Université Paris-Sud XI
Année 2007-2008

Faculté de Médecine Paris-Sud

Mémoire d'habilitation à diriger des recherches

Modèles mathématiques des rythmes physiologiques :

I. Analyse de données cardio-vasculaires et modélisation pour l'étude du système nerveux autonome

II. Chronopharmacologie et optimisation de la chronothérapeutique circadienne en cancérologie

Présenté et soutenu publiquement le 19 décembre 2007 par M. Jean Clairambault
Né le 18 Mars 1950 à Dakar (Sénégal)

Devant le jury composé de :
M. François Dautry, président
M. Jacques Demongeot, rapporteur
Mme France Mentré, rapporteur
M. Jean-Christophe Thalabard, rapporteur
M. Laurent Becquemont, examinateur
M. Michel Laurent, examinateur
M. Jean Maccario, examinateur

Mémoire présenté pour l'obtention de l'habilitation à diriger des recherches en 39e section
(Sciences et technologies pharmaceutiques)

Modèles mathématiques des rythmes physiologiques : I. Analyse de données cardio-vasculaires et modélisation pour l'étude du système nerveux autonome II. Chronopharmacologie et optimisation de la chronothérapeutique circadienne en cancérologie

Jean Clairambault

Décembre 2007

Résumé

Dans ce mémoire sont présentés mes travaux de recherche s'étendant sur 15 ans et divisés en deux thèmes : l'investigation du système nerveux autonome comme coordinateur des rythmes cardio-vasculaires d'une part, et son champ d'application en médecine est la physiologie cardio-vasculaire, et d'autre part celle du système circadien comme coordinateur des rythmes de la prolifération cellulaire, dont le champ d'application médical est d'abord la chronothérapeutique en cancérologie.

Bien que ces deux champs d'application médicale soient aussi séparés que possible l'un de l'autre, l'unité des méthodes théoriques qui permettent cette investigation repose sur une conception de la modélisation des phénomènes observés qui relève en partie de techniques statistiques et de traitement du signal, mais surtout, et c'est pour moi l'aspect le plus intéressant, de méthodes mathématiques de représentation fondées sur l'étude des systèmes dynamiques déterministes, équations différentielles ordinaires et équations aux dérivées partielles.

Dans un premier chapitre la problématique générale de recherche est définie, avec ses deux thèmes d'application à la médecine qui sont présentés chronologiquement. Mon parcours personnel, comprenant cursus, réalisations et liste détaillée de publications est détaillé dans le chapitre suivant. Les chapitres 3 et 4 présentent de façon abrégée les méthodes utilisées et les résultats obtenus, jusqu'aux plus récents. Le chapitre 5 traite des perspectives actuelles pour l'extension de ces travaux et tente de dessiner le paysage scientifique, local et international, dans lequel elle a vocation à s'inscrire. Enfin le chapitre 6 est une sélection de publications venant concrétiser les travaux déjà réalisés.

Je remercie tous mes collègues de l'INRIA (Rocquencourt), en particulier ceux des projets Bang et Sosso dans lesquels j'ai déjà travaillé avec bonheur depuis plusieurs années et continuerai à travailler, mais aussi ceux des projets Contraintes, Estime et Maxplus, avec qui une collaboration s'est ébauchée, qui, je l'espère, ne fera que s'amplifier.

Je remercie tous mes collègues de l'Unité 776 "Rythmes Biologiques et Cancers" de l'INSERM (Villejuif), médecins, biologistes, ingénieurs, mathématiciens, qui m'ont donné la thématique pluridisciplinaire entre cancérologie, tant expérimentale que pharmacothérapeutique, et modélisation mathématique, qui anime mes travaux de recherche actuels.

Je voudrais plus particulièrement distinguer trois personnes dont la bienveillance et les encouragements constants ont été pour moi décisifs :

- *Francis Lévi, médecin clinicien, directeur de l'Unité 776 de l'INSERM, qui dès notre première rencontre s'est montré sensible à nos possibilités de collaboration, et dont la constance dans le maintien de ses objectifs scientifiques contre vents et marées a été pour moi au cours de ces dernières années un point d'ancrage important ;*

- *Benoît Perthame, mathématicien, professeur à l'Université Paris VI, et à l'Ecole Normale Supérieure, responsable scientifique du projet Bang de l'INRIA, qui tout en maintenant un niveau d'exigence mathématique élevé s'est intéressé de plus en plus au cours des dernières années aux problèmes de la biologie et de la médecine actuelles, et m'a toujours soutenu dans ma démarche pluridisciplinaire ;*

- *Daniel Claude, mathématicien, automaticien, homme de contacts et de coopérations, qui était jusqu'à sa retraite récente professeur à l'Université Paris XI et qui m'a fait bifurquer au moment opportun de la modélisation en physiologie cardio-vasculaire à la modélisation pour la chronothérapeutique des cancers tout en conservant la même vision pluridisciplinaire entre mathématiques et médecine, et sans qui rien n'aurait été possible.*

Table des matières

Chapitre 1

Problématique de recherche : la coordination des rythmes physiologiques

1.1 Rythmes physiologiques et modélisation mathématique, intérêt médical en surveillance-diagnostic et thérapeutique

1.1.1 Rythmes physiologiques, essai de définition

Qu'est-ce qu'un rythme physiologique ? On peut le définir comme l'expression temporelle *sensiblement périodique* d'un phénomène biologique résultant de la succession toujours dans le même ordre, reconnaissable, de sous-phénomènes qui le constituent, et qui peut-être macroscopiquement mesurable, tel que le battement du cœur, le mouvement spontané de la respiration pulmonaire, mais aussi de l'expression d'autres variables plus cachées et d'accès nécessitant une technologie élaborée, comme le potentiel d'action des cellules excitables, la pression artérielle, les sécrétions hormonales ou l'alternance activité-repos intrinsèque. Par "*sensiblement périodique*" on entend la qualité pour le phénomène observé de se reproduire à des intervalles temporels de durée sinon constante, du moins s'écartant peu d'une moyenne calculée sur une fenêtre d'observation comprenant un nombre entier raisonnable, disons entre 20 et 100 (notre approximation immédiate de l'infini...), de ses mesures consécutives. La médecine, depuis sa fondation en Occident par la pratique et le corpus théorique de la Collection Hippocratique[1], ne s'est que très peu préoccupée de comprendre les variations de ces rythmes dans les maladies, et "rythme" a longtemps été synonyme de rythme cardiaque, apprécié au pouls. L'insuffisance de moyens de mesure fiables du temps a sans doute été pendant longtemps à l'origine du manque d'intérêt de la médecine pour les rythmes. Souvenons-nous par exemple qu'au XVI^{e} siècle à Pise, le jeune Galilée, déjà plus physicien qu'étudiant en médecine, utilisait son propre pouls comme base temporelle pour mesurer la période des oscillations d'un pendule...

1.1.2 Les rythmes physiologiques, régulateurs des grandes fonctions vitales

On sait aujourd'hui que les grandes fonctions des organismes vivants : métabolismes, transferts d'énergie et d'information, alternance activité-repos, prolifération cellulaire..., et leurs régulations, sont soumises à des rythmes[2, 3] dont la période peut varier de la milliseconde pour les décharges neuronales à l'année pour certains rythmes hormonaux. La coordination des rythmes de ces fonctions physiologiques est essentielle au bon fonctionnement des systèmes qui assurent ces fonctions, permettant à l'organisme de s'adapter au mieux aux variations de l'environnement, par exemple battement cardiaque et respiration ensemble et tous deux au pas d'un coureur à pied.

On s'intéressera surtout dans ce mémoire aux systèmes cardio-vasculaire et respiratoire, et à leur régulation par le système nerveux autonome d'une part, et d'autre part à la régulation de la prolifération cellulaire par le système circadien. Si les composantes du système nerveux autonome sont connues depuis plus d'un siècle, celles du système circadien, dont les mécanismes de base relèvent de la biologie moléculaire des gènes, sont de découverte beaucoup plus récente, des années 1970 à nos jours.

1.1.3 Modélisation des rythmes

Pour rendre compte de ces rythmes et de leur plus ou moins bonne coordination, dans l'organisme sain comme dans la maladie, des modèles mathématiques, reposant autant que faire se peut (suivant l'état des connaissances en biologie) sur la compréhension des mécanismes qui sont à leur origine, ou bien statistiques, analysant de façon plus phénoménologique l'expression simultanée de ces différents rythmes, ont été utilisés depuis une quarantaine d'années au moins, quand mathématiciens, physiciens et ingénieurs ont commencé à appliquer leurs méthodes aux problèmes de la physiologie.

En particulier, des méthodes statistiques et de traitement du signal, utilisant parfois des connaissances physiologiques a priori, ont d'abord été appliquées à l'étude des régulations cardio-vasculaires et cardio-respiratoires à l'effort ou dans l'insuffisance cardiaque. Mais plus récemment, la biologie moléculaire a permis par exemple d'établir des modèles cellulaires à base physiologique de l'excitation membranaire, et, plus récemment encore, du couplage excitation-contraction.

Dans le cas des régulations circadiennes, là aussi des méthodes statistiques et de traitement du signal (analyse spectrale et cosinor) ont d'abord été utilisées. Mais la découverte des mécanismes subcellulaires qui régissent la synthèse de la protéine *PER* (la première à avoir été découverte chez la drosophile) et d'autres protéines constitutives de l'horloge circadienne moléculaire ont heureusement stimulé la construction de modèles mathématiques crédibles des rythmes circadiens[4].

En quoi consistent précisément dans la pratique ces méthodes ? Elles relèvent des domaines suivants des mathématiques appliquées :

– Traitement du signal et des données, autant que possible en utilisant des modèles statistiques fondés sur des connaissances physiologiques a priori ;

– Modélisation multiéchelles, de la molécule à l'organisme entier, utilisant le langage des équations différentielles, des systèmes vivants, avec ou sans intervention d'un contrôle extérieur, représentant la commande thérapeutique, avant tout pharmacologique, du système ;

– Optimisation de la commande (thérapeutique) des modèles ainsi construits, utilisant des méthodes relevant du contrôle optimal.

1.1.4 Intérêt pour le médecin

Quel est l'intérêt pour le physiologiste et pour le clinicien de ces méthodes : traitement statistique des données et modélisation mathématique des mécanismes physiologiques à l'origine des rythmes ? Il est d'abord descriptif et prédictif, donnant de nouveaux outils de mesure du bon fonctionnement de l'organisme (tels que la variabilité du rythme cardiaque, mesure de l'impact du système nerveux autonome sur l'arc baroréflexe), et ces méthodes servent alors dans la surveillance et le diagnostic des pathologies. Mais de plus, la modélisation mathématique des mécanismes physiologiques, lorsqu'elle inclut leur contrôle pharmacologique, a pour but de représenter l'action des médicaments aux niveaux moléculaire, cellulaire, tissulaire et de l'organisme entier, ceci afin d'optimiser les traitements.

1.2 Le système nerveux autonome, coordinateur des rythmes respiratoire, cardiaque et de la pression artérielle, indicateur de bon fonctionnement cardio-vasculaire, et ses mesures non invasives

1.2.1 Mécanismes physiologiques

Le système nerveux autonome, dont les centres sont situés dans le tronc cérébral et le bulbe rachidien, a pour mission chez les mammifères le contrôle à court terme des grandes fonctions vitales : débit cardiaque et circulation sanguine, respiration, oxygénation hiérarchise des teritoires vasculaires, notamment. Ses voies afférentes ont pour origine des capteurs tels que les barorécepteurs aortiques et carotidiens, et rejoignent le noyau du tractus solitaire dans le tronc cérébral ; ses voies efférentes à destination cardiovasculaires sont sympathiques, au départ de l'aire pressive bulbaire et de la corne intermédiolatérale de la moelle, et parasympathiques, au départ du noyau dorsal du vague et ont pour principales destinations le nœud sino-atrial, le myocarde ventriculaire et les muscles lisses des résistances vasculaires périphériques.

L'effet d'une stimulation sympathique, toujours cardioaccélérateur, est relativement lent, de l'ordre d'une dizaine de battements cardiaques, tandis que celui d'une stimulation parasympathique, toujours cardiofrénateur, est beaucoup plus rapide, de l'ordre du battement cardiaque.

Ces différences de comportement entre les deux branches du système nerveux autonome, l'accélératrice lente (sympathique) et la frénatrice rapide (parasympathique), sont à la base de leur étude moderne par l'analyse spectrale du rythme cardiaque, forme la plus élaborée de

l'analyse de la variabilité du rythme cardiaque. En effet, les variations à long terme, ou de basse fréquence, du rythme cardiaque sont le reflet d'un contrôle et sympathique et parasympathique, tandis que les variations à court terme ne représentent que l'influence parasympathique (plus rapide).

Les effets dits dromotropes, bathmotropes, tonotropes et inotropes du système nerveux autonome et des médicaments qui le contrôlent sur le muscle cardiaque échappent à cet outil d'analyse, mais bien sûr ses effets chronotropes au niveau du nœud sino-atrial sont en revanche bien analysés. En fait l'analyse de la variabilité du rythme cardiaque est utilisée pour évaluer le bon fonctionnement du système nerveux autonome tel que le révèle la réponse du baroréflexe à un stimulus, comme par exemple une épreuve d'effort. De ce point de vue, la variabilité du rythme cardiaque est une véritable fenêtre ouverte sur cette variable cachée qu'est le fonctionnement du système nerveux autonome, régulateur principal du système cardio-vasculaire.

La mise en jeu de cette régulation, qui coordonne non seulement la synchronie entre petite et grande circulations, mais aussi la coordination cardio-respiratoire par l'intermédiaire de l'arythmie sinusale resiratoire, se fait en particulier lors du passage à l'orthostatisme et à l'exercice physique, et elle est prise en défaut dans l'insuffisance cardiaque.

1.2.2 Traitement des données

Il s'agit d'abord de données de rythme cardiaque ("signal RR"), obtenues par détection de l'onde R du QRS sur l'électrocardiogramme, puis le traitement par analyse spectrale (transformée de Fourier à court terme) du signal RR, et analyses statistiques unidimensionnelles (tests d'hypothèse, chaînes de Markov cachées) ou multidimensionnelles (analyse en composantes principales, analyse factorielle discriminante) des composantes spectrales extraites.

L'utilisation de méthodes d'analyse non linéaire (dimension de corrélation intégrale, exposants de Lyapounov, prédiction non linéaire...) qui toutes font l'hypothèse d'un "attracteur étrange" pour le signal RR, et de méthodes temps-fréquence (transformée de Wigner-Ville) ou temps-échelle (ondelettes) peut aussi être proposée.

Enfin d'autres techniques associant plusieurs signaux, notamment respiration et rythme RR, peuvent être utilisées, en particulier la démodulation complexe du signal RR au rythme de la respiration, permettant de quantifier en continu l'arythmie sinusale respiratoire (augmentation de la fréquence cardiaque à l'inspiration et diminution à l'expiration -effet du pompage thoracique de sang veineux par abaissement de la coupole diaphragmatique et stimulation de mécanorécepteurs pulmonaires-, elle reflète un bon contrôle du pacemaker sinusal par la branche parasympathique du système nerveux autonome).

1.2.3 Modélisation mathématique

La dépolarisation électrique des cellules cardiaques, au niveau individuel, comme au niveau de l'organe, leur conséquence sur l'entraînement du système cardio-vasculaire (le cœur en tant que pompe) et leur commande par les message du système nerveux autonome, peuvent être représentées par des systèmes d'équations différentielles, ordinaires au niveau d'une cellule, et aux dérivées partielles quand il faut représenter la propagation de l'onde de dépolarisation

dans le myocarde. Le contrôle thérapeutique peut alors se voir comme une modification des paramètres d'excitabilité, de conductivité, de contractilité ou de relaxation des cardiomyocytes.

1.3 Le système circadien, coordinateur des mécanismes de prolifération cellulaire, et ses mesures non invasives ; bases théoriques de la chronothérapie des cancers

1.3.1 Observations initiales et questions physiologiques

Fenêtres d'accès au contrôle physiologique de la prolifération cellulaire par le système circadien, les rythmes de la température centrale et de l'alternance activité-repos mesurée par actimétrie (chez l'homme grâce à un bracelet-enregistreur) permettent d'apprécier non-invasivement le bon fonctionnement de l'horloge circadienne centrale des noyaux suprachiasmatiques (situés dans l'hypothalamus), première horloge circadienne à voir été identifiée.

Il a été observé depuis quelques années grâce aux travaux de l'équipe de Francis Lévi à l'hôpital Paul-Brousse qu'une désorganisation de ces rythmes circadiens chez les patients cancéreux était un facteur de mauvais pronostic et d'autre part qu'une perturbation expérimentale de ces rythmes chez des souris augmentait la vitesse de croissance initiale de tumeurs greffées.

Enfin, la chronothérapie des cancers, pratiquée dans la même équipe et dans d'autres centres hospitaliers, a permis en optimisant théoriquement l'heure du pic d'administration par voie générale des médicaments d'obtenir des résultats significatifs en termes d'amélioration du taux de réponse au traitement, de la tolérabilité clinique et de la survie des patients.

1.3.2 Traitement des données

Le traitement statistique des données expérimentales : courbes de température et d'actimétrie, courbes de croissance du poids tumoral, expression des gènes par qRT-PCR se fait par des méthodes statistiques classiques (tests d'hypothèse) ou par analyse spectrale et par la méthode du cosinor quand un rythme est recherché.

1.3.3 Modélisation mathématique

La modélisation mathématique de la croissance tumorale (avec ou sans traitement) par systèmes dynamiques différentiels est plus originale et tente d'apporter un fondement théorique à la chronothérapie des cancers. Elle nécessite pour cela l'adjonction d'un modèle pharmacocinétique-pharmacodynamique (PK-PD) de l'action des médicaments utilisés et l'introduction de méthodes mathématiques d'optimisation du débit de perfusion prenant pour objectif l'élimination d'un maximum de cellules tumorales sous la contrainte de respecter les cellules saines dans des limites paramétrisables, représentant la capacité du patient, variable selon son état général, à supporter la toxicité du traitement.

Avant de pouvoir procéder à l'optimisation de la fonction de perfusion (le débit d'une pompe programmable en fonction du temps) qui vient contrôler le système dynamique représentant simultanément la croissance tumorale et le maintien de l'homéostasie des tissus sains, il faut représenter l'influence de l'horloge circadienne sur la croissance cellulaire (saine ou tumorale) et sur les systèmes de détoxification cellulaires des molécules exogènes, influence qui est responsable des variations circadiennes observées, sinon toujours expliquées, de l'efficacité antitumorale et de la toxicité non désirée sur les tissus sains.

Cette modélisation peut se faire de manière plus ou moins fine suivant le niveau de description voulu, des interactions moléculaires aux effets globaux en termes de dynamique des populations cellulaires, mais plus les mécanismes à prendre en compte sont nombreux (par exemple des modes d'action différents de médicaments donnés en association, ou encore une toxicité d'un médicament sur l'horloge centrale), plus proche du niveau moléculaire doit être le modèle.

Chapitre 2

Parcours personnel, réalisations, publications

2.1 Curriculum vitæ

Né le 18 Mars 1950, à Dakar (Sénégal).

2.1.1 Formation

1967 Baccalauréat Mathématiques Élémentaires à Angers (Maine-et-Loire).

1969-78 Études de mathématiques à Paris (Paris VI et Paris VII).

1977 Agrégation de mathématiques (91^{e} sur 198).

1978 Doctorat de 3^{e} cycle de mathématiques de l'Université Paris VII sous la direction de F. Norguet et D. Barlet (mention très honorable) ; sujet de la thèse : "Intersections de familles analytiques de cycles".

1978-86 Études médicales au CHU Broussais-Hôtel-Dieu (Paris VI).

1989 Doctorat en médecine de l'Université Paris VI sous la direction de Cl. Gaultier et L. Curzi-Dascalova (mention très honorable) ; sujet de la thèse (soutenue à Paris XI) : "Étude de la variabilité du rythme cardiaque pendant le sommeil de nouveau-nés".

2.1.2 Activités d'enseignement

1981-89 Professeur de mathématiques dans l'enseignement secondaire.

1996-2001 (et à nouveau 2003-04) Professeur agrégé de mathématiques à l'Université Paris VIII (St. Denis). Enseignement des mathématiques en 1er cycle ("Fondements", Intégration, Séries, Calcul différentiel, Algèbre linéaire) et en licence de sciences économiques (Algèbre

linéaire, Systèmes dynamiques) et en licence et maîtrise de mathématiques (Topologie et calcul différentiel, Systèmes dynamiques).

2003-2007 Participation à l'enseignement dans le DU de chronobiologie de l'université Paris VI (Y. Touitou, Pitié-Salpêtrière) : "Traitement des données en chronobiologie" ; participation à l'enseignement dans l'École Doctorale "Innovation thérapeutique" de l'université Paris XI (P. Couvreur, Châtenay-Malabry), dans le module de chronothérapeutique (F. Lévi) et dans le M2 "Pharmacologie-pharmacocinétique-toxicologie" de l'université Paris XI (M. Pallardy).

2007 Chargé d'un cours à option en 3e année (15 h) à l'École Centrale de Paris (Châtenay-Malabry) : Modélisation de la prolifération cellulaire et tissulaire.

2.1.3 Activités de recherche

1976-78 Allocataire de recherche DGRST en mathématiques à l'université Paris VII.

1989-96 Détaché (CR1) à l'INRIA-Rocquencourt (projet SOSSO). Traitement des données de rythme cardiaque et modélisation cardio-vasculaire.

1996-2001 Collaborateur extérieur à l'INRIA (projet SOSSO).

2001-03 Détaché (CR1) à l'INRIA-Rocquencourt (projet SOSSO).

2003-04 Collaborateur extérieur à l'INRIA (projet BANG).

2004-07 Détaché (CR1) à l'INRIA-Rocquencourt (projet BANG). Modélisation du cycle cellulaire et optimisation de la commande thérapeutique.

2001-07 Chercheur dans l'équipe INSERM "Chronothérapeutique des cancers" (E 0118, puis 0354) devenue U 776 "Rythmes biologiques et cancers", directeur F. Lévi, Hôpital Paul-Brousse, Villejuif. Modélisation pour l'optimisation thérapeutique en cancérologie.

2007 Intégré comme chercheur titulaire (CR1) dans le projet BANG de l'INRIA-Rocquencourt.

2.1.4 Activités d'encadrement de la recherche

1990 Juillet-août : Encadrement à l'INRIA de Christopher Leffler, étudiant en médecine et sciences à la Harvard-M.I.T. Division of Health Sciences and Technology (**niveau M1 actuel**). Thème du stage : digitalisation et traitement d'électrocardiogrammes de nouveau-nés.

1990-1991 Février–octobre : Encadrement à l'INRIA de Michael Eiselt, médecin assistant, attaché de recherche à l'Institut de Physiopathologie de l'Université Friedrich-Schiller (Iéna, Allemagne), boursier du gouvernement français dans le cadre d'un accord de coopération avec l'INSERM (**niveau postdoctoral**). Travail effectué : digitalisation et traitement d'électrocardiogrammes de nouveau-nés.

1991 Juin-juillet-août : Encadrement à l'INRIA, en liaison avec G. Celeux, du projet CLOREC, de l'INRIA, de Gino Ranaivoarisoa, stagiaire de 2e année de M.S.T. à l'Université Paris XIII (**niveau M2 actuel**). Thème du stage : analyse des données appliquée à des signaux biomédicaux.

1991-1993 Encadrement à l'INRIA de Ljubomir Spassov, médecin assistant de pédiatrie à la Faculté de Médecine de Sofia (Bulgarie), chercheur à l'INSERM (CJF 89-09, Clamart, Dir. Pr. Cl. Gaultier) sur "poste vert" de mai 1991 à mars 1993 (**niveau postdoctoral**). Travail effectué : digitalisation et traitement d'électrocardiogrammes de nouveau-nés.

1992 Mai–août : Encadrement à l'INRIA, avec G. Celeux, du projet CLOREC, de l'INRIA, de Nadine Colinot, stagiaire de 2e année de l'ISUP (**niveau M1 actuel**). Thème du stage : analyse des données appliquée au rythme cardiaque de nouveau-nés.

1993 Février–juillet : Encadrement à l'INRIA, avec Jacques Henry et Claire Médigue, de Christophe Vermeiren, stagiaire de DEA en génie biomédical (Créteil, **niveau M2 actuel**). Thème du stage : évaluation de méthodes temps-fréquence et de traitement du signal non-stationnaires appliquées à des signaux électrophysiologiques.

1993-94 Décembre-juin : Encadrement à l'INRIA, avec Jacques Henry et Jean-Jacques Codani (Action Génome), d'Alain Gateau, stagiaire de DESS en informatique appliquée à la biologie (Versailles, **niveau M2 actuel**). Thème du stage : développement d'une méthode de reconnaissance par chaînes de Markov des zones codant pour des protéines dans des séquences de génome.

1994 Juillet-août : Encadrement à l'INRIA, avec Claire Médigue et Christophe Vermeiren, d'Alfonso Ehijo, ingénieur et professeur auxiliaire à la Faculté d'Ingénierie de l'Université du Chili (Santiago), dans le cadre d'un contrat de coopération ECOS (**niveau postdoctoral**). Thème du stage : étude des interactions cardiorespiratoires au cours du sommeil ; essai de classification du sommeil en stades à l'aide des signaux respiratoire, de rythme cardiaque, et des mouvements, oculaires et corporels.

2003-05 Participation à l'encadrement de la **thèse de doctorat de mathématiques** de Philippe Michel, soutenue le 5 décembre 2005 à l'université Paris IX-Dauphine, sous la direction de Stéphane Mischler et Benoît Perthame. Sujet de la thèse : "Principe d'entropie relative généralisée et dynamique de populations structurées.".

2005 (Mars-septembre) : Encadrement à l'INRIA (projet BANG) de Houssem Eddine Miled, élève-ingénieur en fin d'études à l'École Polytechnique de Tunisie (**niveau M2 actuel**). Thème du stage : optimisation de la chronothérapeutique en cancérologie.

2005-06 Encadrement avec Benoît Perthame à l'INRIA (projet BANG) de Fadia Bekkal Brikci (**niveau postdoctoral**). Sujet du postdoc : Cinétique de populations cellulaires et thérapeutique du cancer.

2005- Encadrement avec Francis Lévi à l'INSERM d'Ida Iurisci, médecin en **thèse de doctorat ès sciences** entre les universités de Chieti (Italie) et Paris-Sud. Modélisation de l'action cytotoxique du seliciclib, nouvel inhibiteur de kinases cycline-dépendantes (CDKI).

2006 (Février-juin) : Encadrement à l'INRIA (projets BANG et ESTIME) de Jan Stuchly, étudiant du master M2 "Mathématiques de la modélisation" de Paris VI et doctorant de l'Université Charles à Prague. Co-encadrement avec Jean-Charles Gilbert (ESTIME). Thème du stage : Identification d'un modèle sur données expérimentales et évaluation de performances d'algorithmes d'optimisation.

2006-07 (Septembre-mars) : Encadrement à l'INRIA (projets BANG et MAXPLUS) d'Emilio Seijo, stagiaire de M2 (Mexico). Co-encadrement avec Benoît Perthame et Stéphane Gaubert (MAXPLUS). Thème du stage : Contrôle de processus de croissance et optimisation de la valeur propre de Perron.

2007 (Février-juin) : Encadrement à l'INRIA (projets BANG et MAXPLUS) de Thomas Lepoutre, stagiaire de M2 (Paris VI). Co-encadrement avec Benoît Perthame et Stéphane Gaubert (MAXPLUS). Thème du stage : modélisation du cycle cellulaire et contrôle de la valeur propre de Perron.

2007 (Février-juin) : Encadrement à l'INRIA (projet BANG) de Luna Dimitrio, stagiaire de M2 (Paris VI). Thème du stage : modélisation pharmacocinétique-pharmacodynamique intracellulaire d'un anticancéreux.

2007-... (Juin 2007-...) Encadrement à l'INRIA (projet BANG) de la thèse de doctorat d'Annabelle Ballesta (Paris XI). Sujet de la thèse : modélisation moléculaire de la pharmacocinétique-pharmacodynamie intracellulaire d'un anticancéreux.

2007-... (Septembre 2007-...) Co-encadrement à l'INRIA (projet BANG) avec Benoît Perthame (directeur principal) de la thèse de doctorat de Thomas Lepoutre (Paris VI). Sujet de la thèse : modélisation de phénomènes de croissance issus de la biologie.

2.2 Parcours de recherche

2.2.1 Parcours mathématique : formation et recherche

1969-71 1er cycle de mathématiques à Paris, puis Paris VI.
(1970 : DUES 1. Mention Bien. 1971 : DUES 2. Mention Assez Bien.)

1971 Reçu au concours de l'IPES (22e sur 141) à Paris VI en mathématiques.

1973 Maîtrise de mathématiques à Paris VII :

- Topologie générale (A. Revuz). Mention Bien.
- Fonctions analytiques (R. Godement). Mention Très Bien.

– Algèbre (G. Ruget). Mention Assez Bien.
– Calcul différentiel (M. Berger).
– Intégration (J.-L. Verdier). Mention Assez Bien.
– Distributions (F. Norguet).
– Analyse et probabilités (J. Neveu).
– Variétés différentiables (P. Libermann). Mention Très Bien.

1974 CAPES théorique (oral).

1975 CAPES pratique. Mise en sursis d'intégration pour études.

1976 DEA de mathématiques à Paris VII, sous la direction de D. Barlet. Mention Bien :

– 1/2 AEA "Géométrie algébrique élémentaire" (D. Barlet). Mention Bien.
– 1/2 AEA "Variétés analytiques compactes" (J.-L. Stehlé). Mention Assez Bien.
– Mémoire de DEA (directeur : D. Barlet) : "Algèbres de Banach commutatives. Transformation de Gel'fand. Frontière de Shilov.". Mention Très Bien.

1976-78 Boursier DGRST en thèse de 3^e cycle de mathématiques à Paris VII.

1977 Reçu à l'agrégation de mathématiques (91^e sur 198). Option "probabilités et statistiques".

1978 Doctorat de 3^e cycle de mathématiques à Paris VII, sous la direction de D. Barlet et F. Norguet. Mention Très Honorable. Sujet : "Intersections de familles analytiques de cycles".

1977-84 puis à nouveau 1991-95 : Interrogateur en classes préparatoires, au lycée Louis-le-Grand (HX et XP', pendant 7 ans), puis au lycée Hoche, à Versailles (XM et XP), en mathématiques ; en 1995-96 : petites classes à l'ENSTA (MA 103 : analyse, IA 101 : méthodes numériques).

1989-93 Détachement à l'INRIA, et à la suite du doctorat en médecine (sujet de la thèse : "Étude de la variabilité du rythme cardiaque pendant le sommeil de nouveau-nés prématurés et à terme") : Applications de l'analyse de Fourier et de méthodes statistiques multidimensionnelles (analyse en composantes principales, analyse discriminante) au traitement des signaux biomédicaux.

1992-93 Étude par des chaînes de Markov cachées du rythme cardiaque des nouveau-nés (pour y déceler l'état du système nerveux autonome, variable cachée).

1993-94 Étude par des modèles markoviens (chaînes de Markov non cachées) de la reconnaissance de séquences codantes dans des séquences de génome.

1993-95 Étude par des modèles électrophysiologiques de type Hodgkin-Huxley de la dynamique des cellules pace-maker du nœud sinoatrial et de sa régulation par le système nerveux autonome.

1994-96 Étude d'algorithmes évaluant des paramètres déterministes (de type "chaotique"), et application à l'étude de séries de rythme cardiaque selon l'état du système nerveux autonome.

1995-98 Étude d'un modèle en boucle fermée de la régulation du système cardio-vasculaire (rythme cardiaque, pression artérielle) par le système nerveux autonome.

1998-2000 Contrôle de la période d'un modèle d'oscillateur biologique (protéine PER de la drosophile, modèle d'A. Goldbeter) par stimulation intermittente.

2000- Construction d'un modèle d'efficacité antitumorale et de toxicité d'un médicament anticancéreux administré par perfusion chronomodulée.

2003- Modélisation du cycle cellulaire et applications de méthodes de contrôle optimal à la thérapeutique anticancéreuse.

2.2.2 Parcours médical : formation et recherche

1978 Inscription en 1e année de médecine (PCEM1) au CHU Broussais-Hôtel-Dieu (Paris VI).

1979 Reçu au concours de fin de PCEM1 au CHU Broussais-Hôtel-Dieu.

1979-80 PCEM2, et, en parallèle, dans le cadre de la maîtrise de biologie humaine:
Certificat de biochimie générale (Pr. J. Polonovski, CHU St. Antoine), et 1/2 certificat de méthodes statistiques (Pr. Lellouch, CHU Kremlin-Bicêtre).

1980-84 Deuxième cycle des études médicales (DCEM) au CHU Broussais-Hôtel-Dieu. Externat :

- DCEM2 (1981-82) :
  - Consultation de gynéco-endocrinologie (Dr. Canu), hôpital Saint-Michel, Paris.
  - Service de cardiologie (Dr. Droniou), hôpital du Val-de-Grâce, Paris.
  - Laboratoire de biochimie "hormones et protéines" (Pr. Englert), UER biomédicale des Saints-Pères, Paris.
- DCEM3 (1982-83) :
  - Service et consultation de médecine (Pr. Rullière), hôpital Broussais, Paris
  - Service et consultation d'hématologie (Pr. Zittoun), Hôtel-Dieu de Paris.
  - Service et consultation de chirurgie (Pr. Cerbonnet), Hôtel-Dieu de Paris.
- DCEM4 (1983-84) :
  - Service de psychiatrie adolescents (Pr. Flavigny), HIUP, Paris.
  - Service de neurologie (Pr. Laplane), hôpital de la Salpêtrière, Paris.
  - Service de médecine (Pr. Guy-Grand), Hôtel-Dieu de Paris.

1984-86 Troisième cycle des études médicales (TCEM) au CHU Broussais-Hôtel-Dieu. Internat en médecine générale (IMG) :

- Service de psychiatrie-urgences (Dr. Grivois), Hôtel-Dieu de Paris.
- Service de médecine interne (Dr. Krainik), hôpital Léopold-Bellan, Paris (2 semestres).
- Service de psychiatrie-adultes (Pr. Widlöcher), hôpital de la Salpêtrière, Paris.

1987-88 Collaborateur bénévole au laboratoire de biologie du vieillissement (Dr. Sebban), hôpital Charles-Foix, Ivry. Thème d'étude : cartographie électroencéphalographique.

1988-89 Collaborateur bénévole à l'INRIA (projet SOSSO). Thème d'étude : variabilité du rythme cardiaque.

1989 Détachement de l'Education Nationale à l'INRIA, sur (CR1) dans le projet SOSSO. **Décembre 1989 :** Doctorat en médecine au CHU Broussais-Hôtel-Dieu. Sujet de la thèse : " Étude de la variabilité du rythme cardiaque pendant le sommeil de nouveau-nés prématurés et à terme".

2.2.3 Synthèse : recherches entre mathématiques, physiologie et médecine

Après une thèse de **doctorat de 3e cycle en mathématiques** (géométrie analytique, Réf. T1), soutenue en 1978 (dans une situation de pénurie de postes à l'Université), j'ai ressenti le besoin d'explorer un domaine plus proche pour moi des réalités "concrètes" que la cohomologie des faisceaux, qui dominait la recherche en géométrie algébrique et analytique.

Dans cette perspective, la médecine présentait l'intérêt de me rendre rapidement utile en me donnant une activité de terrain dont j'éprouvais la nécessité. Mais aussi j'avais eu connaissance des travaux géométriques de René Thom et de certains de ses élèves (C.P. Bruter, Y. Kergosien) en embryologie et en radiologie notamment, et je pensais qu'il y avait en médecine matière à une réflexion géométrique.

J'ai donc mené, de 1978 à 1986 des **études médicales**, tout en enseignant les mathématiques dans le secondaire. Au cours de ces études, et en préparant pour mes élèves de lycée des cours d'histoire des mathématiques, je me suis aperçu de nombreuses convergences historiques entre médecine et mathématiques, et j'ai envisagé alors de faire une thèse de médecine sur le thème : "Mathématiciens et médecins, convergences et bifurcations", qui aurait fait le point sur le développement parallèle des mathématiques (particulièrement de la géométrie) et de la médecine, depuis l'Antiquité jusqu'aux travaux de R. Thom, en passant par Cardan, Copernic, D. Bernoulli, et quelques autres mathématiciens-médecins. Mais les circonstances m'ont orienté dans une autre direction.

En 1988, en effet, j'ai été amené à m'intéresser au **traitement des signaux biomédicaux**, étant entré en contact avec F. Kauffmann, chercheur à l'INRIA, qui, avec une formation et des intérêts en mathématiques semblables aux miens, étudiait le **rythme cardiaque des nouveau-nés**. Je me suis alors fait détacher de l'Education Nationale à l'INRIA en septembre 1989 et j'ai soutenu en décembre de la même année une **thèse de médecine** sur ce sujet et sous la direction de Mme L. Curzi-Dascalova, chercheur INSERM (CJF 8909, Pr. Cl. Gaultier) à l'hôpital A.-Béclère, Clamart.

A la suite de ma thèse de médecine (Réf. T2) sont venues des publications et communications à des congrès, insistant soit sur l'aspect **traitement du signal** (transformation de Fourier à court terme, Réf. B1, RR1, RR2, O1), soit sur les aspects de **méthodologie statistique** (analyses factorielles, analyses discriminantes, Réf. B2, B3, RR1, O1), soit sur les **aspects physiologiques** (étude de la maturation du système nerveux autonome, Réf. R1, R2, R3, O4, P1) de la méthode et des résultats. Ces travaux, tous menés en collaboration avec Mme L. Curzi-Dascalova, ont montré la possibilité de discriminer selon l'âge les enregistrements du rythme cardiaque de nouveau-nés prématurés et à terme, et l'importance des états de vigilance (stades du sommeil) dans cette discrimination ; ils ont amélioré la compréhension de la **maturation du système nerveux autonome**, montrant qu'elle est différente suivant la branche étudiée, puisqu'elle présente une importante augmentation du tonus parasympathique autour de la 38^{e} semaine d'âge conceptionnel, suivie d'une relative stabilité jusqu'à la naissance, alors que le tonus sympathique connaît une croissance plus régulière de la 31^{e} semaine jusqu'au terme normal. Le but ultime de ces études était de comprendre les causes de la **mort subite inexpliquée du nourrisson**.

Les méthodes mathématiques utilisées dans ces travaux sont tout d'abord du domaine de l'**analyse de Fourier**, pour la décomposition du signal rythme cardiaque en 3 bandes de fréquence ayant chacune une origine physiologique, et de l'**analyse statistique des données multidimensionnelles**, pour l'interprétation des résultats, mais aussi de la modélisation par **chaînes de Markov cachées** (Réf. P2), les états cachés du processus rythme cardiaque (RR, série des intervalles temporels entre battements cardiaques) étant ceux du système nerveux autonome (à prédominance sympathique ou parasympathique).

La modélisation par chaînes de Markov (non cachées) a également été appliquée dans un autre domaine : le **génome**, et a donné lieu à une coopération entre l'INRIA, le Georgia Institute of Technology (Atlanta, USA) et l'Université de Washington (Seattle, USA). Il s'agissait d'adapter et d'intégrer des algorithmes déjà existants (GenMark de M. Borodovsky, MTD de A. Raftery et S. Tavaré) pour obtenir un nouvel outil d'identification des séquences génomiques qui codent pour des protéines. Ce travail a été effectué dans le cadre d'un stage de DESS "informatique et biologie" (Université de Versailles) que j'ai encadré.

Mes recherches se sont ensuite orientées vers une approche plus géométrique de l'étude du rythme cardiaque, considéré comme sortie d'un **système dynamique non linéaire**. Ce système, qui fournit un modèle de l'événement "battement cardiaque", reposant lui-même

sur le modèle de Noma-Irisawa (modèle de type Hodgkin-Huxley) du potentiel d'action de la cellule pace-maker cardiaque, et de son contrôle par le système nerveux autonome. Une étude numérique des orbites périodiques du système de Noma-Irisawa, et également d'un sysème réduit en nombred'équations, et de sa perturbation (paramétrique) par une entrée représentant le système nerveux autonome, a été réalisée, permettant de simuler le rythme cardiaque et sa modulation par le système nerveux autonome (Réf. O6).

Parallèlement à cette approche modélisatrice, des algorithmes de quantification de paramètres, de type "chaotique" (dimension de corrélation intégrale, algorithme de Grassberger et Procaccia, **exposants de Lyapounov**, algorithmes de Wolf et d'Eckmann-Ruelle notamment), ont été évalués sur des séries réelles de rythme cardiaque (Réf. O7, R4, R6). On conjecturait que les séries observées (séries des RR, i.e. pseudopériodes du système perturbé dans le cadre du modèle précédent) étaient en sortie d'un **système dynamique déterministe dissipatif** dont on explorait les propriétés statistiques.
Une collaboration active a été menée entre 1994 et 1997 sur ce sujet avec l'Unité 127 de l'INSERM (biologie et physiopathologie du système cardio-vasculaire, B. Swynghedauw, P. Mansier) et a donné lieu à des communications et publications communes (Réf. R4, R6, O7). On y étudiait le rythme cardiaque de souris soumises à des épreuves pharmacologiques explorant une branche ou l'autre du système nerveux autonome.

Une modélisation globale du système cardio-vasculaire et de la régulation en boucle fermée de la pression artérielle par le système nerveux autonome, aux étapes initiales de laquelle j'ai participé (Réf. SE2, SE3), a ensuite été entreprise dans le projet SOSSO et a donné lieu à trois thèses de doctorat, en Génie Biologique et Médical, en mathématiques appliquées, et en automatique et traitement du signal (1996, 2000 et 2002), sous la direction de J. Henry, M. Sorine et de D. Claude. Mais la réorientation de mes recherches à l'INRIA vers la modélisation en électrophysiologie cardiaque, m'éloignant du traitement du signal pour aller vers une recherche plus théorique (Réf. O6), ce que je souhaitais et à quoi l'INRIA m'incitait, puis surtout mon activité d'enseignement comme PrAg à temps plein à l'université Paris VIII de 1996 à 2001, ne m'ont fait suivre les doctorants concernés que de loin. J'ai néanmoins participé dans ce cadre à une ACI "Technologies de la santé" et plusieurs ARC INRIA (voir ci-dessous : "Participation à des projets nationaux").

Ma rencontre, en 1996, avec D. Claude, alors professeur à l'Université de Paris-Sud, a été le point de départ d'une collaboration qui m'a amené, partant de la modélisation du système cardio-vasculaire, à investir dans des thèmes plus en rapport avec la thérapeutique, s'agissant de la **commande pharmacologique de systèmes biologiques**.

C'est en effet en collaboration avec D. Claude que je me suis intéressé à la **chronobiologie**, étudiant d'abord un modèle d'oscillateur biologique de dimension 5, pour en modifier la période par un stimulus périodique externe (Réf. R7, O8, A3, A4), puis, en collaboration avec F. Lévi, directeur de l'équipe INSERM E 0354 "Chronothérapeutique des cancers" (à partir de 2006 U 776 "Rythmes biologiques et cancers"), un modèle pharmaco-

cinétique-pharmacodynamique (PK-PD) de **chronothérapeutique en cancérologie**, dont le développement est toujours en cours (Réf. SE4, RR4-RR5, R8, R9, R11).

Depuis 2003, cette collaboration s'est élargie à des chercheurs et professeurs de l'École Normale Supérieure (B. Perthame, DMA, également chef du projet BANG à l'INRIA, pour la **modélisation du cycle cellulaire**, Réf. R10, O8, et de la chronothérapeutique anticancéreuse, et C. Basdevant, LMD, pour le **contrôle optimal** d'une chimiothérapie dans un cadre chronobiologique, Réf. R9), et a donné lieu à la participation : a/ à une ACI (2003-2006) : "Nouvelles Interfaces des Mathématiques" ("Apoptose-Nécrose", coordonnateur E. Grenier, UMPA, ENS Lyon) ; b/ à un réseau européen (RTN) "Marie-Curie" (2004-2008) : modélisation de la croissance et de la thérapeutique des cancers, coordonné par N. Bellomo, Turin, et pour sa partie "France-Nord" par B. Perthame, ENS Paris ; c/ à la participation au réseau européen (STREP) "TEMPO" (Temporal genomics for chronotherapeutics) animé par F. Lévi ; et d/ à la soumission de la proposition (2006) à l'ANR BIOSYS "PHYSRYCEL" (Physiologie moléculaire des rythmes : cycle cellulaire, horloge circadienne, métabolisme enzymatique des mdicaments anticancéreux), que j'ai entièrement rédigée.

De plus, je participe au réseau d'excellence européen Biosim (2004-2009) : "Biosimulation, a new tool in drug development", réseau coordonné par E. Mosekilde, Lyngby, Danemark, dont j'ai corédigé avec A. Goldbeter (Bruxelles) le "workpackage" 13 : "Modelling circadian drug effects for cancer therapeutics").

Dans ces deux directions de recherche : modélisation PK-PD de l'action des cytotoxiques, de l'échelle moléculaire à celle de l'organisme entier, et modélisation du cycle cellulaire, le but que je poursuis est la mise en place d'un modèle réaliste et identifiable sur données cliniques de la pharmacologie des anticancéreux, pour lui appliquer des méthodes d'optimisation d'un débit de perfusion. L'optimisation consiste ici à adapter le débit d'un injecteur programmable au profil enzymatique du patient, à ses rythmes circadiens et à sa tolérance clinique d'une part, aux interactions entre cycles cellulaires (suivant les différents tissus cibles) et métabolisme (diffusion, activation, dégradation) des médicaments concernés d'autre part.

2.3 Réalisations

2.3.1 Participation à des projets nationaux

1997-99 Participation au programme de recherche pluridisciplinaire : "Automatique, biologie et santé : modélisation et commande des régulations biologiques." coordonnée par D. Claude (Université Paris-Sud et Laboratoire des signaux et systèmes, CNRS-Supélec).

1997-99 Participation à l'action coopérative INRIA : "Analyse à court et à moyen terme de la variabilité du rythme cardiaque par une approche 'système dynamique'." (CARDIO) (J.

Clairambault, B. Delyon, M. Sorine, projets SIGMA2 et SOSSO). Écriture de la "page Toile" de l'action (`http://www-rocq.inria.fr/sosso/cardio/`).

2000-02 Participation à l'action de recherche coopérative INRIA : "Images de l'activité électromécanique cardiaque." (Projets EPIDAURE, MACS, SINUS et SOSSO (ICEMA) ; coordinatrice : F. Clément).

2002-04 Participation à l'action de recherche coopérative INRIA : "Images de l'activité électromécanique du cœur-2." (Projets INRIA CAIMAN, EPIDAURE, MACS, et SOSSO (ICEMA-2) ; INLN et Université d'Ottawa ; coordinatrice : F. Clément).

2001-03 Participation à l'action incitative "Technologies pour la santé" : "Système Cardio-respiratoire : une approche modélisation et commande" (SCARAMOCO) ; coordonnateur : P.-A. Bliman.

2002-2003 Participation, dans le cadre du GDR "Automatique" du CNRS, au Groupe de Travail "Modélisation et Commande de Systèmes Biologiques" (MCS-Bio) coordonné par D. Claude.

2003-06 Action Concertée Incitative Nouvelles Interfaces des Mathématiques (ACI NIM) "Apoptose-Nécrose", coordonnée par E. Grenier, UMPA, ENS Lyon, réunissant 4 équipes partenaires de recherche (2 ENS, 2 équipes INSERM). Responsable scientifique de l'ACI au sein de l'équipe INSERM U 776 "Rythmes biologiques et cancers" (directeur F. Lévi, hôpital Paul-Brousse, Villejuif), partenaire n^o 2. Programme financé par le Fonds National de la Science.

2006-2008 Action de Recherche Concertée INRIA "Modélisation de la Leucémie Myéloïde Chronique (ModLMC), coordonnée par Mostafa Adimy (Bordeaux).

2.3.2 Participation à des projets internationaux

1992-93 **PROCOPE.** (Programme entre la France et la R.F.A. d'actions intégrées de coopération scientifique et technique) : Coopération avec l'Université Friedrich-Schiller (Institut für Pathophysiologie, Dir. : Prof. U. Zwiener), Iéna, Allemagne. Titre du projet: "Analyse automatique de signaux électrophysiologiques ; application à l'étude de la physiologie et de la physiopathologie du système nerveux du nouveau-né".

1992-93 **INSERM-CONICYT.** Coopération entre le Chili (CONICYT, Unidad de Neurofisiologia del Desarrollo, INTA, Universidad de Chile, Dr. P. Peirano) et la France (INSERM, INRIA, Université de Caen) en recherche biomédicale. Titre du projet : "Contrôle moteur et végétatif chez les anciens prématurés arrivés à l'âge du terme et dans les cas d'hypotrophie intra-utérine". Prise en charge par un accord INSERM-CONICYT. Prise en charge par le ministère des affaires étrangères.

1993-94 **Génome.** Collaboration avec Mark Borodovsky, du Georgia Institute of Technology (Atlanta, GA, USA), Adrian Raftery, de l'Université de Washington à Seattle (USA), et Gilles

Celeux, de l'INRIA-Rhône-Alpes. Thème du projet : utilisation de modèles de Markov pour l'identification de régions de l'ADN codant pour des protéines.

1993-96 **ECOS.** Coopération entre le Chili (CONICYT, INTA) et la France (INRIA, INSERM) en recherche biomédicale. Titre du projet : "Etude en temps réel des interactions entre les rythmes cardiaque et respiratoire et de leur régulation par le système nerveux autonome". Prise en charge par **ECOS** pour 3 ans.

1996-97 **PROCOPE.** Nouveau projet PROCOPE de collaboration avec la même équipe de l'Université d'Iéna (voir ci-dessous) sur le thème : "Estimation quantitative de paramètres déterministes de type chaotique sur des séries temporelles physiologiques. Application à l'étude du système nerveux autonome par l'analyse de données de respiration et de rythme cardiaque." Prise en charge par le ministère des affaires étrangères.

1997-99 **ECOS.** Nouveau projet franco-chilien ECOS avec les mêmes partenaires (voir ci-dessous) : "Etude de la réactivité cardiaque aux stimuli en fonction des stades du sommeil".

2004-09 (6^{e} PCRD) Réseau européen Marie-Curie TUMATHER ("Modelling Tumour Growth and Therapeutics"), coordonné par N. Bellomo (Turin). Réseau financé par l'Union Européenne pour 2004-2008, dans lequel l'École Normale Supérieure (B. Perthame, DMA) représente le pôle "France-Nord", le Laboratoire Rythmes biologiques et Cancers (INSERM E 0354) s'y rattachant dans ce cadre.

2004-09 (6^{e} PCRD) Réseau européen d'excellence pour la santé BIOSIM ("Biosimulation: a new tool for drug development"), coordonné par E. Mosekilde (Lyngby, Danemark). Réseau financé par l'Union Européenne pour 2004-2009. Corédacteur avec A. Goldbeter (Bruxelles) du "workpackage" Modelling circadian drug effects in anti-cancer treatment.

2006-09 (6^{e} PCRD) Réseau européen spécifique (STREP) pour la santé TEMPO ("Temporal genomics for tailored chronotherapeutics"), coordonné par F. Lévi (INSERM U 766, Villejuif.

2.3.3 Organisation d'ateliers et de minisymposia

2004 "Apoptose, cancer et thérapeutique : mécanismes et leur modélisation". Journée de l'ACI "Apoptose-nécrose" (organisateur : Jean Clairambault), Villejuif, septembre 2004 :

1. Modéliser l'apoptose : buts, questions, outils (Jean Clairambault, INRIA, Rocquencourt et INSERM, Villejuif)

2. Contrôle mitochondrial de l'apoptose (Naoufal Zamzami, IGR, Villejuif)

3. Apoptose et AVC Ischémique (Marie-Aimée Dronne, Lyon I)

4. Organisation circadienne de l'apoptose et thérapeutique (Francis Lévi, INSERM, Villejuif)

5. Modélisation et cancer en Europe : développement et nouveaux défis. (Benjamin Ribba, Lyon I)

2005 “Proliferation and growth in tissues”. Minisymposium à la conférence européenne de l’ESMTB, Dresde, juillet 2005 (organisateurs : Dirk Drasdo, Leipzig et Jean Clairambault) :

1. Model based design of dose dense chemotherapy treatments in lymphomas (Markus Loeffler, Leipzig)

2. Analysis and mathematical modeling of cell growth and virus replication of adherent cell lines used in vaccine production (Udo Reichl, Magdeburg)

3. A mathematical model of the cell cycle and its control (Jean Clairambault, INRIA, Rocquencourt and INSERM, Villejuif)

4. On the regulation of tumor growth in-vitro (Dirk Drasdo, Leipzig)

2006 “Coordination of physiological rhythms”. Minisymposium à la conférence internationale IEEE-EMBS, New York, août 2006 (organisateurs : Dirk Hoyer, Iéna, et Jean Clairambault) :

Part I: Fundamentals and circadian rhythms

1. The circadian timing system, a coordinator of life processes (Francis Lévi, INSERM, Villejuif)

2. Importance of circadian rhythms for regulation of the cardiovascular system studies in animal and man (Björn Lemmer, Heidelberg)

3. Cancer symptom complexes related to alterations in molecular circadian axis signalling (Tyvin Rich, Charlottesville, USA)

4. Physiologically based modelling of circadian control on cell proliferation (Jean Clairambault, INRIA Rocquencourt et INSERM, Villejuif)

Part II: Cardiovascular and other coordinated rhythms

1. Why life oscillates - rhythms and health (Maximilian Moser, Graz)

2. Circadian and ultradian rhythms in cardiovascular autonomic modulation (Phyllis K. Stein, St. Louis, USA)

3. Scale-invariant Aspects of Physiologic Dynamics Across Sleep Stages and Circadian Phases (Plamen Ch. Ivanov, Boston, USA)

4. Association between short term and long term communication in pathological autonomic control (Dirk Hoyer, Iéna)

5. Coupled oscillators: Complex but not complicated cardiovascular and brain interactions (Aneta Stefanovska, Lancaster, UK et Ljubljana)

6. Inferring coupling between physiological systems from data: application to cardiorespiratory interaction (Michael Rosenblum, Potsdam)

2006 “Cancer modelling and therapeutic innovation: from theory to clinic”. Atelier international à l’ENS Lyon, septembre 2006 (organisateurs : Benjamin Ribba et Jean Clairambault) :

Tuesday, September 26, 2006

9.00 - 9.15 - Welcome by Benjamin RIBBA

9.15 - 9.30 - Opening remarks by Jean CLAIRAMBAULT

9.30 - 10.00 - Zvia AGUR: Validation in neoadjuvant breast cancer patients of a new solid tumor growth model.

10.00 - 10.30 - Vito QUARANTA: Integrative mathematical model of cancer invasion.

11.00 - 11.30 - Alain PUISIEUX: Escape of cancer cells from failsafe programs: a major step towards tumor progression.

11.30 - 12.00 - Thomas BACHELOT

12.00 - 12.30 - Claire RODRIGUEZ-LAFRASSE

14.00 - 14.30 - Dirk DRASDO: What can we learn from single-cell-based models of tumor growth?

14.30 - 15.00 - Claude VERDIER: Cell interactions in cancer.

15.00 - 15.30 - Luigi PREZIOSI: Modelling the formation of vascular networks.

16.00 - 16.30 - Philip MAINI: Modelling aspects of vascular cancer.

16.30 - 17.00 - Alberto GANDOLFI: Split-dose response to radiation in a tumor cord model.

17.00 - 17.30 - Athanassios ILIADIS: Modelling heterogeneity in cyclosporine pharmacokinetics.

Wednesday, September 27, 2006

9.00 - 9.30 - Dominique BARBOLOSI and Gilles FREYER: Mathematical modelling optimises the Docetaxel-Epirubicin combination in a phase I trial.

9.30 - 10.00 - Francis LÉVI

10.00 - 10.30 - Charles DUMONTET

11.00 - 11.30 - Yann GODFRIN

11.30 - 12.00 - Patrick SQUIBAN

12.00 - 12.30 - Filippo CASTIGLIONE: ImmunoGrid: pushing ahead the immune system simulation.

14.00 - 14.30 - Jean-Yves SCOAZEC: Tumor angiogenesis: Current concepts.

14.30 - 15.00 - Jean-Pierre BOISSEL

15.00 - 15.30 - Randall THOMAS: QCDB: Quantitative database for mathematical models of cancer.

16.00 - 16.30 - Pascal GIRARD

16.30 - 17.00 - Alberto D'ONOFRIO: Metamodeling tumor-immune system interaction and immunotherapy: the interplay between basic science and clinical applications.

17.00 - 17.15 - Closing remarks by Jean-Yves BLAY, Scientific Director of Cancéropôle Lyon Auvergne Rhône-Alpes

2.4 Liste des publications

2.4.1 Thèses

[T1] Clairambault, J. (1978) : "Intersections de familles analytiques de cycles". Thèse de doctorat de 3e cycle de mathématiques (géométrie analytique) soutenue à Paris VII sous la direction de F. Norguet et D. Barlet.

[T2] Clairambault, J. (1989) : "Etude de la variabilité du rythme cardiaque pendant le sommeil de nouveau-nés prématurés et à terme". Thèse pour le doctorat en médecine soutenue à Paris VI sous la direction de Cl. Gaultier et L. Curzi-Dascalova.

[T3] Clairambault, J. (2006) : "Modèles mathématiques des rythmes physiologiques : I. Analyse de données cardio-vasculaires et modélisation pour l'étude du système nerveux autonome. II. Chronopharmacologie et optimisation de la chronothérapeutique circadienne en cancérologie". Mémoire d'habilitation à diriger des recherches en 39e section : Sciences et technologies pharmaceutiques

2.4.2 Analyse de données cardio-vasculaires et modélisation pour l'étude du système nerveux autonome

Articles parus dans des revues internationales :

[R1] Clairambault, J., Curzi-Dascalova, L., Kauffmann, F. Médigue, C., Leffler, C. (1992) : Heart Rate Variability in normal sleeping full-term and preterm neonates. *Early Human Development*, 28, 169-183.

[R2] Eiselt, M., Curzi-Dascalova, L., Clairambault, J., Médigue, C., Peirano, P. (1993) : Heart-rate variability in low-risk prematurely born infants reaching normal term: a comparison with full-term newborns. *Early Human Development*, 32, 183-195.

[R3] Spassov, L., Curzi-Dascalova, L., Clairambault, J., Kauffmann, F., Médigue, C., Peirano, P. (1994) : Heart rate and heart rate variability in small-for-gestational-age newborns. *Pediatric Research*, 35, 500-505.

[R4] Mansier, P., Clairambault, J., Charlotte, N., Médigue, C., Vermeiren, C., LePape, G., Carré, F., Gounaropoulou, A., Swynghedauw, B. (1996) : Linear and non-linear analyses of heart rate variability: a minireview. *Cardiovascular Research*, 31, 371-379.

[R5] Mansier, P., Médigue, C., Charlotte, N., Vermeiren, C., Corabœuf, E., Deroubai, E., Ratner, E., Chevalier, B., Clairambault, J., Carré, F., Dahkli, T., Bertin, B., Briand, P., Strosberg, D., Swynghedauw, B. (1996) : Decreased heart rate variability in transgenic mice overexpressing atrial β_1-adrenoceptors. *American Journal of Physiology*, 271:H1465-H1472.

[R6] Swynghedauw, B., Jasson, S., Clairambault, J., Chevalier, B., Heymes, C., Médigue, C., Carré, F., Mansier, P. (1997) : Myocardial determinants in regulation of the heart rate. *Journal of Molecular Medicine*, 75:860-866.

Articles parus dans des actes de congrès internationaux :

[O1] Clairambault, J., Curzi-Dascalova, L., Kauffmann, F., Médigue, C., Leffler, C. (1991) : Assessment of Heart Rate Variability by Short-Time Fourier Transform and Data Analysis. In: *Computers in Cardiology 1991*, 421-424. Congrès annuel de *Computers in Cardiology*, Venise, septembre 1991.

[O2] Médigue, C., Dupont, F., Clairambault, J., Curzi-Dascalova, L., Spassov, L. (1992) : A Synchronous Language, SIGNAL: application to Heart Rate Variability and Body Movements Analysis in Sleeping Newborns. In: *Computers in Cardiology 1992*, 471-474. Congrès annuel de *Computers in Cardiology*, Durham (NC), octobre 1992.

[O3] Médigue, C., Clairambault, J., Curzi-Dascalova, L. (1992): A real time heart rate variability analysis system using a synchronous language: Signal. In: Actes de la 14^{e} conférence annuelle internationale de l'*IEEE Engineering in Medicine and Biology Society*, 766-767, Paris, octobre 1992.

[O4] Curzi-Dascalova, L., Eiselt, M., Spassov, L., Kauffmann, F., Clairambault, J., Médigue, C., Peirano, P. (1992) : Heart rate variability in normal and at risk newborns. In: Actes de la 14^{e} conférence internationale annuelle de l'*IEEE Engineering in Medicine and Biology Society*, 2638-2639, Paris, octobre 1992.

[O5] Vermeiren, C., Médigue C., Clairambault, J., Curzi-Dascalova, L. (1994) : Beat-to-beat cardio-respiratory demodulation. In: Actes de l'*IFAC Symposium on modelling and control in biomedical systems*, 142-143, Galveston (TX), mars 1994.

[O6] Clairambault, J. (1995) : A model of the autonomic control of heart rate at the pacemaker cell level through G-proteins. In: Actes de la *17^{e} conférence internationale IEEE-EMBS*, 1379-1380, Montréal, septembre 1995.

[O7] Clairambault, J., Mansier, P., Swynghedauw, B. (1995) : Efects of parasympathetic blockade on nonlinear dynamics of heart rate in mice. In: Actes de la *17^{e} conférence internationale IEEE-EMBS*, 31-32, Montréal, septembre 1995.

Rapports de recherche :

[RR1] Clairambault, J., Curzi-Dascalova, L., Kauffmann, F., Médigue, C., Leffler, C., Celeux, G., Guégan, D. (1991) : Heart rate variability in sleeping neonates. *Rapport de Recherche INRIA* n° 1472.

[RR2] Médigue, C., Clairambault, J., Kauffmann, F., Sorine, M., Curzi-Dascalova, L. (1992) : Utilisation du langage SIGNAL pour l'étude d'algorithmes de traitement du signal électrocardiographique. *Rapport de Recherche INRIA* n° 1717.

[RR3] Médigue, C., Bestel, J., Renard, S., Clairambault, J., Garrido, M., Pizarro, F., Peirano, P. (1997) : An application of LARY_C: discrete wavelet transform applied to heart rate variability analysis. Assessment of the autonomic nervous system behaviour in control and iron-deficient anemic infants. *Rapport de Recherche INRIA* n° 3203.

Articles parus dans des bulletins, des actes de colloques ou de séminaires :

[SE1] Clairambault, J., Claude, D. (1996) : Systèmes dynamiques et biologie : quelques exemples. In : *Séminaire* T I P E *sur les systèmes dynamiques*. Journée de formation (ENSTA-UPS) pour les professeurs de Mathématiques Spéciales (organisateur : Max Bezard). Paris, mai 1996.

[SE2] Clairambault, J., Médigue, C., Bestel, J. (1997) : Le système cardio-vasculaire et sa régulation à court terme par le système nerveux autonome. In : *Journées d'Étude "Automatique et Santé" du club EEA* (organisateurs : E. Dombre et A. Fournier). ISIM, Montpellier, juin 1997.

[SE3] Bestel, J., Clairambault, J., Médigue, C., Monti, A., Sorine, M. (1999) : Le système cardio-vasculaire et sa régulation par le système nerveux autonome : modélisation et mesures. In : *Journée d'étude du programme de recherche Automatique, Biologie et Santé : Modélisation et commande de régulations biologiques* (organisateur : Daniel Claude). Paris, mai 1999.

[A1] Curzi-Dascalova, L., Clairambault, J., Kauffmann, F., Médigue, C., Peirano, P. (1991) : Cardiorespiratory variability and development of sleep state organization. In: *Sleep and Cardiorespiratory Control*, colloque INSERM, vol. 217:155-163. Ed : C. Gaultier, P. Escourrou, L. Curzi-Dascalova, Paris, septembre 1991.

[A2] Celeux, G., Clairambault, J. (1992) : Estimation de chaînes de Markov cachées : méthodes et problèmes. In: *Approches markoviennes en signal et images*, pp. 5-19. Ed.: GDR Traitement du signal et images. Colloque au CNRS, Paris, septembre 1992.

[B1] Kauffmann, F., Médigue, C., Clairambault, J., (1991) : Un système d'analyse des signaux biomédicaux. *Bulletin de liaison de la recherche en informatique et automatique*, 130:38-41.

[B2] Clairambault, J., Celeux, G. (1991) : Analyse discriminante appliquée à l'étude du rythme cardiaque. *La Revue de Modulad*, 8, 61-72.

[B3] Celeux, G., Clairambault, J. (1991) : Analyse discriminante appliquée à l'étude du rythme cardiaque: développements méthodologiques. *La Revue de Modulad*, 8:73-80.

2.4.3 Chronopharmacologie et optimisation de la chronothérapeutique circadienne en cancérologie

Articles parus ou à paraître dans des revues internationales :

[R7] Claude, D., Clairambault, J. (2000) : Period shift induction by intermittent stimulation in a Drosophila model of PER protein oscillations. *Chronobiology International*, 17(1):1-14.

[R8] Clairambault, J., Claude, D., Filipski, E., Granda, T., Lévi, F. (2003) : Toxicité et efficacité antitumorale de l'oxaliplatine sur l'ostéosarcome de Glasgow induit chez la souris : un modèle mathématique. *Pathologie-Biologie*, 51:212-215.

[R9] Basdevant, C., Clairambault, J., Lévi, F. (2005) : Optimisation of time-scheduled regimen for anti-cancer drug infusion. *Mathematical Modelling and Numerical Analysis*, 39(6):1069-1086.

[R10] Clairambault, J., Michel, Ph., Perthame, B. (2006) : Circadian rhythm and tumour growth. *C. R. Acad. Sci., Mathématique* (Équations aux dérivées partielles), 342(1):17-22.

[R11] Clairambault, J. (2007) : Modeling oxaliplatin drug delivery to circadian rhythm in drug metabolism and host tolerance. *Advanced Drug Delivery Reviews (ADDR)*, 59:1054-1068.

[R12] Bekkal Brikci, F., Clairambault, J., Ribba, B., Perthame, B. (2007). An age-and-cyclin-structured cell population model for healthy and tumoral tissues. *Journal of Mathematical Biology*, in press.

[R13] Bekkal Brikci, F., Clairambault, J., Perthame, B. (2007). Analysis of a molecular structured population model with possible polynomial growth for the cell cycle. *Journal of Mathematical and Computer Modelling*, in press.

[R14] Clairambault, J., Gaubert, S., Perthame, B. (2007). An inequality for the Perron and Floquet eigenvalues of monotone differential systems and age structured equations. C. R. Acad. Sci. (Paris) Ser. I Mathématique, 345:549-554.

[R15] Clairambault, J. (2008). Physiologically based modelling of circadian control on cell proliferation. *IEEE-EMB Magazine*, in press.

Articles parus dans des actes de congrès internationaux :

[O8] Clairambault, J., Michel, P., Perthame, B. (2006) : A model of the cell cycle and its circadian control. *Actes de la 6e conférence internationale de l'European Society for Mathematical and Theoretical Biology (ESMTB)*, Dresde, juillet 2005.

[O9] Clairambault, J. (2006) : Physiologically based modelling of the circadian control on cell proliferation. *Actes de la 28e conférence internationale IEEE-EMBS*, New York, août 2006.

Rapports de recherche :

[RR4] Clairambault, J, Laroche, B, Mischler, S, Perthame, B. (2003) : A mathematical model of the cell cycle and its control. Présentation à "CANUM 2003", Montpellier. *Rapport de recherche INRIA* no 4892.

[RR5] Basdevant, C., Clairambault, J., Lévi, F. (2004) : Optimal drug infusion strategies for cancer chronotherapy. *Rapport de recherche INRIA* no 5407.

[RR6] Bekkal Brikci, F., Clairambault, J., Ribba, B., Perthame, B. (2006) : A cell population model with proliferation and quiescence for healthy and tumoral tissues. *Rapport de recherche INRIA* no 5941.

Articles parus dans des bulletins, des actes de colloques ou de séminaires :

[SE4] Claude, D., Clairambault, J., Lévi, F. (1999) : Rythmes biologiques et chronothérapeutique : comparaison entre des schémas d'administration théoriques et des thérapeutiques appliquées en cancérologie. *Colloque du Groupe d'Étude sur les Rythmes Biologiques*, Bordeaux, mai 1999.

[A3] Claude, D., Clairambault, J. (1999) : Déplacement de rythme par stimulation intermittente du modèle des oscillations de la protéine PER chez la Drosophile. Numéro spécial de la revue *Traitement du Signal*, 15(6):637-642 : Colloque en l'honneur de B. Picinbono, Paris, mai 1999.

[A4] Claude, D. Clairambault, J., Desmézières, A. (1999) : Travaux pratiques sur les systèmes non linéaires : étude d'un modèle de régulation de la synthèse de la protéine PER chez la Drosophile. *Colloque sur l'Enseignement des Technologies et des Sciences de l'Information et des Systèmes (CETSIS-EEA'99)*, Montpellier, novembre 1999.

Chapitre 3

Travaux de recherche antérieurs (1989-1999) : traitement des données de rythme cardiaque et modélisation en électrophysiologie cardiaque pour l'étude du système nerveux autonome

Au cours des annés 90, mes travaux de recherche, en commençant par ce qui constituait la matière de ma thèse pour le doctorat en médecine, ont porté d'abord sur la variabilité du rythme cardiaque et son intérêt dans l'étude du système nerveux autonome, puis plus généralement sur la modélisation du système cardio-vasculaire et sa commande par le système nerveux autonome, en restant centré sur les aspects *chronotropes* de cette commande, i.e., sur le contrôle de la période du pacemaker du nœud sino-atrial (NSA).

3.1 Analyse des données : la variabilité du rythme cardiaque comme fenêtre d'accès au système nerveux autonome

3.1.1 Rythme cardiaque et système nerveux autonome

Le système nerveux autonome : branche sympathique cardio-accélératrice et branche parasympathique cardio-modératrice, est étudié depuis au moins 70 ans (Rosenblueth et Simeone, 1934[5], plus récemment B. McA. Sayers[6] et Katona et Jyh[7]) par l'intermédiaire des variations du rythme cardiaque. Il est à présent bien établi[8, 9] que les variations rapides (c'est-à-dire de haute fréquence, HF) reflètent le contrôle parasympathique du rythme cardiaque uniquement, alors que les variations moins rapides ou lentes (c'est-à-dire de moyenne ou de basse fréquence, MF, BF) sont un reflet aussi bien du contrôle sympathique que du contrôle parasympathique.

Pour ma thèse de doctorat en médecine, effectuée sous la direction de Mme L. Curzi-Dascalova, alors chercheur INSERM à l'hôpital Antoine-Béclère, et grâce à des collaborations

avec F. Kauffmann, alors à l'INRIA, pour les méthodes de traitement du signal, et G. Celeux, de l'INRIA pour la mise au point de la méthodologie statistique, j'ai utilisé des enregistrements de sommeil d'un groupe de 24 nouveau-nés sains, répartis en trois groupes d'âge : 8 prématurés (de 31 à 36 semaines d'âge conceptionnel), 8 d'âge intermédiaire (37 à 38), et 8 à terme (39 à 41). Considérant deux variables qualitatives, l'âge et le stade du sommeil (SA et SC, codé indépendamment du rythme cardiaque sur des tracés électroencéphalographiques enregistrés simultanément), et posé deux questions :

1/ Dans un groupe d'âge donné, est-il possible de séparer les stades du sommeil à l'aide des variables cardiaques HF, MF et BF ?... Et si oui, quelles sont les variables qui contribuent le plus à cette discrimination ?

2/ Dans un stade de sommeil donné, est-il possible de séparer les nouveau-nés à terme des prématurés à l'aide des seules variables cardiaques HF, MF, et BF ?... Et si tel est le cas, quelle est la contribution de chaque bande de fréquence, et donc des branches sympathique et parasympathique du SNA à cette discrimination ?

Mon but était donc avant tout explicatif : il ne s'agissait pas tant d'obtenir une bonne discrimination entre groupes, mais, ayant obtenu entre eux une discrimination satisfaisante, d'analyser les contributions des variables HF, MF, et BF à cette discrimination et de suivre l'évolution de ces contributions avec la maturation, du prématuré au nouveau-né à terme.

3.1.2 Analyse spectrale

C'est toujours la méthode de référence dans l'étude des phénomènes périodiques. Elle consiste à considérer un signal périodique comme une somme de sinusoïdes à des fréquences et amplitudes distinctes :

$$x(t) = a_1 \cos 2\pi f_1 t + a_2 \cos 2\pi f_2 t + \dots$$

et à représenter le signal dans le domaine fréquentiel (le temps ne figure plus) par le graphe $\{(f_1, a_1), (f_2, a_2), \dots\}$ (spectre de raies).

Dans sa version continue, cette représentation fréquentielle est donnée par le calcul de l'amplitude de la transformée de Fourier :

$$a(f) = \left| \int_{-\infty}^{+\infty} x(t) e^{-2\pi i t f} dt \right|$$

ou dans sa version discrète, pour un signal digitalisé et observé sur une fenêtre de longueur temporelle T et à une fréquence d'échantillonnage $\frac{T}{N}$, i.e., aux instants $x(0), x(T/N), x(2T/N), \dots, x((N-1)T/N)$, par le calcul du périodogramme :

$$a(f) = \left| \sum_{k=0}^{N-1} x\left(\frac{kT}{N}\right) e^{-2\pi i \frac{kf}{N}} \right|$$

.

Il faut mentionner la nécessité, pour que ces calculs aient un sens, de supposer le signal $x(t)$ stationnaire dans l'intervalle de temps étudié, ce qui veut dire (stationnarité faible) que

ses caractères statistiques du premier ordre et du second ordre : moyenne, variance, et fonction d'autocovariance [1] ne varient pas au cours du temps.

Pour répondre à l'objection de non stationnarité du signal, et apprécier de façon continue les *composantes spectrales* instantanées du signal dans des bandes de fréquence données (car aucun signal du monde biologique n'est constitué d'une simple somme de sinusoïdes : on obtient toujours par la transformation de Fourier, non pas un spectre de raies, mais un spectre continu avec des pics aux féquences dominantes), on peut utiliser des méthodes d'analyse spectrale évolutive comme la transformée de Fourier à court terme[10] :

$$A_{f_0}(n) = \left| \sum_{k=0}^{n} x(k) w_\varepsilon(n-k) exp(-2\pi i f_0 k) \right|$$

où [f_0 - ε , f_0 + ε] est la bande de fréquence d'intérêt et (w_ε) est un filtre elliptique (iir) passe-bas, de bande passante [0 , ε]. Ici on a remplacé l'expression du signal digitalisé $x\left(\frac{kT}{N}\right)$ dans la formule précédente, où l'observation se fait sur une fenêtre de longueur finie T par $x(k)$, la fenêtre d'observation n'étant pas limitée : en principe, tous les instants du signal depuis l'origine sont pris en compte ; dans la pratique le filtre utilisé limite le nombre d'instants d'observation nécessaires à au plus quelques centaines en arrière.

Cette méthode relève des méthodes dites de démodulation complexe[11], qui consistent à individualiser dans le signal une composante de fréquence f_0 fixée et à la suivre au cours du temps, en admettant qu'elle est lentement modulée en amplitude et en phase, i.e. de la forme :

$$x_{f_0}(t) = a(t)\cos[2\pi f_0 t + \varphi(t)]$$

où $a(t)$ est l'amplitude instantanée et $\varphi(t)$ est la phase instantanée (entre $-\pi$ et $+\pi$ radians).

En pratique, après avoir choisi la fréquence f_0, on ramène la composante de fréquence f_0 à zéro et on utilise un filtre passe-bas, ce qui donne l'ensemble des composantes du signal dans une bande de fréquence $[f_0 - \Delta f, f_0 + \Delta f]$ autour de f_0. L'amplitude instantanée $a(t)$ indique alors l'intensité du signal dans une bande de fréquence autour de f_0, et la phase instantanée $\varphi(t)$ mesure le glissement en fréquence autour de f_0 : s'il y a un pic isolé en f_0 dans le spectre invariablement au cours du temps, alors la phase $\varphi(t)$ sera toujours à zéro.

Le résultat de ce calcul est constitué de signaux temporels continus représentant les diverses composantes spectrales d'intérêt (sans hypothèse de stationnarité nécessaire), qu'on peut ensuite étudier séquentiellement, par exemple pour le signal RR par plages de 512 battements cardiaques, pour les mettre en rapport avec d'autres signaux physiologiques indépendants obtenus simultanément, comme le stade du sommeil d'un nouveau-né.

La Figure 1 montre l'exemple de 4096 battements cardiaques (intervalles RR) du sommeil d'un nouveau-né à terme et les signaux extraits en haute fréquence (HF, composante spectrale correspondant à des motifs de période entre 3 et 8 battements), moyenne fréquence

1. la fonction d'autocovariance est la transformée de Fourier inverse de la fonction de densité spectrale ; elle peut s'interpréter, pour chaque valeur de u, comme une mesure de la "similarité" moyenne entre la valeur du signal $x(t)$ au temps t et sa valeur $x(t+u)$ au temps $t+u$.

(MF, 10 à 25), et basse fréquence (BF, 30 à 100). L'électroencéphalogramme enregistré simultanément (enregistrement polysomnographique effectué à l'hôpital Antoine-Béclère) a fait indépendamment l'objet d'une classification des stades du sommeil en sommeil agité (SA) et sommeil calme (SC).

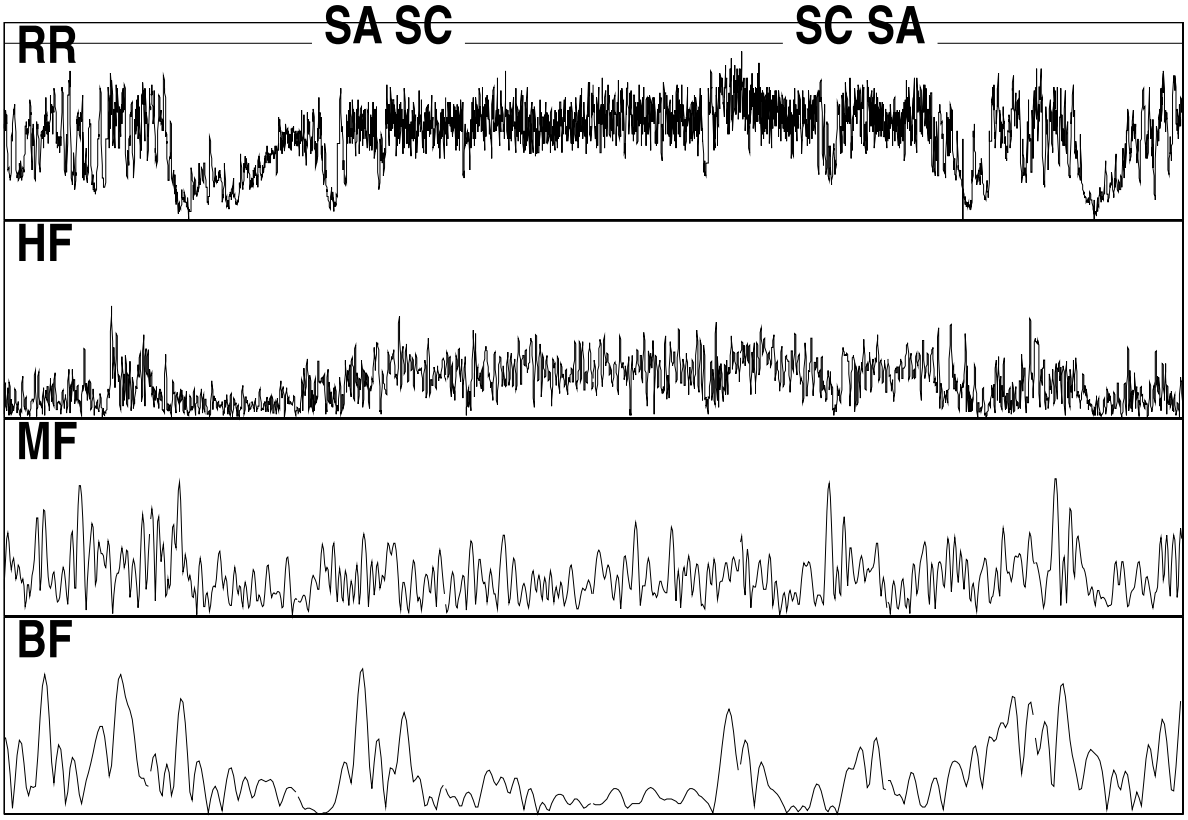

Figure 1. *Séquence de 4096 battements cardiaques d'un nouveau-né à terme, avec (de haut en bas) le signal RR et les 3 signaux extraits HF, MF, et BF. On reconnaît ici une période d'intense activité en HF, avec faible activité en BF, enregistrée en Sommeil Calme (SC), encadrée par deux périodes ayant des caractéristiques opposées, correspondant à du Sommeil Agité (SA).*

3.1.3 Analyse factorielle discriminante : sommeil agité ou sommeil calme ? nouveau-né prématuré ou nouveau-né à terme ?

L'Analyse Factorielle Discriminante[12, 13] est une méthode d'analyse statistique multidimensionnelle (ici, trois variables quantitatives explicatives : HF, MF, BF) qui permet, dans une population dont on sait a priori qu'elle se divise en plusieurs groupes qualitatifs (2, dans le cas simple de l'exemple qui va nous occuper ici), de calculer une *Fonction Linéaire Discriminante*, combinaison linéaire optimale de variables quantitatives choisies, et de donner une règle de discrimination entre ces groupes fondée sur cette Fonction Linéaire Discriminante.

La Figure 2 ci-dessous illustre le cas typique d'une population constituée de 2 groupes nettement séparés, mais qu'aucune des 2 variables (par projection orthogonale sur l'un des axes) ne permet de discriminer de façon satisfaisante. La solution consiste à se ramener à un problème à 1 dimension en projetant le nuage statistique global sur un axe **u** du plan : on sait alors calculer, pour les projetés x'$_{ij}$ sur **u** des points x$_{ij}$ du nuage, la variance intragroupes w(**u**) =$\frac{1}{n_1+n_2}$ [$\sum_j$ (x'$_{1j}$ – g'$_1$)^2 + $\sum_j$ (x'$_{2j}$ – g'$_2$)^2] et la variance intergroupes b(**u**) = $\frac{n_1}{n_1+n_2}$ (g'$_1$ – g')^2 + $\frac{n_2}{n_1+n_2}$ (g'$_2$ – g')^2 (où n$_i$ est le cardinal du groupe G$_i$, de centre de gravité g$_i$).

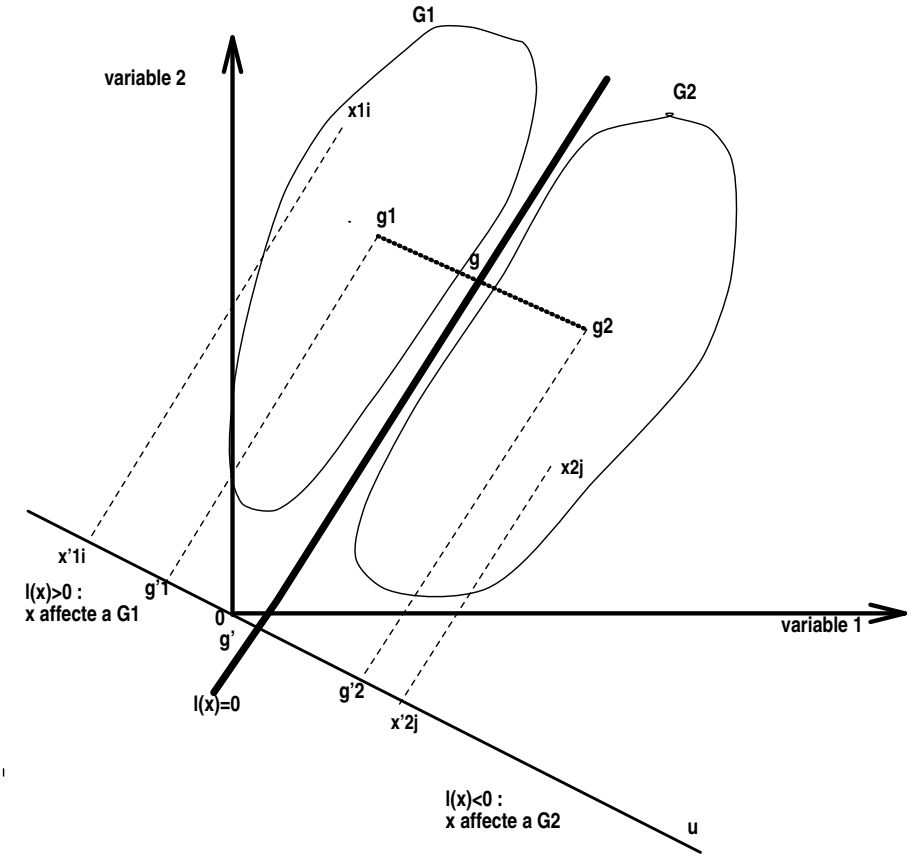

Figure 2. *Schéma d'une Analyse Factorielle Discriminante à 2 variables, dans le cas de 2 groupes qualitatifs, G_1 et G_2.*

Pour discriminer au mieux les deux groupes à l'aide des variables quantitatives considérées, il faut maximiser la 'variable de Fisher' :
F(**u**) = b(**u**)/w(**u**), ou, ce qui revient au même, maximiser la variable
b(**u**)/t(**u**) = b(**u**)/(b(**u**) + w(**u**)) = F(**u**)/(1 + F(**u**)), qui est la part de la variance intergroupes dans la variance totale.

On démontre que l'axe **u** qui maximise cette quantité est l'axe des centres de gravité, dirigé par g$_1$ – g$_2$, et que, si g = $\frac{g_1+g_2}{2}$, l'hyperplan (la droite, à 2 dimensions) qui sépare au mieux les groupes est, dans le cas d'égalité des probabilités a priori p_1 et p_2 des 2 groupes, l'ensemble des x tels que x – g soit orthogonal (au sens de la métrique W^{-1} de Mahalanobis) à g$_1$ – g$_2$. Et dans

le cas général, l'équation de l'hyperplan de discrimination est :
$l(x) = (g_1 - g_2)'\ W^{-1}\ (x - g) - 2 \ln \frac{p_2}{p_1} = 0.$

La Fonction Linéaire Discriminante, appliquée à x,est avec ces notations : $(g_1 - g_2)'\ W^{-1}\ x$.
On peut évaluer la qualité de la discrimination par plusieurs critères :

1. le pouvoir discriminant : c'est le maximum de $b(\mathbf{u})/t(\mathbf{u})$, obtenu pour $\mathbf{u} = (g_1 - g_2)$, c'est-à-dire : $b(g_1 - g_2)/t(g_1 - g_2)$ (≤ 1) ;

2. le pourcentage de bien classés ;

3. la distance de Mahalanobis entre g_1 et g_2 ($\propto b(g_1 - g_2)/w(g_1 - g_2)$) :
$||g_1 - g_2||^2 = (g_1 - g_2)'\ W^{-1}\ (g_1 - g_2)$.

Les résultats ont été publiés en 1992 dans la revue *Early Human Development* (Réf. R1). À titre d'exemple, mentionnons que nous avons (première question) pratiqué des analyses discriminantes entre stades de sommeil, sur l'ensemble des 338 périodes de 512 battements (131 provenant de nouveau-nés à terme, 91 de nouveau-nés d'âge intermédiaire, et 116 de prématurés). les résultats de cette discrimination sont consignés dans le Tableau I, et les coefficients de corrélation de la Forme Linéaire Discriminante (FLD, qui fournit la règle de décision) avec les variables HF, MF, BF dans le Tableau Ibis.

Tableau I
Evolution de la discrimination entre stades du sommeil : analyses discriminantes, à l'aide de HF, MF, et BF, sur les 338 périodes de 512 battements cardiaques (131 provenant de nouveau-nés à terme, 91 de nouveau-nés d'âge intermédiaire et 116 de prématurés).

Groupe d'âge	A F D			D M
'A terme' : n = 131	82%			3.32
	g.o.\g.a.	SA	SC	
(96 en SA et 35 en SC)	SA	94	2	
	SC	21	14	
'Intermédiaires' : n = 91	76%			2.73
	g.o.\g.a.	SA	SC	
(52 en SA et 39 en SC)	SA	43	9	
	SC	13	26	
'Prématurées' : n = 116	71%			0.84
	g.o\g.a.	SA	SC	
(77 en SA et 39 en SC)	SA	71	6	
	SC	28	11	

AFD = Analyse Factorielle Discriminante ; g.o. = groupe d' origine ; g.a. = groupe d' affectation ; SA = périodes de Sommeil Agité ; SC = périodes de Sommeil calme ; DM = Distance de Mahalanobis ; les '%' sont les pourcentages de périodes bien classées (par validation croisée), dans un groupe d'âge donné.

C'est une analyse *factorielle*, c'est-à-dire qu'elle permet d'estimer les coefficients de la meilleure combinaison linéaire (le facteur discriminant) qui sépare les deux groupes (connus a

priori : c'est une méthode de discrimination, pas de classification). Son principal intérêt ici est d'analyser qualitativement la part prise par chaque variable descriptive dans la discrimination, en fonction de l'âge conceptionnel du nouveau-né.

Tableau Ibis
Corrélation de la Forme Linéaire Discriminante (FLD) avec les variables cardiaques : discrimination, à l'aide de HF, MF, et BF, entre SA et SC.

r(FLD,..)	HF	MF	BF
A terme	-0.80	0.14	0.68
Intermédiaires	-0.86	-0.05	0.26
Prématurés	-0.33	0.24	0.76

Du point de vue du physiologiste, les résultats de cette étude montrent que la discrimination à l'aide des variables cardiaques entre stades du sommeil donne des résultats de plus en plus en plus satisfaisants à mesure que l'âge conceptionnel (AC) croît, pour arriver à de bons résultats globaux (excellents pour le sommeil agité, beaucoup plus faibles pour le sommeil calme) chez les nouveau-nés à terme. Cette discrimination est toujours fondée sur une opposition HF/BF, d'autant plus forte que l'AC est plus élevé, la MF ne jouant aucun rôle ; cette opposition est en fait due à une élévation de l'activité HF (parasympathique) en SC, et à une élévation de l'activité BF (sympathique) en SA.

Mais surtout, la discrimination entre groupes d'âge est :
– bonne, surtout en SA, entre nouveau-nés à terme et prématurés, faisant intervenir toutes les variables cardiaques, et toutes dans le même sens : c'est la maturation globale du SNA qui apparaît ici.
– moyenne, un peu meilleure en SA qu'en SC, entre nouveau-nés à terme et d'âge intermédiaire, reposant uniquement sur MF et BF : c'est donc la branche sympathique du SNA qui discrimine ici.
– très bonne en SC, médiocre en SA, entre nouveau-nés d'âge intermédiaire et prématurés, faisant intervenir surtout HF : c'est la branche parasympathique du SNA qui discrimine ici.

Ces résultats suggèrent une maturation précoce, à 37-38 semaines d'AC, du tonus parasympathique, avec une stabilité dans les dernières semaines de la gestation, et une maturation plus lente et régulière du tonus sympathique, de 31 à 41 semaines d'AC (voir la réf. R1).

3.1.4 Chaînes de Markov cachées : un système nerveux autonome à deux états ?

Une autre méthode de discrimination entre stades du sommeil chez un nouveau-né à terme par les variables cardiaques explicatives RR ou HF a consisté à considérer ces variables quantitatives comme sorties d'un système gouverné par un état caché à deux valeurs : tonus sympathique dominant ou tonus parasympathique dominant, ces états pouvant être sommairement identifiés par le stade du sommeil (SA ou SC, respectivement).

J'ai alors programmé en langage *SIGNAL* l'algorithme de restauration-maximisation (alias *"expectation-maximisation"*) [14, 15, 16] "EM à la Gibbs" qu'avait mis au point G. Celeux pour l'appliquer au problème de l'identification de l'état caché du système nerveux autonome sur les signaux de rythme cardiaque RR et HF. Cette méthodologie et ses résultats sont publiés dans des actes d'un colloque au CNRS (réf. A2) et la Figure 3 en donne une illustration, à partir du même signal RR que celui utilisé pour l'analyse factorielle discriminante présentée au paragraphe précédent.

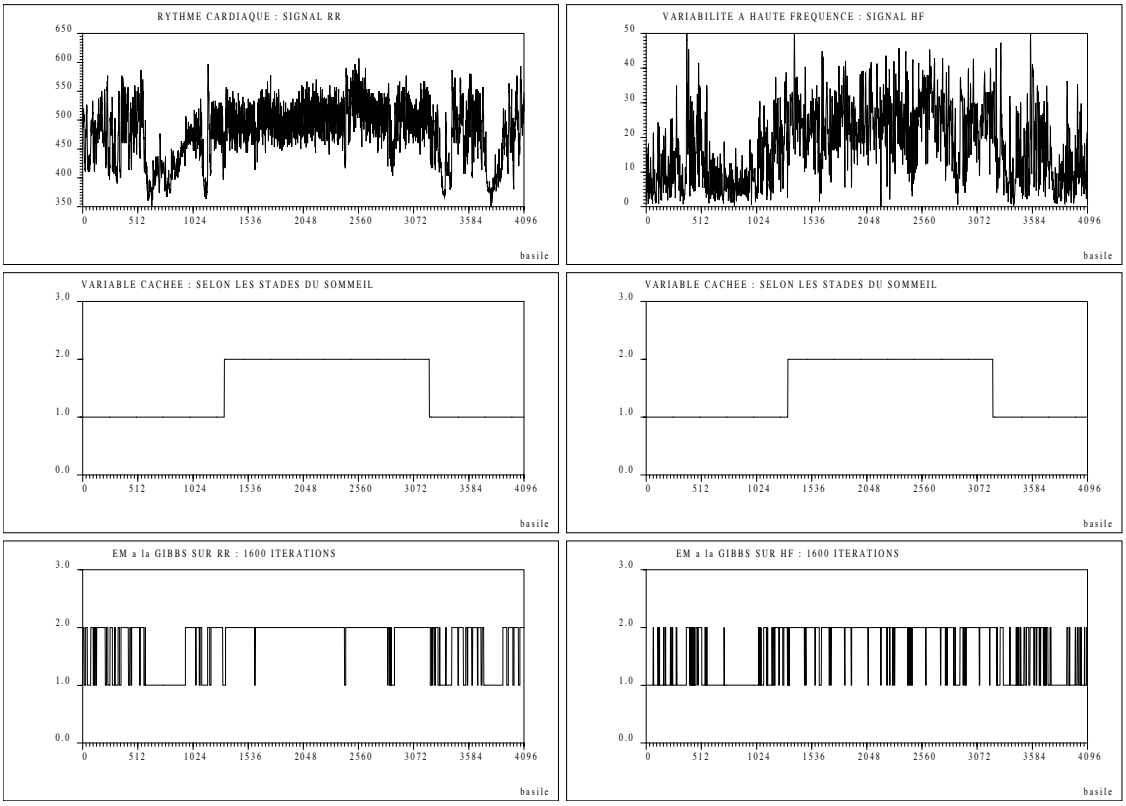

Figure 3. *Identification par l'algorithme EM à la Gibbs d'une variable cachée contrôlant le rythme cardiaque (état sympathique = 1 ; parasympathique =2 du système nerveux autonome), d'une part sur le signal RR brut (à gauche), d'autre part sur le signal HF, variabilité à haute fréquence extraite par transformation de Fourier à court terme du signal RR (à droite).*

3.1.5 Analyses non linéaires

Il est tentant, lorsque les données expérimentales présentent une allure irrégulière, et qu'on soupçonne la présence de non-linéarités dans le système dynamique sous-jacent, de les traiter comme une trajectoire d'un système déterministe différentiable et chaotique, à temps continu ou discret, situé sur un attracteur dans un espace de dimension à déterminer, et dont on n'observe qu'une projection, sur une droite pour un signal unidimensionnel. Sans rien savoir du

modèle sous-jacent, on fait donc l'hypothèse que les données sont situées sur la trajectoire d'un système dynamique déterministe différentiable $x_{n+1} = \Phi(x_n)$ pour un système à temps discret, ou encore $x(s+t) = \Phi^t(x(s))$ pour un système à temps continu, où $t \mapsto \Phi^t$ est le flot du champ de vecteurs ξ tel que l'équation $\dfrac{dx}{dt} = \xi(x)$ admette la trajectoire considérée comme l'une de ses courbes intégrales (bien sûr, on n'a aucun accès à une expression analytique de Φ, ni même de ξ).

On suppose de plus que toutes les trajectoires observées convergent vers un attracteur A, i.e., un ensemble compact de $\mathbb{R}^d$ invariant par Φ, et que de plus ces trajectoires sont chaotiques, c'est-à-dire, si sensibles aux conditions initiales qu'une amplification exponentielle de l'écart entre deux points initiaux rend toute prévision de position autre qu'à très court terme impossible. On suppose aussi que toute trajectoire (ou encore : l'orbite de tout point de A par Φ) est dense dans A, et qu'il existe une unique mesure ρ sur A invariante par Φ, telle que pour toute fonction g continue de $\mathbb{R}^d$ dans $\mathbb{R}$,

$$\int_A g d\rho = \lim_{N\to\infty} \frac{1}{N} \sum_{k=0}^{N-1} g(\Phi^k(x))$$

la limite existant pour presque tout $x \in A$ et étant alors indépendante de x. Cette hypothèse d'ergodicité (la moyenne temporelle définit la moyenne spatiale) est essentielle pour que les calculs ci-dessous aient un sens. L'existence d'une telle mesure est assurée par le théorème de Sinai-Ruelle-Bowen[17] pour les attracteurs hyperboliques, mais on n'a bien sûr aucun moyen de tester l'hyperbolicité d'un système dynamique dont on ne connaît qu'une série de données expérimentales. Tout au plus peut-on essayer d'estimer la stationnarité des données, et ainsi la validité de l'hypothèse ergodique ; mais les tests de stationnarité pour des données de petite taille ($1000 \leq N \leq 10000$) ne sont pas satisfaisants.

On suppose donc que les trajectoires sont ergodiques pour une mesure volume sur l'attracteur qui sera prosaïquement la mesure de comptage de masse totale 1 (les trajectoires visitent chaque région de l'attracteur de manière uniforme), et on cherche alors à estimer des caractéristiques de cet attracteur. En particulier sa dimension de Hausdorff d_0 (qui peut être fractale, l'attracteur est alors dit "étrange"), ou même ses dimensions généralisées de Rényi d_q (dont la dimension d'information d_1 et la dimension de corrélation intégrale d_2), la dépendance sensible des conditions initiales des trajectoires (qui le recouvrent) du système dynamique supposé sous-jacent, à l'aide de ses exposants de Lyapounov, et l'entropie d'une mesure invariante sur cet attracteur, toujours calculée à partir des trajectoires observées.

La première étape est celle de la reconstruction de l'attracteur, à partir de la série de données unidimensionnelles observées, soit x_i, $i = 1, 2, .., N$, dans un espace $\mathbb{R}^d$, pour un $d \in \mathbb{N}$ suffisamment grand pour ne pas "écraser" l'attracteur. On utilise la méthode des retards, proposée en 1985 par Ruelle et Takens[18], qui consiste à construire en partant des x_i une trajectoire $\{X_i = (x_i, x_{i+1}, ..., x_{i+d-1})\ ,\ i = 1, 2, ..., N-d+1\}$ dans $\mathbb{R}^d$, qui est supposée "représentative" de l'attracteur.

Sur ce nouveau jeu de données, on calcule une dimension, en général, non pas la dimension de Hausdorff (ou de *box-counting*) d_0, mais plutôt la dimension d_2, qui est donnée par l'algorithme de Grassberger et Procaccia (1983)[19], les dimensions généralisées de Rényi étant

données par :

$$d_q = \lim_{\varepsilon \to 0} \frac{1}{q-1} \frac{\ln \sum_{i=1}^{M_\varepsilon} p_{i,\varepsilon}^q}{\ln \varepsilon}$$

où M_ε est le nombre de boules $B(X_i, \varepsilon)$ minimum nécessaire pour définir une partition de l'attracteur (ou de ce qu'on en connaît), et :

$$p_{i,\varepsilon} = \rho(B(x_i, \varepsilon)) = \lim_{N \to \infty} \frac{1}{N} \text{card}\{j \ , \ 1 \leq j \leq N \ , \ ||X_i - X_j|| \leq \varepsilon\}$$

Pour que l'attracteur ne soit pas trop écrasé dans cette représentation, il faut que la dimension de plongement d soit correcte. On l'estime généralement en déterminant d_2 pour différentes dimensions de plongement d et en prenant la première, soit D, à partir de laquelle d_2 "ne bouge plus", i.e., a atteint un plateau. Si D, dimension de corrélation intégrale (ce terme trouve son explication dans la méthode de Grassberger et Procaccia) de l'attracteur A peut s'assimiler à la dimension (au sens usuel) d'une variété, un théorème dû à Whitney garantit qu'on peut plonger cette variété dans un espace $\mathbb{R}^{2D}$; d_2 étant en général non entière, on plonge par la méthode des retards les données observées dans un espace $\mathbb{R}^d$, d étant l'entier immédiatement supérieur (ou égal) à $2D + 1$.

Pour $q = 1$,

$$d_1 = \lim_{q \to 1} d_q = \lim_{\varepsilon \to 0} \frac{\ln \sum_{i=1}^{M_\varepsilon} p_{i,\varepsilon}}{\ln \varepsilon}$$

est la dimension d'information. On peut aussi définir l'entropie d'information (de Kolmogorov-Sinai, cf. Eckmann et Ruelle 1985[18]) par :

$$K_1 = \lim_{r \to 0} \lim_{m \to \infty} \lim_{N \to \infty} \left[\phi_N^{m+1}(r) - \phi_N^m(r)\right]$$

où

$$\phi_N^m(r) = \frac{1}{N} \sum_{i=1}^{N} \ln C_i^m(r)$$

et :

$$C_i^m(r) = \frac{1}{N} \sum_{j=1}^{N} H\left(r - ||X_i - X_j||\right)$$

m ($= d$) désignant ici la dimension de plongement et H la fonction de Heaviside (fonction indicatrice de $\mathbb{R}_+$).

Pincus a proposé en 1993[20, 21] de définir une "entropie approchée", qu'il note $ApEn$, et qui est obtenue en fixant N (on n'a de toute façon pas le choix, c'est la taille du jeu de données), $m = 2$, et r étant égal à un pourcentage (5% à 20%) de l'écart-type de la série observée. Il en a

déduit une “mesure de complexité” qu'il a appliquée à des problèmes cliniques tels que la mort subite inexpliquée du nourrisson.

Enfin, une mesure souvent pratiquée sur des données expérimentales (ou aussi d'ailleurs sur des systèmes définis analytiquement) est celle des exposants de Lyapounov, mesure visant à estimer la dépendance sensible des conditions initiales, caractéristique des systèmes chaotiques.

Soient deux trajectoires $t \mapsto X(t, X_0)$ et $t \mapsto X(t, X_0 + \varepsilon)$ du même système dynamique chaotique de flot Φ. Si la divergence des trajectoires à partir des conditions initiales X_0 et $X_0+\varepsilon$ est exponentielle, on aura :

$$||\varepsilon_t|| = ||X(t, X_0 + \varepsilon) - X(t, X_0)|| = ||\Phi^t(X_0 + \varepsilon) - \Phi^t(X_0)|| \simeq ||\varepsilon|| e^{\lambda_1 t}$$

pour un réel positif λ_1, qui est le premier exposant de Lyapounov. On peut se contenter de cette seule mesure de λ_1 ; c'est ce que fait l'algorithme de Wolf (1985)[22].

Mais il y a en fait d exposants de Lyapounov, si d est la dimension de plongement de l'attracteur A, que l'on obtient simplement en enlevant les $||\ ||$ dans l'égalité ci-dessus, à condition de supposer le flot Φ au moins de classe C^1 : le développement de Taylor à l'ordre 1

$$\Phi^t(X_0 + \varepsilon) - \Phi^t(X_0) = J_{X_0}\Phi^t.\varepsilon + o(\varepsilon)$$

(où J_X désigne la matrice jacobienne en X) montre qu'une boule centrée en X_0 pourra être déformée par le flot en un ellipsoïde, différemment suivant la direction considérée, dilatée dans une direction et simultanément contractée dans une autre.

Pour $n \in \mathbb{N}$, ce qui revient à considérer un système dynamique à temps discret, on a donc

$$||\Phi^n(X + \varepsilon) - \Phi^n(X)||^2 \simeq ||J_X\Phi^n.\varepsilon||^2 = \langle (J_X\Phi^n)^* (J_X\Phi^n) .\varepsilon\ ,\ \varepsilon\rangle$$

Or, le théorème ergodique multiplicatif d'Oseledec (1968, cf. Eckmann et Ruelle 1985[18]) nous assure que, pourvu que la fonction $\max(0, \ln ||J_X\Phi||)$ soit intégrable par rapport à la mesure invariante ρ sur l'attracteur A, la limite

$$\lim_{n\to\infty} \{(J_X\Phi^n)^* (J_X\Phi^n)\}^{\frac{1}{2n}} = \Lambda_X$$

existe pour ρ-presque tout $X \in A$.

Ce sont les logarithmes des valeurs propres de la limite Λ_X qui sont les exposants de Lyapounov du système. Le plus grand, λ_1, mesure la divergence exponentielle des trajectoires sur A, mais la somme (la trace de $\ln \Lambda_X$) présente aussi un intérêt : comme

$$(J_X\Phi^n)^* (J_X\Phi^n) \simeq \Lambda_X^{2n} \ \text{ et } \ \text{donc } \ |\det J_X\Phi^n| \simeq \exp\left(n \sum_{i=1}^{d} \lambda_i(X)\right)$$

on aura contraction des volumes par le flot si $\sum_{i=1}^{d} \lambda_i < 0$ (le système est dit dissipatif), conservation si $\sum_{i=1}^{d} \lambda_i = 0$ (système conservatif), dilatation si $\sum_{i=1}^{d} \lambda_i > 0$ (système accrétif). Les systèmes dynamiques du monde physique ne sont jamais accrétifs, et les systèmes chaotiques les plus connus (Hénon, Lorenz, Rössler, etc.) sont dissipatifs (mais le chaos conservatif existe : cf. la transformation du boulanger).

Le calcul des exposants de Lyapounov a été beaucoup pratiqué sur des séries de données[23, 24, 25], en particulier physiologiques, avec des résultats qui varient suivant les algorithmes utilisés, la taille du jeu de données, etc. En tout cas, Eckmann et Ruelle recommandent de disposer d'au moins $N = 10^{D/2}$ mesures, si D est la dimension d_2 de l'attracteur.

3.1.6 Tests de déterminisme et de non-linéarité.

L'application de ces techniques utilisant des propriétés stochastiques des systèmes dynamiques déterministes à n'importe quelle suite de nombres a été justement critiquée. On peut en effet pratiquer ces calculs sur des suites de nombres aléatoires, et trouver des dimensions non entières et des premiers exposants de Lyapounov positifs, il n'y a pourtant pas là d'attracteur étrange, et il faut pouvoir donner des arguments permettant d'exclure le cas de figure de données purement stochastiques imitant du chaos déterministe.

Une première observation est que la somme des exposants de Lyapounov, i.e., la trace de la matrice :

$$\log \lim_{n\to\infty} \left\{ \left(J_X \Phi^n\right)^* \left(J_X \Phi^n\right) \right\}^{\frac{1}{2n}} \ ,$$

si les hypothèses du théorème multiplicatif d'Oseledec sont valides, est négative si on est en présence d'un système chaotique, ou du moins de l'un des systèmes chaotiques tests bien connus : Hénon, Lorenz, etc., et positive pour une suite de nombres aléatoires gaussiens. L'algorithme d'Eckmann-Ruelle permet de tester cette alternative en donnant une estimation de tout le spectre de Lyapounov.

Données substituées

Dans la même veine, J. Theiler[26] a proposé en 1992 de construire systématiquement, pour chaque série temporelle observée, une "série substituée" (*surrogate data*), construite de manière à éliminer toute possibilité de dépendances non linéaires entre points de la série. On procède ainsi : d'abord on fait subir aux données initiales une transformation de Fourier ; puis on procède à une randomisation des phases (*phase shuffling*), i.e., on redistribue les phases au hasard, en conservant les amplitudes ; puis on fait une transformation de Fourier inverse ; on aura pris garde auparavant d'avoir, après la randomisation, symétrisé les phases en remplaçant chaque valeur $z(i),\ i = 1, .., N$ obtenue dans le domaine fréquentiel par $\frac{1}{2}\left[z(i) + \overline{z(N+2-i)}\right]$, afin de récupérer des "données" qui soient bien réelles. Cette procédure ne touche pas au spectre (d'amplitude), et on peut, quitte à faire une modification affine des données, obtenir ainsi une série temporelle ayant même moyenne, même écart-type, et même spectre, mais dont toutes les autres propriétés, à commencer par les non-linéarités, auront été effacées. On compare alors les résultats des calculs (dimension de corrélation, exposants de Lyapounov, entropie) effectués sur les données originales et sur les données substituées : s'il n'y a pas de différence "nette", on rejette l'hypothèse de non-linéarité du système dynamique sous-jacent.

Bien sûr, les générateurs de nombres vraiment aléatoires n'existent pas dans la réalité, et les procédés informatiques utilisés (calcul des restes dans les divisions euclidiennes successives de grands entiers par d'autres grands entiers) sont en fait des procédés déterministes. Mais on

peut utiliser un grand nombre de données substituées (p.ex. 40) construites à partir de la même série expérimentale, avec différents générateurs de nombres aléatoires, pour la randomisation des phases, et comparer les résultats obtenus, en fixant un seuil de rejet de l'hypothèse nulle : p.ex. si la différence avec la moyenne obtenue sur les différents jeux de données substituées n'est pas d'au moins 10 écarts-types, on ne conclut pas au caractère déterministe non-linéaire des données de départ.

Cette technique, quasiment incontournable quand on traite des données expérimentales par des méthodes non linéaires, illustre bien l'embarras dans lequel se trouve l'expérimentateur privé de modèle ; elle a néanmoins le mérite de fournir des tests qui orientent vers la recherche de non-linéarités dans la construction d'un modèle.

Prédiction non linéaire

Il existe de nombreuses méthodes de prédiction non linéaire, et on présentera ici seulement la plus connue : celle de G. Sugihara et R.M. May (1990)[27]. Elle consiste à prédire à court terme grâce à un échantillon d'apprentissage (p.ex. la première moitié des données) la trajectoire suivie par un point sur l'échantillon-test (la deuxième moitié) et à comparer trajectoire réelle et trajectoire prédite. On a plongé les données dans un espace de dimension d suffisante par la méthode de reconstruction d'un attracteur supposé à l'aide de retards (cf. plus haut), et on détermine pour chaque point $X_i = (x_i, x_{i+1}, .., x_{i+d-1})$ ses $d+1$ plus proches voisins, en prenant garde toutefois qu'ils constituent bien un simplexe (un repère affine) contenant X_i ; on suit alors l'évolution dans le temps, k pas plus loin (p.ex. $0 \leq k \leq 15$), des points du simplexe, et on calcule la position Y_{i+k}, prédite à l'instant k, du point X_{i+k}, en gardant les mêmes coordonnées affines dans le nouveau repère (résultat de l'évolution du premier repère, k pas plus loin).

On représente alors graphiquement en fonction de k le coefficient de corrélation, calculé sur l'ensemble de l'échantillon-test, entre les x_{i+k} et les y_{i+k}, projections des Y_{i+k} sur le premier axe de coordonnées dans $\mathbb{R}^d$. Pour des données à base déterministe complètement prévisibles (p.ex. une série sinusoïdale éventuellement parasitée par un bruit gaussien), la valeur du coefficient de corrélation sera à peu près constante, et d'autant plus proche de 1 que le bruitage sera faible (alors qu'un bruit blanc gaussien pur donnera un coefficient de corrélation constamment proche de zéro), mais en tout cas ne présentera pas de décroissance avec k ; ce qui sera le contraire pour une série même complètement déterministe, mais imprévisible à très court terme, car chaotique : on observe une décroissance très rapide du coefficient de corrélation vers zéro.

Ces méthodes d'analyse, qui ont connu une grande vogue dans les années 85-95, sont donc toutes fondées sur l'hypothèse de l'existence d'un "attracteur étrange" vers lequel convergent les trajectoires d'un système dynamique inconnu à l'origine de la série de données expérimentales. Dans le cas du rythme cardiaque, sous l'hypothèse de l'existence d'un système dynamique discret de la forme $\mathrm{RR}_{n+1} = \Phi(RR_n)$ (Φ soit dit en passant n'est pas une application de premier retour de Poincaré, mais bien plutôt un *temps de premier retour*, par exemple temps de retour à une hypersurface de dépolarisation $E = 0$ d'une cellule excitable cardiaque), des paramètres non linéaires : dimension de corrélation (dimension non entière de l'attracteur reconstitué suivant des principes énoncés par J.-P. Eckmann et D. Ruelle en 1985), exposants de Lyapounov, entropie approchée (ApEn), de ce système ont été estimés sur des séries de RR provenant de

données expérimentales de rythme cardiaque de souris, avec ou sans traitement par atropine. Les données provenaient de l'U 127 de l'INSERM (P. Mansier et B. Swynghedauw). Ces travaux ont fait l'objet d'une présentation à une conférence IEEE (réf. O7) et d'un article dans *Cardiovascular Research* (réf. R4). Ils avaient pour but la discrimination sur les seules variables cardiaques (RR) entre groupes d'animaux traités et non traités par des médicaments du système nerveux autonome. La Figure 4 présente un exemple de calcul de dimensions de corrélation qui va bien dans ce sens.

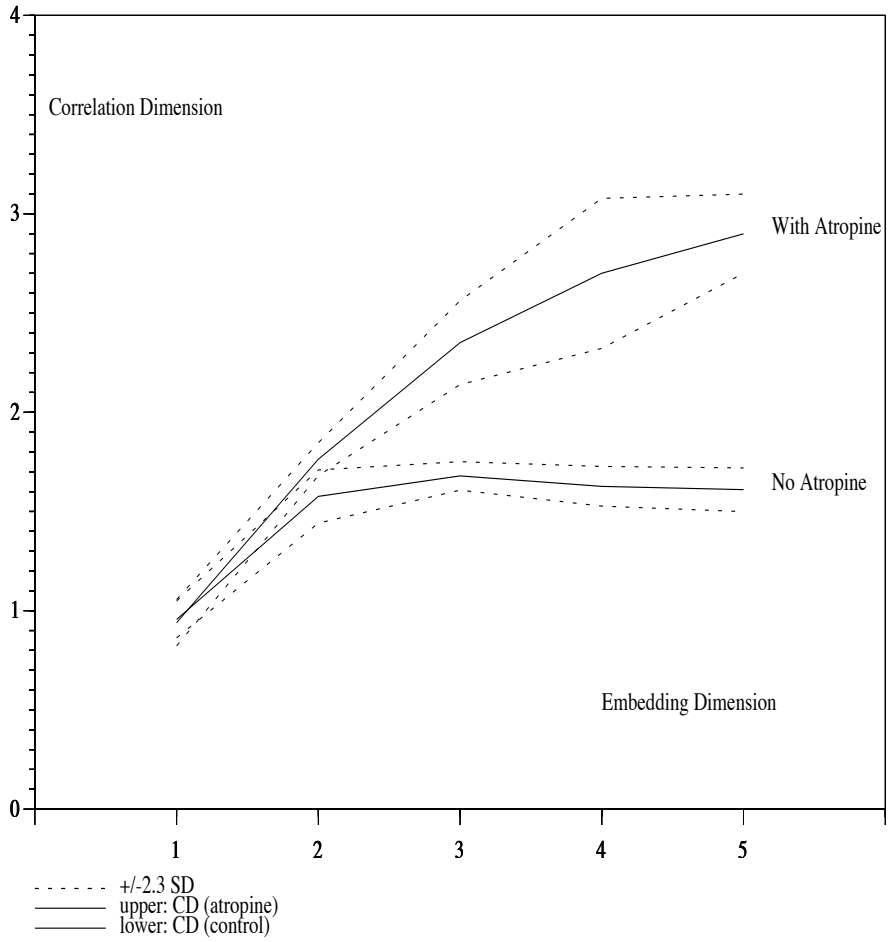

Figure 4. *Dimensions de corrélation intégrale (algorithme de Grassberger et Procaccia) calculées sure une série de 1000 intervalles RR chez une souris avant et après injection IP d'une dose d'atropine. Sur cette figure, les pointillés indiquent +/- 2.3 fois l'écart-type (intervalle de confiance à 95%) de la pente (CD) , calculée par régression linéaire sur 10 points dans la zone linéaire du tracé log-log (log [r] vs. log [C(r)]).*

Sur un petit groupe d'animaux (cinq), on a pu montrer (réf. O7) que tous les indicateurs non linéaires étudiés (dimension de corrélation, premier exposant de Lyapounov, ApEn) sont aug-

mentés par une injection d'atropine, ce qui peut s'interpréter comme une augmentation de "complexité" d'un hypothétique attracteur cardiaque sous-jacent par l'administration d'un parasympatholytique. De même, la somme des exposants de Lyapounov, toujours négative, ce qui signe un système dynamique dissipatif (dans le cas présent dissipation d'énergie à chaque battement cardiaque), se rapproche de 0 avec l'administration d'atropine. Une mission du système nerveux autonome pourrait ainsi être, dans cette vision en termes de dynamique non linéaire, la réduction de la "complexité" du système cardio-vasculaire, réduction consommatrice d'énergie pour diminuer l'entropie du système.

3.2 Modélisation en électrophysiologie cardiaque : contrôle par le système nerveux autonome du chronotropisme cardiaque au niveau du nœud sinusal

Le système nerveux autonome, considéré uniquement par ses efférences sur le nœud sinusal, est un régulateur du rythme cardiaque. Partant du modèle de Yanagihara-Noma-Irisawa (1980)[28] du potentiel d'action de la cellule du nœud sinusal, on peut représenter (réf. O6) à ce niveau unicellulaire l'action, codée en fréquence de décharges neuronales, des deux branches du système nerveux autonome par l'intermédiaire des neuromédiateurs impliqués : acétylcholine et noradrénaline, et de l'action des G-protéines, stimulant ou inhibant les courants ioniques transmembranaires[29], suivant le schéma décrit par la figure 5.

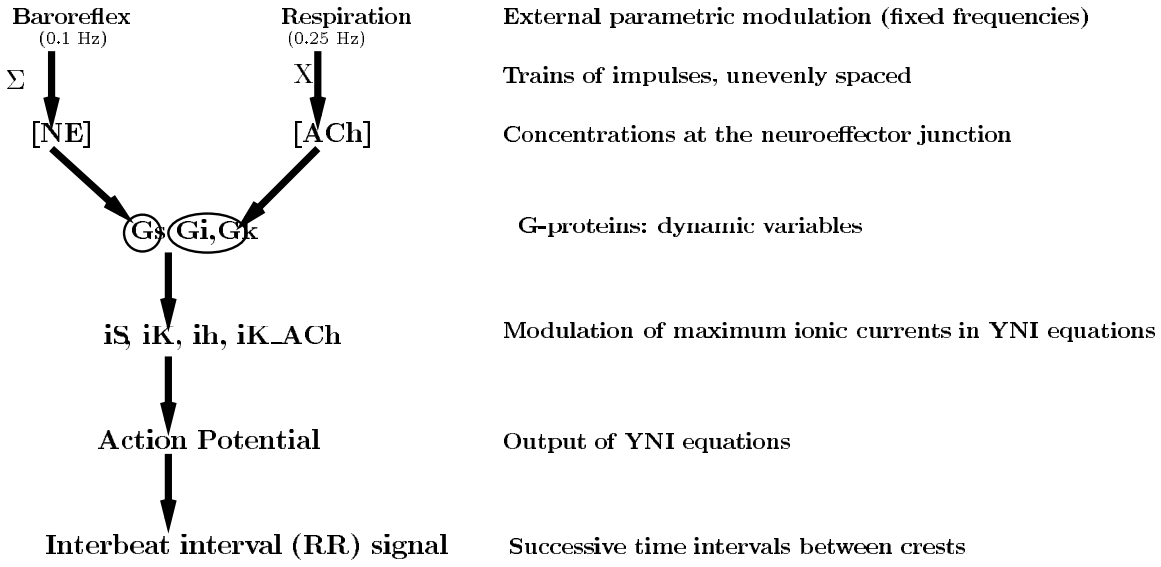

Figure 5. *Principe du modèle de contrôle par le système nerveux autonome de la cellule du nœud sinusal.*

Une illustration du modèle avec contrôle nerveux autonome est présentée sur la Fig. 6 :

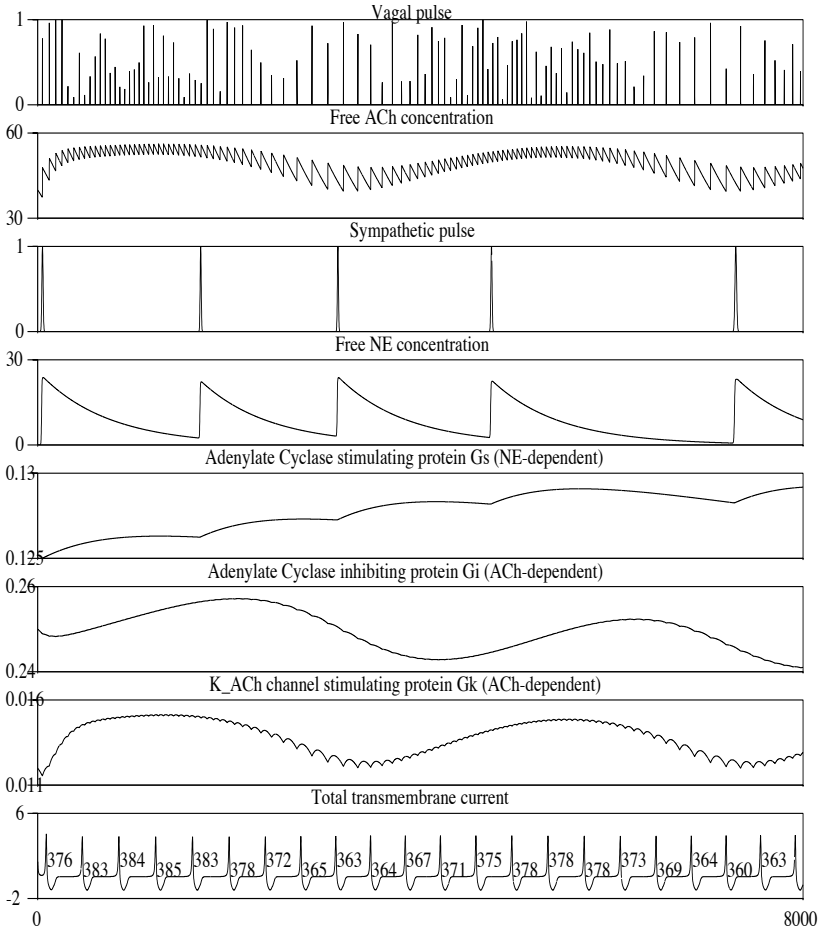

Figure 6. *Modèle de cellule de nœud sinusal contrôlée par le système nerveux autonome.*

L'analyse spectrale du rythme RR ainsi modélisé montre que l'influence vagale est représentée de façon satisfaisante, comme on le constate sur la Figure 7 :

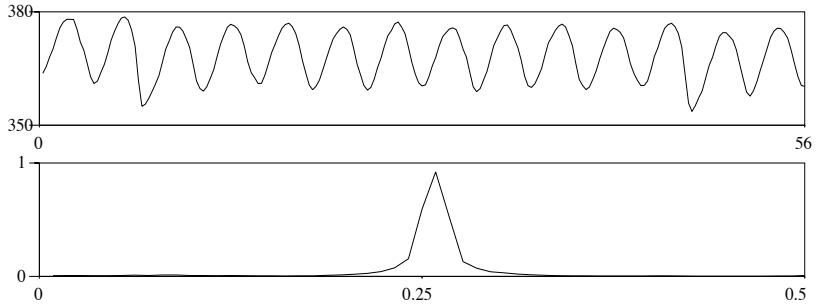

Figure 7. *Signal RR obtenu à partir du modèle de potentiel d'action d'une cellule du nœud sinusal contrôlée par le système nerveux autonome, et son spectre. L'influence du parasympathique (à 0.25 Hz, fréquence de l'arythmie sinusale respiratoire) est bien présente.*

Chapitre 4

Travaux de recherche actuels (2000-. . .) : modèles mathématiques pour l'optimisation de la pharmacothérapeutique en cancérologie

4.1 Un modèle pharmacocinétique-pharmacodynamique réduit de l'action de l'oxaliplatine sur les tissus cancéreux et les tissus sains avec prise en compte de la pharmacodynamie circadienne pour l'optimisation chronothérapeutique

Ce nouveau thème de recherche, en rupture apparente avec mon domaine précédent d'application à la médecine (la physiologie cardio-vasculaire), puisqu'il s'agit d'applications en cancérologie, contient pourtant le même thème : la coordination des rythmes, mais dans le cas présent, en plus du contrôle central (circadien) d'un rythme périphérique (le rythme de division cellulaire), il y est d'emblée question de thérapeutique, ce qui n'était pas au premier plan pour la physiologie cardio-vasculaire.

Le point de départ de mon intérêt pour la modélisation de la pharmacothérapeutique en cancérologie a en effet été ma rencontre en 1999 avec Francis Lévi, qui pratiquait depuis une dizaine d'années déjà en clinique la chronothérapie des cancers[30, 31, 32], en particulier du cancer colorectal métastatique. Suivant une méthodologie mise au point d'abord chez l'animal, puis en clinique, elle consiste à perfuser les médicaments anticancéreux en veillant à les administrer à débit non constant, mais d'allure sinusoïdale avec des pics correspondant à leur heure de moindre toxicité. Qu'une heure de moindre toxicité (qui coïncide le plus souvent, sans qu'on sache pourquoi, avec une heure de plus grande efficacité antitumorale) existe est un apport majeur de la chronobiologie à la pharmacologie en général, et à celle des cancers en particulier.

La Figure 8 illustre un schéma chronothérapeutique classiquement utilisé dans le traitement du cancer colorectal métastatique.

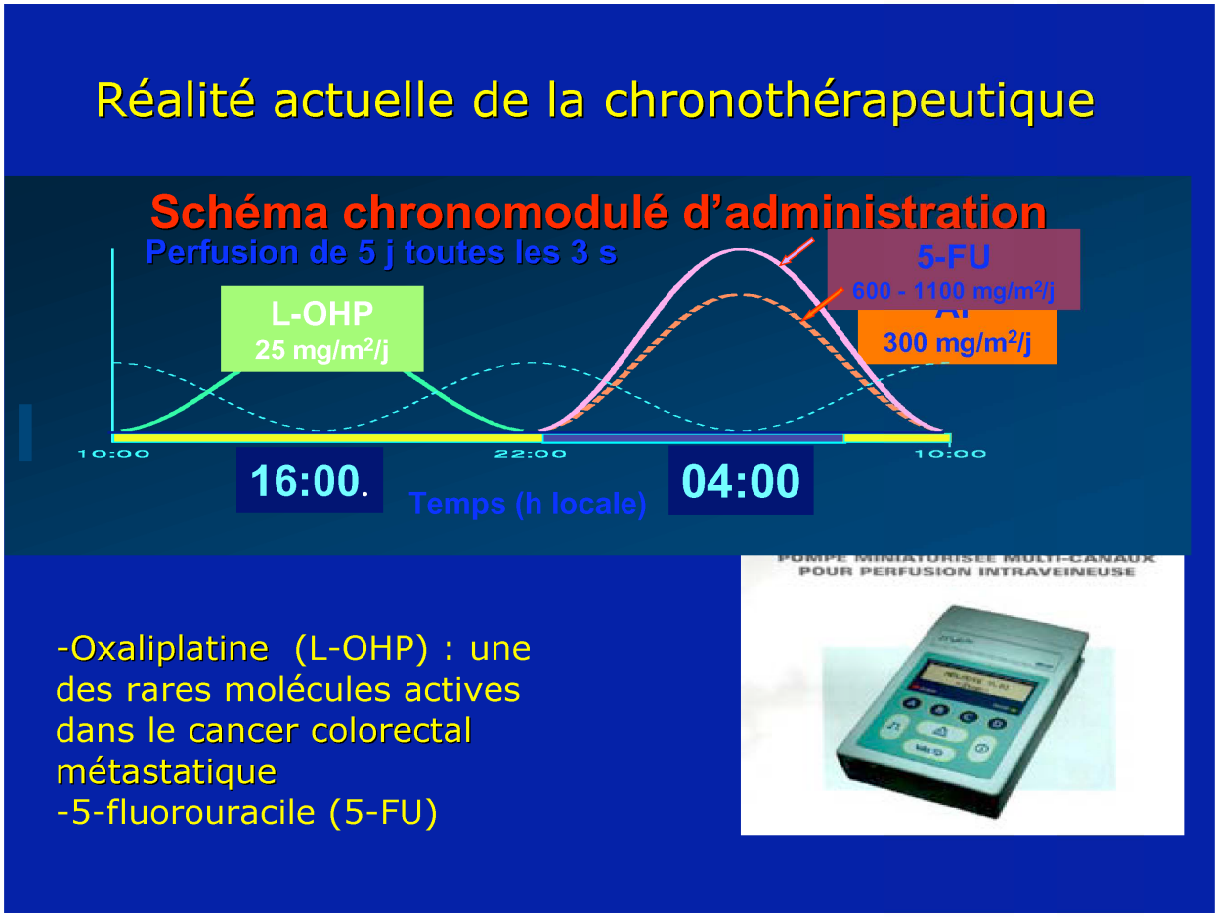

Figure 8. *Schéma chronomodulé sinusoïdal pour la chronothérapie du cancer colorectal : association d'oxaliplatine (L-OHP) et de 5-fluorouracile (5-FU) ; les pics de débit de perfusion sont déterminés pour minimiser la toxicité non désirée sur les organes sains (Unité de chronothérapie clinique, Francis Lévi, hôpital Paul-Brousse.*

Peut-on améliorer ces schémas chronomodulés, ou, à défaut, démontrer leur optimalité ? En considérant dans un premier temps le traitement par le seul oxaliplatine d'une tumeur expérimentale l'ostósarcome de Glasgow de la souris, chez qui la principale toxicité de ce médicament est sur la muqueuse jéjunale[33, 34], j'ai mis au point un modèle pharmacocinétique-pharmacodynamique (PK-PD) macroscopique, i.e., au niveau global de la tumeur et au niveau global de la muqueuse jéjunale, d'efficacité thérapeutique et de toxicité de l'oxaliplatine dans lequel l'influence circadienne est représentée par un simple cosinus venant moduler la pharmacodynamie, c'est-à-dire l'activité du médicament sur la population des cellules tumorales comme sur celle des cellules saines.

Ce modèle (réf. R11) est un système de 6 équations différentielles ordinaires, 3 pour la pharmacocinétique, sanguine et tissulaire, 2 pour la dynamique jéjunale (oscillations stables,

représentant l'homéostasie tissulaire) et 1 pour la croissance tumorale (modèle de Gompertz). Les cinétiques sont d'ordre 1 dans le plasma et dans les tissus périphériques, représentant la fixation irréversible (liaisons covalentes) de l'oxaliplatine sur ses cibles ; la stabilité (hors traitement) de la population jéjunale, due au remplacement des cellules villositaires éliminées dans la lumière intestinale par des celles jeunes en provenance des cryptes est représentée par un système linéaire stable ; enfin la croissance tumorale est supposée être de type gompertzien :

– pharmacocinétique (P, concentration plasmatique, C et D, concentrations jéjunale et tumorale, respectivement, de l'oxaliplatine) :

$$\frac{dP}{dt} = -\lambda P + \frac{i(t)}{V_{di}} \tag{4.1}$$

$$\frac{dC}{dt} = -\mu C + \xi_C P \tag{4.2}$$

$$\frac{dD}{dt} = -\nu D + \xi_D P \tag{4.3}$$

– population des cellules de la muqueuse jéjunale (A, entérocytes villositaires, Z, flux de cellules jeunes en provenance de la crypte, modèle d'oscillateur harmonique amorti) :

$$\frac{dA}{dt} = Z - Z_{eq} \tag{4.4}$$

$$\frac{dZ}{dt} = \{-\alpha - f(C,t)\}\, Z - \beta A + \gamma \tag{4.5}$$

– population des cellules tumorales (B, modèle de Gompertz) :

$$\frac{dB}{dt} = -a.B.\ln(B/B_{max}) - g(D,t).B \tag{4.6}$$

– enfin, la pharmacodynamie chronomodulée est représentée par deux fonctions de Hill, f et g (pour la toxicité et l'efficacité thérapeutique, respectivement), modulées en amplitude par une fonction périodique de période $\mathcal{T}$= 24 h :

$$f(C,t) = F.\left\{1 + \cos\left(2\pi\frac{t-\varphi_S}{\mathcal{T}}\right)\right\}.\frac{C^{\gamma_S}}{C_{S50}^{\gamma_S} + C^{\gamma_S}}$$

$$g(D,t) = H.\left\{1 + \cos\left(2\pi\frac{t-\varphi_T}{\mathcal{T}}\right)\right\}.\frac{D^{\gamma_T}}{D_{T50}^{\gamma_T} + D^{\gamma_T}}$$

En choisissant pour la fonction de ddébit d'injection $t \mapsto i(t)$, commande pharmacologique du système une sinusoïde de période $T = 24$ h, comme la période $\mathcal{T}$ de chronosensibilité

au médicament dans les fonctions de pharmacodynamie f et g, on peut simuler la réponse du système au traitement chronomodulé. Sur la Figure 9 sont représentées les 6 variables du modèle pendant les 5 jours d'une monothérapie chronomodulée à l'oxaliplatine. Le traitement vise à maximiser l'élimination des cellules tumorales (B, dernière trace) tout en préservant le plus possible le cellules saines (A, quatrième trace).

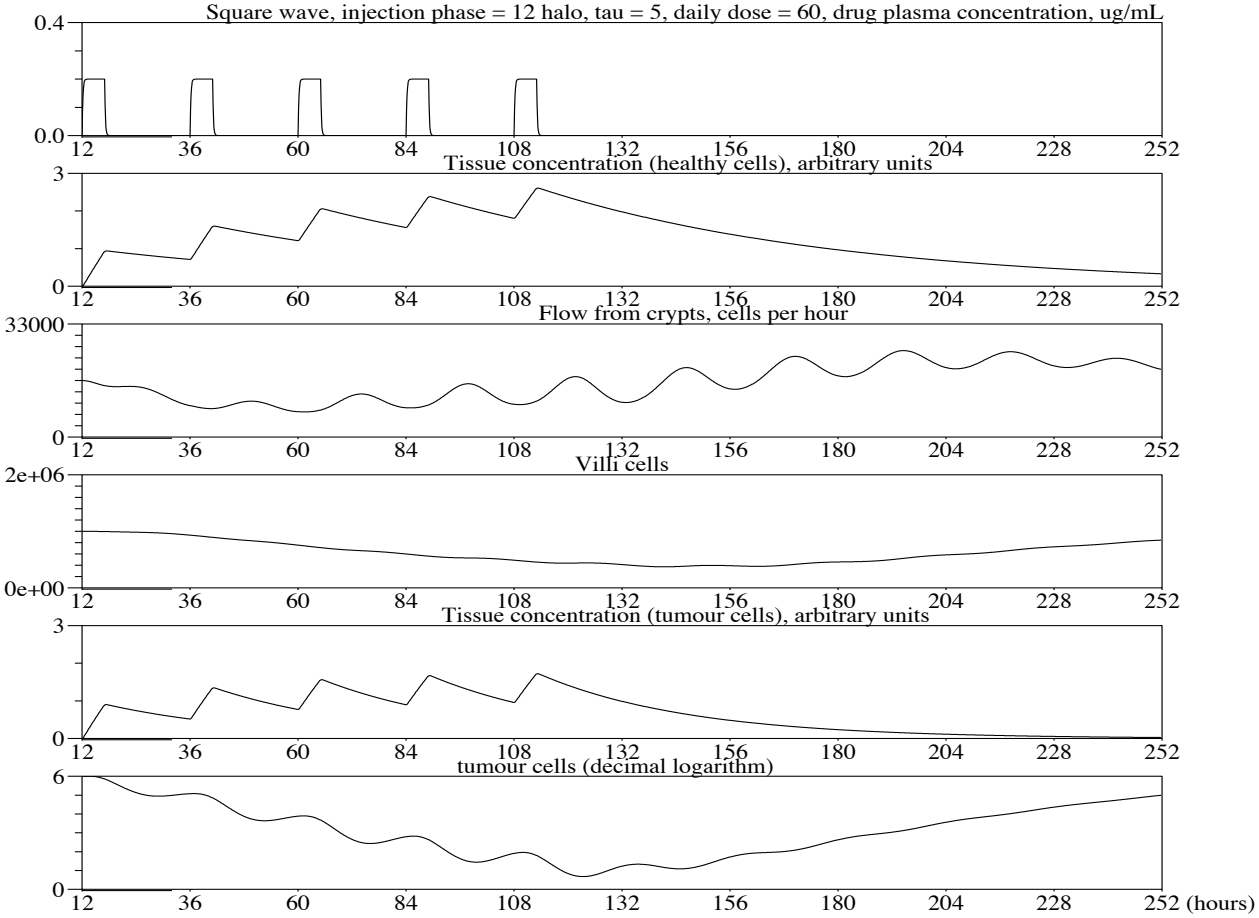

Figure 9. *Evolution des variables du modèle, de haut en bas : P, C, Z, A, D et $\log_{10} B$ sous l'action d'un traitement chronomodulé supposé perfusé par voie générale. Le temps est en heures et les concentrations plasmatiques en $\mu g/mL$, les autres unités sont arbitraires, dépendant de constantes de transfert inconnues du plasma aux tissus, et d'un nombre initial arbitraire pour les populations de cellules.*

Peut-on alors envisager d'autres schémas d'administration chronomodulés, en s'affranchissant du cadre habituel des traitements perfusés à l'hôpital de façon périodique sur une base de 24 h ? En conservant à l'identique ce modèle "chrono-PK-PD", on pose alors la question comme un problème d'optimisation sous contraintes. Quelle est la meilleure fonction de débit instantané d'une pompe programmable qui permette l'élimination maximale des cellules tumorales (fonction objective à minimiser : le nombre de cellules tumorales) tout en préservant les cellules saines suivant une contrainte imposée du nombre de cellules saines à préserver, représentant la tolérabilité du traitement par le patient telle qu'elle peut être estimée par le clinicien. Ce

problème est alors justiciable de l'application de méthodes mathématiques d'optimisation, et une solution élaborée en collaboration avec Claude Basdevant en a été publiée en 2005 (réf. R9). La Figure 10 en donne une illustration.

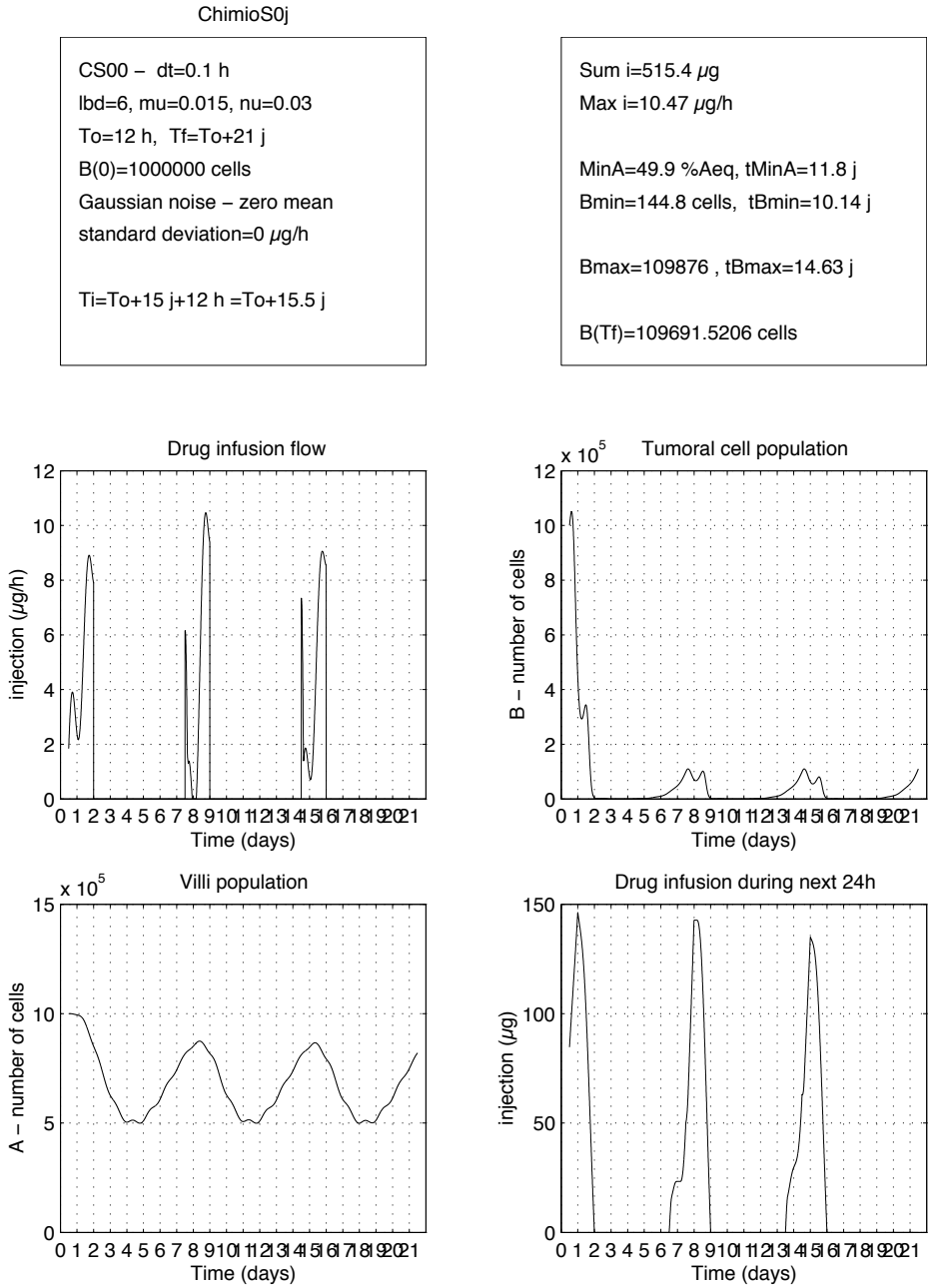

Figure 10. *Traitement de stabilisation de 3 semaines consécutives avec cycles de chronothérapie de 36 heures de perfusion effective suivis de 5 jours 1/2 de récupération. Débit de perfusion calculé suivant des algorithmes d'optimisation mis au point par Claude Basdevant (voir la réf. R9 pour des explications détaillées).*

4.2 Modélisation de la prolifération cellulaire : le cycle de division cellulaire et son contrôle au niveau d'une population de cellules et son contrôle circadien

Le système dynamique précédent présente cependant l'inconvénient de ne pas mentionner le mécanisme d'action du médicament autrement que comme un terme général de mort dans une population de cellules, ce qui ne rend pas possible (autrement que par un modèle de type "boîte noire", avec par exemples des termes linéaires et bilinéaires) la représentation de l'action de plusieurs médicaments aux mécanismes d'action moléculaires distincts et de leurs synergies.

Or les anticancéreux agissent presque tous par inhibition de la division cellulaire, et à des niveaux qui peuvent être très différents. C'est pourquoi il m'est apparu nécessaire de développer un modèle du cycle cellulaire, c'est-à-dire la série d'événements menant à la mitose, dans une population de cellules, avec des points d'entrée pour un contrôle qui doit pouvoir être pharmacologique, mais aussi physiologique, dépendant d'hormones telles que les glucocorticoïdes et de messages en provenance de l'horloge circadienne. On sait en effet que les cyclines, protéines qui conduisent le cycle de division cellulaire, et d'autres protéines qui jouent un rôle dans son contrôle (p53, BAX, BCL2, notamment) ont un rythme circadien de transcription.

C'est pourquoi, avec Benoît Perthame, Stéphane Mischler, Philippe Michel et Béatrice Laroche, nous avons construit entre 2003 et 2006 (réf. RR4, R10) un modèle mathématique pour le cycle de division cellulaire dans une population de cellules. Ce modèle, structuré non pas en espace, mais en âge dans le cycle, repose sur des Équations aux Dérivées Partielles (EDP) qui décrivent l'évolution d'une population durant chaque phase du cycle et la transition à la phase suivante. Ce modèle permet divers types de contrôle : thérapeutique, certaines chimiothérapies étant connues pour agir sur des phases spécifiques du cycle cellulaire ou sur les transitions entre phases) ou physiologique (hormones, rythme circadien). Nous avons étudié alors le comportement asymptotique en temps long de ce système d'EDP en utilisant une méthode d'entropie généralisée et nous avons montré, dans un premier temps grâce à des tests numériques, qu'il était possible de représenter dans ce modèle l'action du contrôle circadien.

Le modèle de densité de population n_i dans la phase i ($1 \leq i \leq I$, I étant le nombre de phases du cycle) à l'instant t et âge a dans la phase s'écrit :

$$\frac{\partial}{\partial t} n_i(t,a) + \frac{\partial}{\partial a}[v_i(a) n_i(t,a)] + d_i(t,a) n_i(t,a) + K_{i\to i+1}(t,a) n_i(t,a) = 0, \quad \text{avec :}$$

$$\begin{aligned} v_i(0) n_i(t, a=0) &= \int_{\alpha \geq 0} K_{i-1\to i}(t,\alpha)\; n_{i-1}(t,\alpha)\; d\alpha \quad 2(\leq i \leq I), \\ n_1(t, a=0) &= 2 \int_{\alpha \geq 0} K_{I\to 1}(t,\alpha)\; n_I(t,\alpha)\; d\alpha, \\ \text{et} \quad \sum_{i=1}^{I} \int_{\alpha \geq 0} n_i(t,a) da &= 1, \end{aligned}$$

Ici, les $d_i(t,a)$ désignent les taux de mort dans les phases, les $K_{i\to i+1}(t,a) = \psi(t)\mathbf{1}_{\{a\geq a_i\}}(a)$ les noyaux (probabilités) de transition entre phases, et les $v_i(a)$ les "vitesses de parcours" dans les phases. Bien sûr, la dernière phase (I) est la phase de mitose. Dans l'expression $K_{i\to i+1}(t,a) = \psi(t)\mathbf{1}_{\{a\geq a_i\}}(a)$, a_i est une durée minimale dans la phase avant qu'une cellule puisse passer dans la phase suivante, est ψ est un contrôle (*a priori* dépendant du temps) sur la transition de phase, par exemple d'origine circadienne ou pharmacologique.

Le principal intérêt de ce modèle est que, grâce à un théorème (Krein-Rutman[35] analogue au théorème de Perron-Fröbenius en dimension finie pour les matrices à coefficients positifs), on peut démontrer sous des hypothèses de compacité de l'opérateur différentiel sous-jacent[1], que le comportement asymptotique des solutions est dominé, quelle que soit la phase i du cycle considérée, par un terme en $e^{\lambda_1 t}$, λ_1 étant la première valeur propre (positive) de l'opérateur. Plus précisément, chaque n_i s'écrit : $n_i(t,a) = e^{\lambda_1 t}\widetilde{N}_i(t,a)$, où les $\widetilde{N}_i$ sont bornés et asymptotiquement et en moyenne sur chaque phase i, constants si le contrôle ψ est constant, et périodiques en temps s'il est périodique.

Cette première valeur propre (dite valeur propre de Perron) mesure donc la croissance d'un processus de croissance exponentiel : en l'absence de phénomènes extérieurs venant limiter cette croissance (cas du stade initial de développement d'une tumeur solide, sans limitations métaboliques ni résistance mécanique du stroma, par exemple), c'est $\lambda_1 = \ln 2/T_d$,où T_d est le temps de doublement de la population. On peut donc contrôler l'évolution d'un tel processus de croissance (d'une population de cellules augmentant par divisions cellulaires dans notre cas) en contrôlant sa valeur propre de Perron. Malheureusement, sauf peut-être dans des cas simples, aucun moyen de calcul analytique de cette valeur propre n'est disponible, et on doit se contenter de l'approcher numériquement.

Ce modèle a été utilisé pour étudier théoriquement le problème du contrôle circadien de la croissance tumorale (tel qu'il a été mis en évidence par les travaux d'Elisabeth Filipski[36] dans l'équipe de Francis Lévi) : une perturbation expérimentale de l'horloge circadienne centrale (par électrocoagulation des noyaux suprachiasmatiques ou par décalage horaire chronique de l'entraînement photique) de souris de laboratoire augmente la vitesse de croissance initiale de tumeurs implantées. On a pu montrer théoriquement (c'est un théorème dû à Benoît Perthame, 2005, cf. réf. R10) que si un contrôle périodique est exercé sur le taux d'apoptose, mais aucun contrôle sur les transitions de phase, c'est le contraire qui doit se produire.

Ceci montre *a contrario* que le contrôle circadien s'exerce (éventuellement uniquement) sur les transitions de phase. Il n'est pas surprenant que l'apoptose ne suffise pas à expliquer dans le cadre de ce modèle le phénomène observé expérimentalement, puisque au moins une influence attendue du rythme circadien (le contrôle de la kinase cdk1 par la kinase-kinase Wee1[37], dont la transcription est elle-même sous la dépendance du gène circadien Bmal1) se situe au

1. Les noyaux $K_{i\to i+1}(t,a)$ positifs, les taux de mort (par apoptose en général) $d_i(t,x) \geq 0$ bornés, et, en posant : $\min_{0\leq t\leq T} K_{i\to i+1}(t,a) : = k_{i\to i+1}(a)$, $\max_{0\leq t\leq T}[d_i + K_{i\to i+1}] : = \mu_i(a)$, et $M_i(a) = \int_0^a \mu_i(\alpha)d\alpha$, la condition : $\prod_{i=1}^{I}\int_{\alpha\geq 0} k_{i\to i+1}(\alpha)e^{-M_i(\alpha)}d\alpha > 1/2$, ceci pour assurer la croissance effective du système (il y a en moyenne plus de renouvellement que de mort).

niveau des transitions de phases et non du taux de mort dans chaque phase. Mais les simulations numériques montrent aussi dans un modèle simplifié à 2 phases que suivant les durées relatives des phases, on peut observer aussi bien une accélération qu'un ralentissement de croissance par l'exercice d'un contrôle périodique sur les transitions (réf. R10, O8).

La Figure 11 montre un cas dans lequel un contrôle périodique diminue effectivement la valeur propre de Perron.

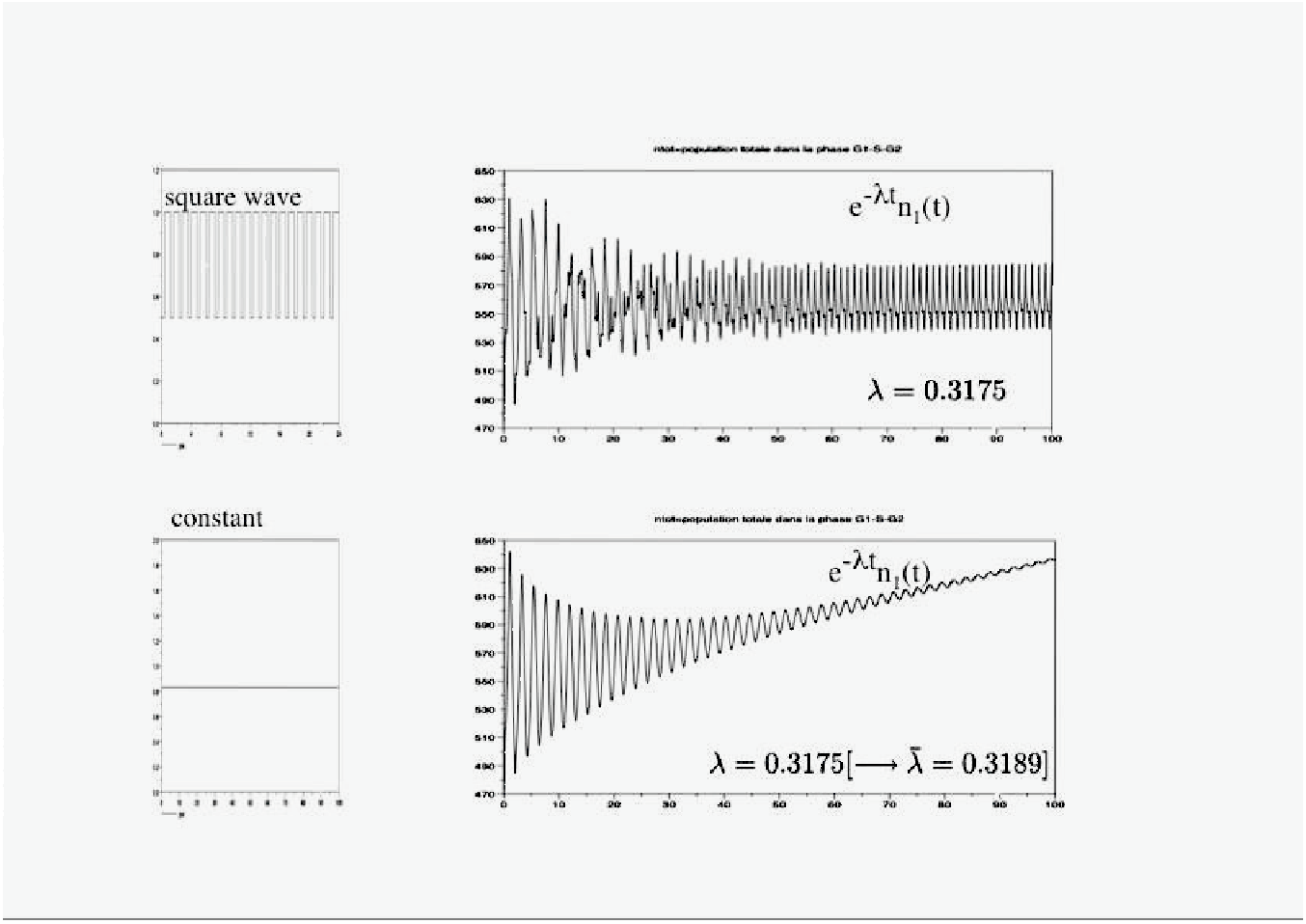

Figure 11. *Effet sur la valeur propre de Perron d'un contrôle périodique du taux de transition entre phases. Pour une même valeur moyenne du contrôle, périodique ou constant, la valeur propre de Perron est dans ce cas particulier réduite par le contrôle périodique, comme dans les observations expérimentales…mais le tableau II montre que ce n'est pas le cas général.*

Le tableau suivant montre en fait qu'aucune hiérarchie claire entre valeurs propres de Perron calculées dans le cas stationnaire et dans le cas périodique n'existe dans l'absolu.

Tableau II

Comparaison des valeurs propres propres de Perron dans le cas d'un contrôle périodique du taux de transition contre une valeur constante de même moyenne pour le taux de transition (λ_{per} / λ_{stat} dans un modèle simplifié à deux phases (G1-S-G2 et M si la transition est G2/M, par exemple). Deux cas de contrôle périodique sont considérés : bref créneau (4 heures à 1 / 20 heures à 0) et créneau régulier (12 heures / 12 heures). Les lignes du tableau indiquent le rapport de durée entre les deux phases. Les valeurs soulignées sont les plus élevées des deux.

G1-S-G2/M, 4-20 sq. w.	λ_{per}	λ_{stat}
1	<u>0.2385</u>	0.2350
2	0.2260	<u>0.2923</u>
3	0.2395	<u>0.3189</u>
4	0.2722	<u>0.3331</u>
5	0.3065	<u>0.3427</u>
6	0.3305	<u>0.3479</u>
7	0.3472	<u>0.3517</u>
8	<u>0.3622</u>	0.3546
10	<u>0.3808</u>	0.3588
20	<u>0.4125</u>	0.3675

G1-S-G2/M, 12-12 sq. w.	λ_{per}	λ_{stat}
1	0.2623	<u>0.2821</u>
2	0.3265	<u>0.3448</u>
3	...	...
4	...	...
5	...	...
6	...	...
7	0.4500	<u>0.4529</u>
8	<u>0.4588</u>	0.4575
10	<u>0.4713</u>	0.4641
20	<u>0.5006</u>	0.4818

Il reste donc encore des points à éclaircir dans les propriétés de ce modèle du cycle cellulaire. Un modèle à au moins trois phases et deux transitions (G1/S et G2/M), plus réaliste, mais aussi plus difficile à identifier, devrait offrir une plus grande richesse de comportement.

Un autre intérêt de ce modèle est qu'il montre la possibilité de l'*entraînement* de la période du cycle cellulaire par la période d'une fonction ψ contrôlant les transitions entre phases (c'est-à-dire que la durée totale du cycle se cale sur la période d'entraînement).

Sur les Figures 12 et 13, on peut voir un exemple de contrôle périodique de la transition de phase par une fonction ψ représentant un contrôle circadien.

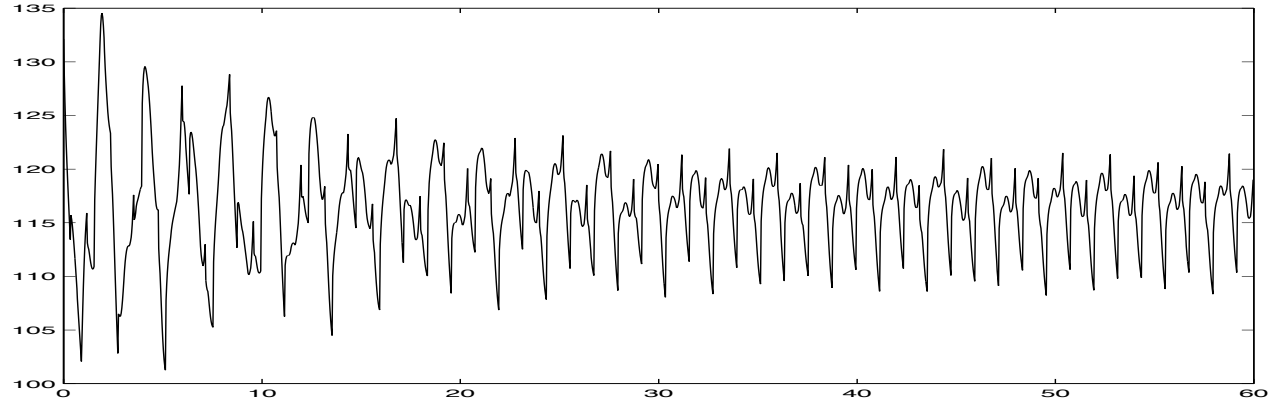

Figure 12. *Solution normalisée $t \mapsto \widetilde{N_1}(t) = e^{-\lambda_1 t} n_1(t)$ de l'EDP pour la population cellulaire en phase* 1 *[moyennée en âge dans la phase] pour un modèle à deux phases de même durée avec contrôle périodique "circadien" (en créneau) de la transition. L'unité de temps est la durée de chaque phase (demi-durée totale du cycle, et le contrôle circadien est de période 1.2 unités de temps.*

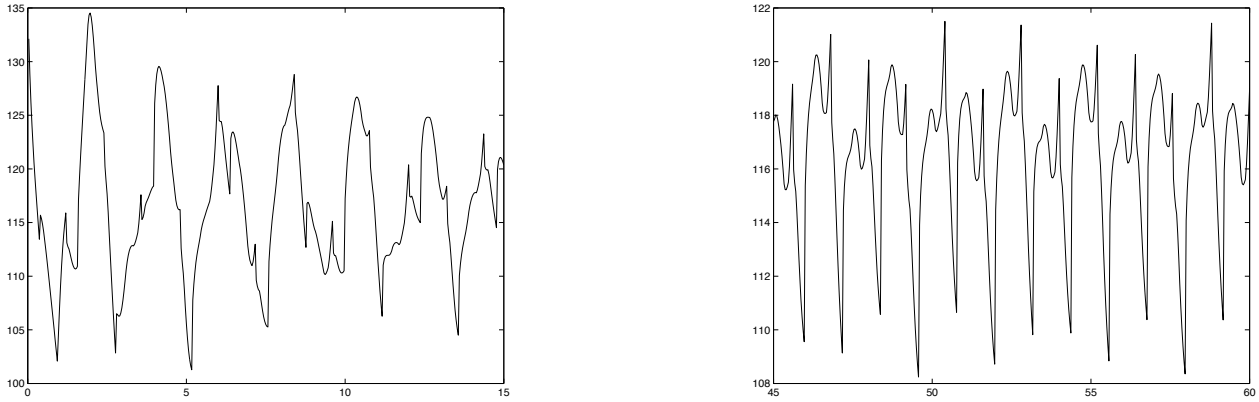

Figure 13. *Détails sur la Figure 12. Au début du tracé (à gauche), la dynamique de la population suit ses oscillations propres, puis après un temps de transition, elle est entraînée à la période circadienne.*

Une autre adjonction au modèle a déjà été faite à l'occasion de l'année de postdoctorat de Fadia Bekkal Brikci, que j'ai encadrée avec Benoît Perthame à l'INRIA sur un sujet que j'avais défini : une phase quiescente a été prise en considération dans le cadre d'un modèle à deux compartiments, quiescent (ou G0) et prolifératif (celui des cellules dans le cycle, ou G1-S-G2-M). Mais comme ces échanges dépendent de façon essentielle du niveau de cycline D contenu dans ces cellules, ce nouveau modèle a été structuré en âge et en cycline.

Les échanges entre ces deux compartiments sont modélisés par deux fonctions. L'une (de fuite de la phase proliférante G1vers la phase quiescente G0) dépend de façon décroissante du niveau de cycline D dans la cellule : lorsqu'un niveau de cycline seuil a été atteint, cette

fonction devient (brusquement), de positive, si proche de zéro que tout retour vers la phase G0 est impossible : ce seuil représente le point de restriction R[38] en fin de phase G1. L'autre (de recrutement dans le cycle) dépend de façon décroissante de la population cellulaire totale et représente une inhibition par la densité de population.

L'introduction de ces fonctions d'échange permet de représenter le comportement de populations de cellules non plus seulement en phase de croissance exponentielle, mais aussi à croissance limitée (de type gompertzienne par exemple) ou illimité, mais polynomiale (par exemple lorsque le volume d'une tumeur solide croît en t^3 avec le temps t comme cela s'observe parfois expérimentalement[39]), ou encore à comportement naturellement homéostatique, comme dans le cas de la prolifération hépatocytaire après hépatectomie partielle.

Le modèle EDP s'écrit ainsi :

$$\begin{cases} \dfrac{\partial}{\partial t}p\left(t,a,x\right)+\dfrac{\partial}{\partial a}\left(\Gamma_0 p\left(t,a,x\right)\right)+\dfrac{\partial}{\partial x}\left(\Gamma_1\left(a,x\right)p\left(t,a,x\right)\right)= \\ -\left(L\left(a,x\right)+F(a,x)+d_1\right)p\left(t,a,x\right)+G\left(N\left(t\right)\right)q\left(t,a,x\right), \\ \dfrac{\partial}{\partial t}q\left(t,a,x\right)=L\left(a,x\right)p\left(t,a,x\right)-\left(G\left(N\left(t\right)\right)+d_2\right)q\left(t,a,x\right). \end{cases}$$

Les variables p et q représentent les populations de cellules proliférantes et quiescentes, respectivement, N la population cellulaire totale (tous âges cellulaires a et charges en cycline x confondus) ; les fonctions L et G sont les fonctions de fuite et de recrutement mentionnées plus haut, F est la fonction de division en fin de phase proliférative, et les Γ (Γ_0, constante, et Γ_1, dépendant de a et x), sont des vitesses d'évolution de a et x par rapport au temps t.

La Figure 14 illustre le comportement du modèle dans le cas d'un tissu sain, par exemple le foie ; mais il pourrait aussi s'agir de la muqueuse digestive ou de la moelle osseuse hématopoïétique.

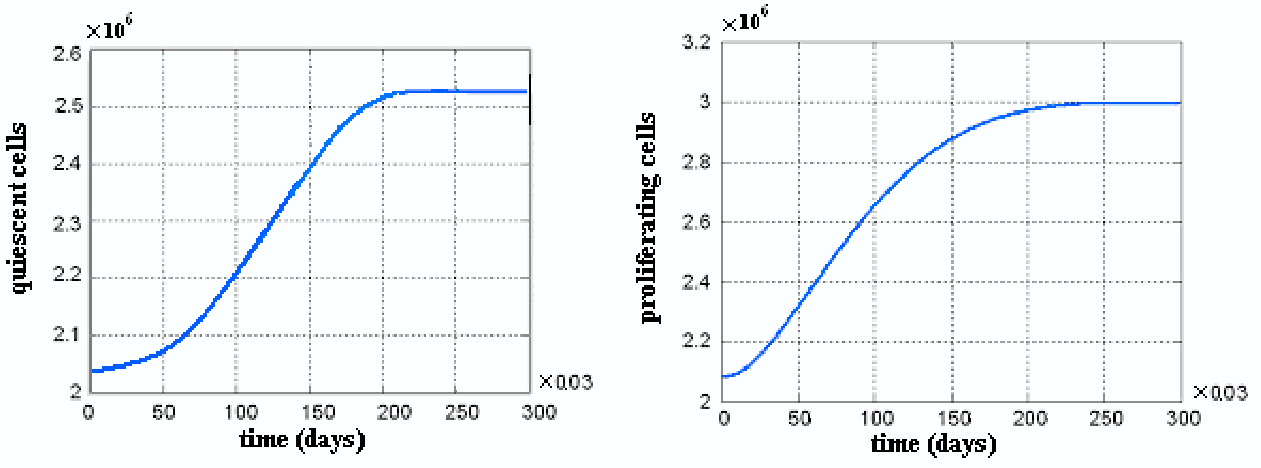

Figure 14. *Evolution des deux populations de cellules (cellules quiescentes à gauche et cellules proliférantes à droite) dans le cas d'un tissu sain.*

Ce modèle est en cours de publication (réf. R12, R13). Il reste à le connecter au modèle de cycle cellulaire à plusieurs phases présenté précédemment. Les fonctions d'échange entre compartiments proliférati f et quiescent sont destinées dans une perspective de modélisation pharmacothérapeutique à représenter les cibles de médicaments inhibiteurs de la croissance *cellulaire* tels que les antagonistes des récepteurs aux EGF (EGFR).

4.3 Modélisation pharmacocinétique-pharmacodynamique (PK-PD) *moléculaire* de l'action des anticancéreux sur la prolifération cellulaire et de son contrôle circadien

Cette partie, encore en cours de construction, est celle que je compte développer en priorité à l'avenir. Dans un premier temps, c'est l'oxaliplatine[40], agent alkylant sans spécificité de phase du cycle, connu pour former des liaisons covalentes sur l'ADN, particulièrement double-brin[41], dont j'ai choisi de représenter l'action. Bien qu'aucune spécificité de phase ne lui soit connue, la cytométrie en flux montre qu'il provoque un arrêt du cycle de division cellulaire principalement à la transition G2/M, et dans une moindre mesure à la transition G1/S.

Un système d'équations différentielles ordinaires (EDO) ayant pour entrée le débit instantané d'une pompe de perfusion programmable doit, pour représenter la pharmacodynamie moléculaire de l'oxaliplatine, avoir pour cible l'ADN libre (i.e., sans adduits d'oxaliplatine) et les autres molécules, protectrices de la cellule, auquel il va aussi se lier de manière irréversible : protéines (et autres molécules de détoxification comme le glutathion) plasmatiques et hépatiques, glutathion intracellulaire.

D'autre part, les principales enzymes connues pour être impliquées dans la résistance à l'oxaliplatine doivent être représentées. Il s'agit de la $GST\pi$[42] pour la liaison (de détoxification) active de l'oxaliplatine au glutathion et des enzymes d'excision $ERCC1$[43] et $ERCC2$ (de réparation -"DNA Mismatch Repair"- de l'ADN endommagé après cassure, au moins simple-brin).

De plus, il est connu qu'il existe un rythme circadien de production des protéines plasmatiques et un rythme circadien (différent du précédent) de synthèse du glutathion[44, 45] (dont l'enzyme limitante est la γ-Glu-cystéinyl ligase (ou synthétase), deux rythmes dont la prise en compte pourrait permettre d'expliquer au niveau moléculaire les variations circadiennes de toxicité et d'efficacité antitumorale de l'oxaliplatine.

Le système d'ED0 ci-dessous répond à ces critères :

$$
\begin{aligned}
\frac{dP}{dt} &= -[\xi + cl + \lambda L]P + i(t) \\
\frac{dL}{dt} &= -\lambda \mathcal{V} P L + \varepsilon \left(N - N_0 - \frac{1}{3}(L - L_0)^3 + r_L(L - L_0) \right) \\
\frac{dN}{dt} &= -\frac{\omega_L^2}{\varepsilon}(L - L_0) \\
\frac{dC}{dt} &= -V_{GST} \frac{C(G - G_0)^2}{K_{GST}^2 + (G - G_0)^2} - k_{DNA} C(F - F_0) + \frac{\xi}{2} \frac{V}{W_j} P \\
\frac{dF}{dt} &= -k_{DNA} C(F - F_0) - k_R(F - F_0) repair \left(g_R, \theta_1, \theta_2, \frac{F_0 - F}{F_0} \right) \\
\frac{dG}{dt} &= -V_{GST} \frac{C(G - G_0)^2}{K_{GST}^2 + (G - G_0)^2} + \delta \left(S - S_0 - \frac{1}{3}(G - G_0)^3 + r_G(G - G_0) \right) \\
\frac{dS}{dt} &= -\frac{\omega_G^2}{\delta}(G - G_0)
\end{aligned}
$$

Les figures suivantes détaillent les mécanismes représentés et la dernière illustre les différences de réponse de l'ADN à l'oxaliplatine suivant la robustesse de la fonction de réparation, supposée liée à l'expression du gène ERCC2.

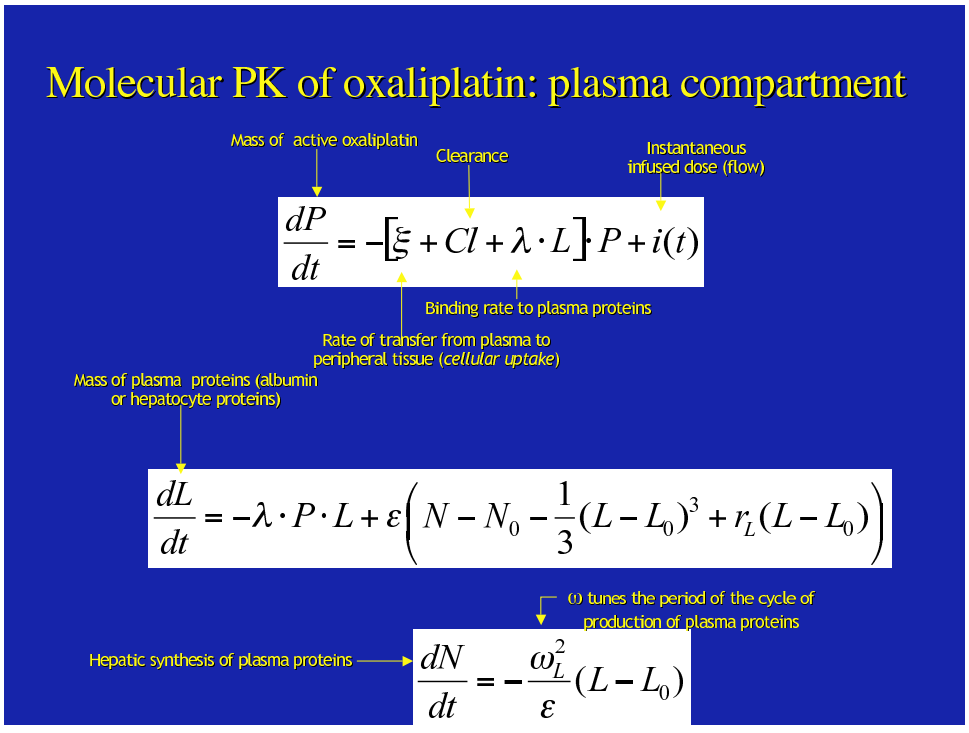

Figure 15. *Pharmacocinétique plasmatique de l'oxaliplatine.*

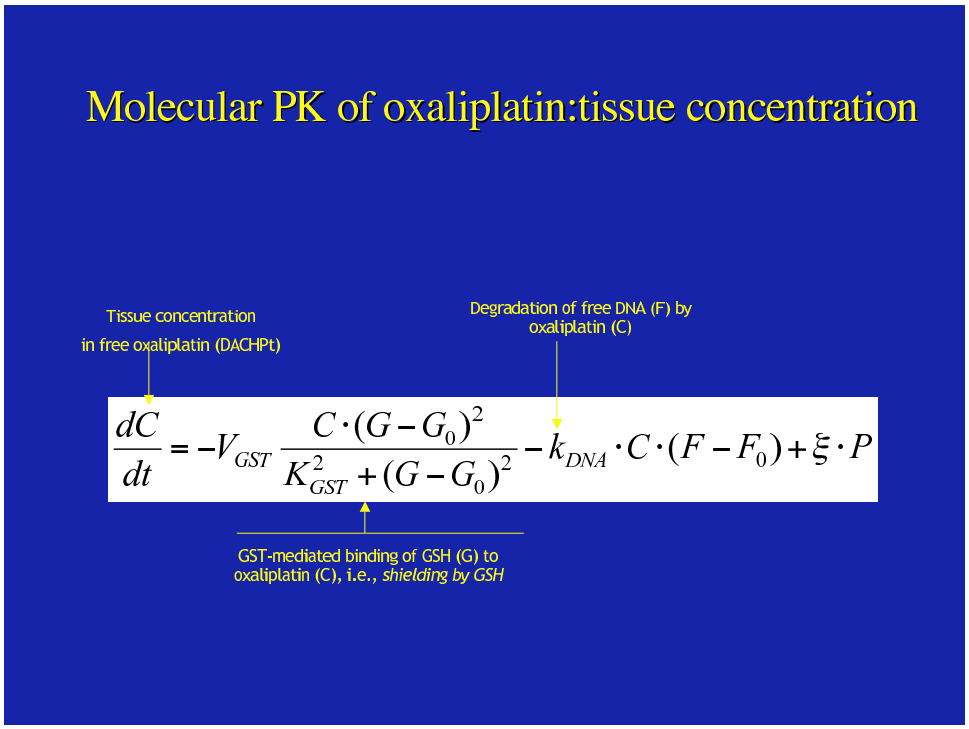

Figure 16. *Pharmacocinétique tissulaire et détoxification cellulaire de l'oxaliplatine.*

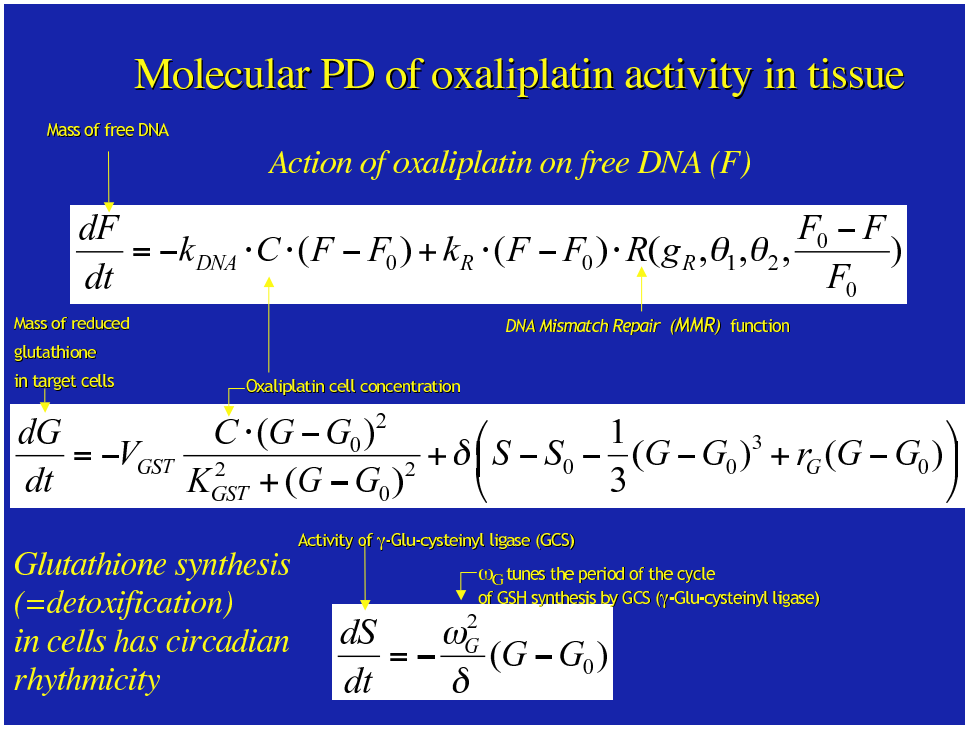

Figure 17. *Pharmacodynamie moléculaire (action sur l'ADN) de l'oxaliplatine.*

Figure 18. *Représentation dans ce modèle du polymorphisme génétique pour ERCC2, gène d'excision ("DNA MMR"), suivant deux types de robustesse de la fonction de réparation.*

Example: representing the action of oxaliplatin on DNA and ERCC2 polymorphism in tumour cells, to take drug resistance into account:

…the same with stronger MMR function (ERCC2-determined):

4.4 Le système circadien : des horloges moléculaires des noyaux suprachiasmatiques aux tissus périphériques

De nombreux modèles de l'horloge circadienne moléculaire ont vu le jour au cours des 10 dernières années. Les plus simples, parmi ceux qui retiennent le mécanisme fondamental de l'horloge : *transcription, traduction, rétroinhibition de la transcription par un produit de la traduction* (par exemple la protéine phosphorylée) sont les modèles d'A. Goldbeter et J.-C. Leloup, publiés à partir de 1995[46, 4, 47], pour la protéine PER de la mouche Drosophila Melanogaster et pour la protéine FRQ de la moisissure Neurospora Crassa.

4.4.1 Contrôle de la période dans un modèle de la protéine *PER*, protéine de l'horloge circadienne moléculaire

En 1999, j'ai commencé à m'intéresser au modèle des oscillations circadiennes de la protéine PER, qu'Albert Goldbeter avait publié en 1995[46] :

$$\begin{cases} \frac{dM}{dt} &= v_s \frac{K_I^n}{K_I^n + P_N^n} - v_m \frac{M}{K_m + M} \\ \frac{dP_0}{dt} &= k_s M - V_1 \frac{P_0}{K_1 + P_0} + V_2 \frac{P_1}{K_2 + P_1} \\ \frac{dP_1}{dt} &= V_1 \frac{P_0}{K_1 + P_0} - V_2 \frac{P_1}{K_2 + P_1} - V_3 \frac{P_1}{K_3 + P_1} \\ & \quad + V_4 \frac{P_2}{K_4 + P_2} \\ \frac{dP_2}{dt} &= V_3 \frac{P_1}{K_3 + P_1} - V_4 \frac{P_2}{K_4 + P_2} - k_1 P_2 \\ & \quad + k_2 P_N - v_d \frac{P_2}{K_d + P_2} \\ \frac{dP_N}{dt} &= k_1 P_2 - k_2 P_N \end{cases}$$

En changeant la valeur du paramètre v_d, représentant le taux de dégradation de la protéine biphosphorylée P_2, supposé génétiquement déterminé, on modélise des cycles circadiens de Drosophiles mutantes -qui existent dans la nature-, à période circadienne plus courte (16 h) ou plus longue (28.5 h) que 24 h (23,71 précisément). Nous avons montré avec Daniel Claude que dans certaines conditions d'entraînement en amplitude et en phase à l'origine, une modification périodique à la période de 24 heures du paramètre k_s, représentant le taux de traduction d'ARN messager en protéine PER (non phosphorylée) pouvait ramener la période des mutantes à la période "physiologique" (i.e., de l'animal non mutant) de 24 heures (réf. R7).

Ces résultats sont illustrés sur les Figures 19 et 20 par des modifications des cycles limites dans le plan de phase (M, PER_{tot}), où M est la concentration en ARN messager et PER_{tot} la concentration en protéine PER totale, phosphorylée et non phosphorylée.

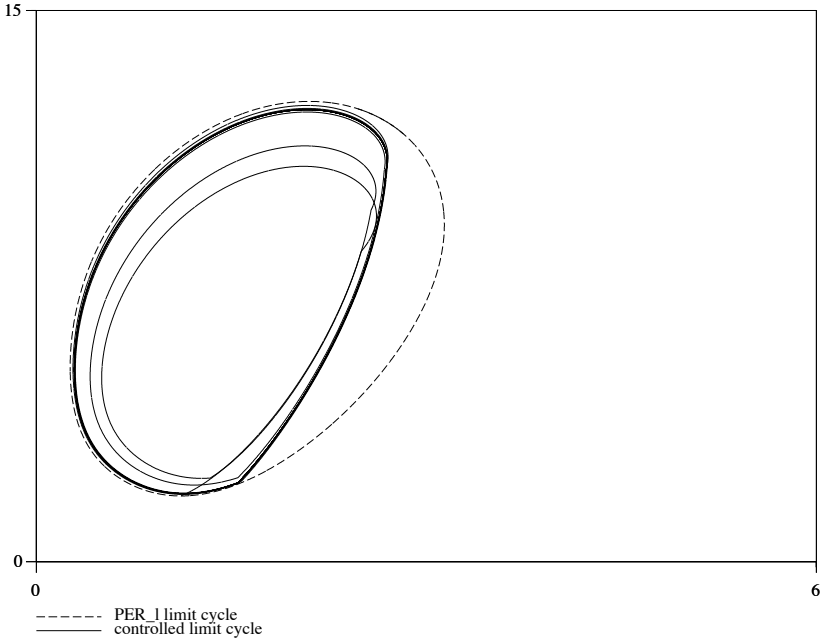

Figure 19. *Modification du cycle limite de la Drosophile mutante longue (pointillés) par un contrôle périodique de k_s le ramenant à un cycle limite parcouru à la période de 24 h.*

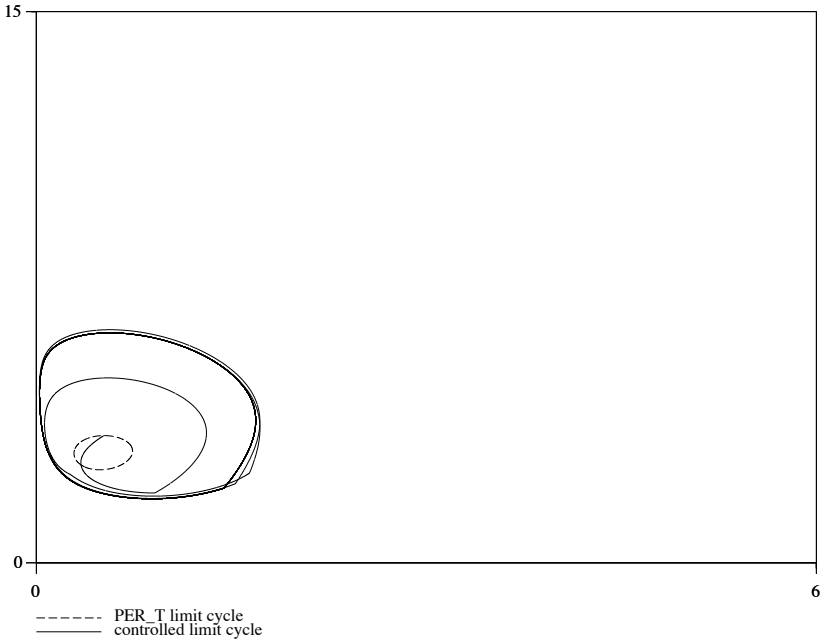

Figure 20. *Modification du cycle limite de la Drosophile mutante courte (pointillés) par un contrôle périodique de k_s le ramenant à un cycle limite parcouru à la période de 24 h.*

4.4.2 Un réseau d'oscillateurs circadiens, des centres à la périphérie

La perturbation des rythmes circadiens centraux, telle qu'elle se manifeste chez certains patients cancéreux au pronostic très réservé ou chez les souris de laboratoire en "jet-lag", par une disparition quasi-complète des oscillations circadiennes de la température et de l'alternance activité-repos, ne peut affecter la prolifération cellulaire en périphérie que si on admet l'existence d'un système circadien, constitué d'horloges moléculaires (présentes de fait dans chaque cellule nucléée où on les a cherchées), et d'un chef d'orchestre central hypothalamique qui coordonne leur activité. Il est donc tentant de considérer l'influence d'une perturbation des rythmes circadiens centraux comme une désorganisation, plus précisément une désynchronisation des horloges circadiennes en périphérie.

Pour représenter dans une perspective pharmacothérapeutique le système circadien, c'est-à-dire les horloges circadiennes des différents tissus périphériques et le pacemaker central des noyaux suprachiasmatiques qui les coordonne, il est nécessaire de modéliser ce système circadien comme un réseau d'oscillateurs.

C'est ce qui est fait, à partir du modèle simple de Neurospora Crassa (transcription : RNA_m ; traduction : PER ; rétroinhibition : Z) pris comme cellule de base du réseau :

$$\begin{cases} \dfrac{dRNA_m}{dt} = V_s \dfrac{K^n}{K^n + Z^n} - V_m \dfrac{RNA_m}{K_m + RNA_m} \\ \dfrac{dPER}{dt} = k_s RNA_m - V_d \dfrac{PER}{K_d + PER} - k_1 PER + k_2 Z \\ \dfrac{dZ}{dt} = k_1 PER - k_2 Z \end{cases}$$

Le réseau est constitué au niveau des noyaux suprachiasmatiques (le pacemaker) par un ensemble d'oscillateurs circadiens (neuronaux) communicant entre eux par couplage diffusif (voir la réf. O9), et au niveau périphérique, par d'autres ensembles d'oscillateurs circadiens, sans communication entre eux, mais tous sous le contrôle d'un messager en provenance du pacemaker, supposé ici inhiber la transcription (par $Z(i) \mapsto Z(i) + W$, où W est le messager périphérique, par exemple un glucocorticoïde) :

$$\begin{cases} \dfrac{dmRNA(i)}{dt} = V_s \dfrac{K^n}{K^n + Z(i)^n} - V_m(i) \dfrac{mRNA(i)}{K_m + mRNA(i)} \\ \dfrac{dPER(i)}{dt} = k_s mRNA(i) - V_d \dfrac{PER(i)}{K_d + PER(i)} - k_1 PER(i) \\ \qquad\qquad + k_2 Z(i) + K_e \displaystyle\sum_{j \neq i} [PER(j) - PER(i)] \\ \dfrac{dZ(i)}{dt} = k_1 PER(i) - k_2 Z(i) \end{cases}$$

La Figure 21 illustre au niveau d'une population moyennée d'oscillateurs circadiens en périphérie la synchronisation / désynchronisation par une alternance lumière / obscurité sur 3 périodes consécutives de 10 jours au niveau des noyaux suprachiasmatiques.

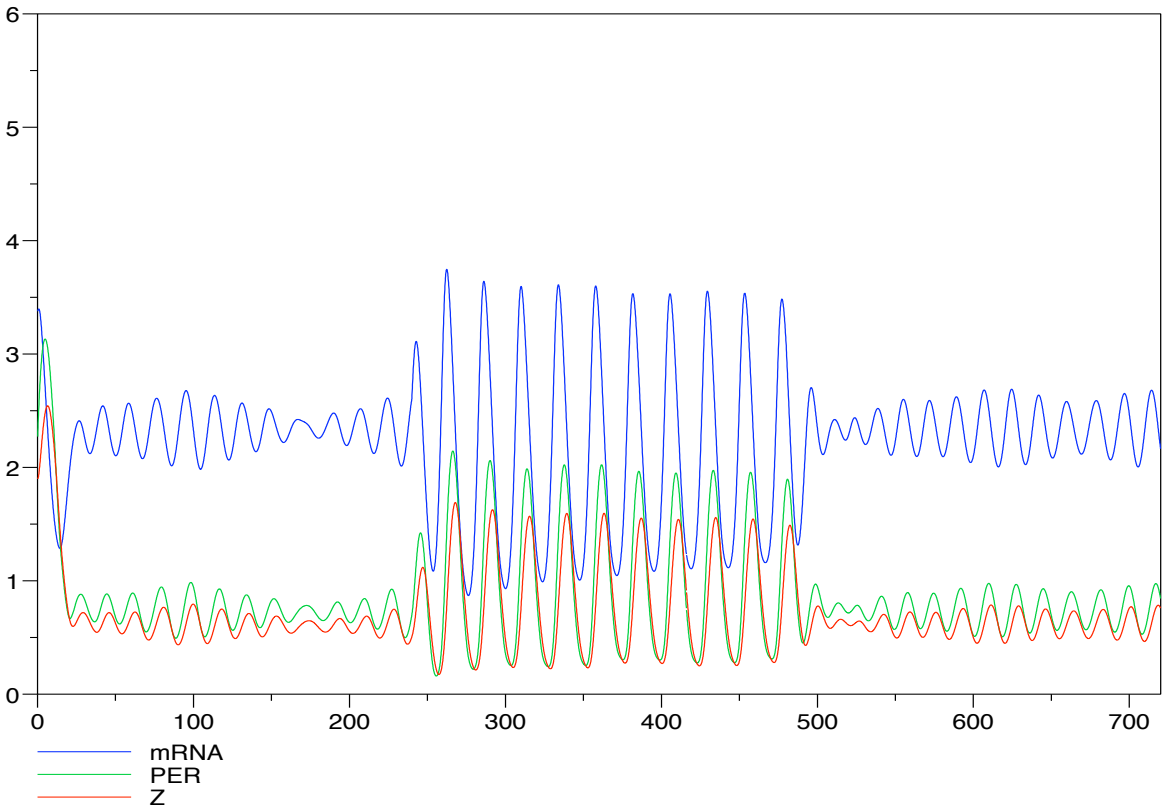

Figure 21. *Entraînement des variables $ARNm$, PER et Z d'une horloge périphérique (moyenne locale d'oscillateurs circadiens) : sans entraînement par la lumière, puis avec, puis à nouveau sans. L'oscillateur périphérique moyenné a une période intrinsèque de 21 h 30, avec une faible amplitude des oscillations résultantes, tandis qu'avec entraînement circadien (10 jours du milieu), la période des oscillations synchronisées résultantes est de 24 h avec une forte amplitude.*

4.4.3 Contrôle circadien sur le cycle de division cellulaire

Ce contrôle a été représenté dans le modèle EDP de cycle cellulaire à deux phases comme le contrôle circadien ψ identifié à la kinase cycline-dépendante CDK1, elle-même obtenue en sortie du modèle minimal d'oscillateur mitotique d'Albert Goldbeter (1991)[48] dans lequel la kinase-kinase Wee1 joue le rôle de cible de l'horloge circadienne, puisque sa transcription est sous la dépendance de l'horloge circadienne. La Figure 22 montre une des étapes de cet entraînement. Mais cet entraînement de CDK1 par (Bmal1 et) Wee1 ne concerne *a priori* que la transition G2/M. Un mécanisme analogue reste à authentifier pour la transition G1/S. Il pourrait impliquer la protéine p21 entraînée par PER2 et agissant sur la kinase CDK2.

De plus, une synchronisation efficace entre les transitions G1/S et G2/M semble nécessaire pour assurer une progression régulière dans le cycle. L'horloge circadienne moléculaire pourrait y jouer l'un de ses rôles (à l'instar, *mutatis mutandis*, du système nerveux autonome assurant la coordination entre rythmes cardiaque et respiratoire).

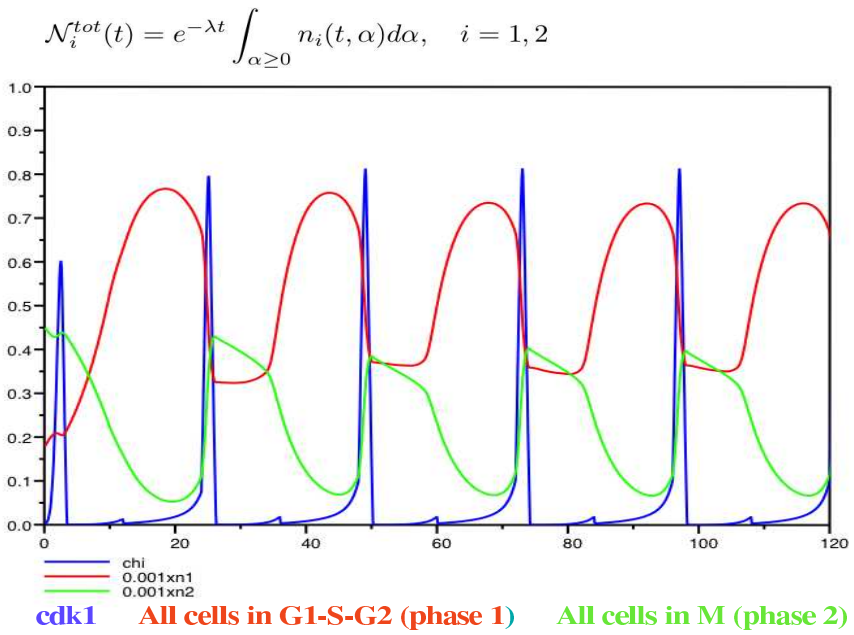

Figure 22. *Entraînement du cycle cellulaire (densité de population cellulaire normalisée) par la kinase CDK1, elle-même entraînée sur un rythme de 24 h par Wee1*

4.4.4 Contrôle circadien sur les mécanismes cellulaires de détoxification ou d'activation

Une représentation par des équations différentielles des mécanismes moléculaires de détoxification des agents exogènes est vraisemblablement la clef de l'explication de la chronotoxicité des médicaments anticancéreux. Glutathion réduit pour l'oxaliplatine, dihydropyrimidine déshydrogénase (DPD) pour le 5-fluorouracile, sont produits sur un rythme de 24 h ; de même, l'activation de l'irinotécan en SN38 par la carboxylestérase. On peut rapprocher de ces mécanismes la réparation après lésion de l'ADN, puisque cerains des gènes (ERCC notamment) qui codent pour cette réparation ont une expression circadienne.

Comprendre comment ces rythmes, et le contrôle des gènes qui les déterminent, diffèrent entre cellules saines et tumorales est un enjeu majeur de la modélisation en pharmacologie des cancers. Beaucoup reste à faire.

Jusqu'ici, seul le contrôle circadien sur la détoxification de l'oxaliplatine a été modélisé et suivant un modèle simplifié d'oscillateur de Van der Pol.

Chapitre 5

Perspectives de recherche : un modèle général de prolifération cellulaire et de son contrôle pour l'optimisation thérapeutique en cancérologie

Des modèles locaux sont à présent en place. Utiliser ces modèles partiels et les mettre bout à bout suivant les besoins pour répondre à une question spécifique, en développant si nécessaire de nouveaux modèles locaux, est l'un des principes qui pour moi doit guider la recherche et le développement de nouvelles méthodes des mathématiques appliquées à la médecine.

Ceci peut se faire dans un cadre général de biologie des systèmes en utilisant un principe de modularité dans le développement des modèles.

5.1 Le cycle cellulaire, son contrôle physiologique et pharmacologique

Il s'agit en particulier de développer des modèles du cycle cellulaire divisé en phases prenant en compte les cyclines, les échanges entre populations de cellules proliférantes et quiescentes, et leur contrôle pharmacologique (PK-PD) moléculaire ou physiologique, notamment circadien. Pour cela, préciser les mécanismes des transitions de phases, de l'induction des enzymes de réparation de l'ADN ou de l'induction de la machinerie apoptotique (p53-dépendante ou non) nécessite des collaborations avec des biologistes fondamentalistes de la cellule comme il en existe notamment sur le site de Villejuif dans l'IFR 89, auquel est rattachée l'U 776.

Du point de vue des méthodes mathématiques, la réduction des systèmes d'EDP utilisés jusqu'ici à des systèmes différentiels à retard est une éventualité qui donnerait facilement lieu à des collaborations, locales ou internationales, et enrichirait l'éventail des techniques d'analyse.

5.2 Populations de cellules : croissance tissulaire non contrôlée ou homéostasie tissulaire

Les modèles de populations de cellules développés jusqu'ici sont fondés sur la division cellulaire représentée sans considération de développement spatial. Le lien avec des modèles spatiaux de type réaction-diffusion, ou à fondement stochastique (IBM, alias "Individual-Based Models") est en discussion à l'intérieur du projet Bang. En particulier des correspondances entre fonctions d'échange abstraites entre phase proliférative et phase quiescente, et limitations spatiales mécaniques ou plus liées au métabolisme (angiogenèse) sont à établir.

5.3 Le système circadien, contrôleur des rythmes physiologiques, son entraînement par l'alternance lumière / obscurité et ses perturbations

5.3.1 Le pacemaker des noyaux suprachiasmatiques

On a déjà représenté ce pacemaker comme contrôlant les processus de prolifération cellulaire. Mais il reste à modéliser, à l'inverse, les impacts d'une part de la cytotoxicité sur les noyaux suprachiasmatiques des cytokines émises par la tumeur ou par le système immunitaire de l'hôte, et d'autre part des médicaments cytotoxiques utilisés en cancérologie eux-mêmes.

Cette toxicité sur le pacemaker central, authentifiée par les mesures, tant invasives (cortisol circulant) que non invasives (température centrale, alternance activité-repos) des rythmes centraux, très perturbés chez les patients cancéreux les plus atteints, mais que rapportent aussi des patients ayant bénénéficié d'un traitement par interféron ($IN\gamma$) se manifeste par des symptômes comparables au "jet-lag" des vols transméridiens. Cette toxicité pose la question d'une contrainte supplémentaire dans l'optimisation thérapeutique en cancérologie : comment limiter la désynchronisation des rythmes circadiens centraux due au traitement ?

Elle pose aussi la question d'une éventuelle thérapie de resynchronisation (mélatonine, cortisol, photothérapie) qui est un moyen d'action adjuvant possible dans l'optimisation thérapeutique.

5.3.2 Les voies de transmissions du centre hypothalamique à la périphérie

Système nerveux autonome et voies hormonales, en particulier glucocorticoïdes, sont les principaux messagers candidats à ce rôle de transmetteurs. La mélatonine y participe-t-elle ? Cela reste à préciser.

Une investigation systématique des voies sympathiques et parasympathiques, et neurohormonales dans la synchronisation des horloges circadiennes périphériques, en particulier pour la prolifération cellulaire, reste entièrement à faire.

5.3.3 Contrôle des horloges circadiennes périphériques et de l'expression des gènes contrôlés par ces horloges

On représentera le contrôle central dans chaque cellule par l'horloge circadienne des gènes du cycle cellulaire d'une part (Wee1, p21, cyclines, cdk, p53,...), des gènes contrôlant les mécanismes d'activation et de détoxification des molécules exogènes d'autre part, et le contrôle de cette horloge circadienne elle-même par les messagers en provenance du pacemaker central.

5.4 Pharmacocinétique-pharmacodynamie moléculaire des médicaments anticancéreux administrés par voie générale

5.4.1 Pharmacocinétique sanguine

Le foie sera considéré comme un filtre sur la circulation générale. Polymorphisme génétique et expression circadienne des protéines circulantes et des enzymes de détoxification hépatiques seront les déterminants d'une pharmacocinétique sanguine moléculaire. La possible toxicité hépatique de certains médicaments sera également prise en compte.

5.4.2 Transports membranaires

Ce thème n'a pas encore été abordé mais présente certainement un intérêt en particulier dans l'étude des résistances aux médicaments.

5.4.3 Mécanismes d'activation et de détoxification cellulaires

Pour chaque molécule étudiée, son devenir dans la cellule : activation, ou dégradation par des molécules génériques comme le glutathion réduit ou par des enzymes spécifiques (par exemple DPD pour le 5-fluorouracile), sera représenté par un modèle dynamique reposant sur des équations différentielles ordinaires.

Les mécanismes d'apparition des résistances aux médicaments pourront être intégrés comme des extensions stochastiques du modèle PK-PD moléculaire (marche aléatoire dans les gènes) et considérés comme une contrainte supplémentaire dans l'optimisation thérapeutique.

La toxicité pour les tissus sains sera représentée (de façon modulaire, i.e., par assemblage de modèles) en fonction des médicaments utilisés et des tissus concernés, pour fournir une fonction de contrainte (de tolérabilité clinique) dans les méthodes d'optimisation.

5.4.4 Protéines sentinelles, réparation ou induction de l'apoptose

p53 et MDM2, qui ont une rythmicité d'expression circadienne, sont les sentinelles des lésions de l'ADN. Elles représentent un lien incontournable entre pharmacologie des cytotoxiques et cycle cellulaire

En effet, en cas de lésions à l'ADN, p53 induit le blocage des transitions de phase G1/S et G2/M et l'expression d'enzymes d'excision (ERCC1, ERCC2) pour la réparation des dommages à l'ADN ; si les dégâts sont irréparables, elle enclenche la voie principale de l'apoptose.

Un modèle de p53 est donc une nécessité pour représenter efficacement la PK-PD moléculaire.

5.4.5 Prise en compte de facteurs métaboliques

En fonction des données et des questions, pH, pression partielle d'oxygène, ATP disponible pourront venir moduler les r'eactions biochimiques prises en compte dans la modélisation PK-PD cellulaire et tissulaire.

5.5 Méthodes d'optimisation de la pharmacothérapeutique

5.5.1 D'autres méthodes d'optimisation sur le modèle macroscopique d'action de l'oxaliplatine

Après le gradient conjugué non linéaire, le lagrangien augmenté a été utilisé pour améliorer les performances de l'algorithme mis au point et employé initialement par Claude Basdevant pour traiter le problème d'optimisation chronothérapeutique, ce qui a fait l'objet d'un stage de fin d'école d'ingénieurs au printemps 2005.

Puis l'application au même problème d'optimisation chronothérapeutique d'autres méthodes d'optimisation : LBFGS_B et SQPAL, ont fait l'objet d'un stage de M2 au printemps 2006. Ces méthodes, qui ont d'abord été utilisées pour identifier les paramètre du modèle PK-PD macroscopique, ont ensuite été employées améliorer les performances des algorithmes précédents. L'évaluation se fait d'une part sur la fonction objectif elle-même (minimisation du nombre de cellules tumorales) mais aussi d'autre part sur la stabilité de la commande optimale (le débit d'injection d'un médicament anticancéreux administré par voie générale) en fonction des paramètres du modèle.

5.5.2 Optimisation du contrôle de la valeur propre de Perron

Cette idée novatrice pour l'étude du contrôle de la prolifération cellulaire repose sur la conception d'une population de cellules en prolifération comme gouvernée dans son évolution par son exposant de Malthus, ou exposant de croissance instantané de la population. Pour un modèle différentiel linéaire, c'est-à-dire à croissance exponentielle, cet exposant est $\frac{\ln 2}{T_d}$, où T_d est le temps de doublement (constant si le modèle est linéaire) de la population cellulaire.

Cette méthode, qui fait partie des techniques mathématiques de contrôle des valeurs propres, fait l'objet d'un stage de M2 de 6 mois, commençant en septembre 2006, entre les projets Bang et Maxplus à l'INRIA.

5.5.3 Réduction de modèles

Nécessaire en fonction de chaque objectif pour pouvoir appliquer des techniques d'optimisation efficaces, la réduction de modèles peut faire appel à des méthodes particulières (notamment de la biologie des systèmes) pour lesquelles des collaborations avec des spécialistes de cette question seront à développer au fur et à mesure des besoins.

5.5.4 Résistances au traitement : une autre contrainte

Si la fonction objective à optimiser est toujours le nombre de cellules tumorales (ou la valeur propre de Perron, qui est une mesure de sa vitesse de croissance), les contraintes peuvent aller au-delà de la toxicité pour les organes sains et concerner l'émergence dans les cellules tumorales de résistances au traitement. L'instabilité génomique des cellules cancéreuses les rend en effet plus aptes que les cellules normales à stimuler l'expression de gènes à l'origine de mécanismes moléculaires qui rendent un médicament inefficace, et cette stimulation est d'autant plus importante que la pression thérapeutique (la dose médicamenteuse) est plus élevée.

Ces mécanismes sont au moins de trois ordres : synthèse des enzymes de détoxification, des enzymes de réparation ("DNA MMR", pour "mismatch repair"), et entrée dans la cellule, et sont tous représentés par des cibles dans les modèles présentés ici. Mais la représentation de la stimulation de ces mécanismes de résistance peut faire appel à une formalisation stochastique (marches aléatoires dans le génome) qui reste à développer.

5.6 Perspectives pratiques

5.6.1 Insertion dans des équipes de recherche : INRIA (projet Bang, Rocquencourt) et INSERM (U 776, Villejuif)

Chargé de recherche dans le projet Bang, qui se développe vers les applications des mathématiques (EDO, EDP, optimisation) à la biologie et, en ce qui me concerne, à la médecine, je suis aussi membre de l'équipe INSERM U 776 "Rythmes biologiques et cancers".

D'autres collaborations, locales, sont souhaitées dans le cadre de Paris XI, et, dans le cadre de réseaux nationaux (GDR) ou européens (FP6 : M3CSTGT- ex-Tumather -, Biosim, Tempo) sont déjà en place et j'y participe activement.

Ma collaboration avec d'autres équipes de l'INRIA (Contraintes, Estime, Maxplus) se développe, et la liste n'est pas close.

5.6.2 Retombées attendues des contrats de recherche nationaux et européens

J'envisage essentiellement, en collaboration à moyen terme avec l'industrie pharmaceutique, le développement de méthodes d'optimisation de la thérapeutique dans tous les domaines de la médecine, en commençant par la cancérologie.

5.6.3 Formation des étudiants à la biologie et à la médecine mathématiques

Il s'agit de la formation de mathématiciens (et pas seulement d'ingénieurs) compétents en médecine et en pharmacie (et pas seulement en biologie), et de médecins et de pharmaciens sensibles à l'intérêt d'une modélisation mathématique dans leurs disciplines.

Sensibilisation dès le lycée des étudiants aux possibilités d'une double formation doctorale en mathématiques et en médecine. Il ne s'agit pas là seulement d'un vœu pieux : tout récemment, un étudiant titulaire d'un M2 de recherche en optimisation mathématique, inscrit en école doctorale, et que j'ai encadré en stage, a commencé ses études de médecine. Je souhaite populariser en Europe cette possibilité d'études.

Développement d'un enseignement des mathématiques appliquées dans les facultés de médecine et de pharmacie. Il y a là un potentiel important car la plupart des étudiants en médecine et en pharmacie ont été sélectionnés au niveau du bac ou bac+1 en grande partie sur leurs compétences en mathématiques, compétences qu'ils n'ont plus guère l'occasion d'exercer dans l'enseignement qu'ils reçoivent en faculté.

5.6.4 Pôle de compétitivité Meditech-Paris-Région

C'est une insertion à développer, souhaitée par l'INRIA, de concert avec l'Institut du Médicament, auquel je participe déjà comme membre de l'U 776.

Chapitre 6

Sélection d'articles

6.1 Analyse de données cardio-vasculaires et modélisation pour l'étude du système nerveux autonome

R1 Clairambault, J., Curzi-Dascalova, L., Kauffmann, F., Médigue, C., Leffler, C. (1992) : Heart Rate Variability in normal sleeping full-term and preterm neonates. *Early Human Development*, 28, 169-183.

A2 Celeux, G., Clairambault, J. (1992) : Estimation de chaînes de Markov cachées : méthodes et problèmes. In: *Approches markoviennes en signal et images*, pp. 5-19. Ed.: GDR Traitement du signal et images. Colloque au CNRS, Paris, septembre 1992.

O6 Clairambault, J. (1995) : A model of the autonomic control of heart rate at the pacemaker cell level through G-proteins. In : Actes de la *17*^{e} *conférence internationale IEEE-EMBS*, 1379-1380, Montréal, septembre 1995.

O7 Clairambault, J., Mansier, P., Swynghedauw, B. (1995) : Efects of parasympathetic blockade on nonlinear dynamics of heart rate in mice. In : Actes de la *17*^{e} *conférence internationale IEEE-EMBS*, 31-32, Montréal, septembre 1995.

R4 Mansier, P., Clairambault, J., Charlotte, N., Médigue, C., Vermeiren, C., LePape, G., Carré, F., Gounaropoulou, A., Swynghedauw, B. (1996) : Linear and non-linear analyses of heart rate variability: a minireview. *Cardiovascular Research*, 31, 371-379.

Early Human Development, 28 (1992) 169–183
Elsevier Scientific Publishers Ireland Ltd.

EHD 01223

Heart rate variability in normal sleeping full-term and preterm neonates

Jean Clairambault[a], Lilia Curzi-Dascalova[b], François Kauffmann[a,c], Claire Médigue[a] and Christopher Leffler[a,b,c]

[a]*INRIA Rocquencourt, France* [b]*INSERM CJF8909 Hospital Antoine-Béclère, Clamart,* [c]*Department of Mathematics University of Caen (France)*

(Received 17 April 1991; revision received 15 November 1991; accepted 21 January 1992)

Summary

To assess maturation of the Autonomic Nervous System (ANS) and sleep states, Heart Rate Variability (HRV) was studied in 24 healthy sleeping newborns, aged from 31 to 41 weeks, conceptional age (CA). Spectral analysis of the interbeat interval (RR) signal, was performed by Short-Time Fourier Transform, in three frequency bands: high (HF), of purely vagal origin, mid (MF), and low (LF), vagal and sympathetic, thus allowing evaluation of both branches of the ANS, observed in Active Sleep (AS = REM Sleep) and in Quiet Sleep (QS = nREM Sleep). Principal Component Analysis, Discriminant Analysis, and hypothesis tests were used to investigate the evolution of spectral variables and their relation with sleep states. HF, MF, LF, and mean RR all increased with age; the differences from the premature to the full-term group, were more marked, as a whole, in AS than in QS. HF showed the highest increase from the premature (31–36 weeks CA) to the intermediate (37–38) group, whereas LF showed equal differences from the premature to the intermediate, and from the intermediate to the full-term (39–41) groups. These results suggest a steep increase in vagal tone at 37–38 weeks CA, with stability afterwards, and a more regular increase in sympathetic tone from 31 to 41 weeks CA

Key words: heart rate variability; spectral analysis; data analysis; sleep; newborn infant; premature.

Correspondence to: J. Clairambault, INRIA, Bâtiment 12, F78153 Rocquencourt, France

0378-3782/92/$05.00
Printed and Published in Ireland

Introduction

The variations of heart rate have long been used as a mean of investigating the Autonomic Nervous System (ANS) [30]. Short-term (or high frequency, HF) variations have been reported to reflect only parasympathetic control of heart rate, and long-term (or low frequency, LF) variations both sympathetic and parasympathetic control [3,12,29,32]. These differences in the frequency domain between the two branches of the ANS (fast vagal and slow sympathetic) may be explained by different response delays in the vagal (about 1 heartbeat duration) and sympathetic (2 to 3 s in adults) pathways [3,38].

HF variations are related to the respiratory cycle (period: 1–3 s, in newborn infants), and carry the part of Heart Rate Variability (HRV) which is referred to as Respiratory Sinus Arrhythmia (RSA) [19,20,29] It is identified, on an adult cardiorespiratory tracing, as an increase in heart rate during inspiration, and a decrease during expiration; it has been classically described as the effect on the centres of a reflex input from lung, atrium, or aortic stretch sensors, but it also might be due to a coupling of respiratory and cardiac vagal medullary motoneurones [17,39].

Various origins (variations in blood pressure due to the baroreflex, thermoregulation, renin/angiotensin system adaptation) have been attributed to LF variations, the period of which ranges from 4 to 30 s in infants [34]. A distinction has been established by numerous authors between low (or mid, MF, period around 10 s) frequency, reported to reflect baroreflex activity, and very low (LF, period usually beyond 20 s) frequency, the origin of which is less clear [3,7,12,32].

In infants from 1 week to 6 months, HF variations have been reported to be higher in quiet sleep (QS) than in active sleep (AS) [15,16,17]; the opposite is true for LF variations [16–18] According to Harper et al, sleep states in infants may be discriminated by HRV variables, on these grounds, with a high degree of accuracy [16].

The physiological importance of these questions is certainly not negligible for a better understanding of early human ontogenesis; furthermore, physiopathological implications are of great interest. This is particularly true for Sudden Infant Death Syndrome, for which a possible role of the ANS has been reported, and in which different studies have analyzed possible differences from controls in heart rate or HRV [2,13,14,24,31,35,36,40].

Regarding normal human ontogenesis, no study so far, to our knowledge, has analyzed by spectral analysis of HRV, maturation of the ANS according to sleep states in healthy premature and full-term newborn infants.

Our aim in this study was to analyze: (1) the age-related modifications of variables quantifying HRV in different frequency bands (and thus parasympathetic and sympathetic tones), in each sleep state and (2) the discrimination between sleep states, as measured by HRV variables, and the evolution of this discrimination with age

Materials and Methods

Subjects

Twenty-four neonates, all clinically and neurologically healthy (in particular,

Apgar score was at least 8 at 1 s, and always 10 at 5 s), were studied between the 2nd and 11th day of extrauterine life (in order to exclude influence of drugs possibly given during labour, or conditions of labour itself, as well as postnatal adaptation of heart rate) by polygraphic sleep recordings (ECG, EEG, eye movements)

They had been divided according to conceptional age (CA) at the time of the recording in three different age groups:

- 8 Full-term; $39 \leq CA \leq 41$ weeks
- 8 Intermediate; $37 \leq CA \leq 38$ weeks
- 8 Premature; $31 \leq CA \leq 36$ weeks.

Recordings

Paper and analog tape recordings were performed in the morning, during a sleep between two meals All neonates were lying supine, either in their beds, at ambient temperature (25–26°C) for full-term and intermediate newborns, or in incubator (30–36°C) for prematures, in order to ensure a normal body temperature for each subject

Recordings were performed until awakening of the subject All recordings contained at least one complete sleep cycle, yielding at least one 512 heartbeat epoch (statistical observation unit) of Active Sleep (AS = REM Sleep) and one of Quiet Sleep (QS = nREM Sleep), coded on paper tracings by using REM and EEG patterns [9,11].

ECG signal processing

ECG recordings were digitized at 282 Hz and processed by a signal-to-noise ratio algorithm [22,23] to obtain the RR series. Every raw RR series (not resampled) was processed by Short-Time Fourier Transform, a non-stationary spectral analysis procedure which uses complex demodulation [28,37], and provides an 'instantaneous' evaluation of spectral amplitude in given frequency bands, one time series for each chosen band.

The estimation of spectral amplitude A_{f_0} of the RR signal in the band $[f_0 - \epsilon, f_0 + \epsilon]$ is given by:

$$A_{f_0}(n) = \left| \sum_{k=0}^{n} RR(k)\omega_\epsilon(n-k) \exp(-2\pi i f_0 k) \right|$$

where (ω_ϵ) is a low-pass elliptic iir filter, with $[0, \epsilon]$ passband If RR(n) is in miltiseconds, so is $A_{f_0}(n)$

In this study, we focused our attention on three types of HRV: High Frequency (HF) variations (with period in heartbeats: 3–8, ranging from 1 to 4 equivalent seconds; (conversion from heartbeats to 'equivalent seconds' is performed by multiplying number of beats by mean RR in a given 512-heartbeat epoch), and two sub-types of low frequency variations mid frequency: (MF) variations (with period in heartbeats: 10 to 25, ranging from 4 to 12 equivalent seconds), and (very) Low Frequency (LF) variations (with period in heartbeats: 30 to 100, ranging from 12 to 50 equivalent seconds).

An illustration of these signals is presented on Fig 1, which shows a rather strik-

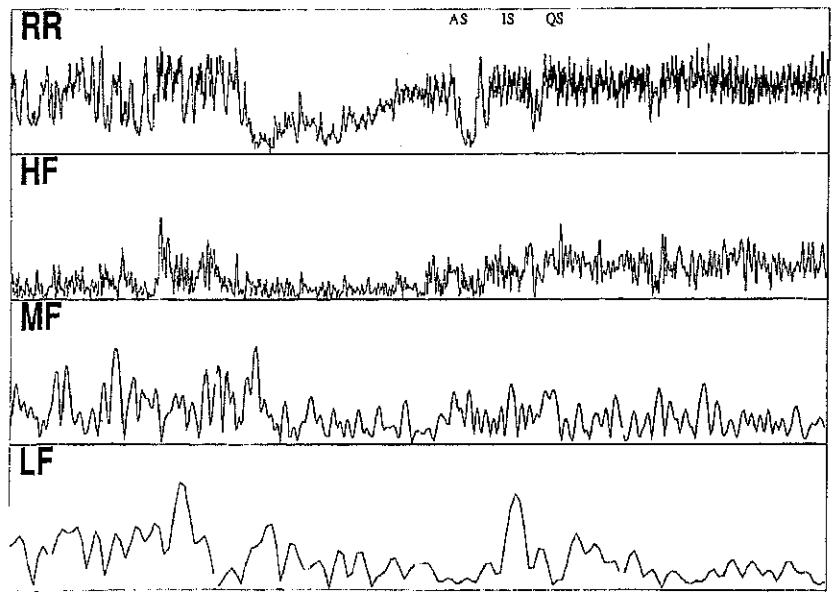

Fig. 1 Raw RR signal and Short-Time Fourier Transform in the three frequency bands: high (HF), mid (MF), and low (LF), from top to bottom, for a series of 2048 consecutive heartbeats, in a full-term newborn (39 weeks, 2 days of life), during about 16 min, and showing a striking transition (middle of page) from Active Sleep (AS) to Quiet Sleep (QS); *y*-scales are from 350 to 650 ms for RR and from 0 to 100 ms for the other signals. Notice the changes in HF (increase from AS to QS) and in LF (decrease from AS to QS)

ing example of what may be seen during the transition from AS to QS, when vagal tone is high enough (here, in a full-term newborn, 39 weeks CA, 2 days of life)

We measured in each epoch of 512 beats the mean amplitude of the raw RR and of the 3 extracted (HF, MF, LF) time signals. These means (338 for each signal) were used as material for subsequent statistical analysis.

Statistical processing

Statistical processing was performed at two levels.

(a) To assess the influence of age and sleep state on each variable separately, and ascertain independence of observations, hypothesis tests were performed on the set of 24 within-individual means, averaged over all 512-heartbeat epochs belonging to the same subject (48 within-individual-and-sleep-state means, for 2-way ANOVA on age and sleep state): *F*-test in analysis of variance, paired and unpaired 2-tailed *t*-tests for the comparison of means between age groups or sleep states

(b) To take into account possible combinations between variables, on the one hand, and within-individual variance for each variable, on the other hand, we performed multivariate data analysis on the set of all 338 epochs, considered as points in the (HF, MF, LF) 3d-space: Principal Component Analysis and Linear Discrimi-

nant Analysis [5,6,26], with cross-validation [27], between age groups or sleep states. Subsequent analysis of the respective parts played by each variable in discrimination was carried through by studying the correlation coefficients of each variable with the discriminant linear function which provides the discrimination rule. RR was not used for these multidimensional analyses, since HF, MF, and LF had been extracted from it.

By using these two complementary classes of methods, we wanted to answer two questions:

(1) Are HRV variables relevant, separately or combined together, to distinguish between age groups, in one given sleep state, or whatever the sleep state? And if it is so, what is the part played by each variable in age group distinction?

(2) Are HRV variables relevant, separately or combined together, to distinguish between sleep states, in one given age group, or whatever the age group? And if it is so, what is the part played by each variable in sleep state distinction ?

Results

Firstly, to examine each variable separately, a two-way analysis of variance was performed on age group and sleep state, by using the 48 within-subject-and-sleep-state means, for HF, MF, LF, and RR.

It may be seen on Table I that RR and all HRV variables are relevant for age distinction, whereas only HF, LF, and, to a lesser extent, RR provide significant between-sleep-state differences. No interaction between age and sleep state has been found.

Then, to go further in the analysis of variance, a normed Principal Component Analysis was performed to analyze, in relation to age (Figs. 2 and 3) and sleep state (Fig. 4) the contribution of each HRV variable to the global variance of the 'statistical cloud' constituted by all 338 epochs of 512 heartbeats, considered as points in the (HF, MF, LF) 3d-space. Equations for the 'principal factor plane':

$$x = 0.69\mathrm{HF} + 0.93\mathrm{MF} + 0.82\mathrm{LF}$$

$$y = 0.71\mathrm{HF} - 0.07\mathrm{MF} - 0.51\mathrm{LF}$$

TABLE I

2-way ANOVA (three ages, two sleep states) on RR and HRV variables.

$n = 48$	F^2_{42} (age group)	F^1_{42} (sleep state)	F^2_{42} (interaction)
HF	9.92**	11.26*	1.08 (NS)
MF	12.37***	0.67 (NS)	0.04 (NS)
LF	11.13**	13.08**	0.87 (NS)
RR	10.56**	6.97*	0.33 (NS)

*$P \leq 0.01$.
**$P \leq 0.001$.
***$P \leq 0.0001$
NS, non-significant.

where numbers are correlation coefficients between variables (HF, MF, LF) and factors (x, y), show that the first factor, x, roughly represents total HRV, and the second one, y, represents a HF/LF opposition; x and y, respectively represent 67% and 26% of the total variance of the statistical cloud

Figure 2 shows the projection of all 338 epochs onto the (x,y) plane. Full-term neonate (39–41 weeks CA) epochs occupy the right part of this figure, and premature (31–36 weeks CA) epochs the left part of it. Intermediate neonate (37–38 weeks CA) epochs are homogeneously displayed along the x-axis. One can therefore see the first factor, x, as a 'maturity factor'

Figure 3 shows a view of all 24 subjects (averages of epochs within each subject, disregarding sleep state) and centres of gravity (mean points) of age groups

Figure 4 shows the same projection as Fig. 2 onto the (x, y) plane, but emphasizes sleep state distinction. AS epochs are predominantly found in the lower part of this figure, and QS epochs in the upper part of it; the second factor, y, thus might be seen as a 'sleep state factor'; but the same HF/LF opposition for y, with a negligible coefficient for MF, was found when performing the same analyses in each sleep state, so that this factor may not be directly related to sleep state

In order to better analyze these general results and answer more precisely the two questions mentioned above about age and sleep state distinction, we performed comparison between groups, first by hypothesis tests for each variable separately, and then by mutivariate discriminant analyses on all HRV variables.

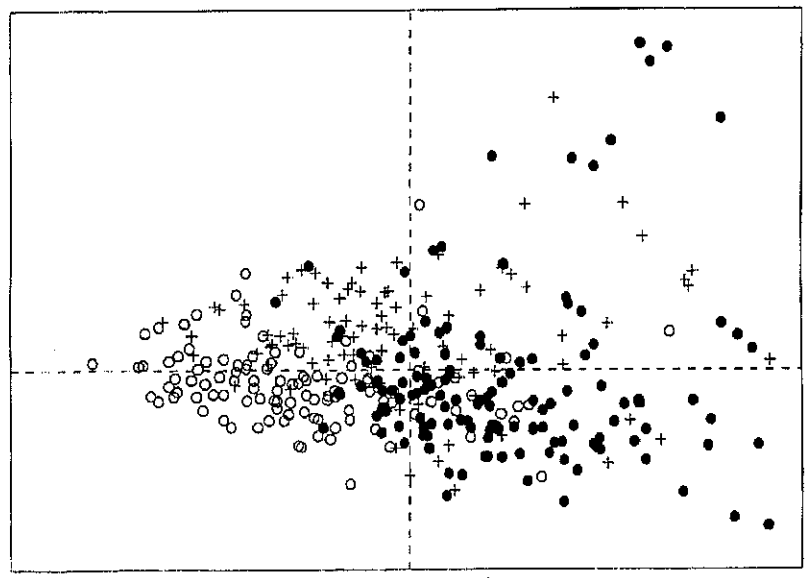

Fig 2 Age group distinction by Principal Component Analysis: projection of all 338 512-heartbeat epochs (corresponding to all 24 newborns studied) onto the principal factor plane: $x = 0.69HF + 0.93MF + 0.82LF$, $y = 0.71HF - 0.07MF - 0.51LF$. Full dots (●) represent full-term neonate epochs, crosses (+) intermediate ones, and empty dots (○) premature ones

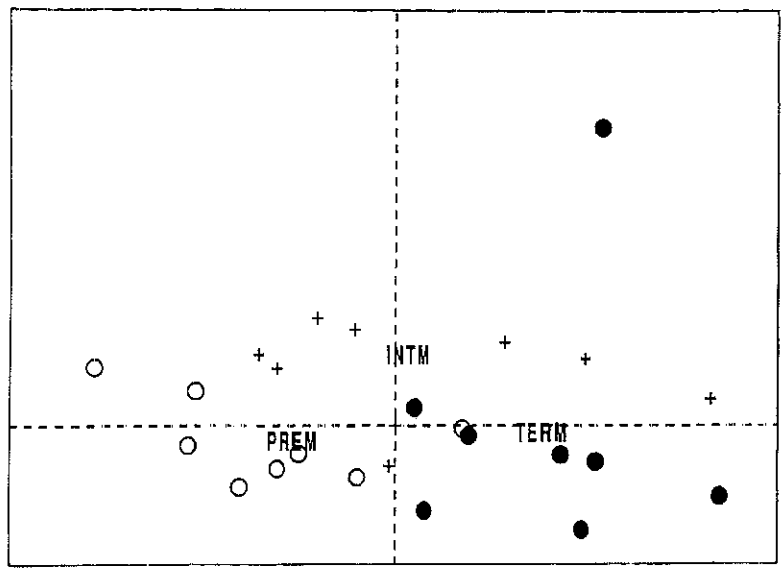

Fig 3 Age group distinction by Principal Component Analysis: projection of all 24 newborns and centres of gravity (mean points) of each age group (TERM for full-term, INTM for intermediate, PREM for premature) onto the principal factor plane: x = 0.69HF + 0.93MF + 0.82LF, y = 0.71HF − 0.07MF − 0.51LF Full dots (●) represent full-term neonate epochs, crosses (+) intermediate ones, and empty dots (○) premature ones; here, the x-axis may clearly be seen as a 'maturity axis'

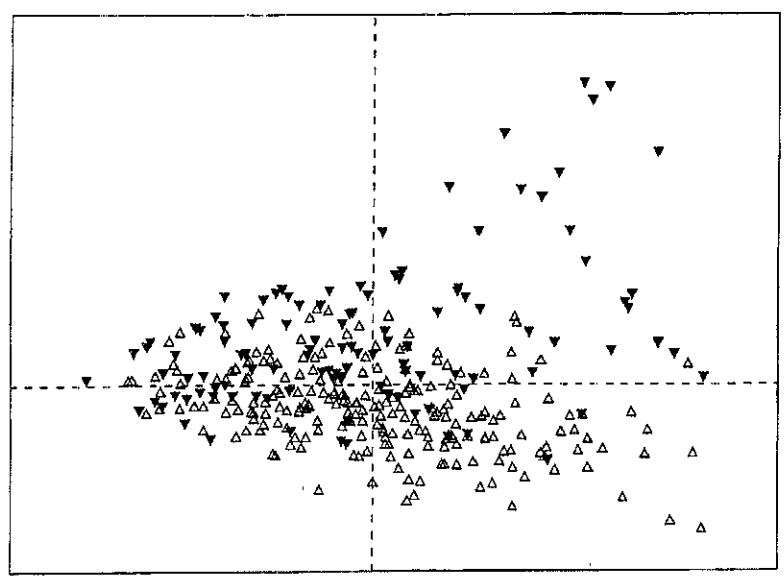

Fig 4 Sleep state distinction by Principal Component Analysis: projection of all 338 512-heartbeat epochs (corresponding to all 24 newborns studied) onto the principal factor plane; Active Sleep epochs are indicated by empty triangles (△), Quiet Sleep epochs by full triangles (▼)

Evolution of HRV variables with age

Trends between age groups, in AS and in QS, are presented on Fig. 5. This figure shows that all HRV variables and mean RR increase with age, but not all with the same regularity. At the two levels of statistical analysis described earlier:

(a) Table II shows the evolution of RR, HF, MF, and LF with age in the 24 neonates, first without consideration of sleep state (top), and then in AS (middle), and in QS (bottom), studied by Student's *t*-test for the comparison of means between couples of age groups. All variables show significant between-age-group differences, and these differences are most emphasized in AS. Studying each variable separately, in contiguous age groups, one can observe that for HF, the strongest changes (on the increase with CA) occur between the premature and intermediate groups; for MF this remains true, but only in AS; as regards LF, differences are nearly significant ($P = 0.06$) between the premature and intermediate groups, and between the intermediate and full-term groups, equally in each case, but only in AS.

(b) Table III assesses the parts played by each variable in multivariate age group discrimination: Linear Discriminant Analysis was performed on the set of 338 512-heartbeat epochs, using HF, MF, and LF, providing percentages of well-classified epochs, Mahalanobis Distance scores, and the correlation coefficients r_{HF}, r_{MF}, r_{LF} of each of these variables with the discriminant linear function, (Mahalanobis Distance between the centres of gravity of groups is a complementary measure of the quality of discrimination [5,6]).

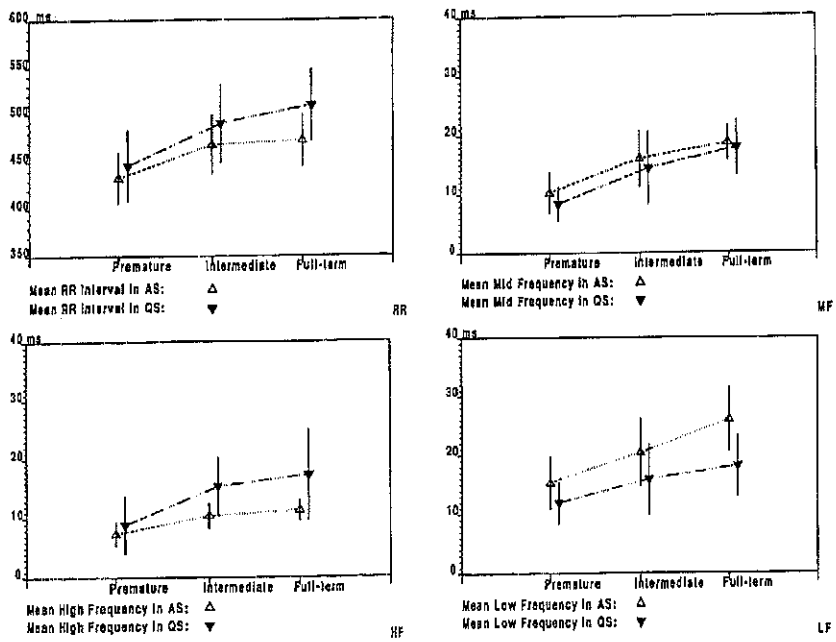

Fig. 5. Trends between age groups, for RR, HF, MF, and LF: mean values in AS (Δ) and in QS (▼); vertical bars indicate ± 1 S.D. around mean values.

TABLE II

Evolution of HRV and RR with age: Student's unpaired *t*-test for the comparison of means between 2 age groups: full-term versus premature (8t/8p), premature versus intermediate (8p/8i), and intermediate versus full-term (8i/8t). From top to bottom: all states mixed, in Active Sleep and in Quiet Sleep.

	8t/8p	8p/8i	8i/8t
All states			
HF	3.41**	4.69***	0.27 (NS)
MF	4.02**	1.66 (NS)	1.71 (NS)
LF	4.47***	1.50 (NS)	2.32*
RR	3.04**	2.54*	0.35 (NS)
Active sleep			
HF	4.98**	3.51**	0.94 (NS)
MF	4.86***	2.51*	1.35 (NS)
LF	4.34***	2.03 ($P = 0.06$)	2.02 ($P = 0.06$)
RR	3.13**	2.59*	0.31 (NS)
Quiet sleep			
HF	2.74*	2.85*	0.60 (NS)
MF	3.41**	1.65 (NS)	1.26 (NS)
LF	2.82*	1.63 (NS)	0.79 (NS)
RR	3.31**	2.19*	0.97 (NS)

(t = full-term newborns (39–41 weeks CA); i = intermediate newborns (37–38 week CA); p = prematures (31–36 weeks CA)
*$P < 0.05$.
**$P < 0.01$.
***$P < 0.001$.
NS, non-significant.

A preliminary attempt to discriminate all 338 epochs in three age groups (full-term, intermediate and premature) had given poor results (less than 50% well-classified epochs), as might have been suspected from the overlapping of groups in Fig. 2. We thus decided to discriminate between all possible pairs of age groups.

Firstly, to distinguish premature from full-term epochs (intermediate ones were temporarily discarded), for all sleep states, and in each sleep state separately, discriminant analyses were performed on the set of 247 non-intermediate epochs. As may be seen on Table III, these analyses yield rather satisfying percentages of well-classified epochs, especially in AS (87%). As may be inferred from the analysis of the correlation coefficients, all HRV variables are relevant and contribute in the same way to age group discrimination.

Secondly, to distinguish premature from intermediate epochs, the same processing was applied to the set of 207 non-full-term epochs. Table III shows satisfying percentages of well-classified epochs, especially in QS (86%); the predominance of HF in discrimination is overwhelming here (r_{HF} as compared to r_{MF}, r_{LF}) which is in favour of a strong enhancement in HF from the premature to the intermediate group.

Thirdly, to distinguish intermediate from full-term epochs, this processing was applied to the set of 222 non-premature epochs. Table III shows results which are a little poorer in AS, but drastically diminished in QS, and a negligible contribution of HF to discrimination. This is in favour of a relative stability of HF, and a moderate increase in MF and LF from the intermediate to the full-term group.

Evolution of sleep state distinction with age

In the same way, to study between-sleep-state differences on each variable separately, paired *t*-tests for the comparison of means within each age group were performed and are presented on Table IV.

The results obtained by 2-way ANOVA are confirmed here: MF is not relevant for sleep state discrimination, whatever the age. HF, and most of all LF, show significant between-state differences among full-term newborns. In the intermediate group, differences in HF and in LF are still significant, but in the premature group, only LF shows significant between-state differences.

In order to assess the parts played by each HRV variable in global (multivariate) discrimination between sleep states, discriminant analyses were also performed on the set of all 338 epochs, for all ages, and in each age group independently.

Table V shows that these analyses yield satisfying percentages of well-classified epochs in the full-term group, but poorer ones in the other groups. The evolution of Mahalanobis distance between the centres of gravity of sleep states shows a constant progression from the premature group to the full-term group.

TABLE III

Between-2-age-group discrimination: Between full-term and premature (131 + 116 = 247 epochs, top), between premature and intermediate (116 + 91 = 207 epochs, middle) and between intermediate and full-term (91 + 131 = 222 epochs, bottom)

	Linear Discr.	Mahalanobis Distance	r_{HF}	r_{MF}	r_{LF}
Full-term/prem.					
All states	85%	3.41	0.75	0.89	0.82
Active Sleep	87%	3.56	0.87	0.94	0.89
Quiet Sleep	77%	3.46	0.90	0.79	0.67
Prem./intermed.					
All states	81%	2.21	0.97	0.42	0.29
Active Sleep	74%	1.91	0.99	0.42	0.27
Quiet Sleep	86%	4.46	0.91	0.39	0.37
Intermed./full-term					
All states	74%	1.17	0.02	0.88	0.91
Active Sleep	79%	1.79	0.18	0.88	0.91
Quiet Sleep	54%	0.40	0.45	0.99	0.69

(Linear Discr : percentages of well-classified epochs, globally or within one given age group; Mahalanobis Distance (between the centres of gravity of groups), a complementary measure of the quality of discrimination; r_{HF}, r_{MF} r_{LF} correlation coefficients of Discriminant Linear Function with HRV variables)

TABLE IV

Evolution of between-state distinction. Means of differences between Active Sleep (As) and Quiet Sleep (QS): paired *t*-test.

t(AS – QS)	Premature (8)	Intermediate (8)	Full-term (8)
HF	−0 80 (NS)	−2 96*	−2 44*
MF	0 39 (NS)	0.79 (NS)	0 94 (NS)
LF	3 63*	2 84*	6 15***
RR	−2.78*	−3.00*	−4 19**

*$P \leq 0.05$.
**$P \leq 0.01$
***$P \leq 0.001$.
NS, non significant

The analysis of the contribution of each variable (r_{HF}, r_{MF}, r_{LF}) to this discrimination confirms that an opposition between HF and LF is an important feature in sleep state distinction As a matter of fact, we also performed the same analyses with only HF and LF: the results proved slightly better, which suggests that MF, which is important in age group discrimination, brings no contribution to sleep state discrimination

Discussion

In this study, we asked the question of the relevance of HRV variables to age or sleep state distinction in premature and full-term newborns, and interpreted the influence of each variable in this distinction. At the two statistical levels considered (within-individual means and all epochs of 512 heartbeats), our results demonstrate two main physiological points

Firstly, HRV parameters are highly discriminant for age, between premature and full-term newborns All HRV variables are on the increase from the premature group

TABLE V

Evolution of between-state discrimination: discriminant analyses, using HF, MF, and LF, performed on all 338 epochs of 512 heartbeats (All ages), 116 premature epochs (Premature), 91 intermediate epochs (Intermediate), and 131 full-term epochs (Full-term)

Age group	Linear Discr.	Mahalanobis Distance	r_{HF}	r_{MF}	r_{LF}
All ages	77%	1 90	−0 66	0 16	0 57
Premature	71%	0 84	−0 33	0 24	0 76
Intermediate	76%	2.73	−0.86	−0 05	0 26
Full-term	82%	3 32	−0 80	0 16	0.68

(Linear Discr.: percentages of well-classified epochs globally or within one given age group; Mahalanobis Distance (between the centres of gravity of groups), a complementary measure of the quality of discrimination; r_{HF}, r_{MF}, r_{LF}, correlation coefficients of Discriminant Linear Function with HRV variables)

(31–36 weeks CA) to the full-term group (39–41 weeks CA), but HF undergoes a rather steep increase from the premature to the intermediate group, remaining relatively stable afterwards, whereas LF grows more regularly from 31 to 41 weeks CA. Since HF reflects only vagal tone, and LF both vagal and sympathetic tones, this is in favour of an important increase of vagal tone at 37 and 38 weeks, with a slower growth afterwards, and of a more constant increase of sympathetic tone from 31 to 41 weeks.

Secondly, concerning sleep organization, we found that according to HRV parameters, sleep states may be discriminated better and better as CA increases, to reach satisfying levels of discrimination (over 80% well-classified epochs) in the full-term group. Between-age differences at hypothesis tests are higher in AS than in QS. This suggests an earlier differentiation of AS, as compared to QS, which is in agreement with previous findings [8,10]. But since significant differences between sleep states in prematures are found only in LF, (higher in AS than in QS), this also suggests earlier maturation of sympathetic heart rate control during AS, HF (lower in AS than in QS) becoming more discriminant later, from 37 weeks on.

This second point is coherent with the first one, developed above, and also with previous findings by Baldzer et al. [4], who used the opposition between LF and Respiratory Sinus Arrhythmia (which is carried by HF) as a parameter for separation in two groups of healthy neonates, and speculated on a later postnatal development of the parasympathetic system as compared to the sympathetic system. From this point of view, we can also suggest an interpretation for the second factor of our Principal Component Analysis, roughly speaking 'HF–LF', higher in full-term newborns than in prematures, and higher in QS than in AS: it may be closely related to vagal tone.

Our results should be compared very cautiously with previous studies on the same subject, since our subjects are healthy premature and full-term neonates recorded in the first days of life, whereas in previous studies, infants were investigated at different postnatal ages [4], QS only being taken into account [1,4], or total HRV only studied [21]. Especially, comparison with interesting results of Harper, Schechtman et al., whose frequency bands are comparable with ours [16,34], may be partially inadequate because of differences in the ages investigated: they studied infants between 1 week and 6 months of age, and while our results may be compared with theirs for 1 week old newborns, this comparison is no more valid in older infants, because of probable fast modifications of autonomic control during the first weeks of postnatal age.

Regarding statistical analysis:

- The relatively small number of subjects in each group (8) is due to the difficulty to find completely healthy newborn babies in the premature group, and we did not want to unbalance our age groups.
- We confirmed the validity of results obtained at parametric tests by performing equivalent non-parametric tests on the same data (Mann-Whitney and Wilcoxon for *t*-test, Kruskal-Wallis for ANOVA): the levels of significance were the same.
- Linear discriminant analysis, which theoretically assumes normality, is robust enough to tolerate violations of the normality assumption [25,26].

- The two levels of statistical processing presented in this study are complementary, and, to our meaning, not interchangeable: apparently good results which would be obtained from hypothesis tests on the set of all epochs, or from discriminant analyses on the set of within-individual means, would be delusive, either forgetting possible non-independence of observations, or considering too few statistical individuals
- To examine a possible dependence of some of the HRV variables upon heart rate, we adjusted them for RR [24], performing Principal Component Analysis and 2-way ANOVA on the same data, but using quotients HF/RR, MF/RR, and LF/RR. The distribution of age and sleep state groups within the statistical cloud was not considerably changed, and levels of significance at Fisher's test were only slightly modified (NS remaining NS, and the other ones remaining at $P \leq 0.01$)

Conclusions

Different statistical approaches converge to sketch the same description of early ANS maturation: a strong enhancement in vagal tone at 37–38 weeks CA, with a relative stability afterwards, and a more constant increase in sympathetic tone from 31 to 41 weeks. These approaches rest mainly on HF and LF, which are the most significant HRV variables and are sufficient to describe maturation of the ANS in normal neonates, premature and full-term

The method of analysis presented here has shown appropriate for studying normal maturation of the ANS, and we purpose to use it now to study heart rate control by the ANS in at-risk and pathological newborns and infants

Acknowledgements

L.C.-D. was supported by grants RGR62 INSERM-CNAMTS and INSERM CJF8909, and C.L. was a visiting student during summer 1990 from the Harvard-MIT Division of Health Sciences and Technology, Cambridge, MA, U.S.A. We are gratefully indebted to Prof. Cl. Gaultier for helping revising the manuscript

References

1 Äärimaa, T., Oja, R., Antila K. and Välimäki, I. (1988): Interaction of heart rate and respiration in newborn babies. Pediatr. Res., 24, 745–750.

2 Antila, K.J., Välimäki, I.A.T., Mäkelä, M., Tuominen, J., Wilson, A.J. and Southall, D.P. (1990): Heart rate variability in infants subsequently suffering sudden infant death syndrome (SIDS). Early Hum. Dev., 22: 57–72.

3 Akselrod, S., Gordon, D., Ubel, F.A., Shannon, D.C., Barger, A.C. and Cohen, R.J. (1981): Power spectrum analysis of heart rate fluctuation: a quantitative probe of beat to beat cardiovascular control. Science, 213: 220–222.

4 Baldzer, K., Dykes, F.D., Jones, S.A., Brogan, M., Carrigan, T.A. and Giddens, D.P. (1989): Heart rate variability analysis in full-term infants: spectral indices for study of neonatal cardiorespiratory control. Pediatr. Res., 26, 188–195.

5 Celeux, G., Diday, E., Govaert, G., Lechevallier, Y. and Ralambondrainy, H. (1989): L'analyse, discriminante. In: Classification Automatique des Données, Ch. 4, pp. 237–275. Dunod, Paris

6 Celeux, G. (1990): Règles statistiques de décision In: Analyse Discriminante sur Variables Continues, pp. 15–36. Editor: G Celeux INRIA, Rocquencourt, France

7 Chess G.F., Tam, R M.K. and Calaresu. F R (1975): Influence of cardiac neural inputs on rhythmic variations of heart period in the cat Am. J. Physiol., 228, 775–780

8 Curzi-Dascalova, L., Peirano, P and Morel-Kahn, F. (1988): Development of sleep states in normal premature and full-term newborns Dev Psychobiol, 21. 431–444.

9 Curzi-Dascalova, L., (1990): Sleep and respiratory control development during the first months of life Ergebn. Exp Med., 53, 137–152

10 Curzi-Dascalova, L., Clairambault, J Kauffmann P, Médigue, C. and Peirano, P. (1991): Cardiorespiratory variability and development of sleep state organization In: Sleep and Cardiorespiratory Control, pp. 155–163. Editors: C Gaultier., P Escourrou, L Curzi-Dascalova. John Libbey, London.

11 Dreyfus-Brisac, C (1979): Ontogenesis of the brain bioelectrical activity and sleep organization in neonates and infants. In: Human Growth, a Comprehensive Treatise, pp 157–182 Editors: F. Falkner, J.M. Tanner Plenum Press, New York

12 Giddens, D.P. and Kitney, R.I. (1985): Neonatal heart rate variability and its relation to respiration J. Theor Biol., 113, 759–780.

13 Gordon, D, Cohen, R J, Kelly, D, Akselrod, S and Shannon, D C (1984): Sudden infant death syndrome: abnormalities in short term fluctuations in heart rate and respiratory activity Pediatr Res, 18: 921–926.

14 Gordon, D., Southall, D P, Kelly D H, Wilson, A., Akselrod, S, Richards, J., Kenet, B., Kenet, R., Cohen, R J. and Shannon, D C. (1986): Analysis of heart rate and respiratory patterns in sudden infant death syndrome victims and control infants. Pediatr. Res., 20: 680–684

15 Harper, R.M., Walter, D.O., Leake, B, Hoffmann, H J., Sieck, G.C., Sterman, M.B, Hoppenbrouwers, T. and Hodgman, J (1978): Development of sinus arrhythmia during sleeping and waking states in normal infants Sleep, 1. 33–48

16 Harper, R.M., Schechtman, V L. and Kluge, K A (1987): Machine classification of infant sleep state using cardiorespiratory measures. Electroencephalogr. Clin Neurophysiol., 67, 379–387.

17 Hathorn, M K S. (1987): Respiratory sinus arrhythmia in newborn infants J Physiol (London) 385, 1–12

18 Hathorn. M.K.S. (1989): Respiratory modulation of heart rate in newborn infants Early Hum Dev, 20, 81–99.

19 Hirsch, J A. and Bishop, B (1981): Respiratory sinus arrhythmia in humans: how breathing pattern modulates heart rate Am. J. Physiol., 241. H620–H629.

20 Katona, P G and Jih, F. (1975): Respiratory sinus arrhythmia: non invasive measure of parasympathetic control. J Appl Physiol., 39, 801–805.

21 Katona, P.G, Frasz, A. and Egbert, J. (1980): Maturation of cardiac control in full-term and preterm infants during sleep Early Hum Dev, 4, 145–159.

22 Kauffmann, F, Clairambault, J. and Médigue, C (1991): Un système d'analyse des signaux biomédicaux. Bull. Liaison Rech. Inf. Autom., (INRIA), 131, 38–41

23 Kauffmann, F and Cauchemez, B (1991): Extraction of cardiorespiratory parameters In: Sleep and Cardiorespiratory Control, pp 105–112. Editors: C Gaultier, P Escourrou and L Curzi-Dascalova. John Libbey, London

24 Kluge, K A, Harper, R.M, Schechtman, V L., Wilson, A J, Hoffman, H J and Southall, D P (1988): Spectral Analysis assessment of respiratory sinus arrhythmia in normal infants and infants who subsequently died of sudden infant death syndrome. Pediatr. Res, 24, 677–682

25 Krzanowski, W.J. (1977): The performance of Fisher's linear discriminant function under non-optimal conditions Technometrics, 19 191–200

26 Lachenbruch, P.A (1975): Discriminant Analysis, Ch 7, Hafner Press, MacMillan Publishing Co

27 McLachlan, G J (1986): Assessing the performance of an allocation rule Comput Math Appl 12A, 261–272

28 Nawab, S H and Quatieri, T.F. (1988): Short-Time Fourier Transform. In: Advanced topics in signal processing, pp. 289–337. Editors: J S. Lim, A V Oppenheim. Prentice-Hall, Englewood Cliffs, New Jersey

29 Pomeranz, B., Macaulay, R.J.B., Caudill, M.A., Kutz, I., Adam, D., Gordon, D., Kilborn, K.M., Barger, A.C., Shannon, D.C., Cohen, R.J. and Benson, H. (1985): Assessment of autonomic function in humans by heart rate spectral analysis. Am. J. Physiol., 248, H151–H153.

30 Rosenblueth, A. and Simeone, F.A. (1934): The interrelations of vagal and accelerator effects on the cardiac rate. Am. J. Physiol., 110, 42–55.

31 Rother, M., Zwiener, U., Eiselt, M., Witte, H., Zwacka, G. and Frenzel, J. (1987): Differentiation of healthy newborns and newborns-at-risk by spectral analysis of heart rate fluctuations and respiratory movements. Early Hum. Dev., 15, 349–363.

32 Sayers, B.McA. (1973): Analysis of heart rate variability. Ergonomics, 16, 85–97.

33 Schechtman, V.L., Kluge, K.A. and Harper, R.M. (1988): Time-domain system for assessing variation in heart rate. Med. Biol. Eng. Comput., 26, 367–373.

34 Schechtman, V.L., Harper, R.M. and Kluge, K.A. (1989): Development of heart rate variation over the first 6 months of life in normal infants. Pediatr. Res., 26, 343–346.

35 Schechtman, V.L., Harper, R.M., Kluge, K.A., Wilson, A.J., Hoffman, H.J. and Southall, D.P. (1989): Heart rate variation in normal infants and victims of the sudden infant death syndrome. Early Hum. Dev., 19, 167–181.

36 Schechtman, V.L., Harper, R.M., Kluge, K.A., Wilson, A.J. and Southall, D.P. (1990): Correlations between cardiorespiratory measures in normal infants and victims of sudden infant death syndrome. Sleep, 13, 304–317.

37 Shaw-Jyh Shin (1989): Assessment of autonomic regulation of heart rate variability by the method of complex demodulation. IEEE Trans. Biomed. Eng., 36, 274–283.

38 Siimes, A.S.I., Välimäki, I.A.I., Antila, K.J., Julkunen, M.K.A., Metsala, T.H., Halkola, L.T. and Sarajas, H.S.S. (1990): Regulation of Heart Rate Variation by the Autonomic Nervous System in Neonatal Lambs. Pediatr. Res., 27, 383–391.

39 Spyer, K.M. (1991): Functional organization of cardiorespiratory control. In: Sleep and Cardiorespiratory Control, pp. 3–8. Editors: C. Gaultier, P. Escourrou and L. Curzi-Dascalova. John Libbey, London.

40 Wilson, A.J., Stevens, V., Franks, C.I., Alexander, J. and Southall, D.P. (1985): Respiratory and heart rate patterns in infants destined to be victims of sudden infant death syndrome: average rates and their variability measured over 24 h. Br. Med. J., 290, 497–501.

Estimation de chaînes de Markov cachées : méthodes et problèmes

Gilles Celeux, Jean Clairambault
INRIA Rocquencourt

Résumé

Nous présentons les principaux algorithmes d'identification des chaînes de Markov cachées : algorithmes de Baum, de Viterbi, estimation bayésienne, utilisation de l'échantillonnage de Gibbs. Nous mettons l'accent sur l'interprétation des chaînes de Markov cachées comme un modèle de mélange de lois de probabilité où les observations sont dépendantes, et sur le fait que le problème statistique posé est un problème à données incomplètes. Les caractéristiques de ces différentes méthodes sont comparées. Nous présentons une application ayant trait à l'analyse du rythme cardiaque de nouveau-nés réalisée à l'aide du langage synchrone SIGNAL.

Mots clés : Mélange de lois, dépendance markovienne, algorithmes de restauration-maximisation, rythme cardiaque.

Abstract

We present the main estimation procedures of Hidden Markov Chains: Baum forward-backward algorithm, Viterbi algorithm, Bayesian estimation and methods using Gibbs sampling. We interpret Hidden Markov Chains as mixtures with dependent data. We regard the statistical problem as an incomplete data model. The characteristics of the methods are discussed. An application, tackled with the synchronous language SIGNAL, concerning heart rate variability of neonates, is presented.

Keywords: Mixture, Markovian dependence, restoration-maximization algorithms, heart rate variability.

1 Le modèle

Soit un processus observé $x_1, ..., x_N$ à valeurs dans $\mathbb{R}^s$ et un processus caché $z_1, ..., z_N$ à valeurs dans $\{1, ..., k\}$ tels que

- les z_i forment une chaîne de Markov homogène et irréductible de matrice de transition $\mathbf{T} = (t_{j\ell} = P(z_{i+1} = \ell | z_i = j))$ et de distribution stationnaire $(p_\ell, \ell = 1, ..., k)(0 < p_\ell < 1)$,
- les x_i sont indépendants conditionnellement aux z_i,
- si $z_i = \ell, x_i$ suit une loi de densité $\phi(x_i|\theta_\ell)$ appartenant à une famille paramétrée. (Par exemple, $\phi(.|\theta)$ est la densité d'une loi normale et $\theta = (\mu, \sigma)$, μ étant la moyenne de la loi et σ sa matrice variance.)

Il s'ensuit que les x_i suivent la loi de densité

$$f(x) = \sum_{\ell=1}^{k} p_\ell \phi(x|\theta_\ell). \tag{1}$$

Ainsi le modèle des chaînes de Markov cachées est un modèle de mélanges pour lequel la traditionnelle hypothèse d'indépendance des données observées $x_1, ..., x_n$ a été remplacée par une hypothèse de dépendance markovienne.

Le problème est d'estimer les paramètres $(\theta_\ell, \ell = 1, ..., k)$, la matrice de transition de la chaîne de Markov cachée $\mathbf{T} = (t_{j\ell}, j = 1, ..., k; \ell = 1, ..., k)$ et sa probabilité stationnaire $(p_\ell, \ell = 1, ..., k)$. Avant de nous intéresser à ce problème, signalons que le modèle de chaînes de Markov cachées (CMC) dont la première étude significative est due à Baum, Petrie, Soulie et Weiss [BAU 70], est devenu un modèle des plus classiques en reconnaissance de la parole (cf., par exemple, [RAB 85], [GUC 90], [JUR 91] ou [AND 92], et, pour un état de l'art récent [GUE 92]). A l'heure actuelle, des applications dans de nombreux domaines se multiplient : données neurophysiologiques ([ALB 91], [LLP 92]), analyse de la structure de l'ADN ([CHU 89],... Quant au présent article, il contient une application à l'analyse du rythme cardiaque du nouveau-né.

2 Algorithmes de restauration-maximisation

Le modèle des CMC rentre typiquement dans les modèles où les données complètes $\mathbf{y} = (y_1, ..., n)$ de densité $g(\mathbf{y}|\eta)$ se décomposent en données observées $\mathbf{x} = (x_1, ..., x_m)$ de densité $f(\mathbf{x}|\eta)$ et en données manquantes $\mathbf{z} = (z_1, ..., z_p)$ (ici, on a $m = p = n$) de densité conditionnelle

$$k(\mathbf{z}|\mathbf{x}, \eta) = \frac{g(\mathbf{y}|\eta)}{f(\mathbf{x}|\eta)}, \tag{2}$$

avec $\mathbf{y} = (\mathbf{x}, \mathbf{z})$. Le fait que les données soient incomplètes rend souvent l'estimation par le maximum de vraisemblance du paramètre η difficile et a

conduit au développement d'algorithmes de *restauration-maximisation* (cf. [QIT 91]) qui fonctionnent comme suit. Partant de η^0, ils utilisent deux étapes :
Restauration : "donner" des valeurs $\mathbf{z}^m$ aux données manquantes sachant $\eta = \eta^m$.
Maximisation : trouver η^{m+1} qui maximise la vraisemblance complétée $g(\mathbf{y}^m|\eta)$ où $\mathbf{y}^m = (\mathbf{x}, \mathbf{z}^m)$.

Fondamentalement, les algorithmes diffèrent par leurs stratégies de restauration dont les principales sont décrites maintenant. Les valeurs manquantes sont remplacées par :

- leur espérance conditionnelle sachant $\mathbf{x}$ et η^m. C'est la stratégie de l'algorithme EM [DLR 77], qui conduit, à chaque itération, à calculer η^{m+1} qui maximise $E[log\ g(\mathbf{y}|.)|\mathbf{x}, \eta^m]$.

- leur valeur la plus probable sachant $\mathbf{x}$ et η^m. Cette stratégie est celle des algorithmes du MAP (maximum a posteriori).

- tirage(s) aléatoire(s) suivant la loi conditionnelle $k(\mathbf{z}|\mathbf{x}, \eta^m)$. C'est la stratégie de l'algorithme SEM [CED 85] où les z_i^m sont issus d'un seul tirage à chaque itération et celle de l'algorithme MCEM [WET 90] où les z_i^m sont obtenus comme moyenne de r tirages aléatoires (r augmentant en général avec le numéro d'itération).

Dans le cadre des CMC, l'algorithme EM, proposé par [BAU 70], est connu sous le nom de *Forward-Backward algorithm* et l'algorithme du MAP est connu sous le nom d'*algorithme de Viterbi*. Notons que l'algorithme du MAP est simplement un algorithme de classification de type nuées dynamiques dans le cadre de mélanges indépendants et l'algorithme ICM de Besag [BES 86] dans le cadre des champs de Markov.

Avant de présenter les algorithmes pour les CMC, il est utile de dresser un rapide panorama de leurs propriétés théoriques et pratiques pour l'identification de mélanges indépendants. (Pour plus de détails, on pourra se reporter à [CEL 92].) C'est en effet un domaine d'investigation très étudié des algorithmes de restauration-maximisation. Et tout laisse à penser que ces caractéristiques sont également valables pour l'identification des CMC et des champs de Markov puisque ces modèles sont également des modèles de mélange.

- L'algorithme du MAP présente l'intérêt de converger en un nombre fini d'itérations et toujours rapidement. Mais il peut fournir des estimations très biaisées, même avec des échantillons de grande taille, pour peu que les paramètres θ_ℓ intervenant dans l'équation (1) soient relativement proches et surtout que les proportions p_ℓ soient assez différentes.

- L'algorithme EM fournit souvent de très bons résultats. Un théorème [REW 84] garantit sa convergence vers la solution consistante des équations de la vraisemblance si sa position initiale est assez proche de cette

solution optimale. Cependant, lorsque les composants du mélange ne sont pas très bien séparés, il fournit des estimations très dépendantes de sa position initiale et converge souvent avec une lenteur insupportable.

- L'algorithme SEM fournit des estimations faiblement dépendantes de sa position initiale. Il parvient à identifier des mélanges assez imbriqués et permet de déceler le nombre de composants du mélange si on en connaît un majorant, pour peu que l'échantillon des données observées ne soit pas trop petit. Pour de très petits échantillons, l'algorithme MCEM est plus fiable que SEM. Sous des conditions techniques assez fortes, on a montré (cf. [DIC 91]) la convergence asymptotique (lorsque n tend vers l'infini) de la loi stationnaire de la suite des estimés fournis par SEM vers une loi normale de variance finie et centrée sur l'estimateur consistant du maximum de vraisemblance.

3 Les algorithmes de Baum et de Viterbi

Nous présentons maintenant les deux algorithmes les plus répandus pour l'identification des CMC. Avant de présenter les formules de l'algorithme EM pour les CMC, il convient de signaler le résultat de consistance de l'approche du maximum de vraisemblance [LER 92] qui conforte cette approche.

Théorème ([LER 92]) *Si le mélange est identifiable*[1]*, si sa matrice de transition* $\mathbf{T}$ *est irréductible, et sous des conditions de régularité classiques (à la Wald), la suite des estimateurs du maximum de vraisemblance tend p.s. vers les vraies valeurs des paramètres du modèle des CMC.*

3.1 L'algorithme de Baum

On peut décrire ainsi l'itération m de l'algorithme EM ou algorithme forward-backward de Baum :
Etape E : l'étape de restauration revient à calculer les quantités

$$D^m_{j\ell}(i) = P(z_{i+1} = \ell, z_i = j \mid \mathbf{x}, \eta^m)(1 \leq i \leq n-1)(1 \leq j, \ell \leq k)$$

$\eta^m = (\mathbf{T}^m, \theta^m_1, \ldots, \theta^m_k)$ étant l'estimation courante des paramètres du modèle. Ces calculs reposent sur l'égalité ([BAU 70])

$$D^m_{j,\ell}(i) = \frac{F^m_i(j) t^m_{j\ell} \phi(x_{i+1}|\theta^m_\ell) B^m_{i+1}(\ell)}{f(\mathbf{x} \mid \eta^m)} \tag{3}$$

avec

$$F_i(j) = P(x_1, \ldots, x_i, z_i = j \mid \eta),$$
$$B_i(\ell) = P(x_{i+1}, \ldots, x_n \mid z_i = \ell, \eta)$$

[1]Un mélange est identifiable ssi $\sum_{j=1}^{k} p_\ell \phi(x, \theta_\ell) = \sum_{j=1}^{k'} p'_\ell \phi(x, \theta'_\ell)$ implique $k = k'$, $p_\ell = p'_\ell$ et $\theta_\ell = \theta'_\ell$ pour tout $\ell = 1, ..., k$.

et $f(\mathbf{x} \mid \eta) = \sum_{j=1}^{k} F_n(j)$.

Le calcul des F_i se fait par la procédure avant suivante :

a) $F_1^m(j) = p_j^m \phi(x_1 \mid \theta_j^m)$ $(j = 1, \ldots, k)$

b) $F_{i+1}^m(j) = \phi(x_{i+1} \mid \theta_j^m) \sum_{\ell=1}^{k} F_i^m(\ell) t_{\ell j}^m$ $(j = 1, \ldots, k)$.

Le calcul des B_i se fait par la procédure arrière suivante :

a) $B_n^m(\ell) = 1$ $(\ell = 1, \ldots, k)$.

b) $B_i^m(\ell) = \sum_{j=1}^{k} t_{\ell j}^m \phi(x_{i+1} \mid \theta_j^m) B_{i+1}^m(j)$ $(i < n)$ $(\ell = 1, \ldots, k)$.

Etape M : l'étape de maximisation conduit à calculer

$$t_{j\ell}^{m+1} = \frac{\sum_{i=1}^{n-1} D_{j\ell}^m(i)}{\sum_{i=1}^{n-1} \sum_{r=1}^{k} D_{jr}^m(i)}$$

Quant à l'estimation des θ_j^{m+1}, elle dépend bien sûr de la famille paramétrée $\phi(x|\theta)$ considérée. Par exemple, dans le cas gaussien réel, $\theta_j = (\mu_j, \sigma_j^2)$, μ_j étant la moyenne de la loi et σ_j^2 sa variance, on obtient

$$\begin{aligned} \mu_j^{m+1} &= \sum_{i=1}^{n} w_j^{m+1}(i) x_i / \sum_{i=1}^{n} w_j^{m+1}(i) \\ (\sigma_j^2)^{m+1} &= \sum_{i=1}^{n} w_j^{m+1}(i)(x_i - \mu_j^{m+1})^2 / \sum_{i=1}^{n} w_k^{m+1}(i) \end{aligned}$$

où $w_j^{m+1}(i) = \sum_{\ell=1}^{k} D_{j\ell}^{m+1}(i)$.

Enfin, les proportions du mélange sont estimées par

$$p_j^{m+1} = \frac{1}{n} \sum_{i=1}^{n} w_j^{m+1}(i).$$

La procédure avant-arrière intervenant dans l'étape E est bien sûr très lourde. De plus, elle induit très rapidement un problème d'"underflow". Aussi, en pratique, on utilise une procédure avant-arrière modifiée pour éviter ce problème. La solution la plus élégante et la plus simple consiste à travailler sur des probabilités conditionnelles (cf. [DEV 85]). On peut écrire (l'indice m d'itération est omis) :

$$D_{j\ell}(i) = \tilde{F}_i(j) t_{j\ell} \tilde{B}_i(\ell)$$

avec

$$\tilde{F}_i(j) = P(z_i = j | x_1, \ldots, x_i, \eta)$$

et

$$\tilde{B}_i(\ell) = \frac{P(x_{i+1}, \ldots, x_n | z_i, \eta)}{P(x_{i+1}, \ldots, x_n | x_1, \ldots, x_i, \eta)}.$$

Et les $\tilde{F}_i$ et les $\tilde{B}_i$ se calculent par des procédures avant et arrière analogues aux précédentes.
Procédure avant :

$$\begin{aligned}\tilde{F}_1(j) &= \frac{t_{j\ell}\phi(x_1|\theta_j)}{\sum_{\ell=1}^k p_\ell \phi(x_1|\theta_\ell)} \\ \tilde{F}_{i+1}(j) &= \frac{\sum_{\ell=1}^k \tilde{F}_i(\ell) t_{\ell j}\phi(x_{i+1}|\theta_j)}{\sum_{r=1}^k\sum_{\ell=1}^k \tilde{F}_i(\ell) t_{\ell r}\phi(x_{i+1}|\theta_r)}.\end{aligned}$$

Procédure arrière :

$$\begin{aligned}\tilde{B}_n(\ell) &= 1 \\ \tilde{B}_i(\ell) &= \frac{\sum_{j=1}^k t_{\ell j}\phi(x_{i+1}|\theta_j)\tilde{B}_{i+1}(j)}{\sum_{r=1}^k\sum_{j=1}^k \tilde{F}_i(j) t_{jr}\phi(x_{i+1}|\theta_r)} \quad (1<i<n) \\ \tilde{B}_1(\ell) &= \frac{\sum_{j=1}^k \phi(x_2|\theta_j)\tilde{B}_2(j)}{\sum_{j=1}^k p_j\phi(x_2|\theta j)}.\end{aligned}$$

3.2 L'algorithme de Viterbi

Cet algorithme est l'algorithme du MAP adapté au modèle des CMC. On décrit ainsi l'itération m de cet algorithme :

Etape C : l'étape de restauration des données manquantes est une étape de classification. On construit $\mathbf{z^m}$ par le principe du MAP. Cela donne (cf., par exemple, [JUR 91]) :

$$z_i^m = arg \max_{\ell=1,\ldots,k} t^m_{z^m_{i-1}\ell}\phi(x_i|\theta^m_\ell)t^m_{z^{m-1}_{i+1}\ell}.$$

Etape M : les termes de la matrice D^{m+1} sont calculés par la formule

$$D^{m+1}_{j\ell} = \frac{1}{n}\sum_{i=2}^n \mathbf{I}_{\{z^m_{i-1}=j,\ z^m_i=\ell\}}$$

De là, on déduit aisément l'actualisation de la matrice de transition $\mathbf{T}$, des θ_ℓ et des proportions p_ℓ par les mêmes formules que celles de l'algorithme de Baum.

Ainsi les formules de l'algorithme de Viterbi sont particulièrement simples et, de plus, cet algorithme converge rapidement. Aussi il peut être recommandé pour l'identification de CMC dont les composants du mélange sont bien séparés ou pour initialiser un algorithme comme celui de Baum. Par contre, il peut s'avérer peu fiable lorsque les composants du mélange sont assez proches. Une simulation illustrant cette caractéristique est présentée dans la section 5.

4 Deux algorithmes stochastiques

L'algorithme SEM (version stochastique naturelle de EM) peut bien sûr s'appliquer sans difficulté pour estimer les CMC. Il a d'ailleurs été utilisé avec succès pour estimer des champs de Markov en analyse d'images (cf., par exemple, [QIT 91] et [MAP 91]). Cependant, cet algorithme n'évite pas le recours à la procédure avant-arrière puisque les tirages aléatoires pour compléter les données se font suivant la loi conditionnelle donné dans la formule (2). Dans cette section, nous allons présenter deux algorithmes stochastiques qui évitent le recours à la procédure avant-arrière grâce à l'échantillonnage de Gibbs qui constitue un outil puissant pour l'approximation de calculs bayésiens. (Voir [GES 90] ou [ROB 92] chapitre 9 pour une présentation détaillée de l'échantillonnage de Gibbs.) Le premier algorithme propose ainsi une solution bayésienne pour estimer une CMC ; le second propose une utilisation de l'échantillonnage de Gibbs dans un cadre fréquentiste et permet de proposer une version stochastique de l'algorithme EM évitant la procédure avant-arrière de l'étape E.

4.1 Estimation bayésienne

Le modèle des CMC nécessite l'estimation de nombreux paramètres. Aussi, l'initialisation des algorithmes est un point sensible pour une bonne estimation des CMC. En règle générale, il vaut mieux partir d'une position proche des bonnes valeurs des paramètres et faire si possible usage des informations a priori disponibles... Ce qui invite à une analyse bayésienne des CMC. Cette analyse a été réalisée par [RCD 92a] et nous la résumons ici.

On suppose que les densités $\phi(x|\theta)$ appartiennent à une famille exponentielle : $\phi(x|\theta) = h(x)\exp(\theta.t(x) - \psi(\theta))$. De la sorte, il existe une loi a priori conjuguée, $\pi(\theta)$, pour θ. On considère que les colonnes $\mathbf{t}_j$ de la matrice de transition $\mathbf{T}$ suivent des lois a priori de Dirichlet indépendantes $\mathcal{D}(\alpha_1^j, \ldots, \alpha_k^j)$.

Dans ce cadre, la loi a posteriori de $\eta = (\theta_1, \ldots, \theta_k, \mathbf{T})$ est

$$\begin{aligned}\pi(\eta|\mathbf{x}) \quad \propto & \Big(\textstyle\sum_{i_2=1}^k \ldots \sum_{i_n=1}^k t_{1,i_2}\phi(x_2|\theta_{i_2}) \ldots t_{i_{n-1},i_n}\phi(x_n|\theta_{i_n}) \Big) \\ & \phi(x_1|\theta_1) \textstyle\prod_{j=1}^k \Big\{ \pi(\theta_j) \Big(\prod_{\ell=1}^k t_{j,\ell}^{\alpha_\ell^j - 1} \Big) \Big\} \end{aligned} \tag{4}$$

Elle est incalculable car elle comporte une somme de k^{n-1} termes. Mais la loi a posteriori conditionnelle $\pi(\eta|\mathbf{x}, \mathbf{z})$ est plus simple :

$$\pi(\eta|\mathbf{x}, \mathbf{z}) \propto \prod_{j=1}^k \Big\{ \pi(\theta_j) \Big(\prod_{\ell=1}^k t_{k,\ell}^{\alpha_\ell^j - 1} \Big) \Big\} \Big\{ \prod_{i=2}^n t_{z_{i-1},z_i} \phi(x_i|\theta_{z_i}) \Big\} \phi(x_1|\theta_1).$$

Ainsi la loi conditionnelle de $\mathbf{t}_j = (t_{j,1}, \ldots, t_{j,k})$:

$$\mathbf{t}_j \sim \mathcal{D}\Big(\alpha_1^j + \sum_{i=2}^n \mathbf{I}_{\{z_{i-1}=j\}}\mathbf{I}_{\{z_i=1\}}, \ldots, \alpha_k^j + \sum_{i=2}^n \mathbf{I}_{\{z_{i-1}=j\}}\mathbf{I}_{\{z_i=k\}} \Big) \tag{5}$$

est facile à simuler. De même, par exemple, si la loi de $\phi(x|\theta_j)$ est une loi normale $\mathcal{N}(\theta_j, 1)$ et si la loi a priori conjuguée est une loi normale $\mathcal{N}(\mu_j, 1)$, on a

$$\theta_j|\mathbf{x}, \mathbf{z} \sim \mathcal{N}\Big(\frac{\sum_{i=1}^n \mathbf{I}_{\{z_i=j\}} x_i + \mu_j}{\sum_{i=1}^n \mathbf{I}_{\{z_i=j\}} + 1}, \frac{\sum_{i=1}^n \mathbf{I}_{\{z_i=j\}}}{\sum_{i=1}^n \mathbf{I}_{\{z_i=j\}} + 1}\Big). \tag{6}$$

Par ailleurs, pour éviter la procédure avant-arrière, on raisonne de même sur la loi conditionnelle de z_i sachant "le reste"

$$\begin{aligned} f(z_i|\mathbf{x}, \eta, z_{j\neq i}) &= f(z_i|x_i, \eta, z_{i-1}, z_{i+1}) \\ &= \frac{t_{z_{i-1},z_i}\, \phi(x_i|\theta_{z_i})\, t_{z_i,z_{i+1}}}{\sum_{j=1}^k t_{z_{i-1},j}\, \phi(x_i|\theta_j)\, t_{j,z_{i+1}}} \\ f(z_n|\mathbf{x}, \eta, z_{j<n}) &\propto t_{z_{n-1},z_n} \phi(x_n|\theta_{z_n}). \end{aligned} \tag{7}$$

Partant de ces équations, on peut utiliser l'échantillonnage de Gibbs pour, à partir d'un vecteur d'état $\mathbf{z}^0$, simuler η^m selon les équations (5) et (6), puis simuler $\mathbf{z}^m$ selon (7). On construit ainsi une chaîne de Markov ergodique $(\eta^m, \mathbf{z}^m)$ dont l'unique densité stationnaire est $\pi(\eta, \mathbf{z}|\mathbf{x})$. De plus, on a le théorème suivant :

Théorème [RCD 92a] *(i) Il existe des constantes $C > 0$ and $0 \leq \varrho < 1$ telles que, quel que soit η^0,*

$$||\pi^m(\cdot) - \pi(\cdot|\mathbf{x})||_1 \leq C\varrho^m.$$

(ii) Pour toute fonction $h(\eta)$ telle que $\mathbf{E}^\pi[|h(\eta)|\,|\mathbf{x}] < +\infty$ et quel que soit $\pi^0(\eta)$, il existe une constante $C' > 0$ telles que

$$|\mathbf{E}^{\pi^m}[h(\eta)] - \mathbf{E}^\pi[h(\eta)|\mathbf{x}]| \leq C'\varrho^m.$$

(iii) Le processus (θ^m) est géométriquement φ-mélangeant.

4.2 EM à la Gibbs

Afin de proposer une version stochastique de EM qui évite la procédure avant-arrière de l'étape E, un algorithme dénommé EM à la Gibbs, qui adapte l'échantillonnage de Gibbs au cadre fréquentiste pour simuler les données manquantes $\mathbf{z}$ à chaque itération, a été conçu [RCD 92b]. Cet algorithme fonctionne ainsi : partant d'une position initiale η^0, le vecteur $\mathbf{z}^m$ est simulé selon la loi de probabilité définie par (7). L'actualisation de η^m dans l'étape de maximisation est identique à celle de l'algorihme de Viterbi (ou de l'algorithme SEM).

Toutefois on doit signaler une précaution numérique. Du fait que $\mathbf{z}^m$ est tiré au hasard, il se peut que des élements de la matrice $\mathbf{T}^{m+1}$ soient nuls. Et dans ce cas ils resteront nuls et la chaîne $\mathbf{z}^m$ ne sera plus irréductible. Pour éviter cela, on stabilise l'estimation de la matrice $\mathbf{T}$ en utilisant la formule

$$p_{j,\ell}^{(m+1)} = \frac{\alpha + \sum_{i=2}^n \mathbf{I}_{\{z_{i-1}^m=j\}} \mathbf{I}_{\{z_i^m=\ell\}}}{\sum_{i=2}^n \mathbf{I}_{\{z_{i-1}^m=j\}} + n\alpha}$$

où α est un nombre positif à choisir petit devant n. De plus, cette modification dans le calcul de $\mathbf{T}^m$ permet d'assurer le théorème suivant :

Théorème [RCD 92b] *La chaîne de Markov* $(\mathbf{z}^m)$ *engendrée par l'algorithme EM à la Gibbs est uniformément géométriquement ergodique et possède une distribution stationnaire unique.*

Ce théorème ne renseigne pas sur la nature de cette distribution stationnaire. On peut conjecturer, et cela est confirmé par la pratique (cf. section 5), que cette distribution se concentre autour de l'estimateur du maximum de vraisemblance. Ainsi l'algorithme EM à la Gibbs apparait comme une version de SEM spécialement adaptée au cadre des CMC.

5 Illustrations

Nous avons programmé deux des algorithmes étudiés plus haut : l'algorithme du MAP (ou de Viterbi) et l'algorithme "EM à la Gibbs" en langage SIGNAL. En effet, SIGNAL est un langage flot-de-données, parallèle et synchrone, conçu pour des applications en temps réel, et notre but à terme est d'identifier sur des fenêtres de taille fixe, en temps réel, des états cachés gouvernant une variable observée.

5.1 Simulations

Dans cette première étude, nous avons testé ces programmes sur une seule fenêtre de 4096 points. La figure 1 illustre les performances de ces deux algorithmes sur un signal simulé, mélange de deux gaussiennes $\mathcal{N}(10, 4)$ et $\mathcal{N}(12, 4)$ suivant une variable d'état simple ne prenant que deux valeurs.

L'algorithme de Viterbi atteint très rapidement (en 20 itérations) un état stationnaire, mais l'identification des paramètres et de la variable d'état est peu satisfaisante : 908 erreurs sur 4096 pour la variable d'état, les lois estimées sont $\mathcal{N}(9.82, 3.06)$ au lieu de $\mathcal{N}(10, 4)$, $\mathcal{N}(12.75, 2.43)$ au lieu de $\mathcal{N}(12, 4)$, et les probabilités de persistante dans un état sont 0.90 et 0.83, au lieu de 0.999... pour les deux états. On retrouve ici la tendance des algorithmes du MAP à surestimer les différences entre moyennes et à sous-estimer les variances (cf. [CEL 92]). En revanche, EM à la Gibbs converge plus lentement, mais très sûrement : on peut voir sur la figure 1 que l'identification est déjà bonne dès 50 itérations, et qu'elle est presque parfaite après 1600 itérations (il subsiste des erreurs d'identification, 38 valeurs erronées sur 4096, aux changements d'état). Les estimations des paramètres[1] : $\mathcal{N}(10.01, 3.89)$ et $\mathcal{N}(11.92, 3.94)$ pour les lois, 0.9991 et 0.9995 pour les probabilités de rester dans un état sont également très satisfaisantes.

[1]Dans cette version, les estimations sont obtenues par un passage d'une itération de Viterbi à l'issue des itérations de EM à la Gibbs.

Signalons que les paramètres ont été initialisés ici à des valeurs ($\mathcal{N}(8,3)$, $\mathcal{N}(14,2)$, 0.98 et 0.99 pour les probabilités de non-transition) pas exagérément éloignées des vraies valeurs, mais que d'autres simulations ont montré qu'EM à la Gibbs supporte des perturbations importantes de ces valeurs initiales, tandis que l'algorithme de Viterbi ne donne plus que des performances très médiocres quand ces valeurs initiales s'éloignent trop des valeurs à identifier.

5.2 Application à l'étude du rythme cardiaque

L'application de modèles de Markov cachés à l'étude de signaux d'origine biologique n'est pas une nouveauté, mais, à notre connaissance, rien n'avait été tenté jusqu'ici sur le rythme cardiaque.

Et pourtant il est depuis longtemps connu que la variabilité du rythme cardiaque est un indicateur de l'état du système nerveux autonome, utilisé notamment en gynécologie-obstétrique (surveillance du bien-être fœtal), en diabétologie (recherche de neuropathie diabétique), et bien sûr en cardiologie (surveillance des sujets à risque de mort subite, après un infarctus du myocarde par exemple). Le système nerveux autonome est subdivisé en deux branches : une branche dite sympathique, cardioaccélératrice, responsable des fluctuations de basse fréquence du rythme cardiaque, et une branche parasympathique, cardiomodératrice, à l'origine de la variabilité de haute fréquence qui se manifeste par un couplage de la respiration et du rythme cardiaque (arythmie sinusale respiratoire) (cf. [CLA 92]).

Il est donc tentant d'aller identifier sur le rythme cardiaque une variable cachée "état du système nerveux autonome", qu'on peut schématiquement classer en deux catégories : à prédominance sympathique ou à prédominance parasympathique.

Mais nous n'avons pas accès, à l'inverse du cas d'un signal simulé, aux "vraies" valeurs de la variable d'état. En revanche, il est connu qu'en sommeil calme, l'état du système nerveux autonome est à prédominance parasympathique, et à prédominance sympathique en sommeil agité (il s'agit du sommeil de nouveau-nés, codé en stades par des cliniciens, au vu du tracé de l'électroencéphalogramme et des mouvements oculaires rapides, donc indépendamment de l'électrocardiogramme). On trouvera sur la figure 2 un extrait de tracé du rythme cardiaque d'un nouveau-né à terme et de sa variabilité à haute fréquence (obtenue par transformation de Fourier à court terme; bande étudiée : oscillations de période allant de 3 à 8 battements). Ce tracé présente une période de forte activité à haute fréquence, encadrée par deux périodes où l'activité à basse fréquence l'emporte. Ces périodes correspondent à une période de sommeil calme encadrée par deux périodes de sommeil agité. Mais bien sûr il subsiste de l'activité à basse fréquence en sommeil calme, et de l'activité à haute fréquence en sommeil agité.

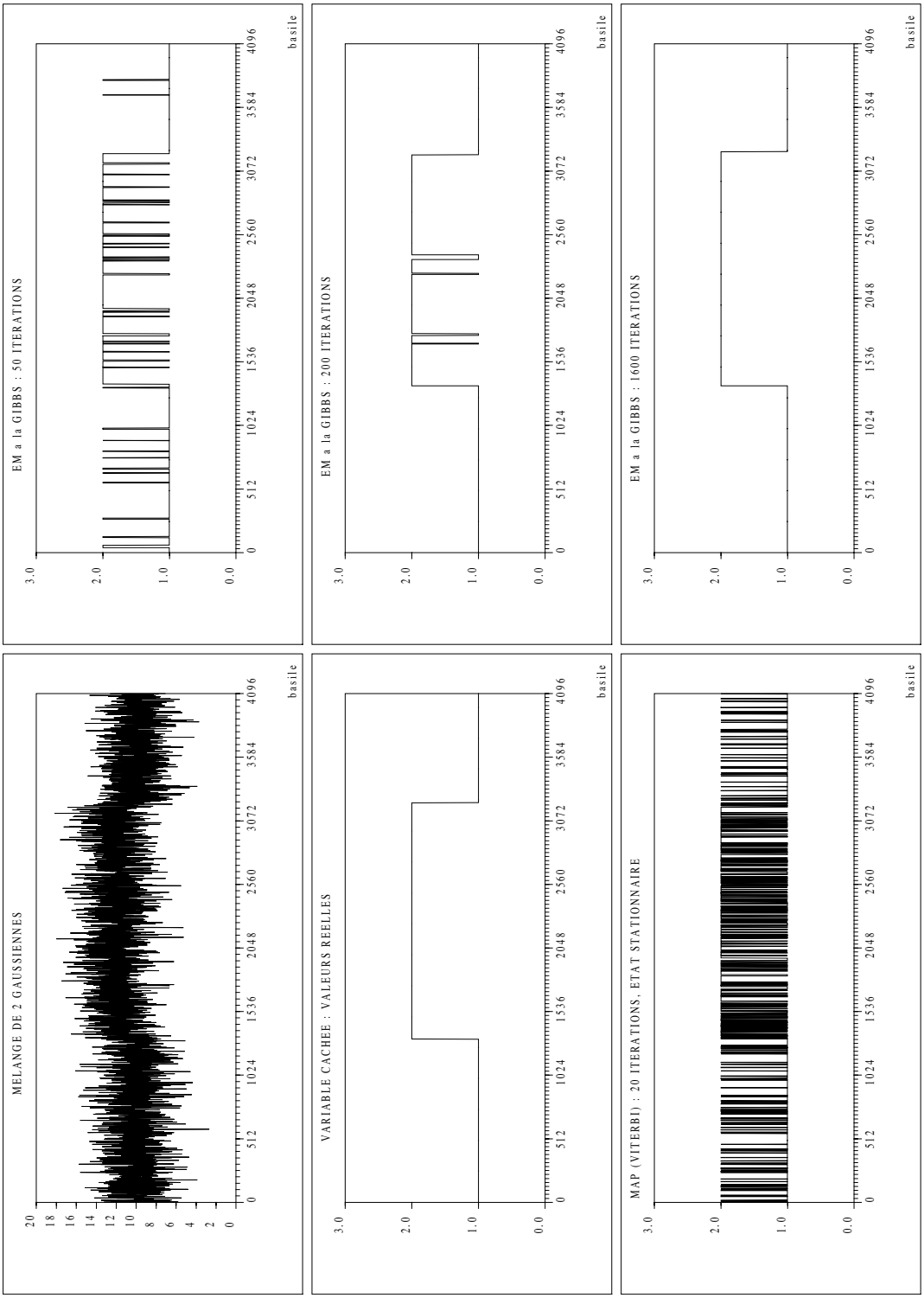

Figure 1. *Performances comparées de l'algorithme du maximum a posteriori (MAP, ou algorithme de Viterbi) et de l'algorithme EM à la Gibbs sur l'identification d'une chaîne de Markov cachée simple à deux états gouvernant un mélange de deux signaux gaussiens.*

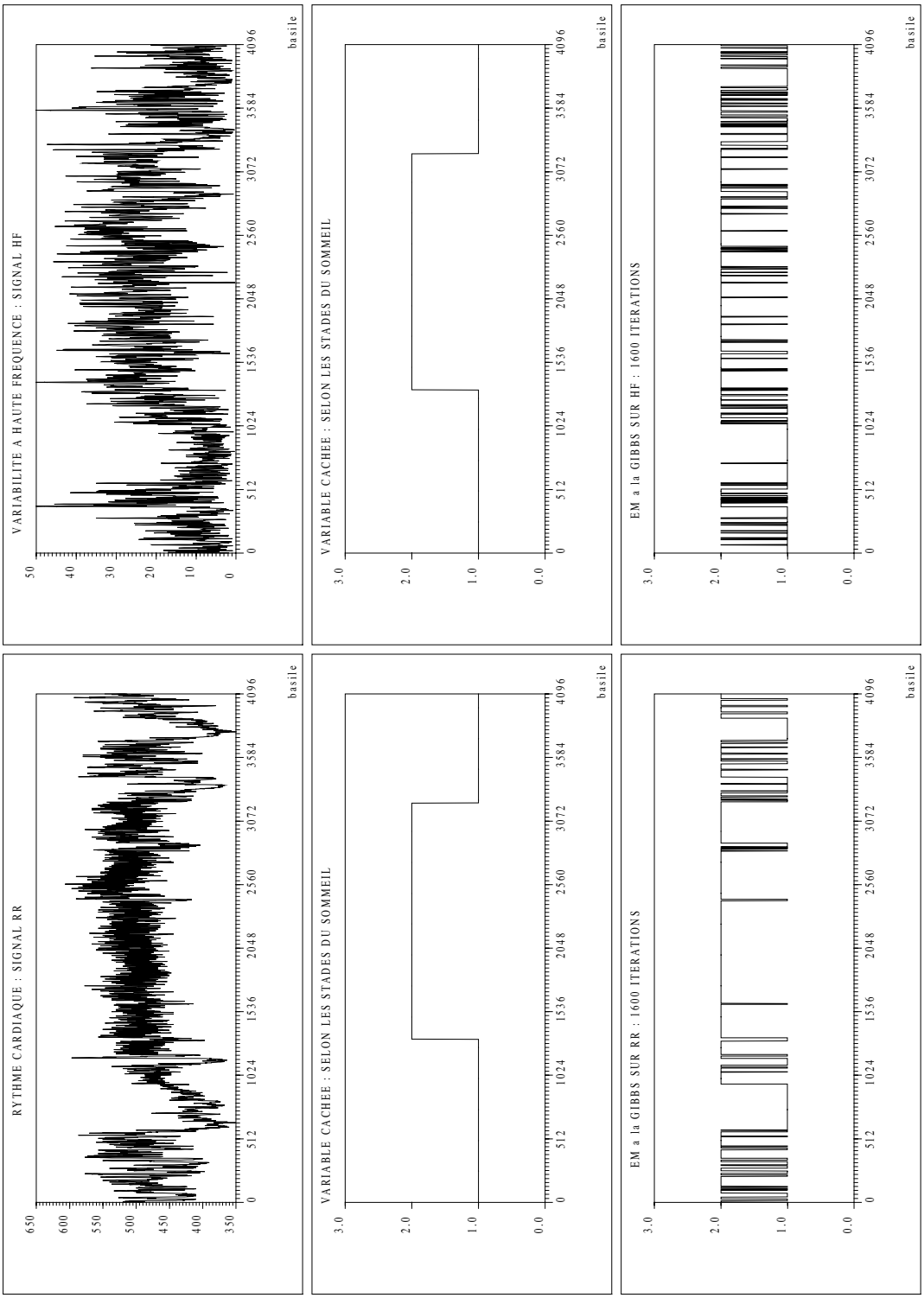

Figure 2. *Tentative d'identification par l'algorithme EM à la Gibbs d'une variable cachée contrôlant le rythme cardiaque (état sympathique vs. parasympathique du système nerveux autonome), d'une part sur le signal RR brut (à gauche), d'autre part sur le signal HF, variabilité à haute fréquence extraite par transformation de Fourier à court terme du signal RR (à droite).*

Il en résulte que l'identification sur ces tracés par l'algorithme EM à la Gibbs d'une hypothétique variable cachée est nécessairement imparfaite. Pourtant, EM à la Gibbs propose une classification du tracé en deux états qui n'est pas si éloignée du codage en stades du sommeil, et qu'une procédure de lissage prenant en compte un temps de séjour minimal dans chaque état, par exemple, permettrait sans doute d'améliorer. Après 1600 itérations de l'algorithme, il y a 2901 valeurs exactes (71%) pour l'identification sur le signal RR, et 3242 valeurs exactes (79%) pour l'identification sur le signal HF (variabilité à haute fréquence); les probabilités estimées de persistance dans un état sont de 0.963 et 0.985 sur RR, et de 0.950 et 0.962 sur HF. Ces résultats donnent à penser qu'un modèle multidimensionnel, qui prendrait en compte les signaux RR, HF, BF (variabilité à basse fréquence), pourrait améliorer encore ces résultats.

Une limitation de ce modèle, dans son état actuel, tient à sa trop grande simplicité : autant les caractéristiques statistiques du rythme cardiaque en sommeil calme sont adéquates au modèle (faible autocorrélation autorisant l'hypothèse d'indépendance, normalité), autant le sommeil agité semble polymorphe et devrait être subdivisé en plusieurs états. Une autre possibilité d'affinement de la méthode serait de remplacer (dans le cas du signal HF) l'estimation d'un modèle gaussien par un modèle de type χ^2.

Il reste aussi à évaluer, concurremment au modèle des chaînes de Markov cachées qui a été étudié ici, des méthodes autorégressives classiques de détection de rupture (cf. [BAB 86]).

Enfin une validation de la méthode par des expérimentations pharmacologiques animales (il existe des médicaments qui bloquent spécifiquement une branche ou l'autre du système nerveux autonome) semble nécessaire et reste à faire.

References

[ALB 91] ALBERT, P. S. : A two-state Markov mixture model for a time series of epilectic seizure counts. *Biometrics*, **47**, 1371-1381, 1991.

[AND 92] ANDRE-OBRECHT, R. : Utilisation des chaînes de Markov cachées en traitement de la parole. Ce volume, 1992.

[BAB 86] BASSEVILLE, M. et BENVENISTE, A. (Eds.) : Detection of abrupt changes in signals and dynamical systems. *Lecture Notes in Control and Information Sciences*, **77**. Springer Verlag, New-York, 1986.

[BAU 70] BAUM L. E., PETRIE T., SOULES G. et WEISS N. : A maximization technique occuring in the statistical analysis of probabilistic functions of Markov chains. *Ann. Math. Statistic.*, **41**, 164-171, 1970.

[BES 86] BESAG, J. : On the statistical analysis of dirty pictures (with discussion). *J.R.S.S.* B, **48**, 192-236, 1986.

[CEL 92] CELEUX, G. : Modèles probabilistes en classifcation. In *Modèles pour l'analyse des données multidimensionnelles*, (Droesbeke,J.-J., Fichet, B. et Tassi. P. éditeurs). Economica, Paris, pp. 165-214, 1992.

[CED 85] CELEUX, G. et DIEBOLT, J. : The SEM Algorithm: a probabilistic teacher algorithm derived from the EM algorithm for the mixture problem. *Computational Statistics Quaterly*, **2**, 73-82, 1985.

[CHU 89] CHURCHILL, G. : Stochastic Models for heterogeneous DNA sequences. *Bull. Math. Biol.* **51**, 79-94, 1989.

[CLA 92] CLAIRAMBAULT, J., CURZI-DASCALOVA, L., KAUFFMANN, F., MEDIGUE, C. et LEFFLER, L. : Heart rate variability in normal full-term and preterm neonates. *Early Human Development,* **28***, 169-183.* Elsevier Scientific Publishers Ireland Ltd., 1992.

[DLR 77] DEMPSTER, A., LAIRD, N. et RUBIN, D. : Maximum likelihood from incomplete data via the EM algorithm (with discussion). *J.R.S.S.* B, **39**, 1-38, 1977.

[DEV 85] DEVIJVER, P.A. : Baum's forward-backward algorithm revisited. *Pattern Recognition Letters* **3**, 369-373, 1985.

[DIC 91] DIEBOLT, J. et CELEUX G. : Asymtotic properties of a stochastic EM algorithm for estimating mixing proportions. Technical Report 228, Departement of Statistics, University of Washington, Seattle, USA, 1991.

[GES 90] GELFAND, A. et SMITH, A.F. : Sampling based approaches to calculating marginal densities. *J. American Statistical Society* **85**, 398-409, 1990.

[GUE 92] GUEDON, Y. : Review of several stochastic speech unit models. Alcatel Alsthom Recherche (soumis à publication), 1992.

[GUC 90] GUEDON, Y. et COCCOZA-THIVENT, C. : Explicit state occupancy modeling by hidden semi-Markov models: application of Derin's scheme. *Computer Speech Language* **4**, 167-192, 1990.

[JUR 91] JUANG, B.H. et RABINER, L.R. : Hidden Markov Models for Speech Recognition. *Technometrics* **33**, 251-272, 1991.

[LLP 92] LE, N. D., LEROUX B. G. et PUTERMAN M. L. : Exact likelihood in a Markov mixture model for time series of seizure counts (reader reaction). *Biometrics* **48**, 317-323, 1992.

[LER 92] LEROUX B. G. : Maximum likelihood estimation for hidden Markov models. *Stochas. Proc. and their Applications* **40**, 127-143.

[MAP 91] MASSON, P. et PIECZYNSKI, W. : Segmentation conceptuelle non surpervisée des images SPOT. *Actes de RFIA 91*, pp. 997-1002, Lyon, 1991.

[QIT 91] QIAN, W. et TITTERINGTON, D.M. : Estimation of parameters in hidden Markov models. *Phil. Trans. Roy. Soc. London* A **337**, 407-428, 1991.

[RAB 85] RABINER, L. R., JUANG, B. H., LEVINSON, S. E. et SONDHI, M.M. : Recognition of isolated digits using hidden Markov models with continuous mixture densities. *ATT Technical Journal* **64**, 1211-1234, 1985.

[REW 84] REDNER, R. A. et WALKER, H. F. : Mixture densities, maximum likelihood and the EM algorithm. *SIAM Review*, **26**, 195-239, 1984.

[ROB 92] ROBERT, C.P. : *L'analyse statistique bayésienne*. Economica, Paris, 1992.

[RCD 92a] ROBERT, C. P., CELEUX, G. et DIEBOLT J. : Bayesian estimation of hidden Markov chains: A stochastic implementation. A paraître dans *Statistics and Probability Letters*, 1992.

[RCD 92b] ROBERT, C. P., CELEUX, G. et DIEBOLT J. : Hidden Markov chains: A stochastic implementation of two estimation schemes. Rapport technique LSTA 161, Université Paris 6, 1992.

[WET 90] WEI, G.C.G. et TANNER, M. : A Monte Carlo implementation of the EM algorithm and the poor man's data augmentation algorithms. *J. American Statist. Assoc.* **85**, 699-704, 1990.

A model of the autonomic control of heart rate at the pacemaker cell level through G-proteins

Jean Clairambault

Abstract— **A mathematical model of the pacemaker cell of the mammal sinoatrial node, based upon the Yanagihara-Noma-Irisawa equations, is presented here. Its aim is to mimic the control of the pacemaker cell, as measured on the resulting heart rate, by both branches of the autonomic nervous system (ANS). It is a simplification of the original model by the suppression of some variables (but no ionic current being removed). It also uses a dynamical model of the G-proteins as actuators of this control in the system, and a construction of the sympathetic and vagal impulses, reflecting respiratory sinus arrhythmia and baroreflex influence. These characteristics make it a model compatible with what is known of the electrophysiological mechanisms of pacemaking at the single cell level, and with the observed spectral characteristics of short-term (respiratory) heart rate variability at the whole heart (electrocardiographic) level, thus partly bridging a gap between these two representation levels of the ANS.**

Keywords— **Electrophysiology, pacemaker cell, heart rate, G-proteins, autonomic nervous system**

I. Introduction

THE autonomic nervous system (ANS) has been for a long time assessed noninvasively by the analysis of heart rate variability. Spectral analysis of the RR signal evidences 2 main peaks in man and other mammals: on the one hand a high frequency one, reflecting the activity of the vagal branch of the ANS, mainly related to respiration, and neurochemically mediated by acetylcholine (ACh), and on the other hand a low frequency one, reflecting both the sympathetic branch of the ANS, strongly influenced by the baroreflex and mediated by norepinephrine (NE), and also, to a lesser extent, the vagal branch[1].

Relatively independently of these heart rate spectral analysis studies, mathematical models of the sinus node pacemaker cell have been proposed in the last 20 years. These models, among which the Yanagihara-Noma-Irisawa (YNI) model[2], usually incorporate the action of ACh on the action potential[2], [3], but seldom the action of NE. Nevertheless, recent studies have incorporated both ACh and NE, on the basis of the YNI model[4], of the Bristow-Clark model[5], or of a model involving less currents[6].

A satisfying model of the pacemaker cell incorporating the complete control by the ANS will be a major stepping stone towards an explicit model of the heart rate as a deterministic dynamical system, which might explain possible chaotic characteristics of it by bifurcation analysis studies (as in [7]), with control parameters linked to ACh and NE concentrations in the neuroeffector junction.

The author is with INRIA-Rocquencourt, B.P. 105, F78153 Le Chesnay Cedex, France. E-mail address: Jean.Clairambault@inria.fr.

II. Methods

The present model takes the YNI model as a basis; it first replaces the variables which give little contribution to the total depolarizing current (h, m, q, as evidenced by I-V plots, see e.g. [8]) by their equilibrium values, letting remain only d, f for the slow inward Ca current, p for the K current, and E for transmembrane potential as dynamic variables. It represents the actions of ACh and NE on the ionic currents by their effects on adenylate cyclase through a dynamic model of the intervention of G-proteins G_s (stimulating, NE-dependent), G_i (inhibiting, ACh-dependent) and G_k (directly active on the K_ACh channel), on the maximum intensity of currents, following ideas developed in [6]. Ach and NE concentrations are simulated according to a model recently proposed for ACh only[3]. Vagal and sympathetic pulse trains follow an original model including oscillations at fixed frequencies (respiratory and baroreflex-linked); the parameters of this last model have been tuned according to what is known of the discharge frequencies of the vagus[9] and of the sympathetic nerve[10]. No stochastic component has been included in the model. Units are milliseconds, millivolts, and nanomoles for ACh and NE concentrations.

Equations for the vagal impulse train are:

$$vag = exp(-5000{x_1}^2) \quad \text{where}$$
$$\dot{x}_1 = x_2, \qquad \dot{x}_2 = -(\tfrac{2\pi(6.5+3.5x_3)}{1000})^2 x_1,$$
$$\dot{x}_3 = x_4, \qquad \dot{x}_4 = -(\tfrac{2\pi\nu_R}{1000})^2 x_3,$$

with $\nu_R = 0.25$ Hz (respiratory frequency). Similar equations were designed for the sympathetic, with other parameters, including a baroreflex-linked frequency $\nu_B = 0.1Hz$.

The vagal impulse train is then used as input to the abovementioned model proposed for ACh[3] (2 more first-order equations, one for the releasable pool of ACh, one for free ACh concentration). The same is done for NE, with different parameters; but in this case, a presynaptic inhibiting factor ($\frac{80}{80+[ACh]}$, as in [6]) modulates the equilibrium value in the 1st-order differential equation for [NE]. Fixed parameters (to be identified) are the maximum increase in [ACh] and [NE] at each vagal or sympathetic pulse.

Then, as in [6], the resulting values of [ACh] and [NE] influence the equilibrium values G_∞ of G_s, G_i, G_k in the 3 1st-order equations $\dot{G} = \alpha(G_\infty - G)$, with time constants: $\alpha_s = 10^{-4}, \alpha_i = 5.10^{-4}, \alpha_k = 10^{-2}$.

Equilibrium values are represented homographically as: $G_{\infty,s} = \frac{[NE]+A_sK_s}{[NE]+K_s}$, $G_{\infty,i} = \frac{[ACh]}{[ACh]+K_i}$, $G_{\infty,k} = \frac{[ACh]A_k}{[ACh]+K_k}$, $A_s = 0.12$, $K_s = 600$, $K_i = 150$, $A_k = 0.6$, $K_k = 2100$.

Some of the numerical constants come from [6], others have been changed to adapt better to the YNI equations

or to the particular setting of the G-proteins variables, the action of which on maximum ionic currents is described by: $\overline{i_s} \rightarrow (1+3G_s)(1-G_i)\overline{i_s}$, $\overline{i_k} \rightarrow (1+G_s)(1-G_i)\overline{i_k}$, $\overline{i_h} \rightarrow (1+2G_s)(1-G_i)\overline{i_h}$, and $\overline{i_{k\_ACh}} \rightarrow G_k\overline{i_{k\_ACh}}$.

The resulting set of 1st-order equations has been numerically integrated on a Sun UNIX workstation with a BDF algorithm, dedicated to stiff sets of equations, using the public domain software SCILAB, developed at INRIA.

III. Results

An illustration of the model is shown on Fig. 1:

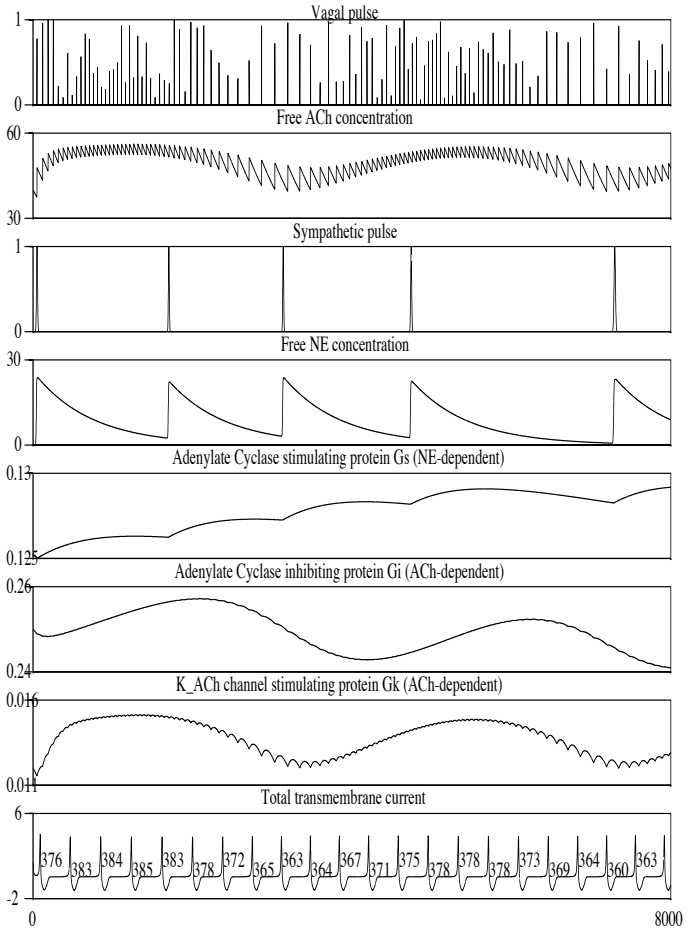

Figure 1. *Results of numerical integration in* SCILAB *of the main features of the model, on a time interval of 8 seconds. Units are milliseconds for time, μamperes for current, and nanomoles/l for concentrations.*

Then a FFT performed on the RR series obtained from the integration of the system over a longer time window (56 seconds) is shown on Fig. 2.

IV. Discussion

This model describes the action of the ANS on heart rate through G-proteins and the adenylate cyclase. It combines ideas published by Mokrane et al.[6], integrating both branches of the ANS, with an original design of the vagal and sympathetic trains, transformed in free [ACh] or [NE] in the neuroeffector junction according to a design proposed by Dexter et al.[3] for ACh, and with the original YNI equations[2].

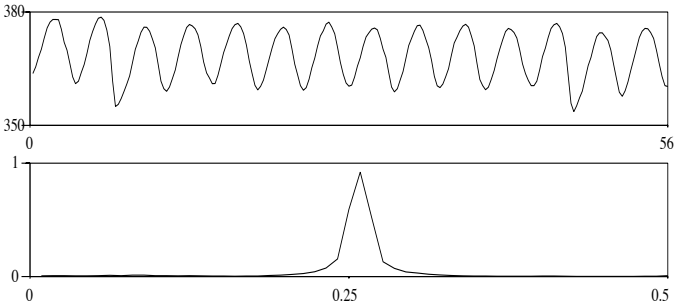

Figure 2. *RR signal resulting from the integration of the system over 56 seconds, and its spectral analysis by FFT. A high frequency peak is present at 0.25 Hz, representing respiratory sinus arrhythmia, but no peak representing baroreflex activity may be seen at the expected frequency of 0.1 Hz.*

The action of the vagal branch of the ANS on the single pacemaker cell is satisfactorily mimicked by this model, but not the action of the sympathetic branch. This shortcoming may be accounted for by unadapted representation of the sympathetic impulse, of the production and degradation of NE, of its influence on the equilibrium value of G_s, or of its action on the main current i_s. Most likely, the direct transposition to NE of the model chosen for ACh[3] is not completely accurate. But it also might be that NE should act on the constants α and β in the YNI equations (as in [4]) for the gating variables d, f, p. Physiological likelihood will lead us on this way to a next step of this model, to study the influence of both branches of the ANS on the pacemaker cell, as measured by heart rate variability.

References

[1] Akselrod, S., Gordon, D., Ubel, F.A., Shannon, D.C., Barger, A.C., Cohen, R.J., *Power Spectrum Analysis of Heart Rate Fluctuation: A Quantitative Probe of Beat-to-Beat Cardiovascular Control*, Science, Vol. 213, pp. 220-222, 1981.

[2] Yanagihara, K., Noma, A., Irisawa, H., *Reconstruction of Sino-atrial Node Pacemaker Potential Based on the Voltage Clamp Experiments*, Jap. J. Physiol. 30, pp. 841-857, 1980.

[3] Dexter, F., Levy, M.N., Rudy, Y., *Mathematical Model of the Changes in Heart Rate Elicited by Vagal Stimulation*, Circ. Res., 65, pp. 1330-1339, 1989.

[4] Riemer, I., Adam, D., *Neural effects on SA Node Action Potential and Interbeat Interval – a Model study*, Proc. of the Computers in Cardiology conference, Durham, NC, USA, pp. 35-38, 1992.

[5] Demir, S.S., Clark, J.W., Giles, W.R., *Cholinergic and Adrenergic Modulation of Ion Channels in a Rabbit Sinoatrial Node Model*, Proc. of the IFAC symposium on modeling and control in biomedical systems, Galveston, TX, USA, pp. 66-67, 1994.

[6] Mokrane, A., LeBlanc, A.R., Nadeau, R., *Modeling of the basic mechanisms of short-term control of heart rate*, Proc. of the IFAC symposium on modeling and control in biomedical systems, Galveston, TX, USA, pp. 142-143, 1994.

[7] Guevara, M.R., Jongsma, H.J., *Three ways of abolishing automaticity in sinoatrial node: ionic modeling and nonlinear dynamics*, Am. J. Physiol., 262: H1268-H1286, 1992.

[8] Demir, S.S., Clark, J.W., Murphey, C.R., Giles, W.R., *A mathematical model of a rabbit sinoatrial node cell*, Am. J. Physiol., 266: C832-C852, 1994.

[9] Katona, P.G., Jih, F., *Respiratory sinus arrhythmia: Noninvasive measure of parasympathetic control*, J. Appl. Physiol., 30, pp. 801-805, 1975.

[10] Somers, V.K., Dyken, M.E., Mark, A.L., Abboud, F.M., *Sympathetic-nerve activity during sleep in normal subjects*, N. Engl. J. Med., 328, pp. 303-307, 1993.

Effects of parasympathetic blockade on nonlinear dynamics of heart rate in mice

Jean Clairambault, Pascale Mansier, Bernard Swynghedauw

Abstract— **The complexity of the heart rate series has been assessed by 3 kinds of nonlinear estimates: correlation dimension (CD), Lyapunov exponents (LE), and approximate entropy (ApEn), in a population of young normal mice before and after IP injection of atropine. The resulting parasympathetic blockade produced an increase in the complexity of the heart rate (RR) series as measured by CD, the first LE and ApEn, and a decrease in heart rate variability, especially in the low frequency component of the RR spectrum. This last feature is a notable difference from the effects of atropine on the human RR spectrum, where it is mainly the high frequency peak which is erased.**

These findings suggest that: 1/ in general, one should not mistake complexity, as measured by these nonlinear estimates, for variability; 2/ the autonomic nervous system of mice, a species of growing interest thanks especially to the recent use of murine transgenic models as tools of cardiovascular exploration, behaves under parasympathetic blockade in a way which is quite different from the human case; 3/ it may be quite hazardous to take without precautions transgenic animals as models in human pathology, since in the control (non transgenic) group, one may encounter very unusual physiological characteristics, as shown on this species.

Keywords— **Nonlinear estimates, heart rate, autonomic nervous system**

I. Introduction

THE autonomic nervous system (ANS) has long been investigated through the variations of heart rate, in man and in various animals. In now classical spectral analysis studies, it has been shown that in man, dog, and other mammals, the parasympathetic branch of the ANS, mediated by acetylcholine (ACh), is reflected on heart rate variability by its high frequency component, whereas the sympathetic branch, mediated by norepinephrine (NE), is reflected mainly by its low frequency component[1]. In the last decade, the growing interest for nonlinear models among physiologists has led to study, as an alternative to spectral analysis parameters, estimates coming from the theory of chaotic dynamical systems. In the absence of an explicit system of equations, it is hardly possible to decide whether or not a physiological time series is chaotic (i.e. coming from a deterministic dynamical system endowed with a strange attractor), although various tests have been proposed to address this question on recorded time series, with varying results. But *assuming* the presence of such an attractor, one may compute estimates of its complexity: dimension of the attractor by correlation dimension (CD), with the help of Grassberger and Procaccia's algorithm[2]; sensitivity to initial conditions and dissipativity: Lyapunov exponents (LE, algorithms by Wolf, Sano and Sawada, Eckmann and Ruelle[3], [4]); and entropy (or approximate entropy, ApEn, as advocated by Pincus[5]). These estimates should indeed be considered as parameters complementary to classical time-domain or spectral measures, which are not to be neglected. We have in this study applied these principles to the analysis of heart rate in a population of mice rather than other laboratory animals because we have developed a model of transgenic mice overexpressing NE $\beta 1$ receptors only in atria, and very little is known of the normal heart rate and ANS in mice. In the first part of the study, only the parasympathetic branch, and only in normal (non transgenic) mice, has been explored, with results presented here.

Jean Clairambault is with INRIA-Rocquencourt, B.P. 105, F78153 Le Chesnay Cedex, France, E-mail: Jean.Clairambault@inria.fr.

Pascale Mansier and Bernard Swynghedauw are with INSERM U127, Hôpital Lariboisière, 41, Bd. de La Chapelle, F75010 Paris, France.

II. Materials and methods

Five young female mice, all healthy and born in our husbandry, non-anesthetized and moving freely, underwent a 3-minute recording of their electrocardiogram (ECG) in the husbandry, before and after intraperitoneal injection of a single dose of atropine (100 mg/kg). The ECG was recorded by means of an intraperitoneal transmitter sending an ultrasound signal to a nearby telemeter (Datasciences Inc., St Paul, MN, USA), then digitized at 3 kHz, stored on a personal computer and submitted to R wave detection by a simple threshold crossing, with the help of the Dadisp software (DSP Development Corp., Cambridge, MA, USA). Careful examination of the detected R waves led us to retain only 5 animals out of a primitive number of 8. The RR interval series were subsequently transferred to be analysed on a Sun UNIX workstation.

The 10 (5 control, 5 with atropine) RR series, *not* filtered, *not* resampled at equally spaced points, were uniformly truncated to keep only the first 1000 values (expressed in milliseconds), and submitted to a nonlinear analysis process involving three public domain softwares: the first one (SCOUNT, by Th.-M. Kruel, University of Würzburg, Germany), an implementation of Grassberger and Procaccia's algorithm, allowed us to estimate for each series $log(r)$ vs. $log(C(r))$ and $log(r)$ vs. $\overline{log(C_i(r))}$ plots, necessary to calculate its CD and ApEn; the second one (DLIA, by K. Briggs, University of Adelaide, Australia), used as an implementation of Eckmann and Ruelle's algorithm, gave us an estimation of its LE's; and the third one (SCILAB, by the Scilab group at INRIA) was used for all other calculations and graphical representations, including the ones leading to CD and ApEn.

The first and second statistical moments were also calculated, and a spectral analysis by means of classical FFT performed for each one of the 10 RR series.

III. Results

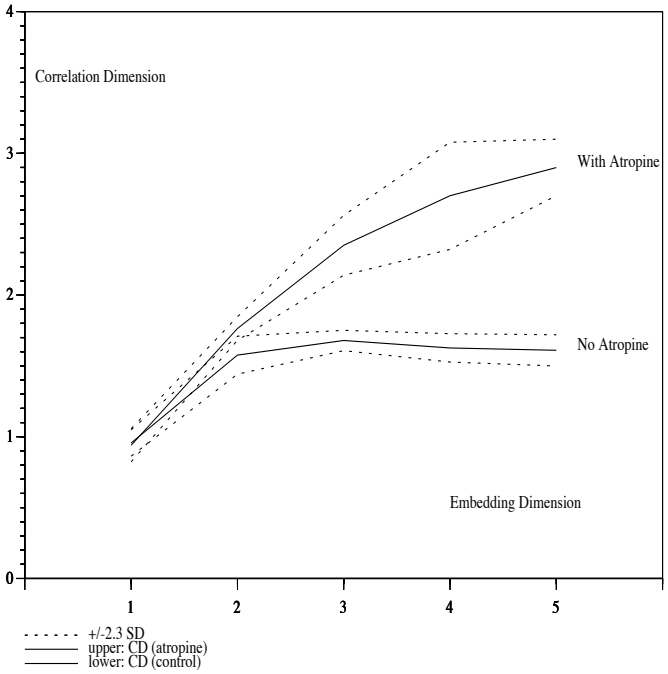

Figure 1. *Correlation dimensions of a series of 1000 RR in one mouse before and after IP injection of atropine (animal number 3). On this figure, dotted lines indicate +/- 2.3 times the standard deviation (95% confidence interval) of the slope (CD), calculated by linear regression on 10 points in the linear zone of the log(r) vs. log(C(r)) plot, and assuming normality of the error.*

We calculated correlation dimension (CD) and Lyapunov exponents (LE) for embedding dimensions ranging from 1 to 5. CD's are given in Tables 1 and 2. An illustration of CD contrasts in one animal is presented on Figure 1.

Table 1. *CD for control recordings (before injection).*

	CD for embedding dimension:				
	1	2	3	4	5
Animal 1	0.81	1.36	1.42	1.07	1.22
Animal 2	0.97	1.89	2.41	2.32	2.70
Animal 3	0.96	1.58	1.68	1.63	1.61
Animal 4	1.01	1.84	2.27	2.24	2.21
Animal 5	0.91	1.61	1.99	2.01	1.98

Table 2. *CD for recordings after atropine injection.*

	CD for embedding dimension:				
	1	2	3	4	5
Animal 1	0.81	1.77	2.24	2.07	1.92
Animal 2	0.90	1.78	2.37	2.44	2.76
Animal 3	0.94	1.76	2.36	2.70	2.90
Animal 4	0.95	1.71	2.45	2.78	2.82
Animal 5	0.83	1.58	1.99	2.07	1.98

Wilcoxon's matched-pairs signed rank 2-sided test gave a $p < 0.1$ in dimensions 3, 4 and 5. Assuming normality, a 2-sided Student's test gave $p < 0.07$ in dimensions 4 and 5, non significant in dimension 3; the limited number of animals, resulting from a rigorous selection of the recordings, did not allow us to improve these results (p cannot be under 0.1 for $n = 5$ at Wilcoxon's test).

LE's were calculated in dimensions 3 to 5; only the results in dimension 3 are presented in Table 3, but the tendency to increase the first LE with atropine injection persisted in dimensions 4 and 5, and the sum of all LE's was always negative (an argument in favour of dissipativity).

Table 3. *Lyapunov exponents in dimension 3.*

	Control:			Atropine:		
	λ_1	λ_2	λ_3	λ_1	λ_2	λ_3
Animal 1	0.84	-0.08	-0.96	0.95	-0.04	-0.93
Animal 2	0.79	0.03	-0.94	0.88	-0.03	-0.98
Animal 3	0.90	0.00	-0.90	1.10	-0.04	-1.22
Animal 4	0.93	0.01	-0.97	1.09	-0.05	-1.16
Animal 5	0.85	-0.06	-1.29	0.85	-0.13	-1.12

Again, at Wilcoxon's test, $p < 0.1$ (all differences < 0) for the first LE. ApEn values ($m = 2$ and r equal to 0.05 times the standard deviation of each series) were the following (control / *atropine*): 0.03 / *0.10*; 0.18 / *1.00*; 0.08 / *0.45*; 0.19 / *1.57*; 0.96 / *0.65*; at Wilcoxon's test: $p < 0.1$.

IV. Discussion

Atropine had a marked effect on these nonlinear estimates (CD, 1st LE and ApEn), suggesting an increase in complexity of the underlying dynamics; but the overall heart rate variability, as measured by standard deviation of the RR series (in milliseconds) was constantly decreased by atropine injection: 9.4 / *6.5*; 10.9 / *4.2*; 11.7 / *6.9*; 11.9 / *1.7*; 3.9 / *2.7*, as may also be evidenced on spectral representations (not shown) by a global erasing of the spectrum, more visible in its lower part which carries most of the variability. Mean RR (110–160 ms) was not significantly changed by atropine. These actions of atropine are quite different from the human case, where mean RR is decreased, and the variability is erased mainly in the high frequency component. It is possible that mice, unlike humans, have a permanent leading sympathetic tone, with a vagal correction, rather than the contrary. But, independently of this discussion on the particular species under study, a more general conclusion may be drawn from these results: it is not true that increasing the variability of a time series will result in an increase of its complexity. Indeed, we have shown that the opposite may happen.

References

[1] Akselrod, S., Gordon, D., Ubel, F.A., Shannon, D.C., Barger, A.C., Cohen, R.J., *Power Spectrum Analysis of Heart Rate Fluctuation: A Quantitative Probe of Beat-to-Beat Cardiovascular Control*, Science, Vol. 213, pp.220-222, 1981.

[2] Grassberger, P., Procaccia, I., *Measuring the strangeness of strange attractors*, Physica 9D, pp. 189-208, 1983.

[3] Eckmann, J.-P., Ruelle, D., *Ergodic theory of chaos and strange attractors*, Rev. of Mod. Phys. Vol.57, pp. 617-656, 1985.

[4] K. Briggs, *An improved method for estimating Liapunov exponents of chaotic time series* Phys. Letters A, Vol. 151, pp. 27-32, 1990.

[5] Pincus, S.M., Goldberger, A.L., *Physiological time-series analysis: what does regularity quantify?*, Am. J. Physiol., 266: H1643-H1656, 1994.

ELSEVIER

Cardiovascular Research 31 (1996) 371–379

Cardiovascular Research

Review

Linear and non-linear analyses of heart rate variability: a minireview

Pascale Mansier [a,*], Jean Clairambault [b], Nathalie Charlotte [a], Claire Médigue [b], Christophe Vermeiren [b], Gilles LePape [c], François Carré [d], Athanassia Gounaropoulou [a], Bernard Swynghedauw [a]

[a] U127-INSERM, IFR Circulation, Hôpital Lariboisière, 41 Bd de la Chapelle, 75010 Paris, France
[b] INRIA-Rocquencourt, Domaine de Voluceau, BP 105, 78153 Le Chesnay Cedex, France
[c] Laboratoire d'Ethologie et de Psychophysiologie, Faculté des Sciences et Techniques, Parc de Grandmont, 37200 Tours, France
[d] Laboratoire de Physiologie Médicale, Faculté de Médecine de Rennes, 2–4 Av. du Pr. Leon Bernard, 35043 Rennes, France

Received 15 March 1995; accepted 20 October 1995

Abstract

To complete traditional time- and frequency-domain analyses, new methods derived from non-linear systems analysis have recently been developed for time series studies. A panel of the most widely used methods of heart rate analysis is given with computations on mouse data, before and after a single atropine injection.

Keywords: Linear analysis; Non-linear analysis; Heart rate variability

1. Introduction

Heart rate can be computed from an electrocardiogram (ECG): it is based on the RR series which represents the successive interbeat intervals. Within the same individual, important variations from the mean RR value are observed in every species studied, from man [1] (mean RR of 1 s) to mouse [2] (mean RR of 0.1 s). Heart rate variability (HRV) is defined as the fluctuations of the RR intervals around this mean value. HRV analysis assumes sinus rhythm and ectopic ventricular beats should be rejected. The influence of the Autonomic Nervous System (ANS) has long been recognized in these fluctuations, short-term variability being mediated by the parasympathetic system, and long-term variability by both the sympathetic and parasympathetic pathways [3–7].

Epidemiological studies, beginning in the late seventies, have shown that a decrease in HRV is one of the best predictors of arrhythmic events or sudden death after myocardial infarction [8–13]. Search for better methods of analysis has therefore more than an academic interest. HRV depends on various determinants including the baroreflex, cortical influences, but also, as recently suggested in our laboratory [15], the myocardial phenotype. The myocardial β-adrenergic/muscarinic receptors ratio is modified during cardiac failure and experimental data have shown that these alterations parallel the decrease in HRV [14,15]. To verify such a hypothesis, independently of any baroreflex influence, we have developed a model of transgenic mice overexpressing β_1-adrenergic receptors exclusively in atria [16]. Preliminary results reveal substantial alterations of sinus rhythm variability [2].

To illustrate a large panel of HRV analysis methods, we have purposely focussed our study on RR series obtained from the same young female mouse, before and after intraperitoneal (IP) injection of a single dose of atropine (100 mg/kg). The mouse is a model of growing interest because of the use of murine transgenic models in the cardiovascular domain [17–19]. The ECGs were recorded by telemetry and the RR series were computed using DADISP software (DSP Development Corporation) and

* Corresponding author. Tel. (+33-1) 42-85-80-65; Fax (+33-1) 48-74-23-15.

Time for primary review 21 days.

0008-6363/96/$15.00
PII S0008-6363(96)00009-0

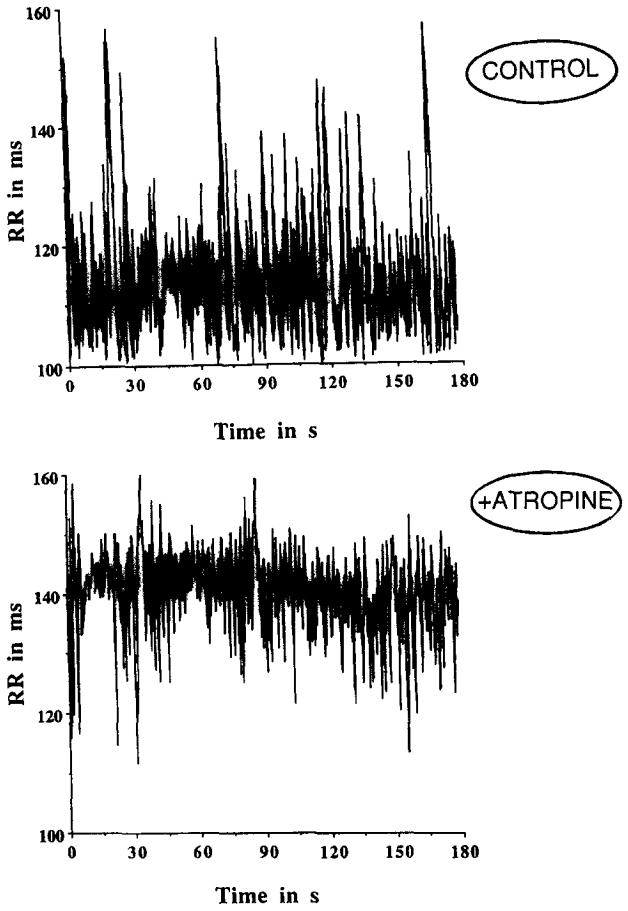

Fig. 1. Effects of atropine on heart rate in a mouse. A: control. B: after injection of a single dose of atropine (100 mg/kg). Tachograms. Heart rate recording uses a biocompatible ETA transmitter (DataSciences Inc, St Paul, MN, USA) via a telemetric device on a non-anaesthetized and freely moving young female mouse (4 months old; body weight 22.3 g). Sampling frequency: 3 kHz. Such a frequency ensures R wave detection with an accuracy < 1 ms. Signal digitized on a PC-based system (Axotape) and stored for further analysis on a Unix workstation. RR series were obtained from the ECG recordings using DADISP software and a level cross method to detect the R waves.

the effects of atropine injection are shown in Fig. 1A and B.

In the present review, methods of HRV analysis will be presented, derived from both classical signal processing and non-linear dynamics. The review will focus on a few points: (a) time-domain, spectral and time-frequency analyses are not exclusive of non-linear analysis; (b) the use of non-linear methods should not be restricted to proven deterministic chaos [20]; (c) a rather large panel of methods has to be used to provide reasonable evidence of chaotic, or at least non-linear, behaviour.

2. Methods of analysis of HRV

2.1. Spectral and non-spectral methods of analysis

Several articles have been published on this topic [4–6,21,22] and this section is a review of some of the classical methods in use.

2.1.1. Time domain methods; Variability indexes

Apart from the mean RR value, the effective calculation of the standard deviation gives a coarse quantification of the variability, without distinguishing between short-term and long-term fluctuations. In our example, the heart rate of the mouse is round 500 bpm, with a mean RR value of 113 ± 9 ms. Interestingly, atropine lowers the heart rate and increases the mean RR to 140 ± 6 ms, instead of accelerating the heart rate as it does in most of the animal species, suggesting that mice have no vagal tone. Standard deviation was diminished from 9 to 6 ms. The calculation of the autocorrelation function is also instructive [correlation of the RR(i) with the RR($i + t$), with varying t], which gives the standard deviation for $t = 0$. Furthermore, the autocorrelation function is periodic if the original series is periodic.

Many different variability indexes have been defined in various fields such as obstetrics [23] and cardiology [24] and some of them are widely used (Yeh's indexes in obstetrics [23], and SDANN or SDNN50 [12,13,24] in cardiology). It is worth noting that most of the epidemiological studies demonstrating the prognostic value of a decrease in HRV after myocardial infarction have been based upon such indexes [13].

2.1.2. Frequency domain methods; Spectral analysis

Spectral analysis consists in converting information in the time domain into information in the frequency domain. The most widely used method for processing the studied signal is the Fast Fourier Transformation, FFT. The result of FFT is a complex number for each frequency; its squared modulus is the spectral power, and the set of all spectral powers for the different frequencies is the Power Spectral Density (PSD) function; its graph is the spectrum of the signal. Results are expressed in Power Spectral Density (PSD), the squared amplitude calculated for each frequency. The spectrum of the signal is the graph of the PSD function (y-axis) plotted against frequency (x-axis). Partitioning in High or Low Frequency variabilities, HF and LF, gives the short-term or long-term variability of the time series. The total HRV is obtained by calculating the total area under the PSD curve. Spectral analysis methods have been widely applied to both HRV and blood pressure variability. Nevertheless, spectral analysis presents intrinsic limitations, especially in relation to the possible non-stationarity of the signals [25]. The FFT requires a stationary signal: the statistical properties of the signal should be the same when their estimation is performed at different time intervals within the same recording. It also assumes that the recorded oscillations are symmetrical.

Fig. 2 (left) gives the result of a spectral analysis of the RR series performed by FFT using a Hamming window, and shows apparent activity in various frequency bands: a HF band around 2.4 Hz, a LF band around 0.6 Hz, and a very low frequency band below 0.4 Hz. The spectrum is complex, and the quantification difficult due to the ex-

treme variability of the heart rate in this animal species. In the presence of atropine, there is an overall decrease in HRV which is more pronounced in the LF range.

2.1.3. Time-frequency methods of analysis

In order to be free from the stationarity assumption underlying spectral analysis, time-frequency methods have been developed. They evaluate the spectrum over moving windows, attributing a value of the PSD to each point in time and to each frequency, and produce instantaneous, or evolutionary, spectra. The most widely used time-frequency methods are the short-time Fourier transform and the Wigner-Ville transform [26,27].

The smoothed pseudo Wigner-Ville transform has been used in our laboratory to analyse HRV in mice because the heart rate of this animal species varies quickly [2]. The signal is analysed simultaneously in the time and in the frequency domains, with a third dimension on a horse representation representing the spectral power (Fig. 2 right). It is then also possible to determine two main frequency bands: a Low Frequency band, LF, centered at 0.6 Hz (one oscillation every 1.6 s), and a High Frequency band, HF, centered at 2 Hz (one oscillation every 0.5 s). Quantification is obtained by averaging the peak spectral power values at each instant in every band. Atropine decreases the spectral power in the two bands, but has a more pronounced effect on the Low Frequency oscillations than at high frequency (from 22 150 to 12 650 ms^2/Hz for LF and from 3250 to 3000 ms^2/Hz for HF). In this mouse, atropine decreases mainly the LF part of the spectrum, in contrast to human RR recordings, in which atropine mainly erases the HF activity [6]. Whether this is a consequence of a peripheral effect of atropine, or an intrinsic difference in the regulation of heart rate by the ANS between mice and men, is an open question.

2.2. Methods derived from fractal geometry

The basic property of a fractal object is self-similarity or scale invariance; the details of the structure are similar when zooming at different resolutions. The fractal dimension measures this irregularity. It can be estimated from the minimal number $N(r)$ of (hyper)cubes with given edge length r, and in the case of a fractal object, this fractal dimension is a non-integer number. It is also called capacity, or box-counting dimension [28–30].

Several fractal measures of irregularity are applicable to heart rate. The fractal dimension of the RR series can be calculated, usually by box-counting, time being here irrelevant [31]. Another measure may be computed on the spectrum, with the help of the exponent β in the approximate $1/f^{\beta}$ expression for the PSD [32]. In our example, on a mouse, performing such a log-log representation is not really advisable because of the shortness of the data sets. Let us nevertheless mention that the calculation gives for the atropine data sets a lower β exponent in the upper part of the spectrum, and no differences in the lower part.

HRV may also be considered as a mixture of influences

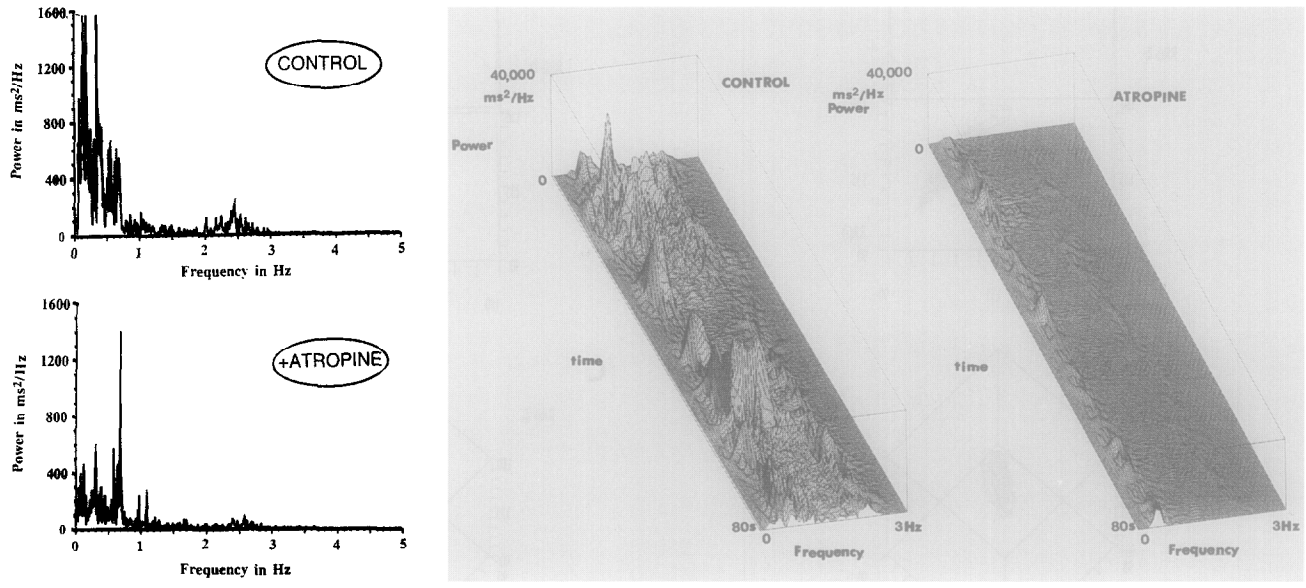

Fig. 2. Effects of atropine on heart rate in a mouse. Left: Fast Fourier Transform, performed with a Hamming window on 80 seconds of the same data, before and after (B) atropine injection. Right: Smoothed pseudo Wigner-Ville Transform applied to 80 seconds of the same data as in the fast Fourier transform. The input is a high-pass filtered version of the signal, to eliminate very low frequency noise (< 0.4 Hz). The analysis was performed with Lary_C software (INRIA, Rocquencourt, France and TNI, Brest, France). High resolution was achieved by independent time and frequency smoothing using a moving 16-point (= 1.6 seconds) window (for time) and a 128-point window (for frequency). Evaluation of spectral power, in ms^2/Hz was performed for each window by taking the maximal amplitude in both high and low frequency bands. In each band, the results were averaged over all time windows considered.

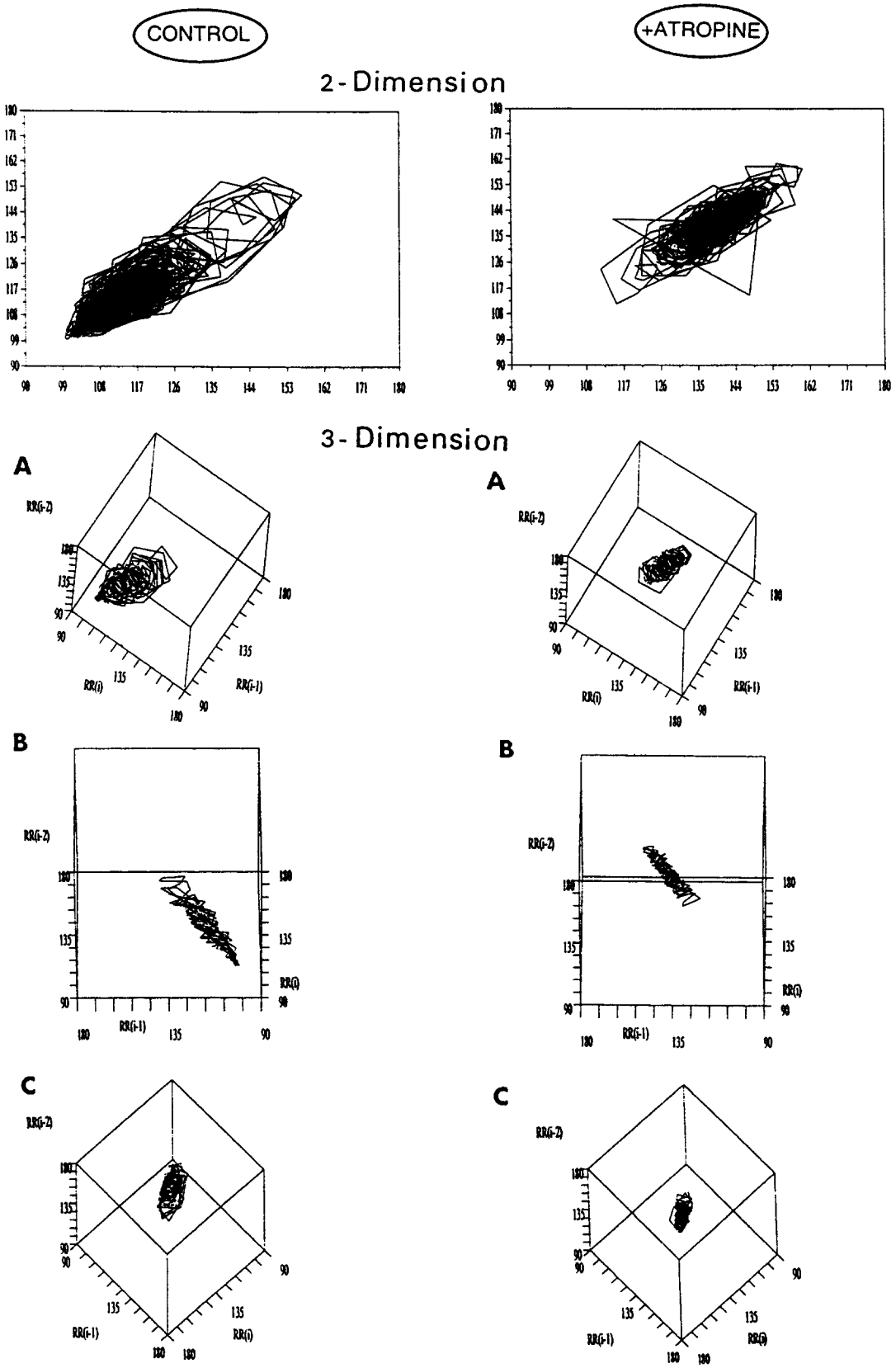

Fig. 3. Effects of atropine on heart rate in a mouse. Left panel: control. Right panel: after atropine. Phase portraits (scatterplots) in 2 or 3 dimensions. A: 2D projection onto the principal factor plane. B, C: 3D projections on the other two factor planes. In the case of non-linear analysis procedures we used a raw RR signal with a non-equidistant sampling.

from the ANS ("harmonic component") and a remaining "fractal component": calculation will then consist in extracting this fractal part of the HRV in the spectrum, computing its relative importance in the spectrum (fractal percentage) and determining a fractal exponent from the remaining part of the spectrum [33–35].

2.3. Methods of non-linear dynamics; Chaotic behaviour

Sets of differential or difference equations describing the evolution of a system can display solutions that are totally unpredictable in the long run, because of "sensitive dependence on initial conditions", even though the trajectories remain in a bounded region of the space. In other words, the divergence between two initially close trajectories of the system is such that any estimation of the position of one point at a given time is impossible. And yet the system has nothing to do with chance: it is theoretically determined by its equations and a starting point [36–39].

2.3.1. Attractors and chaos

From a "dynamical" point of view, a discrete time series, such as an RR series, is seen as the projection on a line of one trajectory of an unknown discrete deterministic dynamical system in m-dimensional space. If this evolution is not subject to abrupt changes induced by external factors, such a trajectory will converge to an attractor, i.e. a closed set of points in m-dimensional space which is a limit set for all trajectories of the system, and one trajectory is supposed to cover the attractor if the time series is long enough. Many deterministic dynamical systems present attractors, but not all of them are chaotic. A chaotic attractor is defined by sensitive dependence on initial conditions for the trajectories on them; if, furthermore, it is a fractal object, with a non-integer dimension, then it is a strange attractor and displays no simple geometric structure [40,41]. Chaos occurs only in non-linear systems. Widely known examples of strange attractors are Hénon's and Lorenz's attractors [36–39].

2.3.2. The case of heart rate

Application to biological systems is relatively new and has been recently reviewed [42–44]. The ECG may be viewed as a deterministic continuous dynamical system. The RR series is then considered as the sequence of "first return times" corresponding to the intersections of the trajectories with a fixed hyperplane, e.g. zero crossing for the action potential. In this respect, [RR_n vs RR_{n+1}] plots, or [RR_n, RR_{n+1}, RR_{n+2}] plots [45] are not Poincaré maps or first return maps but rather "first return time maps" of a continuous dynamical system; they are sometimes termed scatterplots [46], but the most widely used term is "phase portraits" [47]. Two- and three-dimensional phase portraits are shown in Fig. 3 for data obtained with a mouse. The control plots are geometrically ordered, in a cone-like structure, whereas the atropine plots are distributed in a less ordered aspect.

2.3.3. Reconstructing a cardiac attractor from the RR series

Let us assume that a dynamical system of unknown dimension m underlies the RR series. Packard, Ruelle and Takens showed that one-dimensional projected data were sufficient to reconstruct an original m-dimensional attractor with the method of delays [48]. It consists in considering the time series $\{RR(t),\ t = 1,2,...N\}$, as the projection on one coordinate axis of an m-dimensional series $\{\mathrm{RR}_t = [RR(t),\ RR(t+\tau),\ RR(t+2\tau),\ldots,\ RR(t+(m-1)\tau],\ t = 1,2,\ldots,N\}$, taken as a trajectory on an attractor. As far as the RR series are concerned, a time lag $\tau = 1$ seems to be the most reasonable choice, since longer lags may induce undue loss of spatial correlation between points. The dimension m of the space in which one thus embeds the trajectory is called the embedding dimension. If it is chosen large enough (one should take $m > 2\ d_2 + 1$ [48], where d_2 is the correlation dimension, see below), then the geometrical properties of the trajectory and of the reconstructed attractor are conserved by this processing. Statistical and geometrical invariants of the attractor, such as dimension, Lyapunov exponents and entropy, may then be computed.

2.3.4. Measuring a cardiac attractor

2.3.4.1. Dimension. The dimension of an attractor can be given by the fractal dimension d_0 obtained by box-counting, the information dimension d_1 obtained by computing the information entropy, and the correlation dimension d_2 obtained by the Grassberger-Procaccia algorithm [49–51] or its variants [52]. If the experimental data are regularly distributed on the attractor, these three modes of calculation give the same result. Such algorithms are limited by data length: $10^{d_2/2}$ points are necessary to estimate dimension d_2 [53]. For heart rate series, even a 24-h recording of heart rate (100 000 beats for a human heart, 700 000 beats for a mouse) cannot allow any estimation of the correlation dimension over 10. Furthermore, such a processing assumes that the attractor has not changed during the recording period. Such limitation in the length of data implies in particular that only low-dimensional chaos may be evidenced by dimension computation.

In the case of the mouse RR series, the atropine injection induces an increase in the correlation dimension, regardless of the embedding dimension (Table 1) which clearly suggests that atropine enhances the "complexity" of the RR series (increased "complexity" simply meaning an increased dimension or number of degrees of freedom of a system). An embedding dimension of 3 is then apparently enough to estimate d_2. In fact, we have also calculated d_2 for embedding dimensions up to 10, and have obtained a permanent decrease of d_2 after 5, instead

Table 1
Non-linear analysis of HRV in a mouse. Effects of atropine. Correlation dimensions

Embedding dimension	1	2	3	4	5
Control					
Original data	0.88	1.42	1.46	1.37	1.30
Surrogate data	0.97	1.82	2.29	2.31	2.42
+ Atropine					
Original data	0.93	1.81	2.24	2.10	1.92
Surrogate data	0.97	1.83	2.31	2.37	2.48

Table 2
Non-linear analysis of HRV in a mouse. Effects of atropine. Lyapunov spectrum for embedding dimension 3. Λ is the sum of $\lambda_1 + \lambda_2 + \lambda_3$

Lyapunov exponent	λ_1	λ_2	λ_3	Λ
Control				
Original data	0.838	−0.082	−0.958	−0.203
Surrogate data	2.502	0.240	−1.304	1.437
+ Atropine				
Original data	0.951	−0.038	−0.930	−0.017
Surrogate data	2.973	0.201	−1.352	1.823

of an increase which would have been expected with purely random data.

2.3.4.2. Lyapunov exponents. They allow the quantification of sensitive dependence on initial conditions [48,54–58]. On strange attractors, two points on distinct trajectories will see their distance after a time t multiplied by a factor $\exp(\lambda_1 t)$ (with a positive λ_1, so that $\exp(\lambda_1 t) > 1$). This exponent λ_1 is the first Lyapunov exponent of the system, but not the only one. If we consider a small volume element, the deformation of this volume element after a time t will vary according to the directions considered. It will be expanded if a multiplicative factor of the form $\exp(\lambda t)$, $\lambda > 0$, accounts for the deformation in this direction, and shrunk in another direction when $\lambda < 0$. Consequently, to accurately analyse the dynamical system, computation of the complete Lyapunov spectrum $(\lambda_1, \lambda_2, \ldots, \lambda_m$, with $\lambda_1 > \lambda_2 > \ldots > \lambda_m,)$ is necessary. The first exponent λ_1, has to be positive for the system to be chaotic, but the following ones may be positive or negative. The sum $\Lambda = \lambda_1 + \lambda_2 + \ldots + \lambda_m$ gives the exponential rate Λ of contraction (if it is negative: $\exp(\Lambda t) < 1$), or expansion (if the sum is positive: $\exp(\Lambda t) > 1$) of the volume. The system is said to be dissipative for $\Lambda < 0$, conservative for $\Lambda = 0$, and accretive for $\Lambda > 0$. These terms are related respectively to dissipation, conservation, or accretion of energy.

In our example, in control conditions, the first Lyapunov exponent λ_1 is positive, and the sum Λ is negative, which favours a deterministic dissipative chaotic system for the heart rate of our mouse. Atropine injection increases both λ_1 and Λ and draws the sum Λ close to zero (Table 2). Such results are also in favour of an increased "complexity" in the presence of atropine. The Lyapunov spectrum was also calculated in embedding dimensions 4 and 5, with comparable results, the first two exponents being positive, and not only the first one. A short data length is again a limiting factor in Lyapunov spectrum estimation: for an attractor of correlation dimension d_2, a correct evaluation of $\lambda_1, \lambda_2, \ldots, \lambda_m$ requires 10^{d_2} points [53], a condition fulfilled by the present heart rate series.

2.3.4.3. Entropy. K_1, the information entropy, is a quantification of the information uniformity carried by the probability distribution; in the case of a strange attractor where the measure considered is the counting measure on the trajectory, K_1 is lower than the sum of positive Lyapunov exponents [48]. Other definitions are available, particularly a topological entropy K_0 and a "correlation-like" entropy K_2. Both K_1 and K_2 are computed by variants of the Grassberger-Procaccia algorithm. A variant of K_1 has been proposed by Pincus and co-workers: "ApEn", for Approximate Entropy, which is likely to be less sensitive to noise and usable for short stationary time series [59,60].

In the case of our mouse, the injection of atropine results in an increase in ApEn (Table 3) which again

Table 3
Results of a panel of linear and non-linear methods applied to the analysis of HRV in a mouse. Effects of atropine

	Control	Atropine
Heart rate		
Mean RR (ms)	113	140
SD (ms)	9	6
Visual observation of tachygram (Fig. 1)		
		RR series more regular
Fast Fourier transform (Fig. 2)		
		⇓ power all frequencies, ⇓⇓ Low Frequency
Time-frequency analysis (Wigner-Ville Transformation, Fig. 3)		
HF peak (ms^2/Hz)	3250	3000
LF peak (ms^2/Hz)	22150	12650
Phase portraits (Fig. 4)		
		more compact
Correlation dimension (Table 1)		
For $m = 3$	1.46 ± 0.13	2.24 ± 0.19
Lyapunov exponents (Table 2)		
For $m = 3$		
λ_1	0.838	0.951
Λ	−0.203	−0.017
ApEn [a]		
	0.03	0.10
Non-linear prediction (Fig. 5)		
		worse
Surrogate data: see Tables 1 and 2, Fig. 5.		
Correlation dimension:	in favour of a non-linear component	
Lyapunov spectra:	strongly in favour of a non-linear component	
ApEn:	in favour of a non-linear component	
Non-linear prediction:	in favour of a non-linear component	

[a] The ApEn statistic has been calculated for $N = 1000$ points, $m = 2$, $r = 0.05$ s.d.

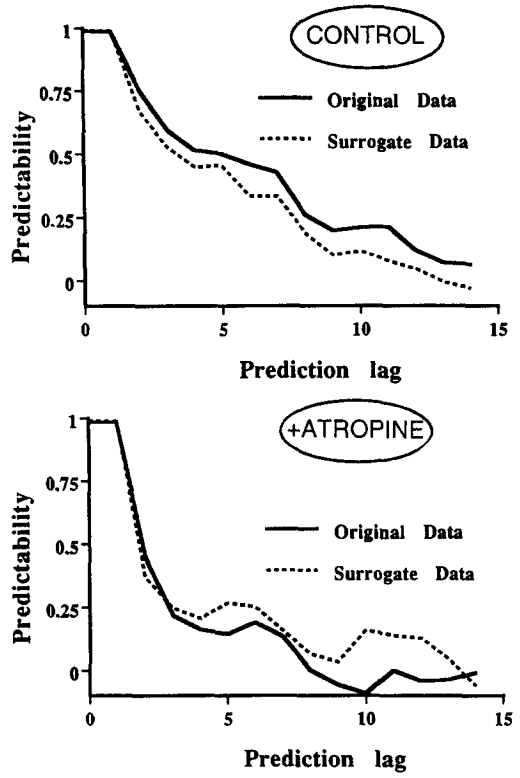

Fig. 4. Effects of atropine on heart rate in a mouse. A: control. B: after atropine. Comparison between experimental and the surrogate series. Non-linear prediction by Sugihara and May's method [61] in embedding dimension 3. Correlation coefficient between observed and predicted values, in number of beats as a function of the prediction time. The prediction is determined by using the first 500 points of the RR series, and the actually observed values are the following 500 points of the same series (total number of RR: 1000 points). Predictability is defined by the the capacity to predict the RR value. The prediction lag is taken here as the number of beats.

favours an increased "complexity" due to the drug, in the same time as variability decreases, showing that these two terms are not synonymous.

2.3.5. Non-linear determinism and randomness

All these estimates derived from non-linear dynamics assume that the RR series is the output of a deterministic dynamical system. This assumption is naturally not to be taken for granted, and tests of non-linear prediction [61], as well as comparison tests with surrogate data [62], have been proposed to address this question. A surrogate series is a time series in which non-linear dependences have been wiped out by some "random shuffling procedure", but which retains all linear characteristics of the original time series, including its spectrum.

We have used non-linear prediction in our mouse, as an example. The predictability is shown in Fig. 4A and B. Before atropine, the prediction index is better for the experimental series than for its surrogate series; by contrast, after atropine injection, one no longer sees differences between the original and the surrogate series. The same results were obtained using the correlation dimension (Table 1). Most important, in the case of the Lyapunov spectra, striking differences between original and surrogate series are obtained for both control and atropine data (Table 2). The results for surrogate series reveal an apparently stochastic behaviour with a very high first Lyapunov exponent λ_1, in an accretive system ($\Lambda > 0$). By contrast, the original series show a lower (but still positive) λ_1, in a dissipative (control) or at most conservative (atropine) system ($\Lambda \leq 0$). The ApEn values calculated for surrogate data are much higher than for the original series: 0.32, instead of 0.03 for the original RR series before atropine, and 0.53, instead of 0.10 for the original RR series under atropine.

These differences between original and surrogate data are thus in favour of a non-linear, deterministic and chaotic dynamical system for the RR series under study. They are quite clear for all series on the Lyapunov spectrum (obtained by the public-domain program DLIA [56], following Eckmann-Ruelle's algorithm) and on ApEn values, but remain clear only for the control series on correlation dimension calculations (public-domain program SCOUNT [51], completed by the scientific programs package SCILAB, developed at INRIA), as well as on non-linear prediction. This illustrates the necessity of a large panel of analysis techniques, rather than a single one, to investigate time series.

3. Concluding remarks

Numerous methods of analysis, derived from classical signal processing or non-linear dynamics, are available and no single measure is more appropriate than the others for physiological research or clinical practice (Fig. 5). Therefore, and following Drazin [39], we propose to use a panel of measures, as presented in Table 3. The detailed analysis that we had performed on our mouse case allowed us to conclude that an atropine injection is likely to result in an increased complexity of an assumed heart rate attractor.

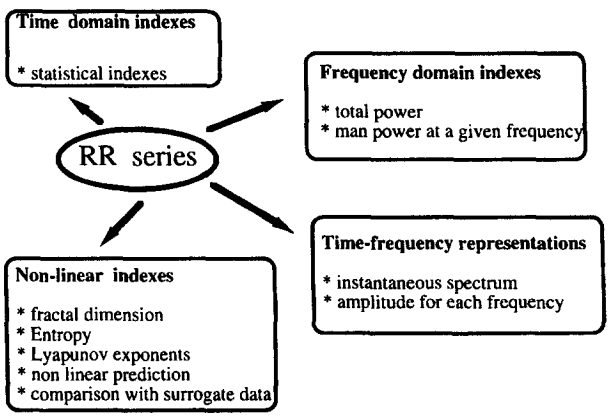

Fig. 5. Qualitative illustrations and quantitative indexes which may be obtained from experimental time series.

The existence of a cardiac strange attractor which would have as output the RR series is as yet far from being fully demonstrated. Although explicit equations are presently lacking to fully justify these techniques, we do not have any real argument to reject them. Whether they rely on sound theoretical grounds or not may even appear irrelevant to pragmatists, provided they allow clear distinction between physiologically distinct groups of subjects [20].

The ApEn statistic is advocated by Pincus and coworkers [63,64] and is independent of the assumption of a cardiac strange attractor. ApEn is a product of the work achieved in the last ten years in non-linear dynamics: the original idea of ApEn, even if it now relies on other theoretical grounds, was first an approximation to the entropy of an invariant measure on an attractor [48]. And one may expect still other interesting parameters, coming from non-linear systems analysis, to be helpful in physiological research or clinical practice.

Acknowledgements

The help of Dr Bernard Cazelles in non-linear prediction and Dr Dirk Hoyer in surrogate data is gratefully acknowledged.

References

[1] Angelone A, Coulter NA. Respiratory sinus arrhythmia: a frequency dependent phenomenon. J Appl Physiol 1964;19(3):479–482.
[2] Mansier P, Charlotte N, Médigue C, Clairambault J, Vermeiren C, Carré F, Bertin B, Swynghedauw B. Heart rate variability is reduced in transgenic mice expressing human b1-adrenoceptors in atria. Circulation 1994;90:I-267(Abst).
[3] Rosenblueth A, Simeone FA. The interrelations of vagal and accelerator effects on the cardiac rate. Am J Physiol 1934;110:42–55.
[4] Akselrod S, Gordon D, Ubel FA, Shannon DC, Barger AC, Cohen RJ. Power spectrum analysis of heart rate fluctuation: a quantitative probe of beat-to-beat cardiovascular control. Science 1981;213:220–222.
[5] Pomeranz B, Macaulay RJB, Caudill MA, Kutz I, Adam D, Gordon D, Kilborn KM, Barger AC, Shannon DC, Cohen RJ, Benson H. Assessment of autonomic function in humans by heart rate spectral analysis. Am J Physiol 1985;248:H151–153.
[6] Appel ML, Berger RD, Saul JP, Smith JM, Cohen RJ. Beat-to-beat variability in cardiovascular variables: noise or music?. J Am Coll Cardiol 1989;14:1139–1148.
[7] Randall DC, Brown DR, Raisch RM, Yingling JD, Randall WC. SA nodal parasympathectomy delineates autonomic control of heart rate power spectrum. Am J Physiol 1991;260:H985–988.
[8] Wolf M, Varigos G, Hunt D, Sloman J. Sinus arrhythmia in acute myocardial infarction. Med J Aust 1978;2:52–53.
[9] Kleiger RE, Miller JP, Bigger JT Jr, Moss, and the Multicenter Postinfarction Research Group. Decreased heart rate variability and its association with increased mortality after acute myocardial infarction. Am J Cardiol 1987;59:256–262.
[10] LaRovere MT, Specchhia G, Mortata A, Schwartz PJ. Baroreflex sensitivity, clinical correlates and cardiovascular mortality among patients with a first myocardial infarction: a prospective study. Circulation 1988;78:816–824.
[11] Odemuyiwa O, Malik M, Farrell T, Bashir Y, Poloniecki J, Camm J. Comparison of the predictive characteristics of heart rate variability index and left ventricular ejection fraction for all-cause mortality, arrhythmic events and sudden death after acute myocardial infarction. Am J Cardiol 1991;68:434–439.
[12] Bigger JT Jr, Fleiss JL, Rolnitzky LM, Steinman RC, Schneider WJ. Time course of recovery of heart period variability after myocardial infarction. J Am Coll Cardiol 1991;18:1643–1649.
[13] Bigger JT Jr, Fleiss JL, Rolnitzky LM, Steinman RC. Predicting mortality after myocardial infarction from the response of RR variability to antiarrhythmic drug therapy. J Am Coll Cardiol 1994;23:733–740.
[14] Carré F, Lessard Y, Coumel P, Ollivier S, Besse S, Lecarpentier Y, Swynghedauw B. Spontaneous arrhythmias in various models of cardiac hypertrophy and senescence in rats. A Holter monitoring study. Cardiovasc Res 1992;26:698–705.
[15] Carré F, Maison-blanche P, Ollivier L, Mansier P, Chevalier B, Vicuna R, Lessard Y, Coumel P, Swynghedauw B. Heart rate variability in two models of cardiac hypertrophy in rats in relation to the new molecular phenotype. Am J Physiol 1994;266:H1872:1878.
[16] Bertin B, Mansier P, Makeh I, Briand P, Rostene W, Swynghedauw B, Strosberg AD. Specific atrial overexpression of G-protein coupled human b1-adrenoceptors in transgenic mice. Cardiovasc Res 1993;27:1606–1612.
[17] Brosnan J, Mullins J. Transgenic animals in hypertension and cardiovascular research. Exp Nephrol 1993;1:3–12.
[18] Field L. Cardiovascular research in transgenic animals. Trends Cardiovasc Med 1992;2:237–245.
[19] Koretsky A. Investigation of cell physiology in the animal using transgenic technology. Am J Physiol 1992;262:C261–C275.
[20] Glass L, Kaplan D. Time series analysis of complex dynamics in physiology and medicine. Med Prog through Techn 1993;19:115–128.
[21] Kitney RI, Rompelman O. The Study of Heart Rate Variability. Oxford: Clarendon Press, 1980.
[22] Malliani A, Pagani M, Lombardi F, Cerutti S. Cardiovascular neural regulation explored in the frequency domain. Circulation 1991;84:482–492.
[23] Parer WJ, Parer JT, Holbrook RH, Block BSB. Validity of mathematical methods of quantitating fetal heart rate variability. Am J Obstet Gynecol 1985;153:402–409.
[24] Bigger JT, Fleiss JL, Steinman RC, Rolnitzky LM, Kleiger RE, Rottman JN. Frequency domain measures of heart period variability and mortality after myocardial infarction. Circulation 1992;85:164–171.
[25] Coumel P, Hermida JS, Wennerblöm B, Leenhardt A, Maisonblanche P, Cauchemez B. Heart rate variability in left ventricular hypertrophy and heart failure and the effects of beta-blockade. A non-spectral analysis of heart rate variability in the frequency domain and in the time domain. Eur Heart J 1991;12:412–422.
[26] Novak P, Novak V. Time/frequency mapping of the heart rate, blood pressure and respiratory signals. Med Biol Eng Comput 1993;31:103–110.
[27] Novak V, Novak P, de Champlain J, Le Blanc AR, Martin R, Nadeau R. Influence of respiration on heart rate and blood pressure fluctuations. J Appl Physiol 1993;74(2):617–626.
[28] Mandelbrot BB. The Fractal Geometry of Nature. New York: Freeman, 1983.
[29] Keipes M, Ries F, Dicato M. Of the British coastline and the interest of fractals in medicine. Biomed Pharmac 1993;47:409–415.
[30] Goldberger AL, Rigney DR, West BJ. Chaos and fractals in human physiology. Sci Am 1990;46:42–51.
[31] Glenny RW, Robertson HT, Yamashiro S, Bassingthwaighte. Applications of fractal analysis to physiology. J Appl Physiol 1991;70:2351–2367.
[32] Kobayashi M, Musha T. 1/f fluctuation of heartbeat period. IEEE Trans Biomed Eng 1982;29:456–457.

[33] Butler GC, Yamamoto Y, Xing HC, Northey DR, Hughson RL. Heart rate variability and fractal dimension during orthostatic challenges. J Appl Physiol 1993;75:2602–2612.
[34] Yamamoto Y, Hughson RL. Extracting fractal components from time series. Physica D 1993;68:250–264.
[35] Yamamoto Y, Hughson RL. On the fractal nature of heart rate variability in humans: effects of data length and β-adrenergic blockade. Am J Physiol 1994;268:R40–R49.
[36] Bergé P, Pomeau Y, Vidal C. L'ordre dans le Chaos. Paris: Hermann, 1984.
[37] Baker GL, Gollub JP. Chaotic Dynamics, an Introduction. Cambridge University Press, 1990.
[38] Schuster HG. Deterministic Chaos. Weinheim, Germany: VCH Verlag, 1989.
[39] Drazin PG. Nonlinear Systems. Cambridge University Press, 1992.
[40] Ruelle D, Takens F. On the nature of turbulence. Commun Math Phys 1971;20:167–192 and 23:343–344.
[41] Li T, Yorke J. Period three implies chaos. Am Math Monthly 1975;82:985–992.
[42] Denton TA, Diamond GA, Helfant RH, Khan S, Karagueuzian H. Fascinating rhythm: a primer on chaos theory and its application to cardiology. Am Heart J 1990;6:1419–1440.
[43] Skinner JE, Molnar M, Vybiral T, Mitra M. Application of chaos theory to biology and medicine. Int Physiol Behav Sci 1992;27:39–53.
[44] Elbert T, Ray WJ, Kowalik ZJ, Skinner JE, Graf KE, Birnbaumer N. Chaos and physiology: deterministic chaos in excitable cell assemblies. Physiol Rev 1994;74:1–47.
[45] Schechtman VL, Raetz SL, Harper RK, Garfinkel A, Wilson AJ, Southall DP, Harper RM. Dynamic analysis of cardiac RR intervals in normal infants and in infants who subsequently succumbed to the sudden infant death syndrome. Pediatr Res 1992;31:606–614.
[46] Copie X, Le Heuzey JY, Iliou MC, Khouri R, Lavergne T, Pousset P, Guize L. Correlation between time-domain measures of heart rate variability and scatterplots in post-infarction patients. Pace 1995; in press.
[47] Zbilut JP, Mayer-Kress G, Geist K. Dimensional analysis of heart rate variability in heart transplant recipients. Math Biosci 1988;90:49–70.
[48] Eckmann JP, Ruelle D. Ergodic theory of chaos and strange attractors. Rev Modern Phys 1985;57:617–656.
[49] Grassberger P, Procaccia I. Measuring the strangeness of strange attractors. Physica D 1983;9:189–208.
[50] Ding M, Grebogi C, Ott E, Sauer T, Yorke JA. Estimating correlation dimension from a chaotic time series: when does plateau onset occur? Physica D 1993;69:404–424.
[51] Kruel Th-M, Freund A. SCOUNT: a program to calculate the correlation and information dimension from attractors by the method of sphere-counting. 1986–1993. Documentation to the program (1986, last revised 1993) available on internet by anonymous `ftp` from the archive `lyapunov.ucsd.edu`.
[52] Fraedrich K, Wang R. Estimating the correlation dimension of an attractor from noisy and small data sets based on re-embedding. Physica D 1993;65:373–398.
[53] Eckmann JP, Ruelle D. Fundamental limitations for estimating dimensions and Lyapunov exponents in dynamical systems. Physica D 1992;56:185–187.
[54] Wolf A, Swift JB, Swinney HL, Vastano JA. Determining Lyapunov exponents from a time series. Physica D 1985;16:285–317.
[55] Eckmann JP, Oliffson Kamphorst S, Ruelle D, Ciliberto S. Lyapunov exponents from time series. Phys Rev A 1986;34:4971–4979.
[56] Briggs K. An improved method for estimating Lyapunov exponents of chaotic time series. Physics Lett A 1990;151:27–36.
[57] Brown R, Bryant P, Arbanel HDI. Computing the Lyapunov spectrum of a dynamical system from an observed time series. Phys Rev A 1991;43:2787–2806.
[58] Kruel TM, Eiswirth M, Schneider FW. Computation of Lyapunov spectra: effect of interactive noise and application to a chemical oscillator. Physica D 1993;63:117–137.
[59] Pincus SM, Goldberger AL. Physiological time-series analysis: what does regulatory quantify? Am J Physiol 1994;266:H1643–H1656.
[60] Pincus SM, Cummins TR, Haddad GG. Heart rate control in normal and aborted-SIDS infants. Am J Physiol 1993;264:R638–646.
[61] Sugihara G, May RM. Nonlinear forecasting as a way of distinguishing chaos from measurement error in time series. Nature 1990;344:734–741.
[62] Theiler J, Eubank S, Longtin A, Galdrikian B. Testing for non-linearity in time series: the method of surrogate data. Physica D 1992;58:77–94.
[63] Skinner JE, Carpeggiani C, Landisman CE, Fulton KW. Correlation dimension of heartbeat intervals is reduced in conscious pigs in myocardial ischemia. Circ Res 1991;68:966–976.
[64] Yamamoto Y, Hughson RL, Sutton JR, Houston CS, Cymerman A, Fallen EL, Kamath MV. Operation Everest II: an indication of deterministic chaos in human heart rate variability at simulated extreme altitude. Biol Cybern 1993;69:205–212.

6.2 Chronopharmacologie et optimisation de la chronothérapeutique circadienne en cancérologie

R7 Claude, D., Clairambault, J. (2000) : Period shift induction by intermittent stimulation in a Drosophila model of PER protein oscillations. *Chronobiology International*, 17(1):1-14.

R9 Basdevant, C., Clairambault, J., Lévi, F. (2005) : Optimisation of time-scheduled regimen for anti-cancer drug infusion. *Mathematical Modelling and Numerical Analysis*, Vol. 39(6):1069-1086.

R10 Clairambault, J., Michel, Ph., Perthame, B. (2006) : Circadian rhythm and tumour growth. *C. R. Acad. Sci. Paris, Mathématique* (Équations aux dérivées partielles), 342(1):17-22.

R11 Clairambault, J. (2007) : Modeling oxaliplatin drug delivery to circadian rhythm in drug metabolism and host tolerance. *Advanced Drug Delivery Reviews (ADDR)*, 59:1054-1068.

R12 Bekkal Brikci, F., Clairambault, J., Ribba, B., Perthame, B. (2007) : An age-and-cyclin-structured cell population model for healthy and tumoral tissues. *Journal of Mathematical Biology*, sous presse.

O9 Clairambault, J. (2006) : Physiologically based modelling of the circadian control on cell proliferation. *Actes de la 28*e *conférence internationale IEEE-EMBS*, New York, août 2006.

CHRONOBIOLOGY INTERNATIONAL, 17(1), 1–14 (2000)

PERIOD SHIFT INDUCTION BY INTERMITTENT STIMULATION IN A *DROSOPHILA* MODEL OF PER PROTEIN OSCILLATIONS

Daniel Claude[1,*] and Jean Clairambault[2,†]
[1]Université Paris XI and INRIA Rocquencourt
[2]Université Paris VIII and INRIA Rocquencourt
INRIA, Bât. 12, Domaine de Voluceau, B. P. 105,
78153 Le Chesnay cedex, France

ABSTRACT

PER protein circadian oscillations in *Drosophila* have been described by Goldbeter according to a five-dimensional model that includes the possibility of genetic mutation described by changing one parameter, the maximum degradation rate of the PER protein. Assuming that, in a mutant *Drosophila* this parameter is unreachable, we modify another parameter, the translation rate between the mRNA and the nonphosphorylated form of PER protein, by periodic intermittent activation or inhibition. We show how such a modification, simulated in the model by a periodic, on/off, piecewise constant stimulation (which increases or decreases this parameter) allows the entrainment of oscillations exactly at, or close to, a desired period. In a different context, this suggests that some diseases may be corrected using pharmacological agents according to specific periodic delivery schedules. (*Chronobiology International, 17(1), 1–14, 2000*)

Key Words: Control theory—Chronotherapy—Entrainment—Oscillations—Periodic intermittent stimulation

Received February 4, 1999; returned for revision April 21, 1999; accepted July 20, 1999.
*E-mail: Daniel.Claude@inria.fr
†E-mail: Jean.Clairambault@inria.fr

INTRODUCTION

Biological systems are nonlinear by nature and often show stable periodicities. In particular, circadian rhythms have been observed in many plants or animals and in human beings (Sweeney 1969; Bünning 1973; Winfree 1980; Touitou and Haus 1992; Goldbeter 1995; Vanden Driessche et al. 1996; Boisssin and Canguilhem 1998; Hartmann et al 1998). Some diseases, called *dynamical diseases* by Bélair et al. (1995), are observed when one or more of these rhythms are altered Changes in the characteristics of these rhythms may be the result of a mutation, modifying biochemical oscillations, and cellular rhythms (Goldbeter 1996), as is the case with the insect *Drosophila*. In previous articles (Claude and Nadjar 1994; Claude 1995) and in another biological context, the problem of shifting a pathological dynamic system toward a physiological one is tackled. Here, we consider the problem of shifting a mutant *Drosophila* PER protein cycle (per^l or per^T) toward a normal ("wild") one using distribution laws common in applied pharmacokinetics.

THE MODEL AND ITS CONTROL

In a recent article (Goldbeter 1995), Goldbeter proposed a model for the circadian oscillations of the PER protein in *Drosophila* (Fig. 1) This five-dimensional biochemical model describes the cycle of production and degradation of the various forms (nonphosphorylated, monophosphorylated, or diphosphorylated) of the PER protein and its mRNA.

This model is described by the following set of equations:

$$\begin{cases} \dfrac{dM}{dt} = v_s \dfrac{K_I^n}{K_I^n + P_N^n} - v_m \dfrac{M}{K_m + M} \\ \dfrac{dP_0}{dt} = k_s M - V_1 \dfrac{P_0}{K_1 + P_0} + V_2 \dfrac{P_1}{K_2 + P_1} \\ \dfrac{dP_1}{dt} = V_1 \dfrac{P_0}{K_1 + P_0} - V_2 \dfrac{P_1}{K_2 + P_1} - V_3 \dfrac{P_1}{K_3 + P_1} + V_4 \dfrac{P_2}{K_4 + P_2} \\ \dfrac{dP_2}{dt} = V_3 \dfrac{P_1}{K_3 + P_1} - V_4 \dfrac{P_2}{K_4 + P_2} - k_1 P_2 + k_2 P_N - v_d \dfrac{P_2}{K_d + P_2} \\ \dfrac{dP_N}{dt} = k_1 P_2 - k_2 P_N \end{cases} \tag{1}$$

where M is PER mRNA, and P_0, P_1, P_2, and P_N are the nonphosphorylated, monophosphorylated, diphosphorylated, and nuclear forms of the protein, respectively The parameters of the model were taken from Goldbeter (1995):

$v_s = 0.76$ μM h^{-1}, $K_I = 1$ μM, $n = 4$, $v_m = 0.65$ μM h^{-1}, $K_m = 0.5$ μM, $k_s = 0.78$ h^{-1}, $V_1 = 3.2$ μM h^{-1}, $K_1 = 2$ μM, $V_2 = 1.58$ μM h^{-1}, $K_2 = 2$ μM, $V_3 = 5$ μM h^{-1}, $K_3 = 2$ μM, $V_4 = 2.5$ μM h^{-1}, $K_4 = 2$ μM, $k_1 = 1.9$ h^{-1}, $k_2 = 1.3$ h^{-1}, $K_d = 0.2$ μM, $v_d = 1.6$ μM h^{-1} (wild), $= 2$ μM h^{-1} (per^l), or $= 0.5$ μM h^{-1} (per^T)

We illustrate the oscillatory behavior of the PER production cycle by a phase representation in the (M,P_t) plane, where $P_t = P_0 + P_1 + P_2 + P_N$; asymptotically, for $t \to +\infty$,

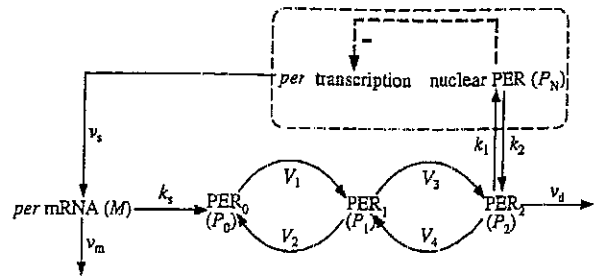

FIGURE 1. The biochemical pathways of PER protein synthesis, phosphorylation, and degradation (After Goldbeter 1995, Fig. 1.)

one thus obtains a closed curve representing a stable limit cycle, which is a geometrical characteristic of the system (Goldbeter 1996).

In a subsequent publication (Leloup and Goldbeter 1997), this dynamic system (PER) was coupled to another one (TIM), which allowed modeling of PER protein oscillations in a more complete way. This more elaborate system also shows a circadian rhythm and offers, in the light of experimental observations, other explanations, associated with changes in different parameters, for the mutant phenotypes. However, in the present paper, we only considered the simpler model, given by Eq. 1 above, in which nonmutant (wild) and mutant *Drosophila* strains were characterized tentatively by different values of v_d ($v_d = 1.6$ μM h^{-1} for the wild type, resulting in an endogenous period of 23.71h, $v_d = 2$ μM h^{-1} for the long per^l type, with a period of 28.5h, and $v_d = 0.5$ μM h^{-1} for the ultrashort per^T type, with a period of 16h), the values of the other parameters being the same. These different types exhibit different limit cycles (see Fig. 2).

Here, we consider the problem of shifting a mutant *Drosophila* PER cycle toward the wild-type *Drosophila* PER cycle, setting its period precisely to 24.00h. We use the present model as a paradigm to explain how we can restore altered rhythms by a general method, bearing in mind possible applications to applied pharmacokinetics.

In the present model (unlike the more elaborate one designed by Leloup and Goldbeter 1998), the v_d parameter represents the only "genetic" component, specific for the *Drosophila* type considered here: wild, long (per^l), or ultrashort (per^T). If it were possible to modify the value of v_d in a mutant *Drosophila*, for instance, by gene therapy, to recover the wild-type value of 1.6 μM h^{-1}, then this problem would be resolved directly. We assumed here that the parameter v_d cannot be recovered by pharmacological or other physical means, and that we had to find an indirect way to change the period of the limit cycle.

A modification of temperature may be considered, but it would also change other parameters of the system (Leloup and Goldbeter 1997), and from the model, we cannot derive information on the temporal variation of all the parameters with respect to temperature.

Since we are dealing with a closed-loop system, we could a priori act on any step of this biochemical pathway. However, from our control law on the system, we also wished to achieve sufficient *robustness* with respect to the inevitable errors that affect the programming of either quantity or time when applying any stimulation scheme

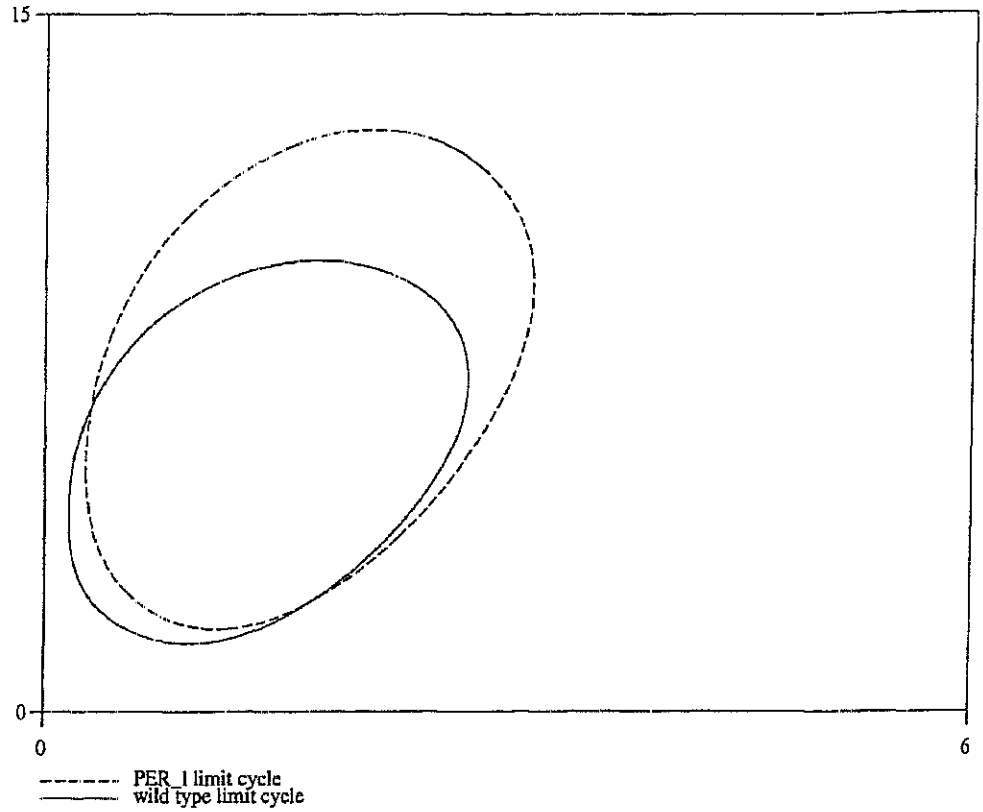

(a)

FIGURE 2. (a) The per^l mutant *Drosophila* limit cycle (dashed line) compared with the wild-type limit cycle (solid line) for PER protein oscillations; representation in the (M,P_t) plane without any external control (see text for details) (b) The per^T *Drosophila* limit cycle (dashed line) compared with the wild-type limit cycle (solid line) for PER protein oscillations; representation in the (M,P_t) plane without any external control (see text for details).

Considering the biochemical loop described in Fig. 1, we chose to focus on the two main parameters that appear between M and $P_t = P_0 + P_1 + P_2 + P_N$, namely, the constants v_s and k_t (see Eq. 1). These parameters represent plausible pharmacological targets: v_s is a chemical reaction velocity, and k_t is a rate constant (here, a factor multiplying mRNA concentration M). These two parameters could be changed or adapted in the real physical world using a chemical activator or inhibitor.

We controlled both parameters, but do not present results for v_s here. Indeed, v_s, which measures the transcription rate from DNA to mRNA, proved to be more delicate to handle and was thus less robust with respect to possible errors in the amplitude, period, or phase of the stimulation scheme.

Starting from mutant *Drosophila* parameter values, we focused on the activation or inhibition of the translation rate of the PER *mRNA* into the nonphosphorylated form

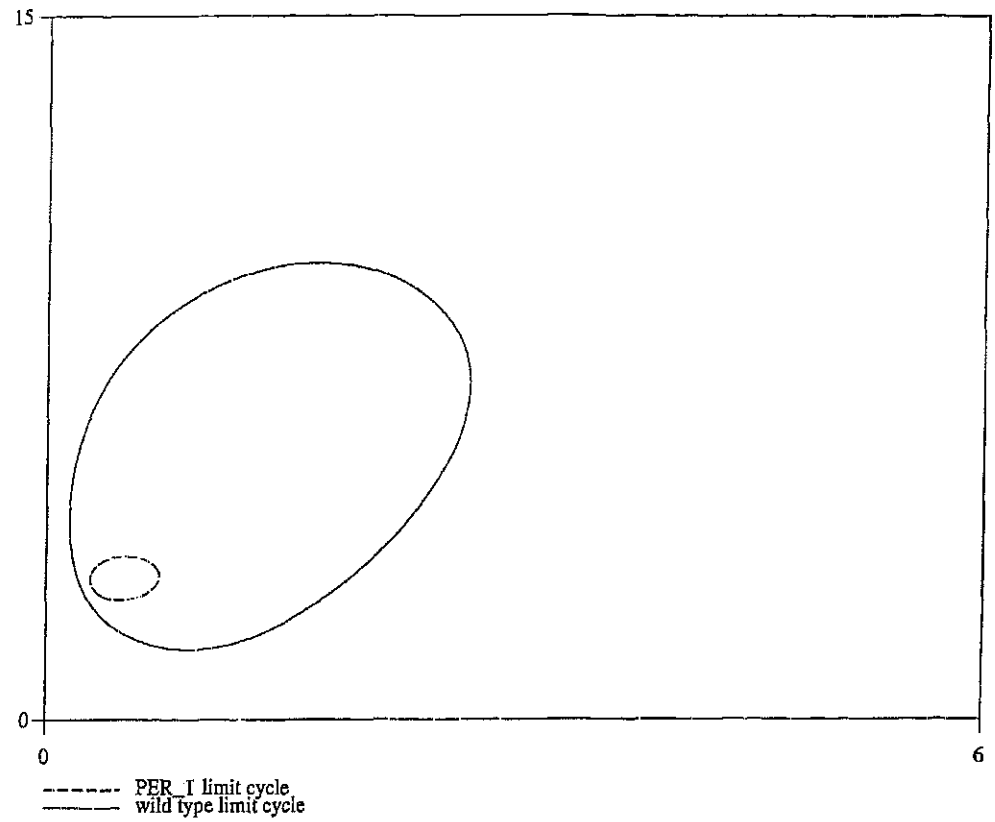

(b)

FIGURE 2. Continued.

of the PER protein, which is measured by the parameter k_s in the above set of equations.

Based on control laws common in applied pharmacokinetics, we used three different stimulation time schemes, each with activating or inhibiting effect on the control parameter:

1. Constant stimulation
2. 24h periodic bolus (one quasi-instantaneous on-off stimulation of very short duration (3 or 6 minutes) every 24h)
3. Rhythmic intermittent stimulation with a period of 24.00h and effective long durations of 1h, 2h, 3h, 4h, 6h, 8h, or 12h (see Fig. 3), at peak or trough time for P_i in the original mutant model.

Activation or inhibition was obtained, starting from the basis value of $0.78h^{-1}$ for k_s, given by Goldbeter in 1995, by adding or subtracting a constant level of amplitude ranging between $0.2h^{-1}$ and $2.0h^{-1}$ for activation and between $-0.2h^{-1}$ and $-0.7h^{-1}$ for inhibition.

Thus, our first aim was to obtain, by modifying k_s, an endogenous rhythm close to 24h for a mutant *Drosophila* and, if possible, phases (peak or trough time, counted from zero, modulo 24h) and oscillation values for the different dynamic variables of the controlled mutant model, which should be close to the ones observed in the nonmutant model.

Second, although we used an open-loop control, we wished to obtain a control law that was sufficiently robust with respect to possible errors in amplitude, period, or phase.

Third, inasmuch as a 24h period was in fact obtained for the controlled limit cycle, we also desired to reach it with transients as short as possible, preferably within 1 week.

Finally, we wanted to obtain transients that were close enough to the final (controlled) limit cycle, thus discarding control laws that showed transient behaviors that were too large or erratic.

RESULTS

The aforementioned system of ordinary differential equations was solved numerically using the public domain software SCILAB (scilab@inria.fr), with integration step = 0.01h (36 seconds, occasionally 0.005h = 18 seconds in case of a brief bolus) and total integration time 216h (= 9 days), occasionally 432h or even 648h. For each mutant (per^l and per^T), two sets of initial values were used: one corresponding to the maximum value of the total PER protein P_t for the noncontrolled cycle (peak) (Fig. 4) and the other one to its minimum value (trough).

Most Common Modes of Control: Bolus and Constant Stimulation

None of these modes of control reached the objective of setting the period of PER oscillations to 24h in a robust way.

First, starting from the per^l type v_d value of 2.0 $\mu M\ h^{-1}$, constant stimulation by setting $k_s = 0.78 + 0.5 = 1.28\ h^{-1}$ leads to a period of 26.5h, closer to 24h, but with oscillation amplitudes much higher than those obtained for the wild-type cycle (with $v_d = 1.6$ $\mu M\ h^{-1}$), whereas inhibition by setting $k_s = 0.28\ h^{-1}$ leads toward oscillations with a lower amplitude and a limit cycle of period 37.5h (Fig. 4a). These oscillation values are thus incompatible with the wild-type values that are our target.

In the same way, starting from the per^T type v_d value of 0.5 $\mu M\ h^{-1}$, stimulation by setting $k_s = 0.78 + 0.5 = 1.28\ h^{-1}$ suppresses the oscillations (Fig. 4b), and inhibition by setting $k_s = 0.28\ h^{-1}$ leads to a period of 22.6h, with a very low amplitude of the oscillations.

In both cases, when applying various stimulation amplitudes according to a $0.1h^{-1}$ grid, we could never obtain a 24h periodicity by such a constant stimulation. However, with the per^T type, taking $k_s = 0.78 - 0.5375 = 0.2425h^{-1}$, we obtained a controlled limit cycle with exactly a 24h period. We did not find this control law to be robust enough to be retained. First, such a control law would demand too high precision, incompatible with the real conditions in applied pharmacokinetics. Second, even if a slight modification in the control parameter values causes only a small period shift in our case, it may give rise to drastic changes and may even lead to a bifurcation in other nonlinear systems.

We then used a brief stimulation by a periodic bolus of 3-minute or even 6-minute duration and a 24h periodicity. Trying various stimulation amplitudes and phases (stimu-

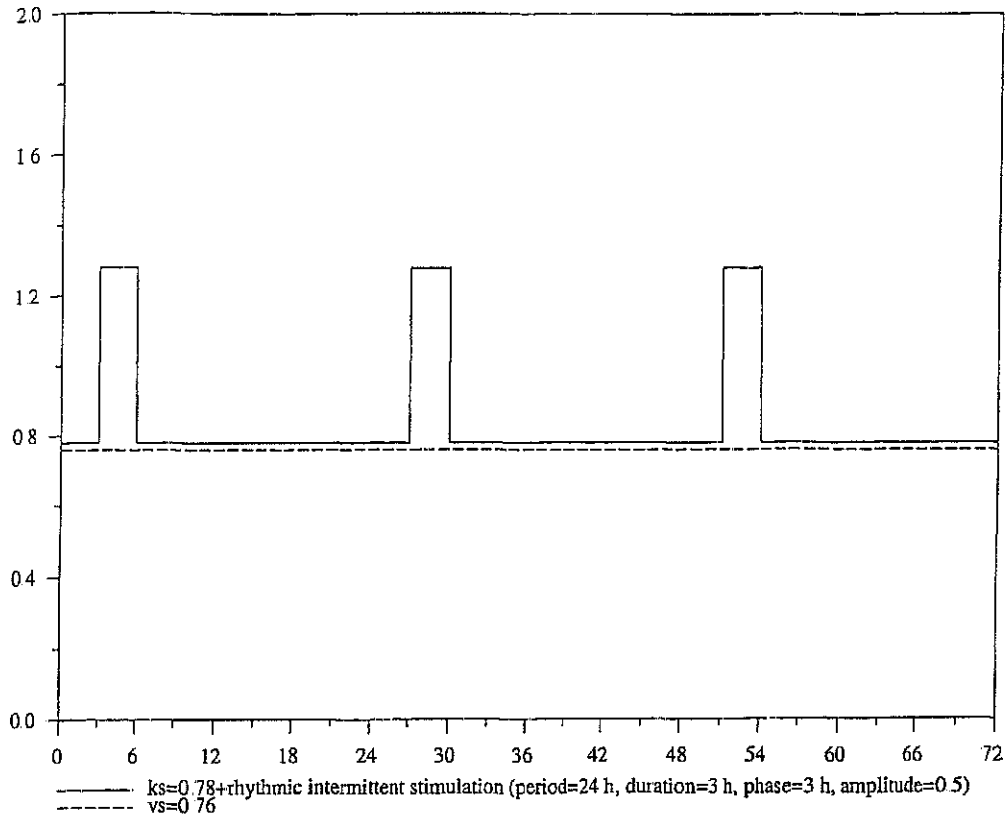

FIGURE 3 Control law applied to the parameter k_s: square wave characterized on this figure by period = 24h, effective duration = 3h, amplitude (activation) = $0.5h^{-1}$, phase from origin = 3h. Bolus would be represented in the same way, but with a much shorter effective duration (3 or 6 minutes) of the stimulus

lation at peak or trough of the noncontrolled cycle), we could never obtain any significant deviation from the initial limit cycle. This probably illustrates the stable nature of the limit cycle, whether for the per^l or the per^T mutant.

Forcing PER Oscillations by Periodic Intermittent Stimulation

We finally used a long 24h periodic stimulation, according to the rhythmic intermittent schemes mentioned above, in amplitude, phase, and time (long time, between 1h and 12h, unlike 0.05h or 0.1h in the bolus scheme). In both mutants and both modes of stimulation, we obtained good entrainment at the desired 24h rhythm in particular zones of the stimulus amplitude and effective stimulation time. The existence of such *zones* (and not only well-defined values) ensures natural robustness of the periodic intermittent stimulation with respect to errors in stimulus period, amplitude, duration, and initial phase (peak or trough or another phase).

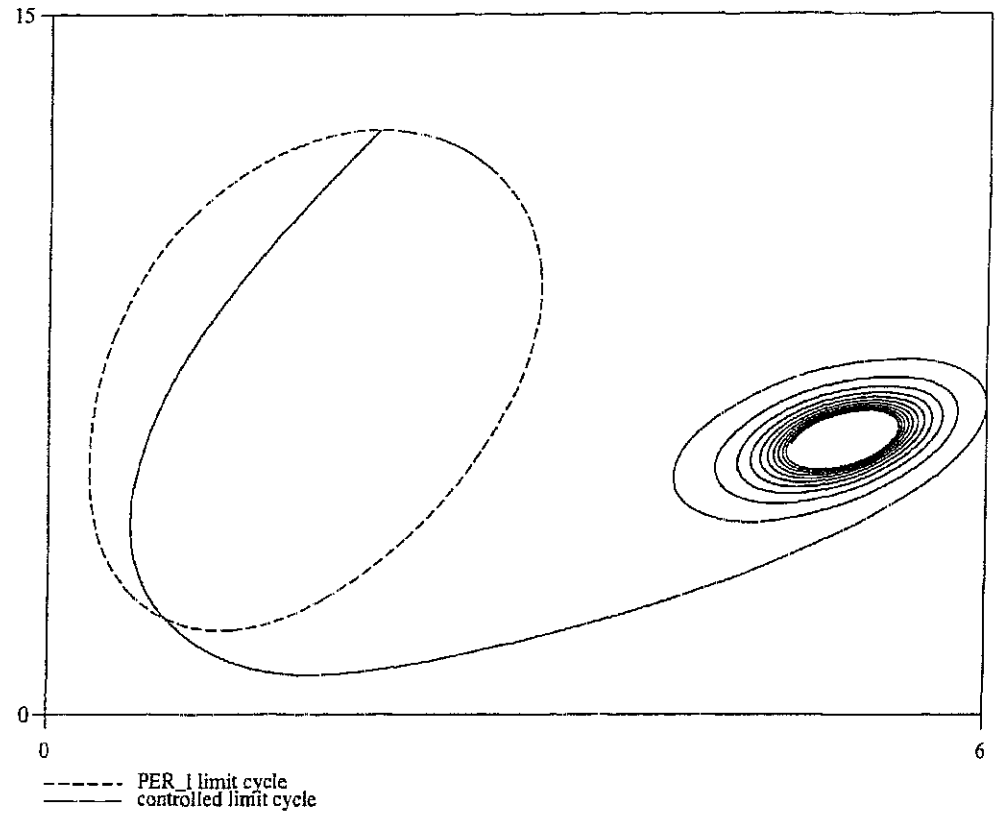

(a)

FIGURE 4. (a) The per^{l} mutant *Drosophila* limit cycle controlled by constant inhibiting stimulation (solid line), with stimulus amplitude $-0.5h^{-1}$, starting at peak time of the noncontrolled per^{l} limit cycle (dashed line) (b) The per^{T} mutant *Drosophila* limit cycle controlled by constant activating stimulation (solid line), with stimulus amplitude $0.5h^{-1}$, starting at peak time of the noncontrolled per^{T} limit cycle (dashed line)

We present, in Tables 1 and 2, lower and upper bounds for the intervals of values added to k_s, in which entrainment was obtained and some additional intermediate values within these intervals. Outside these intervals, various types of behavior were observed: no disruption at all, apparent period doubling with a limit cycle appearing as an invaginated eight (Pascal's "limaçon"), or even completely erratic.

For per^{l} (see Fig. 5a and Table 1), the activation proved to be much better than inhibition, with a good 1-1 entrainment, a satisfying limit cycle, and satisfying transient behavior obtained from only 1h of effective activation, provided that stimulus amplitude was chosen high enough ($1.5h^{-1}$ or $2h^{-1}$), up to 12h of effective activation, with lower amplitude levels (from $0.3h^{-1}$ to $0.7h^{-1}$, for 12h, 8h, and 6h), whereas inhibiting entrainment demanded at least 4h of effective inhibition, with an amplitude as low as $-0.3h^{-1}$, down to $-0.4h^{-1}$, for 12h. The different stimulation schemes shown in Table 1 produced

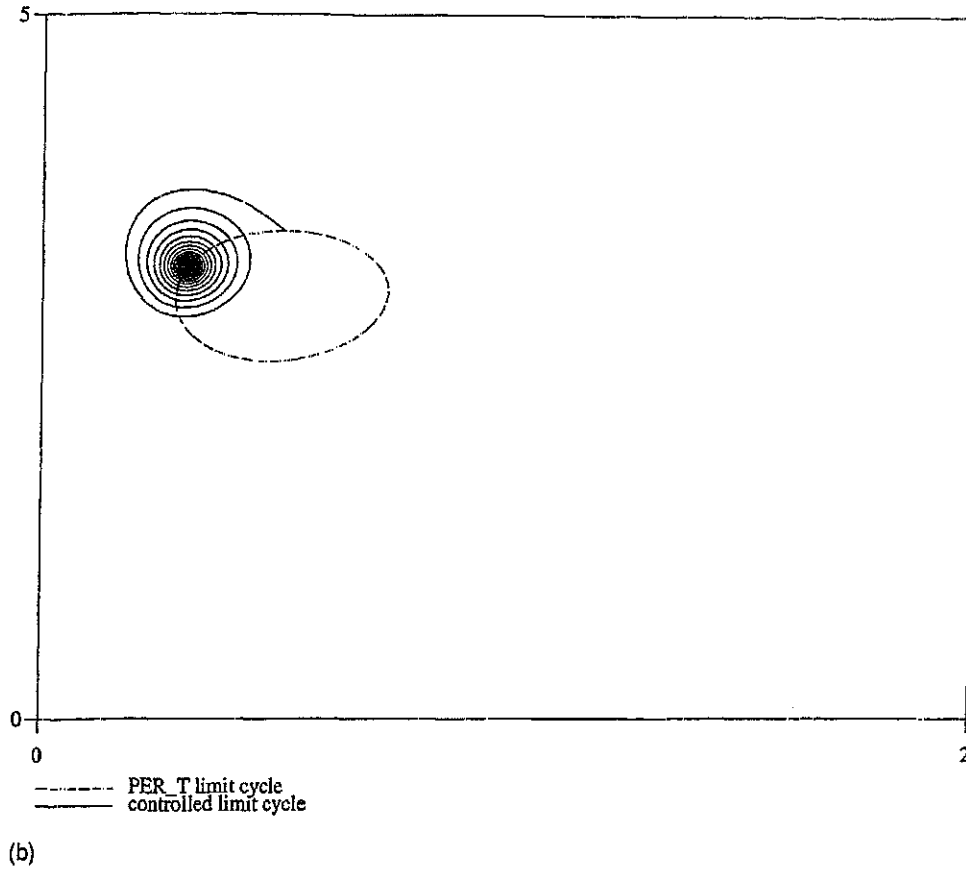

(b)

FIGURE 4. Continued

Table 1. 24h Periodic Intermittent Stimulation of *per*^{l}: Exposure Duration Versus Amplitude of the Activating (Positive Values) or Inhibiting (Negative Values) Stimulus Producing a 1-1 Entrainment, Regardless of the Chosen Initializing Phase, Peak, or Trough of the Original Mutant *P*, Protein Concentration

	Activating							Inhibiting				
1h	—	—	—	—	—	1.5	2	—	—	—	—	—
2h	—	—	—	0.7	1	1.5	—	—	—	—	—	—
3h	—	—	—	0.7	1	—	—	—	—	—	—	—
4h	—	—	0.5	0.7	1	—	—	—	—	—	—	−0.7
6h	0.3	0.4	0.5	0.7	—	—	—	—	—	—	−0.5	−0.7
8h	0.3	0.4	0.5	—	—	—	—	—	−0.35	−0.4	−0.5	−0.7
12h	0.3	0.4	—	—	—	—	—	−0.3	−0.35	−0.4	—	—

Table 2. 24h Periodic Intermittent Stimulation on per^T: Exposure Duration Versus Amplitude of the Activating (Positive Values) or Inhibiting (Negative Values) Stimulus Producing a 1-1 Entrainment Regardless of the Chosen Initializing Phase, Peak, or Trough of the Original Mutant P_t Protein Concentration

	Activating			Inhibiting			
4h	—	—	—	—	—	—	−0.6
6h	—	—	2	—	−0.45	−0.5	—
8h	—	1.5	2	−0.4	−0.45	—	—
12h	1.2	1.5	—	−0.4	−0.45	—	—

a 1-1 entrainment whatever the chosen initial phase was, but usually gave rise to faster convergence if the stimulation started at peak time rather than at trough time, except for the long exposure duration (8h or 12h).

On the other hand, for per^T (see Fig. 5b and Table 2), inhibition proved to be easier than activation. Entrainment was obtained with only 4h of exposure for inhibition (versus 6h for activation) and an amplitude within a narrow range ($-0.4h^{-1}$ to $-0.5h^{-1}$ for high exposure durations of 6h, 8h, and 12h), whereas activating entrainment was obtained only for a stimulus amplitude over 1. Stimulation at peak time usually gave rise to faster convergence than at trough time, with shorter transients and oscillation amplitudes for the limit cycle and transients that were closer to those of the wild type.

DISCUSSION

We could not obtain a 24h period by constant or periodic bolus stimulation in a robust way. From a mathematical point of view, a permanent change in stimulus amplitude may produce a deformation of the limit cycle, modification of its period, or even bifurcation of the dynamic system; as for a brief bolus, it usually produces only phase resetting (cf. Winfree 1980).

The inspection of the good entrainment zones suggested the possibility of a "law of areas" that may define a daily dose for an activator or inhibitor of the reaction: A 1-1 entrainment exists only if the total delivered dose during 24h (the amplitude times the effective stimulation time) lies within an "efficacy interval." Outside this interval, we observed the following unadapted types of behavior:

- too long transients
- no entrainment at all, with the cycle returning to the original mutant cycle and consequently to its original period
- a limit cycle with amplitude values or shape that were too far away from the wild type
- 1-2 entrainment with a 48h period for the controlled limit cycle
- even more complicated trajectories in the (M,P_t) phase plane, with a very disorderly appearance

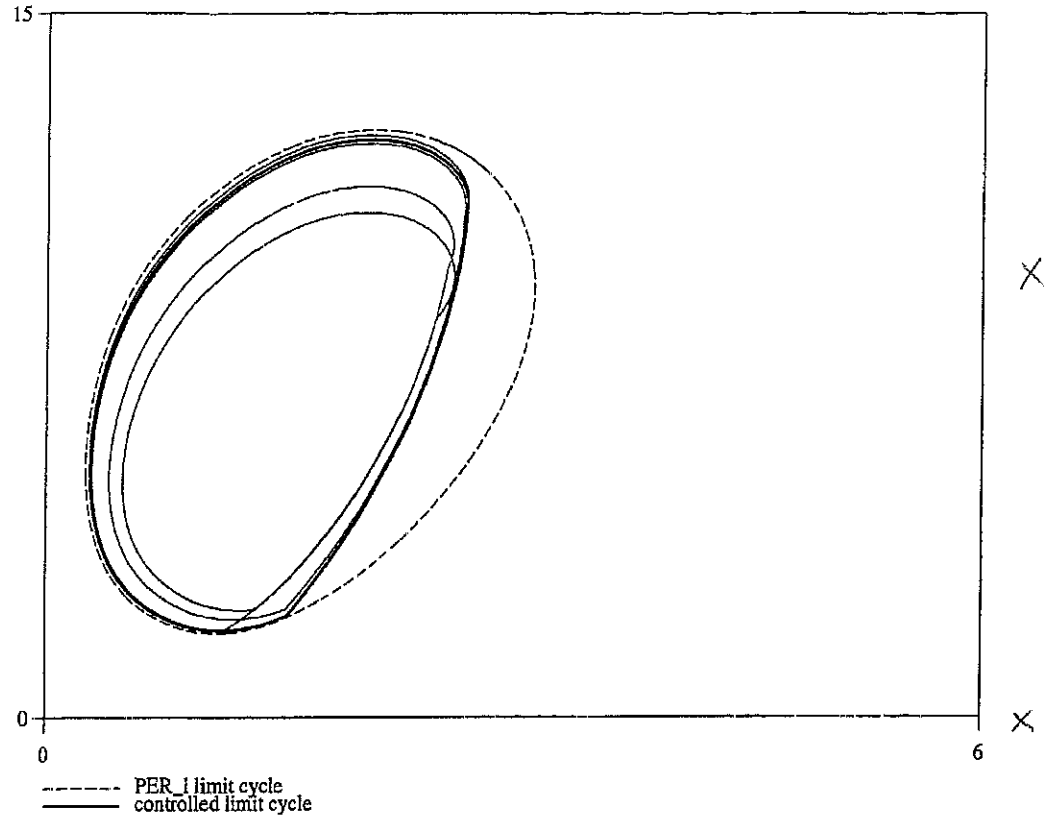

(a)

FIGURE 5 (a) The per^l mutant *Drosophila* limit cycle controlled by 24h periodic intermittent activating stimulation (solid line), with stimulus amplitude $0.4h^{-1}$, exposure duration 6h, starting at trough time of the noncontrolled per^l limit cycle (dashed line). Successful 1-1 entrainment was obtained, with a period of exactly 24h for the controlled per^l limit cycle. (b) The per^T mutant *Drosophila* limit cycle controlled by 24h periodic intermittent inhibiting stimulation (solid line), with stimulus amplitude $-0.4h^{-1}$, exposure duration 8h, starting at peak time of the noncontrolled per^T limit cycle (dashed line). Successful 1-1 entrainment was obtained, with a period of exactly 24h for the controlled per^T limit cycle.

(continued)

Beginning stimulation at peak time or at trough time usually gave the same entrainment results, but not at an equal speed: Very long and/or disorderly transients were observed when the initial phase (peak or trough) was not adapted.

We thus obtained a very good 1-1 entrainment at the desired period of 24h when particular parameters for the control law (stimulus amplitude, effective duration of stimulation, and initial phase) were chosen. We may also fit the phase of the controlled cycle by choosing the pair (amplitude, effective stimulation time). For instance, with the per^l mutant, a good 1-1 entrainment was obtained for a total "delivered daily dose" (of an activator or inhibitor of the reaction) equivalent to a stimulus amplitude for k_s of $+0.8h^{-1}$

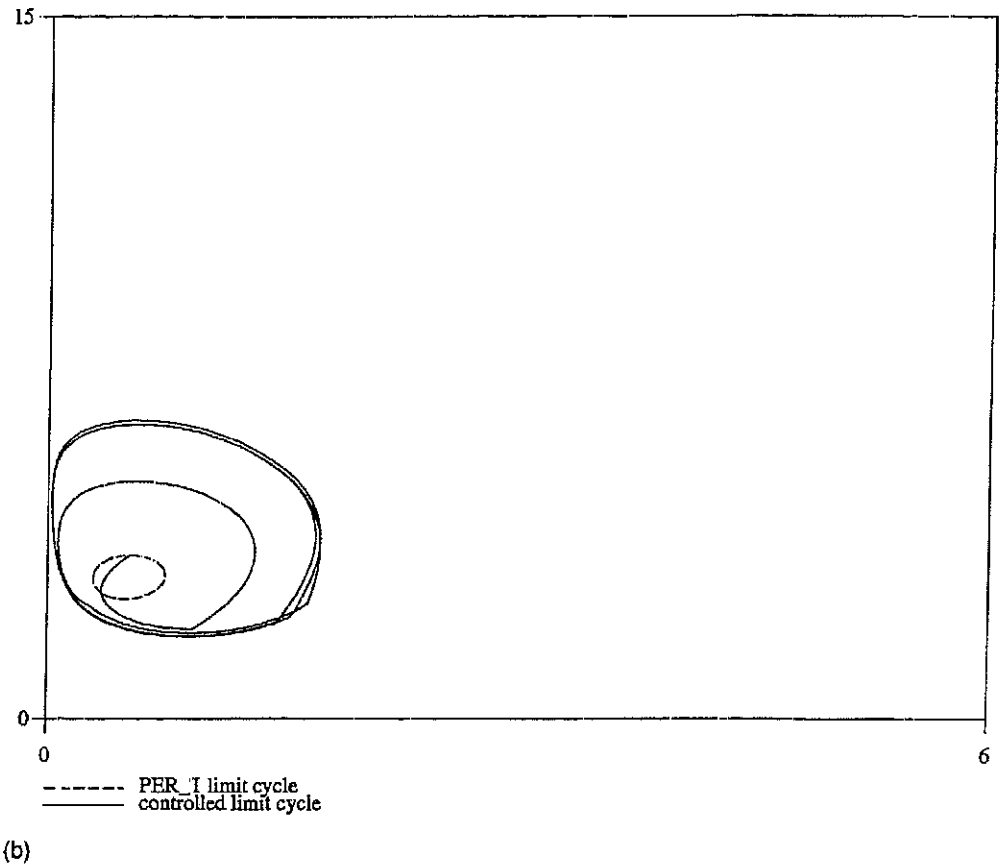

FIGURE 5 Continued.

for 3h, or $+0.6h^{-1}$ for 4h, or $+0.4h^{-1}$ for 6h, or $+0.3h^{-1}$ for 8h, with corresponding P_t peaks at 8.27h, 8.85h, 10.27h, and 12.35h, modulo 24h, from initial time regardless of the choice of the initial phase, peak, or trough time for P_t.

Thus, in this low-dimensional model, which may be taken as a general paradigm of the numerous biological systems in which protein synthesis regulation is involved, we have shown that, using an adapted daily dose, one can shift the period of a "pathological" cycle toward a "physiological" one by varying three factors: total dose, exposure duration, and time of start of exposure (phase). Later, we may improve this tool by frequency coding (Goldbeter 1991, 1993) of the entrainment stimulus, using intermittent burst delivery.

Chronotherapy, until now, has consisted mostly of the rhythmic delivery of medications to improve treatment tolerance and/or efficacy (Lévi 1997; Lévi et al. 1997). Nevertheless, rhythmic alterations of physiological variables have been reported in several diseases, including cancer (Canon and Lévi 1992; Mormont and Lévi 1997) and could also benefit from chronotherapeutic strategies, based on the principle of periodic intermittent drug delivery, developed in this paper.

ACKNOWLEDGMENTS

We are gratefully indebted to A Goldbeter for useful suggestions concerning the choice of control parameters and to F Lévi for helpful remarks during the writing of this work.

This research was supported by the GdR "Automatique" of the French CNRS.

REFERENCES

Bélair J, Glass L, an der Heiden U, et al. 1995. Dynamical disease: Identification, temporal aspects and treatment strategies of human illness. In: Bélair J, Glass L, an der Heiden U, et al, editors. Dynamical disease: mathematical analysis of human illness. Woodbury, New York: American Institute of Physics Press. Reprint of Chaos, 5(1):1–7 1995

Boissin J, Canguilhem B. 1998. Les rythmes du vivant. Origine et contrôle des rythmes biologiques. Paris: Nathan

Bünning E. 1973. The physiological clock. Circadian rhythms and biological chronometry. 3rd rev ed. Berlin: Springer Verlag

Canon C, Levi F. 1992. Immune system in relation to cancer. In: Touitou Y, Haus E, editors. Biological rhythms in clinical and laboratory medicine. Berlin: Springer Verlag, pp. 633–47.

Claude D. 1995. Shift of a limit cycle in biology: from pathological to physiological homeostasia. In: Bélair J, Glass L, an der Heiden U, et al., editors. Dynamical disease: mathematical analysis of human illness. Woodbury, New York: American Institute of Physics Press. Reprint of Chaos, 5(1):162–66.

Claude D, Nadjar N. 1994. Nonlinear adaptive control of adrenal-postpituitary imbalances and identifiability analysis. Math Biosci. 121:155–92

Goldbeter A. 1991. Du codage par fréquence des signaux intercellulaires à l'ébauche d'une chronopharmacologie généralisée. Bulletin et Mémoires de l'Académie de Médecine de Belgique 146:113–27.

Goldbeter A. 1993. Du codage par fréquence des signaux intercellulaires à l'ébauche d'une chronopharmacologie généralisée. Bulletin du Groupe d'étude des Rythmes Biologiques. 25(7):131–45.

Goldbeter A. 1995. A model for circadian oscillations in the *Drosophila* period protein (PER). Proc R Soc Lond B 261:319–24.

Goldbeter A. 1996. Biochemical oscillations and cellular rhythms. Cambridge, UK: Cambridge University Press.

Hartmann C, Joseph C, Millet B. 1998. Biologie et physiologie de la plante. Age chronologique, âge physiologique et activités rythmiques. Paris: Nathan.

Leloup J-C, Goldbeter A. 1997. Temperature compensation of circadian rhythms: control of the period in a model for circadian oscillations of the PER protein in *Drosophila*. Chronobiol Int. 14(5):511–20.

Leloup J-C, Goldbeter A. 1998. A model for circadian rhythms in *Drosophila* incorporating the formation of a complex between the PER and TIM proteins. J Biol Rhythms. 13(1):70–87

Lévi F. 1997. Chronopharmacology of anticancer agents. In: Redfern PH, Lemmer B,

editors Handbook of experimental pharmacology, Vol : physiology and pharmacology of biological rhythms. Berlin: Springer Verlag, pp. 299–331.

Lévi F, Zidani R, Misset J-L. 1997. Randomised multicentre trial of chronotherapy with oxaliplatin, fluorouracil, and folinic acid in metastatic colorectal cancer. Lancet. 350(9079):681–86.

Mormont MC, Lévi F. 1997. Circadian-system alterations during cancer processes: a review. Int J Cancer. 70:241–47.

Sweeney BM. 1969. Rhythmic phenomena in plants. New York: Academic.

Touitou Y, Haus E, editors. 1992, 1994. Biological rhythms in clinical and laboratory medicine. Berlin: Springer Verlag.

Vanden Driessche Th, Guisset J-L, Petiau-deVries GM, editors. 1996. Membranes and circadian rhythms. Berlin: Springer Verlag.

Winfree AT. 1980. The geometry of biological time. Vol. 15. Berlin: Springer Verlag.

ESAIM: M2AN
Vol. 39, N° 6, 2005, pp. 1069–1086
DOI: 10.1051/m2an:2005052

ESAIM: Mathematical Modelling and Numerical Analysis

OPTIMISATION OF TIME-SCHEDULED REGIMEN FOR ANTI-CANCER DRUG INFUSION

Claude Basdevant[1], Jean Clairambault[2] and Francis Lévi[3]

Abstract. The chronotherapy concept takes advantage of the circadian rhythm of cells physiology in maximising a treatment efficacy on its target while minimising its toxicity on healthy organs. The object of the present paper is to investigate mathematically and numerically optimal strategies in cancer chronotherapy. To this end a mathematical model describing the time evolution of efficiency and toxicity of an oxaliplatin anti-tumour treatment has been derived. We then applied an optimal control technique to search for the best drug infusion laws. The mathematical model is a set of six coupled differential equations governing the time evolution of both the tumour cell population (cells of Glasgow osteosarcoma, a mouse tumour) and the mature jejunal enterocyte population, to be shielded from unwanted side effects during a treatment by oxaliplatin. Starting from known tumour and villi populations, and a time dependent free platinum Pt (the active drug) infusion law being given, the mathematical model allows to compute the time evolution of both tumour and villi populations. The tumour population growth is based on Gompertz law and the Pt anti-tumour efficacy takes into account the circadian rhythm. Similarly the enterocyte population is subject to a circadian toxicity rhythm. The model has been derived using, as far as possible, experimental data. We examine two different optimisation problems. The eradication problem consists in finding the drug infusion law able to minimise the number of tumour cells while preserving a minimal level for the villi population. On the other hand, the containment problem searches for a quasi periodic treatment able to maintain the tumour population at the lowest possible level, while preserving the villi cells. The originality of these approaches is that the objective and constraint functions we use are L^∞ criteria. We are able to derive their gradients with respect to the infusion rate and then to implement efficient optimisation algorithms.

Mathematics Subject Classification. 49M29, 92B05, 92C50.

Received: March 18, 2005.

Introduction

An important issue in the treatment of cancer is its tolerability by patients. Drugs that show good therapeutic effects by killing tumour cells are always limited in their use by their toxicity on healthy tissues. Such unwanted toxicity usually depends on the particular drug in use, but since they all act by hindering cell proliferation, the

Keywords and phrases. Dynamical systems, optimisation, circadian rhythms, drugs, therapeutics, cancer.

[1] Université Paris-Nord, Villetaneuse and École Normale Supérieure, 75005 Paris, France. basdevant@lmd.ens.fr

[2] INRIA, projet BANG, 78153 Rocquencourt, France. jean.clairambault@inria.fr (corresponding author)

[3] INSERM E 0354, Hôpital Paul-Brousse, 94800 Villejuif, France. levi-f@vjf.inserm.fr

most exposed healthy cell populations are found in normal fast renewing tissues, such as intestinal mucosa or bone marrow, where cell proliferation is as active as in tumour tissues – though under control.

It is thus of the greatest importance to find differences in the behaviours of healthy and cancer cells towards aggression by anti-tumour treatments. In this respect, to our knowledge, no clear molecular mechanisms have been documented as yet on these differences. But various observations at the macroscopic, cellular or molecular levels have been made and used to try and propose improved chemotherapy treatments in patients with cancer. In particular, according to these observations, the mean cell cycle time is often different between healthy and cancer cells, and even if it is the same, its variance should be higher in cancer cells, due to lack of synchronisation between cells in the cycle; this has led to propose pulsed chemotherapies of cell-cycle phase-specific drugs with the aim to destroy electively proliferating cancer cells [1,9–11,34]. More recently, it has been proposed that the ability to undergo apoptosis (programmed cell death) induced by cytotoxic drugs could be higher in tumour cells than in normal healthy cells, thus explaining the already observed good therapeutic index (anti-tumour efficacy *vs.* unwanted toxicity) of these drugs [14].

But another fact, which has also been observed for a rather long time at the experimental and clinical levels, is that a circadian rhythmicity of the pharmacosensitivity to these drugs (as for most drugs) exists, its phase depends on the particular drug in use, and it is different in cancer and in healthy cells [27]. A molecular basis supporting the influence of circadian clock genes on the expression of genes involved in cell cycle progression and apoptosis has recently been found [16, 17, 28], and chronobiological research is at the present time very active on this topic, even if until now no molecular mechanism has been evidenced for circadian rhythm differences between normal and cancer cells.

The chronotherapy concept thus takes advantage of these observed circadian rhythmicity differences by maximising therapeutic efficacy on a tumour while minimising undesirable toxicity on healthy tissues [27]. One should point out that unlike pulsed therapies with an artificial external period, which may eventually present the drawback of resynchronising a desynchronised population of tumour cells according to this artificial period [2], circadian chronotherapy uses a natural period (circa 24 h), which is present in healthy cells [22] and to a lesser extent in tumour cells [7], for pharmacological sensitivity, to deliver cytotoxic drugs to treat cancer. Furthermore, peripheral cells – and the subjects bearing them –, endowed with this common natural period, are also naturally phase-synchronised by inputs from the light-dark cycle[1].

The object of the present paper is to investigate mathematically and numerically optimal strategies in (circadian) cancer chronotherapy. To this end a mathematical model describing the time evolution of efficacy and toxicity of intravenous oxaliplatin, one of the few drugs active on metastatic colorectal cancer, has been derived [8]. We have then applied an optimal control technique to obtain the best law for the drug infusion flow.

Many authors have previously addressed optimal control problems, often with L^1 or L^2 criteria, for anticancer chemotherapy. They did so mostly by taking into account acquired resistance of tumour cells to cytotoxic drugs, with or without cell cycle phase specificity (reviews in [15,25,33]), but usually without pharmacokinetic-pharmacodynamic (PK-PD) modelling. We address here neither drug resistance nor cell cycle phase specificity, but rather focus on a balance between anti-tumour efficacy and healthy tissue toxicity of cytotoxic drugs, as has also been done in [23, 24]. In this limited setting, we consider our approach original inasmuch as it uses pure L^∞ criteria (though using a nonlinear conjugate gradient method), includes PK-PD modelling, and takes into account drug circadian effects.

Section 2 will be devoted to the study of mathematical models for the cell populations submitted to drug infusion. We will first consider the healthy tissues and then the tumour cells. We will show that the minimal (or maximal) cell population during a given time interval happens to be a differentiable function of the drug infusion law, the gradient of which can be derived. In Section 3 two different optimisation problems are addressed; the eradication problem consists in finding the drug infusion law leading to the smallest, and possibly vanishing, tumour population; the containment problem looks for a treatment that forces the number of tumour cells to

[1]Through a retinohypothalamic tract, a central circadian pacemaker located in the hypothalamus, and pathways from there to peripheral tissues still remaining to be elucidated, but which include the autonomic nervous system and corticoid hormones [27].

remain at the lowest possible level while preserving an acceptable level for the healthy tissues. In Section 4 numerical results are presented; discussion and conclusion follow in Section 5.

1. The model

1.1. Experimental and pharmacological background

Given the scarcity of long followup human data on untreated tumour growth, we used animal experimentation. Oxaliplatin, one of the few drugs active on metastatic colorectal cancer, is also known to be active on Glasgow osteosarcoma in mice. This murine tumour, transplanted under the skin of the animal, is easily measurable at the laboratory with a caliper, which allows obtaining tumour growth curves, with or without treatment, in whole living animals[18] (animals in which tumours had reached 10% of their total body weight were sacrificed for ethical reasons).

The main toxicities of oxaliplatin in Man are on bone marrow, peripheral sensory nerves, and the jejunum[26]. In mice, the main toxicity is on the jejunum (producing extended necrosis of the mucosa)[4, 5], which led us to design a simple model for jejunal mucosa proliferation and homeostasis, which one may take as a paradigm of fast renewing healthy tissue behaviour subject to drug toxicity, within a global model designed to represent both therapeutic efficacy and toxicity.

Plasma pharmacokinetic parameters for oxaliplatin (a drug which binds covalently, *i.e.* irreversibly to its targets or to detoxicating molecules in living cells) have been taken from published data[4, 5] and input to a simple first order model; tissue pharmacokinetic parameters (measuring the decrease of drug quantities in both types of tissues, tumour and jejunal mucosa) were identified either from published data[4, 5], or by an overall estimation when data were not available. The efficacy or toxicity function describing the cell kill effect was chosen of the Hill type, taking into account pharmacological uses and recent published studies [13, 30], its maximum being modulated by a 24 h-periodic cosine representing circadian pharmacosensitivity. Tissue pharmacodynamic parameters – including maximal and minimal pharmacosensitivity phases – were identified as much as possible from laboratory curves[18] (comparison between treated and untreated tumour growth) or else only estimated on the basis of likeliness after other drug or tissue data when no relevant data were available.

1.2. The healthy tissue: jejunal villi cells

We chose for the representation of jejunal mucosa homeostasis a simple damped linear model, which mimics in a satisfactory way what is known of the recovery behaviour of enterocytes subject to radiotoxic or cytotoxic insult[31]. It may be thought of as the linearisation of a more complex nonlinear model[6] about a stable equilibrium point, which from a pathophysiological point of view is actually a very stable equilibrium point, representing tissue homeostasis. The drug toxicity effect was supposed to be active only on the compartment representing the influx of young cells to the jejunal villi, since mature cells are unable to proliferate in the jejunal mucosa, and oxaliplatin, as most anti-cancer drugs, is active mainly on proliferating cells.

1.2.1. *Mathematical model for villi population*

The mathematical model for the villi population $A(t)$ at time t consists in a set of four coupled differential equations:

$$\frac{\mathrm{d}P}{\mathrm{d}t} = -\lambda P + \frac{i(t)}{V_{\mathrm{dist}}}\Phi(t) \tag{1}$$

$$\frac{\mathrm{d}C}{\mathrm{d}t} = -\mu C + \xi_C P \tag{2}$$

$$\frac{\mathrm{d}Z}{\mathrm{d}t} = \{-\alpha - f(C,t)\}\, Z - \beta A + \gamma \tag{3}$$

$$\frac{\mathrm{d}A}{\mathrm{d}t} = Z - Z_{eq}. \tag{4}$$

Here P and C stand, respectively, for drug concentrations in the plasmatic and target cell population compartments (plasma and the jejunal mucosa, target of toxicity, *i.e.* of unwanted side effects of the drug). V_{dist} is the distribution volume, *i.e.* the volume of the central (plasmatic) compartment, in which the active drug is infused. A is the number of mature (villi) jejunal enterocytes, Z is the instantaneous flow to villi from crypts, rate of renewal to make up for natural elimination of villi enterocytes in the intestinal lumen. $\Phi(t)$ is given, equal to 1 during authorized infusion periods and 0 elsewhere and $i(t) \geq 0$ is the time dependent drug infusion law. Function f represents the drug toxicity on the healthy jejunal mucosa, assumed to be periodic, more precisely here to have circadian variations with period T_A; it is given by:

$$f(C,t) = F\left(1 + \cos\left(2\pi \frac{t-\varphi_A}{T_A}\right)\right) \frac{C^{\gamma_A}}{C_{50}^{\gamma_A} + C^{\gamma_A}}$$

$\lambda, \mu, \xi_C, \alpha, \beta, \gamma, Z_{eq}, F, \varphi_A, \gamma_A, C_{50}$ are positive constants. These equations represent drug diffusion and elimination by first order pharmacokinetics for concentrations in the plasmatic and target cell compartments (P and C), and normal jejunal mucosa homeostasis by a linear system showing a stable focus at $(Z_{eq}, A_{eq} = \beta^{-1}(\gamma - \alpha Z_{eq}))$, perturbed by the drug toxicity function which comes to strengthen the natural self-regulation coefficient α.

Classical ODE theorems demonstrate that, initial conditions at time t_0 been given for $X_A(t) = (P(t), C(t), Z(t), A(t))$, and a piecewise continuous infusion profile $i(t)$ been prescribed, system (1–4) has a continuous, piecewise C^1, solution for $t \in [t_0, t_f]$ (for any $t_f > t_0$). Moreover:

$$i \in L^2([t_0,t_f]) \longrightarrow A \in H^4([t_0,t_f])$$

is a continuous, weakly continuous, differentiable application, $A(t)$ being a C^3, piecewise C^4, function of time[2].

Remark 1. Functions P, C, Z, A and most functions in the following will be considered as functions of time t and of i the infusion law (which is also itself a function of time), however we will omit to note the i-dependency whenever there is no ambiguity, hence writing A or $A(t)$ rather than $A(i,t)$.

Remark 2. Functions P and C are drug concentrations and thus positive quantities; equations (1) and (2) ensure they remain positive. Unfortunately equations (3)–(4) do not ensure the positivity of A, a population count; however, when $A(t)$ reaches zero the animal (or the patient: it is noteworthy that in clinical settings severe jejunal depletion may yield diarrhoeas which may be fatal) is already dead and the model is no longer valid!

In order to find optimal infusion laws by means of descent algorithms, we need to know the gradients with respect to the infusion law of objective or constraint functions, that is, if $W(i)$ is such a differentiable real function of $i \in L^2([t_0,t_f])$, and $\dfrac{\partial W}{\partial i}$ its differential with respect to i, the gradient $\nabla_i W(i)$ is the element of $L^2([t_0,t_f])$ such that:

$$\frac{\partial W}{\partial i}.di = \langle \nabla_i W(i), di \rangle$$

[2]In fact, solution of (1) reads:

$$P(t) = P(t_0)\mathrm{e}^{-\lambda t} + \int_{t_0}^{t} \frac{i(\tau)}{V} \Phi(\tau) \mathrm{e}^{-\lambda(t-\tau)} \mathrm{d}\tau,$$

thus, if i is in L^2, P is in H^1 and the application from L^2 to H^1 is affine, continuous, weakly-continuous, differentiable. Moreover if i is piecewise continuous, P is continuous and piecewise C^1.
The behaviour of (2) is similar; if P is H^1 then C is an infusion profile piecewise continuous, C is C^1 and piecewise C^2 in time.
Now system (3-4) is linear with piecewise C^2 coefficients, thus system (3-4) has a solution that is C^2 and piecewise C^3, for a piecewise continuous infusion, therefore A is C^3 and piecewise C^4. Function $f(C,t)$ being a Lispchitz function of C, A is a regular function of C and then a continuous, weakly continuous, differentiable application of i.

where $\langle \nabla_i W(i), di \rangle$ is the scalar product of $L^2([t_0, t_f])$:

$$\langle \nabla_i W(i), di \rangle = \int_{t_0}^{t_f} \nabla_i W(i)(\tau) di(\tau) \mathrm{d}\tau$$

This will be done in the following paragraphs.

1.2.2. *A first function of the villi population*

Let us define, for η a given time in $]t_0, t_f[$, a function $\tilde{F}_A$ of the drug infusion law by

$$\tilde{F}_A(i, \eta) = \tau_A - \frac{A(\eta)}{A_{eq}}$$

where A_{eq} is a reference level for the villi population and $\tau_A \in]0, 1]$ a tolerable fraction of this reference level. We know that F_A is a continuous, weakly continuous, differentiable function of $i \in L^2([t_0, t_f])$. To obtain its gradient, we will demonstrate the following lemma:

Lemma 1. *The gradient $\nabla_i \tilde{F}_A$ of $\tilde{F}_A$ with respect to the infusion profile i is defined in $L^2([t_0, t_f])$ by:*

$$\nabla_i \tilde{F}_A = \begin{cases} \dfrac{\Phi(t)}{V_{\text{dist}}} P_{a1}(t) & \forall t \in [t_0, \eta] \\ 0 & \forall t > \eta \end{cases} \tag{5}$$

where P_{a1} is given by the adjoint system, defined for $t_0 \leq t \leq \eta$:

$$\frac{\mathrm{d}P_{a1}}{\mathrm{d}t} = \lambda P_{a1} - \xi_C P_{a2} \tag{6}$$

$$\frac{\mathrm{d}P_{a2}}{\mathrm{d}t} = \mu P_{a2} + P_{a3} Z \frac{\partial f}{\partial C}(C, t) \tag{7}$$

$$\frac{\mathrm{d}P_{a3}}{\mathrm{d}t} = \{\alpha + f(C, t)\} P_{a3} - P_{a4} \tag{8}$$

$$\frac{\mathrm{d}P_{a4}}{\mathrm{d}t} = \beta P_{a3} \tag{9}$$

with initial conditions at time η:

$$P_{a1}(\eta) = P_{a2}(\eta) = P_{a3}(\eta) = 0 \quad \textit{and} \quad P_{a4}(\eta) = -\frac{1}{A_{eq}}.$$

The proof of the lemma can be obtained by mere identification. Indeed, one has to verify that for any $di \in L^2([t_0, t_f])$:

$$\frac{\partial \tilde{F}_A}{\partial i}.di = -\frac{\bar{A}(\eta)}{A_{eq}} = \int_{t_0}^{t_f} \nabla_i \tilde{F}_A(\tau)\, di(\tau)\, \mathrm{d}\tau \tag{10}$$

where $\bar{A} = \dfrac{\partial A}{\partial i}.di$, the differential of A with respect to i applied to di, is defined by the following linear tangent system, defined for $t \geq t_0$:

$$\frac{\mathrm{d}\bar{P}}{\mathrm{d}t} = -\lambda \bar{P} + \frac{di(t)}{V_{\mathrm{dist}}}\Phi(t) \tag{11}$$

$$\frac{\mathrm{d}\bar{C}}{\mathrm{d}t} = -\mu \bar{C} + \xi_C \bar{P} \tag{12}$$

$$\frac{\mathrm{d}\bar{Z}}{\mathrm{d}t} = \{-\alpha - f(C,t)\}\,\bar{Z} - \frac{\partial f}{\partial C}(C,t)\,\bar{C}\,Z - \beta \bar{A} \tag{13}$$

$$\frac{\mathrm{d}\bar{A}}{\mathrm{d}t} = \bar{Z} \tag{14}$$

with vanishing initial conditions at $t = t_0$.

The calculation then goes as follows; if $\nabla_i \tilde{F}_A$ is defined by (5), then:

$$\begin{aligned}\int_{t_0}^{t_f} \nabla_i \tilde{F}_A(\tau)\, di(\tau)\, \mathrm{d}t &= \int_{t_0}^{\eta} \nabla_i \tilde{F}_A(\tau)\, di(\tau)\, \mathrm{d}\tau \\ &= \int_{t_0}^{\eta} P_{a1}(\tau)\frac{\Phi(\tau)}{V_{\mathrm{dist}}}\, di(\tau)\, \mathrm{d}\tau\end{aligned}$$

and using equations (11)–(14):

$$\begin{aligned}= \int_{t_0}^{\eta} \Bigg\{ & P_{a1}(\tau)\left(\frac{\mathrm{d}\bar{P}}{\mathrm{d}t} + \lambda \bar{P}\right) + P_{a2}(\tau)\left(\frac{\mathrm{d}\bar{C}}{dt} + \mu \bar{C} - \xi_C \bar{P}\right) \\ & + P_{a3}(\tau)\left(\frac{\mathrm{d}\bar{Z}}{\mathrm{d}t} + \{\alpha + f(C,t)\}\,\bar{Z} + \frac{\partial f}{\partial C}(C,t)\,\bar{C}\,Z + \beta \bar{A}\right) \\ & + P_{a4}(\tau)\left(\frac{\mathrm{d}\bar{A}}{\mathrm{d}t} - \bar{Z}\right)\Bigg\}\,\mathrm{d}\tau\end{aligned}$$

doing one integration by parts, the result (10) is obtained using equations (6)–(9) and the boundary conditions at t_0 for the $\bar{P}, \bar{C}, \bar{Z}, \bar{A}$ and at η for $P_{a1}, P_{a2}, P_{a3}, P_{a4}$.

1.2.3. *The minimal villi population*

Now consider the constraint:

$$F_A(i) = \tau_A - \min_{t \in [t_0, t_f]} \frac{A(t)}{A_{eq}} \leq 0,$$

where again A_{eq} is a reference level for the villi population and $\tau_A \in]0,1]$ a tolerable fraction of this reference level. We know that F_A is a continuous, weakly continuous, real function of $i \in L^2([t_0, t_f])$. The following theorem tells us that in most cases the gradient of F_A exists and can be computed using the adjoint system (6)–(9).

Theorem 1. If in the vicinity of infusion i the minimum of $A(t)$ is unique, belongs to $]t_0, t_f[$ with a strictly positive second derivative, then F_A is a differentiable function of i. If we denote by $t_A(i)$ the time at which A reaches its minimum, then the gradient $\nabla_i F_A$ is given by:

$$\nabla_i F_A(i)(t) = \begin{cases} \nabla_i \tilde{F}_A(i, t_A)(t) & \forall t \in [t_0, t_A] \\ 0 & \forall t > t_A. \end{cases}$$

Let us show first that, under these hypothesis, t_A is a differentiable function of i. In fact t_A is locally in time defined by the equation $\frac{\partial A(i, t_A(i))}{\partial t} = 0$. With the hypothesis that $\frac{\partial^2 A(i, t_A(i))}{\partial t^2} > 0$, and the property that A is

a differentiable function of i, the implicit function theorem applied to the equation $\frac{\partial A(i,t)}{\partial t} = 0$ gives the result. Then the computation of the gradient relies on the differentiation chain rule: as $F_A(i) = \tilde{F}_A(i, t_A)$,

$$\frac{\partial F_A(i)}{\partial i}.di = \frac{\partial \tilde{F}_A(i,t_A)}{\partial i}.di + \frac{\partial \tilde{F}_A(i,t_A)}{\partial t}\frac{\partial t_A}{\partial i}.di.$$

The minimum of $A(t)$ been reached at time t_A it follows that $\frac{\partial \tilde{F}_A(i,t_A)}{\partial t} = 0$ and the results follows.

1.3. **The tumour cell population**

Tumour growth was modelled according to a Gompertz law, which is one of the simplest laws classically used for this purpose [12, 20, 21]. The variable B which stands for tumour cell population number (see equations below) is in this model bound to eventually reach a plateau B_{max}, after an initial exponential growth, following an S-shaped curve. The accuracy of the Gompertz model for tumour growth has often been questioned, but also justified on refined modelling grounds (using quiescent and proliferative subpopulations inside the tumour); it is generally accepted at least as a first intention simple modelling approach for this purpose, and we decided to use it in this sense.

1.3.1. *Mathematical model for the tumour cell population*

The mathematical model for the tumour cell population $B(t)$ at time t consists in a set of three coupled differential equations:

$$\frac{\mathrm{d}P}{\mathrm{d}t} = -\lambda P + \frac{i(t)}{V_{\mathrm{dist}}}\Phi(t) \tag{15}$$

$$\frac{\mathrm{d}D}{\mathrm{d}t} = -\nu D + \xi_D P \tag{16}$$

$$\frac{\mathrm{d}B}{\mathrm{d}t} = -aB\ln\left(\frac{B}{B_{\max}}\right) - g(D,t)B \tag{17}$$

where equation (15) is the same as (1), D stands for drug concentration (assumed to be homogeneously diffused) in the tumour and B is the number of tumour cells. Function g, which represents anti-tumour drug efficacy, is assumed (as is function f for toxicity) to present circadian variations with period T_B; it is given by:

$$g(D,t) = H\left(1 + \cos\left(2\pi\frac{t-\varphi_B}{T_B}\right)\right)\frac{D^{\gamma_B}}{D_{50}^{\gamma_B} + D^{\gamma_B}}$$

where $\lambda, \nu, \xi_D, a, B_{\max}, H, \varphi_B, \gamma_B, D_{50}$ are positive constants.

Initial conditions at time t_0 been given for $X_B(t) = (P(t), D(t), B(t))$, and a piecewise continuous infusion profile $i(t)$ been prescribed, system (15)–(17) has a continuous, piecewise C^1, solution for $t \in [t_0, t_f]$ for any $t_f > t_0$. Moreover:

$$i \in L^2([t_0,t_f]) \longrightarrow B \in H^3([t_0,t_f])$$

is a continuous, weakly continuous, differentiable application, $B(t)$ being a C^2, piecewise C^3, function of time. The demonstration is similar to the one for A (note that Eq. (17) is a linear equation for the unknown $\ln(B)$).

Remark 3. Equations (15)–(17) ensure the positivity of P, C and B. Nevertheless we will consider that the tumour has been completely destroyed if $B(t) < 1$, thus integration of equation (17) has to be stopped when this arises.

Equation (17) is made of the Gompertz law for the tumour cell population growth and of a linear destruction law (modulated by the circadian effect) for the anti-tumour efficacy. The latter has at least two drawbacks.

First, the drug is less and less efficient when the tumour gets smaller, one may wonder if this behaviour is realistic. Conversely, the drug is more and more efficient when the tumour gets larger. These two extreme behaviours explain why the numerical results are in practice nearly independent of the initial size $B(0)$ of the tumour. An alternative modelling assumption could be to replace $-g(D,t)B$ by a non linear term such as $-g(D,t)\frac{B}{1+B}$ in equation (17). But in the absence of experimental or clinical data supporting this hypothesis, we decided to keep the growth inhibition term in its linear form.

1.3.2. *A first function of the tumour cell population*

Let us define, for $\eta \in [t_0, t_f]$, a function $\tilde{F}_B$ of the drug infusion law by:

$$\tilde{F}_B(i,\eta) = B(\eta).$$

We know that F_B is a continuous, weakly continuous, differentiable function of $i \in L^2([t_0,t_f])$. We will demonstrate the following lemma:

Lemma 2. *The gradient $\nabla_i \tilde{F}_B$ of $\tilde{F}_B$ with respect to the infusion profile i is defined in $L^2([t_0,t_f])$ by:*

$$\nabla_i \tilde{F}_B = \begin{cases} \dfrac{\Phi(t)}{V_{\text{dist}}} P_{b1}(t) & \forall t \in [t_0, \eta] \\ 0 & \forall t > \eta \end{cases}$$

where P_{b1} is given by the adjoint system, defined for $t_0 \le t \le \eta$:

$$\frac{\mathrm{d}P_{b1}}{\mathrm{d}t} = \lambda P_{b1} - \xi_D P_{b2} \tag{18}$$

$$\frac{\mathrm{d}P_{b2}}{\mathrm{d}t} = \nu P_{b2} + P_{b3} B \frac{\partial g}{\partial D}(D,t) \tag{19}$$

$$\frac{\mathrm{d}P_{b3}}{\mathrm{d}t} = P_{b3}\left(a \ln\left(\frac{B}{B_{\max}}\right) + a - g(D,t)\right) \tag{20}$$

with initial conditions at time η:

$$P_{b1}(\eta) = P_{b2}(\eta) = 0 \quad \textit{and} \quad P_{b3}(\eta) = 1.$$

As it has been done for $\tilde{F}_A$, the proof of the lemma can be obtained by mere identification. For any $di \in L^2([t_0,t_f])$:

$$\frac{\partial \tilde{F}_B}{\partial i}.di = \bar{B}(\eta) = \int_{t_0}^{t_f} \nabla_i \tilde{F}_B(\tau)\, di(\tau)\, \mathrm{d}\tau$$

where $\bar{B} = \dfrac{\partial B}{\partial i}.di$, the differential of B with respect to i applied to di, is obtained by solving the following linear tangent system, defined for $t \ge t_0$:

$$\frac{\mathrm{d}\bar{P}}{\mathrm{d}t} = -\lambda \bar{P} + \frac{di(t)}{V_{\text{dist}}}\Phi(t) \tag{21}$$

$$\frac{\mathrm{d}\bar{D}}{\mathrm{d}t} = -\nu \bar{D} + \xi_D \bar{P} \tag{22}$$

$$\frac{\mathrm{d}\bar{B}}{\mathrm{d}t} = -a\bar{B}\ln\left(\frac{B}{B_{\max}}\right) - a\bar{B} - g(D,t)\bar{B} - \frac{\partial g}{\partial D}(D,t)\bar{D}B \tag{23}$$

with vanishing initial conditions at $t = t_0$.

1.3.3. *The maximal (or minimal) tumour cell population*

Now consider the objective function:

$$J_B(i) = \max_{t\in[t_1,t_f]} B(t),$$

where t_1 is a given time after the initial phase of the treatment. We know that J_B is a continuous, weakly continuous, real function of $i \in L^2([t_0,t_f])$. The following theorem tells us that in most cases the gradient of J_B exists and can be computed using the adjoint system (18)–(20).

Theorem 2. If in the vicinity of infusion i the maximum of $B(t)$ in $]t_1,t_f[$ is unique with a strictly negative second derivative, then J_B is a differentiable function of i. If we denote by $t_B(i)$ the time at which B reaches its maximum, then the gradient $\nabla_i J_B$ is given by:

$$\nabla_i J_B(i)(t) = \begin{cases} \nabla_i \tilde{F}_B(i,t_B)(t) & \forall t \in [t_0,t_B] \\ 0 & \forall t > t_B. \end{cases}$$

The proof of the theorem is similar to the one for the villi population and relies on the differentiation chain rule as $J_B(i) = \tilde{F}_B(i,t_B)$.

Remark 4. A similar result is valid for $G_B(i) = \min_{t\in[t_0,t_f]} B(t)$.

2. Two optimisation problems

2.1. The eradication problem

Let us consider the problem of finding the infusion law leading to the smallest, and possibly vanishing, tumour population while preserving a minimal villi population. Mathematically this can be written: find the infusion law $i \in L^2([t_0,t_f])$, $i(t) \geq 0$, that minimises the objective function:

$$G_B(i) = \min_{t\in[t_0,t_f]} B(t)$$

subject to the constraint

$$F_A(i) = \tau_A - \min_{t\in[t_0,t_f]} \frac{A(t)}{A_{eq}} \leq 0.$$

As F_A is weakly continuous, the ensemble of admissible solutions

$$U = \left\{ i \in L^2([t_0,t_f]) \mid 0 \leq i\,,\, F_A \leq 0 \right\}$$

is weakly closed in $L^2([t_0,t_f])$; as the infused drug destroys the villi population U is also bounded; G_B being weakly continuous, this ensures the existence of an optimal infusion law for the eradication problem. However neither the objective function, nor the constraint are convex functions of the infusion law. The optimum may not be unique (indeed $i(t)$ remains undefined where $\Phi(t) = 0$) and, moreover, there may exist local minima. Nevertheless the results from previous sections allow us to define descent algorithms to find quasi-optimal strategies. A Uzawa-like saddle-point algorithm (see *e.g.* [3]) for solving the eradication problem is:

(1) Start with a Lagrange multiplier $\alpha_A^0 > 0$.
(2) Find i^k, minimising $J(i) = G_B(i) + \alpha_A^k F_A(i)$ in $L^2([t_0,t_f]) \cap \{i \geq 0\}$.
(3) Define α_A^{k+1} by $\alpha_A^{k+1} = \max\left\{\alpha_A^k + \rho F_A(i^k), 0\right\}$.
(4) Until $F_A(i^k) \approx 0$.

In step (3) the coefficient $\rho > 0$ has to be chosen adequately (in fact this step corresponds to a gradient algorithm for the dual problem). In practice we found more efficient to use for step (3) a bisection or a secant algorithm to find the Lagrange multiplier α_A associated to the active constraint $F_A = 0$.

Remark 5. If other constraints are to be imposed on the infusion law, such for example a bound for the total infusion or a maximum instantaneous infusion rate, these constraints can be treated either in step (2) or using more Lagrange multipliers.

2.2. **The containment problem**

Unfortunately there may not exist a treatment that destroys down to a sufficiently low level the tumour cells while keeping a sufficiently high level of villi cells. As the number of villi cells is in clinical settings of primary importance for the patient's life, one has then to reduce the infusion rate and consequently the treatment course will end with a non negligible number of residual tumour cells. Due to the Gompertz law, the tumour will then grow up rapidly after the end of the course. In that context one has to look for a containment treatment, that is a treatment repeated periodically in time that forces the number of tumour cells to remain at the lowest possible level while preserving an acceptable number of villi cells. Mathematically this can be written: find the infusion law $i \in L^2([t_0, t_f])$, $i(t) \geq 0$, that minimises the objective function:

$$J_B(i) = \max_{t\in[t_1,t_f]} B(t)$$

subject to the constraint

$$F_A(i) = \tau_A - \min_{t\in[t_0,t_f]} \frac{A(t)}{A_{eq}} \leq 0.$$

In that case function $\Phi(t)$, that defines infusion periods, should for example take the value 1 during two days, then 0 during five days (no treatment), and then repeatedly until t_f; as for t_1 it can be taken to be 1 or 2 days after t_0 in order to allow the initial infusion to reduce significantly the tumor.

In the same way as for the eradication problem, J_B is a weakly continuous function on a bounded weakly closed ensemble, thus the optimal infusion exists, however the minimum may not be unique and local minima may also exist.

The Uzawa-like algorithm defined previously can be applied similarly to the containment problem:

(1) Start with a Lagrange multiplier $\alpha_A^0 > 0$.
(2) Find i^k, minimising $J(i) = J_B(i) + \alpha_A^k F_A(i)$ in $L^2([t_0, t_f]) \cap \{i \geq 0\}$.
(3) Define α_A^{k+1} by $\alpha_A^{k+1} = \max\left\{\alpha_A^k + \rho F_A(i^k), 0\right\}$.
(4) Until $F_A(i^k) \approx 0$.

2.3. **A descent algorithm**

We will briefly describe a descent algorithm designed to solve the minimisation problem in step (2) of the Uzawa procedure for the containment problem (or the eradication problem).

(1) Start from an initial infusion profile i_0.
(2) Given the infusion profile i_k, integrate the dynamical system (1)–(4) and (16)–(17) from t_0 until t_f to obtain villi and tumour populations.
(3) Search for t_A and t_B and compute the value of J_B, F_A and J. (Note: if accidentally an extremum value is reached at multiple times, choose the largest).
(4) Integrate the adjoint system (6)–(9) of F_A from t_A down to t_0 and the adjoint system (18)–(20) of J_B from t_B down to t_0, to obtain the gradient of J.
(5) Determine a descent direction d_k using the gradient of J and previous descent directions (non-linear conjugate gradient, see *e.g.* [3])).
(6) Determine i_{k+1} by minimising $J(i_k + sd_k)$ along direction d_k (one-dimensional search) under the constraint $i \geq 0$.
(7) Loop to step 2 until convergence.

Remark 6. The one-dimensional search of step (6) asks for one or several evaluations of J and eventually its gradient (Wolfe's search, see *e.g.* [3]), that is integrations of the dynamical system and of the adjoint systems.

Remark 7. During the one-dimensional search of step (6), several infusion profiles are tested with respect to the minimum of J. But incidentally one of them may be a good solution for the containment problem. It is then worthwhile (and costless) to compare, on the fly, with respect to F_A and J_B, these infusion profiles to the best profile already encountered.

Remark 8. It is in practice efficient to take for i_0 in step 1 of the descent algorithm a combination of $i^{(k-1)}$, the last obtained infusion in the Uzawa procedure, and a constant infusion rate. Also a small random perturbation may be applied to i_0 in order to improve the exploration of the phase space.

2.4. **Optimisation with respect to the infusion period**

Let us suppose that the authorised infusion period is a single interval, thus $\Phi(t) = \chi_{[t_0,t_i]}(t)$. Then, in the eradication problem, the objective function G_B and the constraint F_A can be considered as functions of i and of t_i; the optimisation can be conducted on the product space $L^2([t_0,t_f]) \times [t_0,t_f]$. The only difference with the previous developments is that we need to compute the gradient of the various functions with respect to t_i (gradients are in fact simple derivatives in this case). These are, for $F_A(i,t_i) = \tau_A - \min\limits_{t\in[t_0,t_f]} \dfrac{A(t)}{A_{eq}}$:

$$\nabla_{t_i} F_A(i,t_i) = \begin{cases} -\dfrac{\check{A}(t_A)}{A_{eq}} & \text{if } t_i < t_A \\ 0 & \text{if not} \end{cases}$$

with $A(t_A) = \min\limits_{[t_0,t_f]} A(t)$, and $\check{A}$ given by the linear tangent system, defined for $t \geq t_i$:

$$\frac{\mathrm{d}\check{P}}{\mathrm{d}t} = -\lambda\check{P} + \frac{i(t)}{V_{\text{dist}}}\delta(t-t_i) \tag{24}$$

$$\frac{\mathrm{d}\check{C}}{\mathrm{d}t} = -\mu\check{C} + \xi_C\check{P} \tag{25}$$

$$\frac{\mathrm{d}\check{Z}}{\mathrm{d}t} = \{-\alpha - f(C,t)\}\,\check{Z} - \frac{\partial f}{\partial C}(C,t)\,\check{C}\,Z - \beta\check{A} \tag{26}$$

$$\frac{\mathrm{d}\check{A}}{\mathrm{d}t} = \check{Z} \tag{27}$$

where $\delta(t)$ is the Dirac function at origin and with vanishing initial conditions at $t = t_i$.

And for $G_B(i,t_i) = \min\limits_{t\in[t_0,t_f]} B(t)$:

$$\nabla_{t_i} G_B(i,t_i) = \begin{cases} \check{B}(t_B) & \text{if } t_i < t_B \\ 0 & \text{if not} \end{cases}$$

with $B(t_B) = \min_{[t_0,t_f]} B(t)$, and $\check{B}$ given by the linear tangent system, defined for $t \geq t_i$:

$$\frac{\mathrm{d}\check{P}}{\mathrm{d}t} = -\lambda\check{P} + \frac{i(t)}{V_{\mathrm{dist}}}\delta(t - t_i) \tag{28}$$

$$\frac{\mathrm{d}\check{D}}{\mathrm{d}t} = -\nu\check{D} + \xi_D\check{P} \tag{29}$$

$$\frac{\mathrm{d}\check{B}}{\mathrm{d}t} = -a\check{B}\ln\left(\frac{B}{B_{\max}}\right) - a\check{B} - g(D,t)\check{B} - \frac{\partial g}{\partial D}(D,t)\check{D}B \tag{30}$$

with vanishing initial conditions at $t = t_i$.

3. Numerical experiments

We conducted several numerical experiments for both the containment and eradication problems. These experiments used the following data:

- For drug infusion:
  $\lambda = 6\ \mathrm{h}^{-1}$; $V_{\mathrm{dist}} = 10\ \mathrm{cm}^3$ (distribution volume for oxaliplatin in a mouse).
- For the villi population:
  $\mu = 0.015\ \mathrm{h}^{-1}$, $\xi_C = 1\ \mathrm{h}^{-1}$, $A_{eq} = 10^6$ cells, $Z_{eq} = 16500$ cells/h, $\alpha = 0.0153\ \mathrm{h}^{-1}$, β[3]$= 0.002\ \mathrm{h}^{-2}$, $\gamma = \beta A_{eq} + \alpha Z_{eq} = 2213.8$ cells/h, $F = 0.5\ \mathrm{h}^{-1}$, $\varphi_A = 10$ h, $T_A = 24$ h, $\gamma_A = 1$, $C_{50} = 10\ \mu\mathrm{g/cm}^3$.
- For the tumour population:
  $\nu = 0.03\ \mathrm{h}^{-1}$, $\xi_D = 1\ \mathrm{h}^{-1}$, $a = 0.015\ \mathrm{h}^{-1}$, $B_{max} = 5.3\,10^6$ cells,
  $H = 2\ \mathrm{h}^{-1}$, $\varphi_B = 21$ h, $T_B = 24$ h, $\gamma_B = 1$, $D_{50} = 10\ \mu\mathrm{g/cm}^3$.

These numerical data have been deduced from laboratory experiments; however, a large uncertainty remains on most of them, thus the goal of the subsequent numerical results is only to prove the feasibility of our approach rather than to obtain clinically relevant results.

All the experiments start with initial conditions: $P_0 = C_0 = D_0 = 0\ \mu\mathrm{g/cm}^3$, $A_0 = 10^6$ cells, $B_0 = 10^6$ cells, $Z_0 = 16500$ cells/h. The initial time t_0 was noon and the time step 0.1 hour.

3.1. **Eradication problem**

The results presented were obtained in the framework of the eradication problem when optimising with respect both to i, the injection rate, and t_i, the infusion period. Together with the constraint to preserve a given level τ_A of the villi population, a constraint was also imposed on the instantaneous infusion rate, namely $i(t) \leq 10\ \mu\mathrm{g/h}$[4]. Experiments started with a treatment duration of 48 hours ($t_i - t_0 = 2$ days), and they converged to a treatment of almost 32 hours.

Figures 1 to 3 display respectively, as a function of time, the best infusion rate $i(t)$, the villi population $A(t)$ and the tumour cell population $B(t)$ for three different values of the minimal admissible fraction of the villi population $\tau_A = 0.4$, 0.5 and 0.6. In Figure 1, the impact of the different circadian rhythms for the villi and tumour populations is clearly seen as they impose a strong chronomodulation on the infusion rate. This impact is enhanced when the constraint to preserve the villi population is stronger. Note also the effect of the limitation of the instantaneous infusion rate. The chronomodulation is also seen on the villi population behaviour displayed in Figure 2.

[3] $\alpha = \frac{1}{72}\ln 3$, $\beta = (\frac{\alpha}{2})^2 + (\frac{2\pi}{144})^2$, these values correspond to coefficients of a damped harmonic oscillator of period 6 days and dampening coefficient $\frac{1}{3}$ over one period, a behaviour estimated after literature data.

[4] The ensemble of admissible solutions is then $U = \{i \in L^2([t_0,t_f]) \mid 0 \leq i \leq 10\ \mu\mathrm{g/h}\,,\ F_A \leq 0\}$; the maximal constraint on infusion rate is treated in step 2 of the algorithm (see Rem. 6).

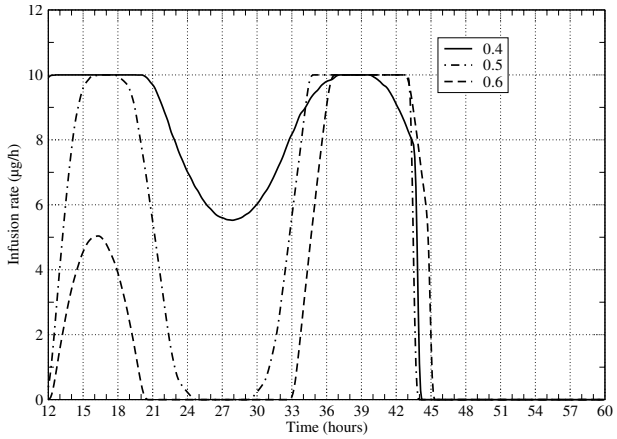

FIGURE 1. One week eradication treatment with 1.5+5.5 days cycle: optimised infusion flows for $\tau_A = 0.4$, 0.5 and 0.6.

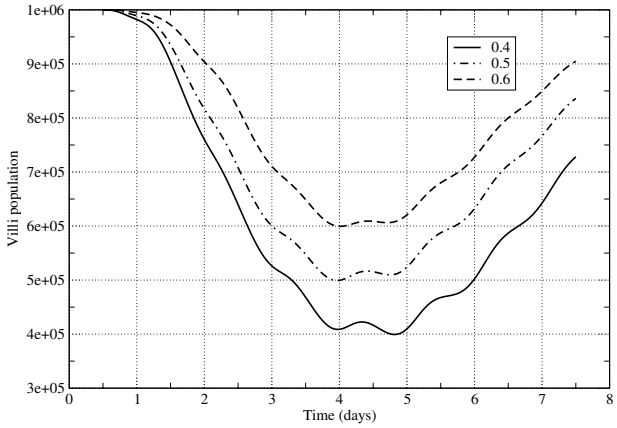

FIGURE 2. One week eradication treatment with 1.5+5.5 days cycle: villi population for $\tau_A = 0.4$, 0.5 and 0.6.

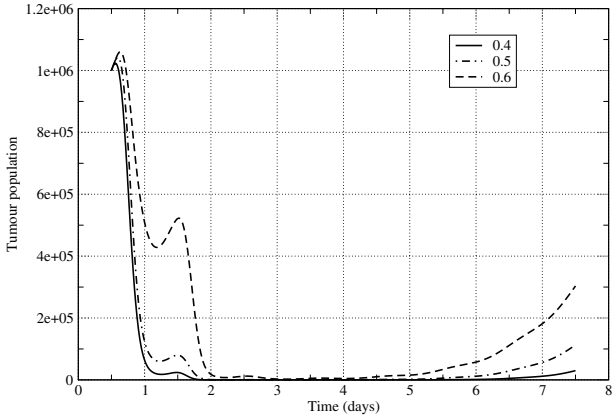

FIGURE 3. One week eradication treatment with 1.5+5.5 days cycle: tumour cell population for $\tau_A = 0.4$, 0.5 and 0.6.

TABLE 1. Treatment durations and residual tumour cell numbers (eradication).

τ_A	(days) $t_i - t_0$	(hours) $t_i - t_0$	$\min_t B(t)$
0.4	1.33	31.9	3.4
0.5	1.32	31.7	114
0.6	1.38	34	2374

Table 1 presents the best treatment duration $t_i - t_0$ and objective function $\min_t B(t)$ for the best infusion rate i, for the three experiments. The tumour population is strongly reduced when τ_A decreases, however, with the data we used, the complete eradication of the tumour ($B < 1$) would require to diminish the villi population lower than 39% of the reference number, whatever the duration of the treatment, a level which, in a clinical context, is not admissible for the patient. Thus, for the experiments presented, a few tumour cells remain after

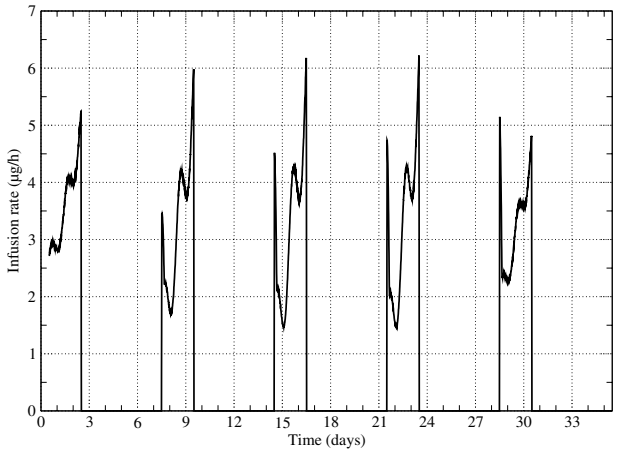

FIGURE 4. Five weeks containment treatment with 2+5 days cycle: optimised drug infusion flow for $\tau_A = 0.5$.

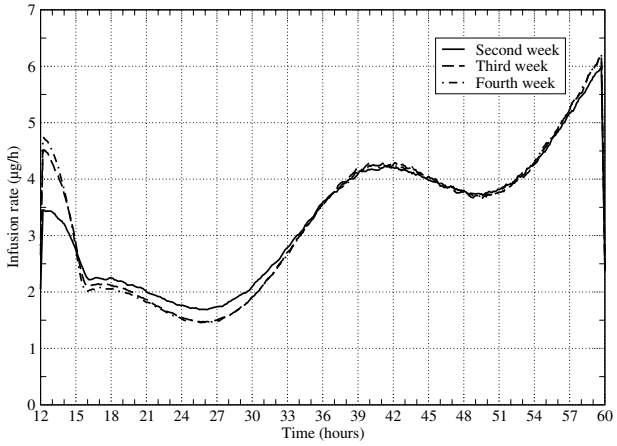

FIGURE 5. Five weeks containment treatment with 2+5 days cycle: optimised drug infusion flows for $\tau_A = 0.5$, according to the week of treatment.

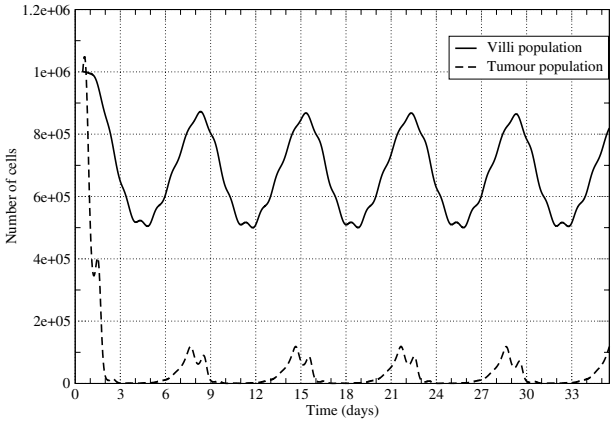

FIGURE 6. Five weeks containment treatment with 2+5 days cycle: cell populations for $\tau_A = 0.5$.

the end of the treatment (see Fig. 3), and, due to its exponential growth the tumour population will, without treatment, rapidly recover and overtake its initial level. This is why we studied the containment problem which should be applied to control tumour growth when the complete eradication is out of reach.

3.2. **Containment problem**

Figures 4 to 6 present the results for the containment problem with a weekly scenario of an infusion period of 2 days followed by 5 days of recovery, and an acceptable fraction $\tau_A = 0.5$ for the villi population. The calculation was performed on a five weeks time interval. Figure 4 presents the infusion law, some details of which are shown in Figure 5. The infusion law is, as expected, strongly chronomodulated. Also, after the initial decrease of the tumour population, the infusion law evolves toward a periodic profile; indeed in Figure 5, curves become quickly intertwined. The tumour and villi population, displayed in Figure 6, have also this periodic

TABLE 2. Tumour cell population (containment) for a treatment of 2+5 days.

τ_A	$\max_t B(t)$	$\min_t B(t)$
0.4	36 000	21
0.5	119 000	390
0.6	352 000	5900

TABLE 3. Tumour cell population (containment): 2.5 days of treatment + 4.5 days of recovery, chonomodulated and equivalent constant treatment.

τ_A infusion	$\max_t B(t)$ chronomodulated	$\max_t B(t)$ constant
0.4	18 400	38 500
0.5	75 300	129 600
0.6	247 000	367 000

tendency ensuring that the treatment can be repeated while controlling tumour growth. Table 2 presents the best objective function, $\max_t B(t)$ for the best infusion rate i, after an initial treatment period of 3 days, for infusion cycle experiments of 2+5 days and three different values of the minimal admissible fraction of the villi population $\tau_A = 0.4$, 0.5 and 0.6. Table 2 also presents the minimum tumour population reached with this best infusion rate. While the tumour population can be brought to a very low level, due to the exponential growth of the tumour, the maximal number of tumour cells, after a initial period of 3 days, remains quite high, though under control.

Table 3 corresponds to experiments performed in a four weeks course, with an infusion cycle of 2.5 days followed by 4.5 days of recovery. In this particular setting, we also assessed here the gain obtained by the chronomodulated scheme as compared to an equivalent constant infusion scheme: the best objective function, $\max_t B(t)$ after a 3 days initial treatment period, is given for the chronomodulated infusion law and for a constant infusion law (applied during the 2.5 days infusion periods) with an infusion rate equal to the mean of the corresponding chronomodulated instantaneous infusion flow.

One should not be surprised that for the same chronomodulated scheme, a weekly containment treatment with an infusion period of 2.5 days leads to a lower level of tumour cells than the same with an infusion period of 2 days: the longer the recovery period, the higher the tumour can grow up. A trade-off has to be found between the length of the necessary recovery period and the admissible maximal level for the tumour. Furthermore, Table 3 also shows the net gain obtained by the chronomodulation strategy: the number of tumour cells is significantly reduced when the treatment takes benefit of the circadian rhythm.

4. Discussion and conclusion

4.1. **Optimisation method**

In this paper, we have detailed an optimisation procedure taking into account objective and constraint functions that are optimised in an L^∞ manner, and not according to a quadratic L^2, or L^1 criterion, as has already been done before in the literature. To our knowledge, this approach is original, as are the differentiability results stated here. This approach is intended to stick to the actual clinical or experimental problem, and in this respect extreme values are of uppermost importance as they may be fatal for the patient, our L^∞ approach controls them whereas L^2 or L^1 integrated criteria don't. It is clear however that our mathematical model is still too simple as it should take into account different toxicities (other than the intestinal, such as bone marrow toxicity or sensory neuropathy, as is the case with oxaliplatin in clinical settings). This would lead to more

equations and more constraints, with possible weighting – left to the clinician – between them, but our approach extends easily to such far more complicated cases.

From the algorithmic point of view, although we cannot assert that our optimisation algorithm reaches a global minimum, the multiplicity of iterations and the storing of the best solution at each iteration, together with the use of some random walk to explore the phase space gives us hints of its actual optimality and robustness.

4.2. **Why a purely deterministic model?**

It is noteworthy that, as stated in the introduction, circadian rhythms in living organisms are synchronised by natural light [and by social rhythms in Humans], which implies – and is observed in experimental and clinical settings – that all subjects show the same periods and time peaks in drug sensitivity. At the cell population level, variabilities in circadian drug sensitivity phases may occur in each compartment, healthy or tumoral, but both phases are synchronised by the central pacemaker located in the hypothalamus (suprachiasmatic nuclei). These phases and their variabilities may be assessed at the peripheral tissue level by measuring clock gene (Per2, Clock, Bmal1) expression or clock-controlled gene expression of apoptosis proteins such as BAX or BCL2 as a function of circadian time [19], and at the central level by body rhythm recordings, such as temperature. Taking them into account would only add a new parameter to the model: the robustness of circadian control. This will surely be of interest in a future model, for describing differences in the quality of individual circadian synchronisation within a population of individuals (laboratory animals or patients). But this was not our primary concern in setting this frame for presenting the optimisation procedure. In the same way, artificially adding stochastic components to the model would hardly be of any interest for this presentation.

4.3. **Limits of this model**

The model we used addresses the optimisation of cancer chemotherapy using pharmacokinetic-pharmacodynamic and circadian modelling with a toxicity constraint. It does not address the problem of drug resistance and its evolution in tumour cell populations, which is also an important limitation in cancer chemotherapy, and has been studied by various authors already [15, 25, 33]. Nor does it address the fact that most anti-cancer drugs (but not oxaliplatin, to our knowledge) are known to show cell cycle phase specificities. The former should be taken into account by an extension of our simple model to subpopulations for tumour growth, quiescent, proliferative drug-sensitive and proliferative drug-resistant. The latter implies future modelling of cell cycle progression and apoptosis at the tissue level for tumour cell populations, with coupling to local circadian clocks – a coupling which has been shown experimentally to be unidirectional, *i.e.* control of cell proliferation by the clock, at least for the regenerating liver in mice [28, 32]. These approaches are complementary, and according to the particular tumour and drug involved, partial or extended models should be used for chemotherapy optimisation.

4.4. **Model identification and future clinical applications**

We must stress that the numerical results presented are highly dependent on the values of parameters used, some of which had to be grossly estimated in our dataset – besides, the dataset should be completely different for other tumours and other cytotoxic drugs –, so that any generalisation of these results to clinical conclusions would at this stage be completely hazardous. Yet, as far as equivalent modelling equations and their parameters may be identified in other settings, the same optimisation procedure could be successfully applied.

We will not hide that identifying cell and tissue pharmacokinetics and pharmacodynamic dose-effects (even if these two aspects are merged together) means acquiring knowledge of hidden mechanisms which are not easily accessible in everyday clinical routine, and this remains today a shortcoming of the method proposed here. Nevertheless, we have reasonable hopes that such data, provided by the development of modern pharmacokinetics-pharmacodynamics (PK-PD) and molecular biology techniques, will become more and more available in the next future.

This in our meaning justifies developing such optimisation methods which make it necessary to model intimate tissue mechanisms for drug efficacy and toxicity effects. Whole organism modelling and PK-PD development

could lead us to use other observable than cell population numbers – for instance, as far as oxaliplatin is concerned, peripheral sensory neuropathy has recently been proposed to be linked to insults to nucleoli in nerve ganglia [29], not measurable by cell kill evaluations-, but such future, more detailed, models will still be liable for the optimisation method we presented here.

Finally, one may notice that it gives a rationale, not only for circadian chronotherapy theoretic studies which first motivated it, but also, using optimisation in the product space $L^2([t_0, t_f]) \times [t_0, t_f]$, for so-called intensive therapies, in which the stress is put on the best treatment course and between courses durations making possible a necessary increase in the delivered dose when classical therapeutic schemes have failed.

Acknowledgements. This work was supported by the EU Network of Excellence BIOSIM, contract 005137.

References

[1] Z. Agur, R. Arnon and B. Schechter, Effect of the dosing interval on myelotoxicity and survival in mice treated by cytarabine. *Eur. J. Cancer* **28A** (1992) 1085–1090.
[2] L.K. Andersen and M.C. Mackey, Resonance in periodic chemotherapy: a case study of acute myelogenous leukemia. *J. Theor. Biol.* **209** (2001) 113–130.
[3] J.F. Bonnans, J.C. Gilbert, C. Lemarechal and C.A. Sagastizabal, *Numerical Optimization: Theoretical and Practical Aspects.* Springer Universitext (2003).
[4] N.A. Boughattas, F. Lévi, *et al.*, Circadian Rhythm in Toxicities and Tissue Uptake of 1,2-diamminocyclohexane(trans-1)oxaloplatinum(II) in Mice. *Cancer Research* **49** (1989) 3362–3368.
[5] N.A. Boughattas, B. Hecquet, C. Fournier, B. Bruguerolle, A. Trabelsi, K. Bouzouita, B. Omrane and F. Lévi, Comparative pharmacokinetics of oxaliplatin (L-OHP) and carboplatin (CBDCA) in mice with reference to circadian dosing time. *Biopharmaceutics and drug disposition* **15** (1994) 761–773.
[6] N.F. Britton, N.A. Wright and J.D. Murray, A mathematical model for cell population kinetics in the intestine. *J. Theor. Biol.* **98** (1982) 531–541.
[7] L. Canaple, T. Kazikawa and V. Laudet, The days and nights of cancer cells. *Cancer Research* **63** (2003) 7545–7552.
[8] J. Clairambault, D. Claude, E. Filipski, T. Granda and F. Lévi, Toxicité et efficacité antitumorale de l'oxaliplatine sur l'ostéosarcome de Glasgow induit chez la souris : un modèle mathématique. *Pathologie-Biologie* **51** (2003) 212–215.
[9] L. Cojocaru and Z.A. Agur, Theoretical analysis of interval drug dosing for cell-cycle-phase-specific drugs. *Math. Biosci.* **109** (1992) 85–97.
[10] B.F. Dibrov, M.A. Zhabotinski, Yu.A. Neyfakh, M.P. Orlova and L.I. Churikova, Mathematical model of cancer chemotherapy. Periodic schedules of of phase-specific cytotoxic agent administration increasing the selectivity of therapy. *Math. Biosci.* **73** (1985) 1–34.
[11] B.F. Dibrov, Resonance effect in self-renewing tissues. *J. Theor. Biol.* **192** (1998) 15–33.
[12] L. Edelstein-Keshet, *Mathematical Models in Biology.* NY: McGraw-Hill (1988) 210–270.
[13] A.W. El-Kareh and T.W. Secomb, A mathematical model for cisplatin cellular pharmacodynamics. *Neoplasia* **5** (2004) 161–169.
[14] S. Faivre, D. Chan, R. Salinas, B. Woynarowska and J.M. Woynarowski, DNA Single Strand Breaks and apoptosis induced by oxaliplatin in cancer cells. *Biochemical Pharmacology* **66** (2003) 225–237.
[15] K.R. Fister and J.C. Panetta, Optimal control applied to cell-cycle-specific cancer chemotherapy. *SIAM J. Appl. Math.* **60** (2000) 1059–1072.
[16] L. Fu, H. Pellicano, J. Liu, P. Huang and C.C. Lee, The Circadian Gene Period2 Plays an Important Role in Tumor Suppression and DNA Damage Response In Vivo. *Cell* **111** (2002) 41–50.
[17] L. Fu and C.C. Lee, The circadian clock: pacemaker and tumour suppressor. *Nature Reviews* **3** (2003) 351–361.
[18] T.G. Granda, R.-M. D'Attino, E. Filipski, *et al.*, Circadian optimisation of irinotecan and oxaliplatin efficacy in mice with Glasgow osteosarcoma. *Brit. J. Cancer* **86** (2002) 999–1005.
[19] T.G. Granda, X.H. Liu, R. Smaaland, N. Cermakian, E. Filipski, P. Sassone-Corsi and F. Levi, Circadian regulation of cell cycle and apoptosis proteins in mouse bone marrow and tumor. *FASEB J.* **19** (2005) 304.
[20] M. Gyllenberg and G.F. Webb, Quiescence as an explanation of gompertzian tumor growth. *Growth, Development and Aging* **53** (1989) 25–33.
[21] M. Gyllenberg and G.F. Webb, A nonlinear structured population model of tumor growth with quiescence. *J. Math. Biol.* **28** (1990) 671–694.
[22] M.H. Hastings, A.B. Reddy and E.S. Maywood, A clockwork web: circadian timing in brain and periphery, in health and disease. *Nat. Rev. Neurosci.* **4** (2003) 649–661.
[23] A. Iliadis and D. Barbolosi, Optimising drug regimens in cancer chemotherapy by an efficacy-toxicity mathematical model. *Computers Biomed. Res.* **33** (2000) 211–226.

[24] A. Iliadis and D. Barbolosi, Optimising drug regimens in cancer chemotherapy: a simulation study using a PK-PD model. *Computers Biol. Med.* **31** (2001) 157–172.
[25] M. Kimmel and A. Swierniak, *Using control theory to make cancer chemotherapy beneficial from phase dependence and resistant to drug resistance.* Technical report #7, Ohio State University, Nov. 2003, available on line at `http://mbi.osu.edu/publications/techreport7.pdf` (2003).
[26] F. Lévi, G. Metzger, C. Massari and G. Milano, Oxaliplatin: Pharmacokinetics and Chronopharmacological Aspects. *Clin. Pharmacokinet.* **38** (2000) 1–21.
[27] F. Lévi (Ed.), Cancer Chronotherapeutics. *Special issue of Chronobiology International* **19** #1 (2002).
[28] T. Matsuo, S. Yamaguchi, S. Mitsui, A. Emi, F. Shimoda and H. Okamura, Control mechanism of the circadian clock for timing of cell division in vivo. *Science* **302** (5643) (2003) 255–259.
[29] M.C. McKeage, T. Hsu, G. Haddad and B.C. Baguley, Nucleolar damage correlates with neurotoxicity induced by different platinum drugs. *Br. J. Cancer* **85** (2001) 1219–1225.
[30] M. Mishima, G. Samimi, A. Kondo, X. Lin and S.B. Howell, The cellular pharmacology of oxaliplatin resistance. *Eur. J. Cancer* **38** (2002) 1405–1412.
[31] C.S. Potten and M. Loeffler, Stem cells: attributes, cycles, spirals, pitfalls and uncertainties. Lessons for and from the crypt. *Development* **110** (1990) 1001–1020.
[32] U. Schibler, Circadian rhythms. Liver regeneration clocks on. *Science* **302** (5643) (2003) 234–235.
[33] G. Swan, Role of optimal control theory in cancer chemotherapy. *Math. Biosci.* **101** (1990) 237–284.
[34] G.F. Webb, Resonance phenomena in cell population chemotherapy models. *Rocky Mountain J. Math.* **20** (1990) 1195–1216.

Available online at www.sciencedirect.com
SCIENCE DIRECT®
C. R. Acad. Sci. Paris, Ser. I 342 (2006) 17–22
COMPTES RENDUS MATHEMATIQUE
http://france.elsevier.com/direct/CRASS1/

Partial Differential Equations

Circadian rhythm and tumour growth

Jean Clairambault [a,d], Philippe Michel [b,c], Benoît Perthame [a,b]

[a] *INRIA, projet BANG, domaine de Voluceau, BP 105, 78153 Le Chesnay cedex, France*
[b] *Département de mathématiques et applications, UMR 8553, École normale supérieure, 45, rue d'Ulm, 75230 Paris cedex 05, France*
[c] *CEREMADE, université Paris 9 Dauphine, place du Maréchal de Lattre de Tassigny, 75775 Paris cedex 16, France*
[d] *INSERM E 0354 « Rythmes biologiques et cancer », hôpital Paul-Brousse, 14, avenue Paul-Vaillant-Couturier, 94807 Villejuif cedex, France*

Received 21 September 2005; accepted 28 September 2005

Available online 28 November 2005

Presented by Philippe G. Ciarlet

Abstract

We address the following question: can one sustain, on the basis of mathematical models, that for cancer cells, the loss of control by circadian rhythm favours a faster growth? This question, which comes from the observation that tumour growth in mice is enhanced by experimental disruption of the circadian rhythm, may be tackled by mathematical modelling of the cell cycle. For this purpose we consider an age-structured population model with control of death (apoptosis) rates and phase transitions, and two eigenvalues: one for periodic control coefficients (via a variant of Floquet theory in infinite dimension) and one for constant coefficients (taken as the time average of the periodic case). We show by a direct proof that, surprisingly enough considering the above-mentioned observation, the periodic eigenvalue is always greater than the steady state eigenvalue when the sole apoptosis rate is concerned. We also show by numerical simulations when transition rates between the phases of the cell cycle are concerned, that, without further hypotheses, no natural hierarchy between the two eigenvalues exists. This at least shows that, if such models are to take account of the above-mentioned observation, control of death rates inside phases is not sufficient, and that transition rates between phases are a key target in proliferation control. ***To cite this article: J. Clairambault et al., C. R. Acad. Sci. Paris, Ser. I 342 (2006).***

Résumé

Rythme circadien et croissance tumorale. L'objet de cette Note est de questionner, sur des bases mathématiques, le fait expérimental que les populations de cellules de souris cancéreuses échappant au contrôle circadien, ont tendance à se développer plus vite. Pour cela nous considérons un modèle du cycle cellulaire avec contrôle des taux de mort (apoptose) et de transition entre phases, et deux valeurs propres. L'une est associée aux coefficients périodiques via la théorie de Floquet (dans une version de dimension infinie), l'autre est associée au problème stationnaire avec des coefficients moyens. Nous montrons par une preuve directe que, de façon inattendue si l'on considère l'observation expérimentale évoquée plus haut, la valeur propre périodique est plus grande que la valeur propre stationnaire dans le cas où le contrôle périodique est effectué sur l'apoptose. Nous montrons aussi, par des tests numériques dans le cas où le contrôle périodique est effectué sur le taux de transition d'une phase à l'autre du cycle cellulaire, qu'il n'existe alors aucune hiérarchie naturelle entre les deux types de valeurs propres. Ceci montre au moins que, pour que de tels modèles puissent rendre compte des observations expérimentales ci-dessus, le seul contrôle des taux de mort dans

E-mail addresses: jean.clairambault@inria.fr (J. Clairambault), Michel@dma.ens.fr (P. Michel), Benoit.Perthame@ens.fr (B. Perthame).

1631-073X/$ – see front matter
doi:10.1016/j.crma.2005.10.029

chaque phase est insuffisant, et que les taux de transition entre phases sont une cible clef pour le contrôle de la prolifération. ***Pour citer cet article : J. Clairambault et al., C. R. Acad. Sci. Paris, Ser. I 342 (2006).***

Version française abrégée

Nous étudions dans cette Note au moyen de modèles mathématiques et de simulations numériques l'idée suivante, qui est à l'origine de la chronothérapie des cancers : les rythmes circadiens influencent la prolifération cellulaire. En particulier, on a pu observer que la croissance tumorale est favorisée par une perturbation de ces rythmes, mesurés notamment par l'enregistrement de la température corporelle ou du cycle repos/activité. Plusieurs études épidémiologiques ont ainsi montré que des travailleurs soumis à des variations prolongées de leurs rythmes de travail sont plus exposés au risque de cancer colorectal que ceux ayant un rythme de travail régulier. On peut donc se demander si la perte du contrôle circadien sur le cycle cellulaire peut entraîner une accélération de la progression tumorale. Cette hypothèse s'appuie sur une bonne compréhension des mécanismes moléculaires contrôlant l'apoptose et les transitions entre phases du cycle cellulaire, sous l'influence de protéines telles que p53, mais aussi des cyclines et cycline-kinases (cdk). En effet certains de ces mécanismes, comme la phosphorylation du dimère CycB-cdk1 par la kinase Wee1, sont directement contrôlés par des gène circadiens, comme Bmal1.

Notre approche repose sur l'analyse mathématique de modèles du cycle cellulaire qui sont maintenant bien établis. Nous introduisons le rythme circadien comme une périodicité de certains des coefficients de ces modèles, et examinons si cette périodicité diminue ou non la croissance du système par rapport au modèle à coefficients constants (même moyenne). Notre but est de déterminer si ce niveau de modélisation peut rendre compte du fait expérimentalement observé qu'une diminution du contrôle circadien favorise la croissance tumorale.

Il existe de nombreuses références classiques, s'appuyant éventuellement sur des comparaisons expérimentales, sur le sujet des populations structurées et, comme cas particulier, du cycle cellulaire, voir [1–3,8,11,15]. Pour une analyse récente de ces systèmes s'appuyant sur des méthodes d'entropie on peut consulter [12,13]. Nous retenons, suivant en cela une étude précédente [4], le système d'équations aux dérivées partielles (1) pour décrire la densité de cellules $n_i(t,x) \geqslant 0$ d'âge x dans la phase $i = 1, \ldots, I$ à l'instant t. Ici nous identifions la phase 1 à la phase $I+1$. Le coefficient $d_i(t,x)$ représente le taux d'apoptose et $K_{i\to i+1}$ les taux de transition d'une phase à la suivante (on a choisi pour la transition $I \to 1$ la mitose terminée par le doublement du nombre des cellules). Ces coefficients peuvent être constants en temps (pas de contrôle circadien) ou avoir une période T lorsqu'on prend en compte le rythme circadien. Des hypothèses sur ces coefficients sont données en (2) et (3), qui permettent de prouver que l'opérateur différentiel sous-jacent admet un premier vecteur propre positif non seulement dans le cas des coefficients constants (théorie de Krein–Rutman), associé à une valeur propre notée λ_s (s pour « stationnaire »), classiquement appelée valeur propre de Perron dans le cas de la dimension finie, mais aussi dans le cas des coefficients périodiques (théorie de Floquet, généralisée ici au cas de la dimension infinie), vecteur propre associé à une valeur propre notée λ_{per} (per pour « périodique »).

En ce qui concerne le contrôle périodique par l'apoptose (les $K_{i\to i+1}$ sont alors pris constants), nous démontrons que, de façon surprenante au regard des résultats des expérimentations animales, on a toujours $\lambda_{per} > \lambda_s$. Pour le contrôle par les taux de transition, les simulations numériques montrent qu'il n'y a pas d'ordre général entre ces deux valeurs propres, alors que les données physiopathologiques sur la transition de G1-S-G2 à M obtenues à partir de courbes expérimentales de croissance tumorale sur des animaux de laboratoire vont toutes dans le sens $\lambda_s > \lambda_{per}$.

Il n'est pas surprenant que l'apoptose ne suffise pas à expliquer dans le cadre de ce modèle le phénomène observé expérimentalement, puisque l'influence attendue du rythme circadien se situe, du moins en ce qui concerne le mécanisme bien identifié du contrôle circadien de la kinase cdk1, au niveau des transitions de phases et non du taux de mort dans chaque phase.

1. Cell cycle and circadian rhythm

The goal of this Note is to address by means of mathematical and numerical models the following fact which underlies chronotherapy [9,14]: circadian rhythms influence cell proliferation. In particular, tumour growth has been shown to be favoured by disruptions of the circadian rhythm, as assessed e.g. by body temperature or rest-activity

recordings [5]. This is supported by clinical observations according to which patients with cancer *and* disrupted circadian rhythms are less responsive to chemotherapy and have poorer prognosis than others with the same diseases but strong circadian rhythmicity [9,14]. Furthermore, molecular mechanisms underlying circadian control on apoptosis and cell cycle phases through proteins such as p53 and cyclins are currently being unveiled [6,10,16].

Our approach relies on equations for the cell cycle which are well settled nowadays, see [1–3,8,11,15] for references on structured population dynamics and the cell cycle, and [12,13] for a more recent approach based on entropy properties. We introduce circadian control through periodic coefficients and assess the hypothesis according to which periodicity diminishes the system growth as compared to constant coefficients (same average), in order to decide if a loss of circadian control theoretically favours tumour growth. Here and following earlier work [4], we model our population of cells by a Partial Differential Equation for the density $n_i(t,x) \geqslant 0$ of cells with age x in the phase $i = 1, \ldots, I$, at time t.

$$\begin{cases} \dfrac{\partial}{\partial t} n_i(t,x) + \dfrac{\partial}{\partial x} n_i(t,x) + \big[d_i(t,x) + K_{i\to i+1}(t,x)\big] n_i(t,x) = 0, \\ n_i(t,x=0) = \displaystyle\int_{x'\geqslant 0} K_{i-1\to i}(t,x')\, n_{i-1}(t,x')\,\mathrm{d}x', \quad 2 \leqslant i \leqslant I, \\ n_1(t,x=0) = 2\displaystyle\int_{x'\geqslant 0} K_{I\to 1}(t,x')\, n_I(t,x')\,\mathrm{d}x'. \end{cases} \tag{1}$$

Here and below we identify $I+1$ to 1. We denote by $d_i(t,x) \geqslant 0$ the apoptosis rate, $K_{i\to i+1}$ the transition rates from one phase to the next, the last one ($i = I$) being mitosis. These coefficients can be constant or T-periodic in time in order to take into account presence or absence of circadian control. Our assumptions are

$$K_{i\to i+1}(t,x) \geqslant 0,\ \mathrm{d}_i(t,x) \geqslant 0 \quad \text{are bounded}, \tag{2}$$

and, setting $\min_{0\leqslant t\leqslant T} K_{i\to i+1}(t,x) := k_{i\to i+1}(x)$, $\max_{0\leqslant t\leqslant T}[d_i + K_{i\to i+1}] := \mu_i(x)$, $M_i(x) = \int_0^x \mu_i(y)\,\mathrm{d}y$,

$$\prod_{i=1}^{I} \int_0^{\infty} k_{i\to i+1}(y)\, \mathrm{e}^{-M_i(y)}\,\mathrm{d}y > \frac{1}{2}. \tag{3}$$

Classically, one can introduce the growth rate of the system λ_{per} (Malthus parameter, first eigenvalue) such that there is a unique T-periodic *positive* solution to

$$\begin{cases} \dfrac{\partial}{\partial t} N_i(t,x) + \dfrac{\partial}{\partial x} N_i(t,x) + \big[d_i(t,x) + \lambda_{\mathrm{per}} + K_{i\to i+1}(t,x)\big] N_i(t,x) = 0, \\ N_i(t,x=0) = \displaystyle\int_{x'\geqslant 0} K_{i-1\to i}(t,x') N_{i-1}(t,x')\,\mathrm{d}x', \quad 2 \leqslant i \leqslant I, \\ N_1(t,x=0) = 2\displaystyle\int_{x'\geqslant 0} K_{I\to 1}(t,x') N_I(t,x')\,\mathrm{d}x', \qquad \displaystyle\sum_{i=1}^{I} \int N_i(t,x)\,\mathrm{d}x = 1. \end{cases} \tag{4}$$

Under our assumptions (2) and (3), the existence of a solution to (4), with $\lambda_{\mathrm{per}} > 0$, follows from an infinite dimensional version of Floquet theory and one has (see for instance [12])

$$\sum_i \int \big| n_i(t,x)\, \mathrm{e}^{-\lambda_{\mathrm{per}} t} - \rho N_i(t,x) \big| \varphi_i(t,x)\,\mathrm{d}x \to 0 \quad \text{as } t \to \infty,$$

where $\varphi_i(t,x)$ is the periodic positive solution of the adjoint problem to (4) normalised by $\sum_i \int N_i(t,x)\varphi_i(t,x)\,\mathrm{d}x = 1$, and $\rho = \sum_{i=1}^{N} \int n_i(t=0,x)\varphi_i(t=0,x)\,\mathrm{d}x$. In other words, the periodic solution is the observed stable state after renormalisation by the growth rate λ_{per}.

One can also introduce the coefficients averaged in time

$$\big\langle K_{i\to i+1}(x) \big\rangle := \frac{1}{T}\int_0^T K_{i\to i+1}(t,x)\,\mathrm{d}t, \qquad \big\langle d_i(t,x) \big\rangle := \frac{1}{T}\int_0^T d_i(t,x)\,\mathrm{d}t,$$

and consider the associated steady state solution. This allows us to define another growth rate λ_s, and a steady state solution $\overline{N}_i$ to

$$\begin{cases} \dfrac{\partial}{\partial x}\overline{N}_i(x) + \big[\big\langle d_i(x)\big\rangle + \lambda_s + \big\langle K_{i\to i+1}(x)\big\rangle\big]\overline{N}_i(x) = 0, \\ \overline{N}_i(x=0) = \displaystyle\int\limits_{x'\geqslant 0} \big\langle K_{i-1\to i}(x')\big\rangle \overline{N}_{i-1}(x')\,\mathrm{d}x', \quad 2\leqslant i\leqslant I, \\ \overline{N}_1(x=0) = 2\displaystyle\int\limits_{x'\geqslant 0} \big\langle K_{I\to 1}(x')\big\rangle \overline{N}_I(x')\,\mathrm{d}x', \quad \displaystyle\sum_{i=1}^{I}\int \overline{N}_i(x)\,\mathrm{d}x = 1. \end{cases} \tag{5}$$

For these problems, we address the hypothesis that circadian control reduces growth, i.e., that $\lambda_{\mathrm{per}} \leqslant \lambda_s$. In Section 2, we prove that, surprisingly enough, the opposite is true, i.e., $\lambda_{\mathrm{per}} \geqslant \lambda_s$ when the control acts only on the apoptosis rate. In Section 3, we show by numerical experiments that no hierarchy exists between the two eigenvalues when the control acts on the transition rate $K_{1\to 2}$ in a reduced 2-phase model. Section 4 sums up these results and gives hints toward designing physiologically based models of the cell cycle for cancer therapeutics.

2. Control by apoptosis

In this section, we consider the case when circadian control only acts on apoptosis, i.e., $K_{i\to i+1}$ depends only upon x.

Theorem 2.1. *Assume that* $d_i(t,x) \geqslant 0$, $K_{i\to i+1}(x) \geqslant 0$ *are bounded and that* (3) *holds, then the eigenvalue problems* (4), (5) *have unique solutions* $(\lambda_{\mathrm{per}}, N(t,x))$, $(\lambda_s, \overline{N}(x))$, *and*

$$\lambda_{\mathrm{per}} \geqslant \lambda_s. \tag{6}$$

Proof. The existence part for the two problems is standard and we do not prove it again (see [4,12]). Now consider the function $q_i(x) = \langle \log(N_i(t,x)/\overline{N}_i(x))\rangle$. It satisfies

$$\frac{\partial}{\partial x} q_i + \lambda_{\mathrm{per}} - \lambda_s = 0, \quad \text{and} \quad q_i(x=0) = \left\langle \log\left[\int K_{i-1\to i}(x) \frac{\overline{N}_{i-1}(x)}{\bar{N}_i(0)} \frac{N_{i-1}(t,x)}{\overline{N}_{i-1}(x)}\,\mathrm{d}x \right] \right\rangle.$$

Since $d\mu_i(x) = K_{i-1\to i}(x)(\overline{N}_{i-1}(x)/\bar{N}_i(0))\,\mathrm{d}x$ is a probability measure thanks to the condition $\bar{N}_i(0)$ (a factor 2 should be included for $i=1$), we also have

$$\begin{aligned} q_i(x=0) &\geqslant \left\langle \int \log \frac{N_{i-1}(t,x)}{\overline{N}_{i-1}(x)}\,\mathrm{d}\mu_i(x) \right\rangle \quad \text{(by Jensen's inequality)} \\ &= \int q_{i-1}(x)\,\mathrm{d}\mu_i(x) = \int \big[q_{i-1}(0) + (\lambda_s - \lambda_{\mathrm{per}})x\big]\,\mathrm{d}\mu_i(x). \end{aligned}$$

Therefore, summing over i, $0 \geqslant (\lambda_s - \lambda_{\mathrm{per}}) \sum_{i=1}^{I} \int_{x=0}^{\infty} x\,\mathrm{d}\mu_i(x)$, and the result follows. □

3. Control by phase transition

We have performed numerical tests for the cell cycle systems (4), (5) based on a classical upwind scheme with $CFL = 1$ which gives the exact transport solver (see [4] for details). We have taken a simplified version of the cell cycle with two phases ($I = 2$): G1-S-G2 and M. The apoptosis rate has been taken constant and the transition rates are: $K_{1\to 2}(t,x) = \psi(t)\mathbb{1}_{\{x\geqslant x_*\}}$, and $K_{2\to 1}(t,x) = \mathbb{1}_{\{x\geqslant x_{**}\}}$.We have in mind the following order of magnitudes for several animal tumour cells: total cycle duration is 21 h, 8 h for G1, 8 h for S, 4h for G2, 1 h for M (therefore in this case $x_* = 20$ h and $x_{**} = 1$ h). But we will also consider different duration ratios x_*/x_{**} between the 2 phases, from 1 to 20. In fact, although the G2/M transition is known to be a circadian control target with a well identified mechanism (Bmal1→Wee1→cdk), another control target, with another molecular mechanism in which genes *per* and *cMyc* have been shown to be involved [6], also takes place at the G1/S transition, and the G1 phase may have a

Table 1
The periodic and stationary eigenvalues for 2 periodic phase transition functions and different duration ratios between the first and second phases. See text for details

Tableau 1
Les valeurs propres stationnaires et périodiques pourun modèle à deux phases avec transitions périodiques et différentes durées relatives de phases

G1-S-G2/M, brief sq. w.	λ_{per}	λ_s	G1-S-G2/M, 12-12 sq. w.	λ_{per}	λ_s
1	0.2385	0.2350	1	0.2623	0.2821
2	0.2260	0.2923	2	0.3265	0.3448
3	0.2395	0.3189	3	–	–
4	0.2722	0.3331	4	–	–
5	0.3065	0.3427	5	–	–
7	0.3472	0.3517	7	0.4500	0.4529
8	0.3622	0.3546	8	0.4588	0.4575
10	0.3808	0.3588	10	0.4713	0.4641
20	0.4125	0.3675	20	0.5006	0.4818

very variable duration. So that while in principle testing here the G2/M transition, we may also be testing the G1/S gate control by an unknown 24 h-rhythmic factor. The function $\psi(t)$ has 24 h period. We have tested for ψ 2 square waves, a brief one with 4 hours at value 1 and the remaining 20 hours at 0, mimicking the shape of the cdk1 kinase behaviour, with entrainment by 24 h-rhythmic Wee1, according to Goldbeter's model of the mitotic oscillator [7], the other one with 12 hours at 1 and 12 hours at 0, a version of the same cdk1 model, with no entrainment, but fixed coefficients yielding also a 24 h period. In Table 1, we show a comparison between the two eigenvalues (periodic and stationary), for the tested ψ periodic transition functions.

Thus no clear hierarchy can be seen between the two eigenvalues (even though some regularity may be suspected, and these simulations show cases favourable to our initial hypothesis in the interval $2 \leqslant$G1-S-G2/M$\leqslant 7$). It is likely that 2 phases only are not sufficient to account for the experimental observation which guided us in this modelling work, and that, as it is, this model aggregates in a too simplistic way circadian effects on the G1/S and G2/M transitions.

4. Concluding remarks

(1) This model allows to study the interactions in proliferating tissues between the cell cycle and physiological control systems such as the circadian clock.
(2) More than 2 phases and better knowledge of other mechanisms (e.g. control of Cyclin E-cdk4 at G1/S transition) might be necessary to further investigate the first eigenvalues of the periodic and stationary problems.
(3) The result $\lambda_{per} \geqslant \lambda_s$ for apoptosis control suggests that the sole control of death rate inside cell cycle phases might be unable to describe control of proliferation by cytotoxic drugs in cancer treatment. Transition rates should be considered in a therapeutic perspective.

Acknowledgements

We are gratefully indebted to S. Gaubert for discussions on theoretical and numerical aspects, and to B. Laroche and S. Mischler for the derivation of the model.

References

[1] O. Arino, A survey of structured cell population dynamics, Acta Biotheor. 43 (1995) 3–25.
[2] B. Basse, B.C. Baguley, E.S. Marshall, W.R. Joseph, B. van Brunt, G. Wake, D.J.N. Wall, A mathematical model for analysis of the cell cycle in cell lines derived from human tumors, J. Math. Biol. 47 (4) (2003) 295–312.
[3] G. Chiorino, J.A.J. Metz, D. Tomasoni, P. Ubezio, Desynchronization rate in cell populations: mathematical modeling and experimental data, J. Theor. Biol. 208 (2001) 185–199.
[4] J. Clairambault, B. Laroche, S. Mischler, B. Perthame, A mathematical model of the cell cycle and its control, INRIA Research Report # 4892, 2003.
[5] E. Filipski, P.F. Innominato, M.W. Wu, X.M. Li, S. Iacobelli, L.J. Xian, F. Lévi, Effect of light and food schedules on liver and tumor molecular clocks in mice, J. Natl. Cancer Inst. 97 (7) (2005) 507–517.

[6] L. Fu, H. Pelicano, J. Liu, P. Huang, C.C. Lee, The circadian gene *Per2* plays an important role in tumor suppression and DNA damage response in vivo, Cell 111 (2002) 41–50.
[7] A. Goldbeter, Biochemical Oscillations and Cellular Rhythms, Cambridge University Press, 1996.
[8] J.L. Lebowitz, S.I. Rubinow, A theory for the age and generation time distribution of a microbial population, J. Math. Biol. 1 (1977) 17–36.
[9] F. Lévi (Ed.), Cancer Chronotherapeutics, Chronobiol. Int. 19 (1) (2002) (Special issue).
[10] T. Matsuo, S. Yamaguchi, S. Mitsui, A. Emi, F. Shimoda, H. Okamura, Control mechanism of the circadian clock for timing of cell division in vivo, Science 302 (2003) 255–259.
[11] J.A.J. Metz, O. Diekmann, The dynamics of physiologically structured populations, Lecture Notes in Biomath., vol. 68, Springer-Verlag, 1986.
[12] P. Michel, S. Mischler, B. Perthame, The entropy structure of models of structured population dynamics. General relative entropy inequality: an illustration on growth models, J. Math. Pures Appl. 84 (9) (2005) 1235–1260.
[13] S. Mischler, B. Perthame, L. Ryzhik, Stability in a nonlinear population maturation model, M3AS 12 (12) (2002) 1751–1772.
[14] M.-C. Mormont, F. Lévi, Cancer chronotherapy: principles, applications and perspectives, Cancer 97 (1) (2003) 155–169.
[15] M. Rotenberg, Transport theory for growing cell populations, J. Theor. Biol. 103 (1983) 181–199.
[16] U. Schibler, Liver regeneration clocks on, Science 302 (2003) 234–235.

Available online at www.sciencedirect.com
ScienceDirect
Advanced Drug Delivery Reviews 59 (2007) 1054–1068
Advanced DRUG DELIVERY Reviews
www.elsevier.com/locate/addr

Modeling oxaliplatin drug delivery to circadian rhythms in drug metabolism and host tolerance ☆

Jean Clairambault *

INSERM U 776 "Rythmes Biologiques et Cancers", Paul-Brousse Hospital, F9480 Villejuif, and INRIA Rocquencourt, Domaine de Voluceau, BP 105, F78153 Rocquencourt, France

Received 1 May 2006; accepted 25 August 2006
Available online 28 June 2007

Abstract

To make possible the design of optimal (circadian and other period) time-scheduled regimens for cytotoxic drug delivery by intravenous infusion, a pharmacokinetic–pharmacodynamic (PK–PD, with circadian periodic drug dynamics) model of chemotherapy on a population of tumor cells and its tolerance by a population of fast renewing healthy cells is presented. The application chosen for identification of the model parameters is the treatment by oxaliplatin of Glasgow osteosarcoma, a murine tumor, and the healthy cell population is the jejunal mucosa, which is the main target of oxaliplatin toxicity in mice. The model shows the advantage of a periodic time-scheduled regimen, compared to the conventional continuous constant infusion of the same daily dose, when the biological time of peak infusion is correctly chosen. Furthermore, it is well adapted to using mathematical optimization methods of drug infusion flow, choosing tumor population minimization as the objective function and healthy tissue preservation as a constraint. Such a constraint is in clinical settings tunable by physicians by taking into account the patient's state of health.

Keywords: Theoretical models; Cancer drug toxicity; Pharmacokinetics-pharmacodynamics; Treatment outcome; Chronotherapy; Drug-delivery optimization

Contents

☆ This review is part of the *Advanced Drug Delivery Reviews* theme issue on "Chronobiology, Drug Delivery and Chronotherapeutics".

* Tel.: +33 1 39 63 55 43; fax: +33 1 39 63 58 82.
E-mail address: jean.clairambault@inria.fr.

0169-409X/$ - see front matter © 2007 Elsevier B.V. All rights reserved.
doi:10.1016/j.addr.2006.08.004

1. Physiological and pharmacological background

1.1. Chronobiology and cancer chronotherapeutics

Circadian rhythms have long been known in animals and humans, and taken into account in the therapy of cancer in humans during the past 20 years by various teams of clinicians in Europe, China, Canada and the United States. Recently, molecular biology has brought new insight about the mechanisms by which such rhythms are generated [1–3]. New understanding has been realized at the molecular level revealing connections between circadian clocks and cancer therapeutics [4–6] (see also the review in [7] for a state-of-the-art in cancer chronotherapeutics).

Our goal here is to provide a tool that is applicable in clinical settings. Herein, we design a model depending on parameters that are identifiable, relying on experimental observations at the scale of the living organism, to yield a macroscopic representation of the evolution of cell populations exposed to cytotoxic drugs used in cancer therapeutics. Even though the model is clearly dedicated to cancer therapeutics, we wish to point out that its pharmacokinetic–pharmacodynamic (PK–PD) part originated primarily from models commonly used in antibiotherapy, and from more general chronophar-macological considerations, as described in [8]. Thus we believe that this model can be generalized to other medical fields.

1.2. Aims of this study

Various teams of oncologists worldwide now take into account the fact that for a given cytotoxic drug, improved anti-tumor efficacy and reduced toxicity are possible when delivered at a determined circadian time, depending on the particular drug used. This approach has led to significant improvements in life expectancy and quality, for example, in patients with colorectal cancer.

To our knowledge, there is no theoretical model as yet that explains or predicts the qualitative behavior of an organism undergoing different time-scheduled anti-tumor therapeutic regimens. The aim of this article is to partially fill this void, by providing physicians and drug-delivery scientists with a practical tool to enable them to improve the clinical efficacy of anti-tumor treatments while minimizing their toxic effects on healthy tissues by using optimally designed time-scheduled regimens.

Since time matters in *chronotherapeutics*, such a tool must be dynamic and be composed of PK–PD differential equations describing the observed chronosensitivity of tumor growth and healthy tissue homeostasis on a drug delivered by intravenous infusion, the flow of which (as a function of time) is the external control law to be optimized.

The six variables of the dynamic system considered here (first presented in [9]) are the concentrations in active drug (in the general circulation compartment, in the tumor, and in the jejunal mucosa), the population of jejunal enterocytes and the tumor cell population. The time-dependent sensitivity of both the tumor and healthy cells to the drug is taken into account by 24-hour periodic modulation of the maximum of the PD function inducing cell death. The identification of model parameters was performed as far as possible on experimental laboratory data, precisely tumor size evolution curves during active treatment, i.e., a sequence of oxaliplatin injections, versus inactive treatment, i.e., the same sequence of injections of the sole drug vehicle.

1.3. Application chosen for this feasibility study

Oxaliplatin is one of the few drugs active on human metastatic colorectal cancer [10]. It is also known to be active on Glasgow osteosarcoma (GOS) in $B6D2F_1$ mice, and the treatment of this murine tumor has been extensively studied in our laboratory (INSERM U 776 "Biological Rhythms and Cancers", Paul-Brousse Hospital, Villejuif, France) according to various time-scheduled dose regimens [11].

Fragments of Glasgow osteosarcomas, about 1 mm^3 in volume that were sampled from fresh tumors in $B6D2F_1$ mice, were inoculated by subcutaneous puncture into both flanks of animals of the same lineage. Tumor size, from the moment it had become palpable just under the skin in the tumor-bearing animals until their sacrifice on ethical grounds, was measured with a caliper by its highest and lowest diameter, three times per week. The time evolution of tumor weight, deduced from these measures by an approximation formula (proportional to $L \times l^2$, longer and shorter diameters, respectively), was the basis for assessing tumor growth and therapeutic efficacy [11]. Within four weeks, all mice were dead, by toxicity or tumor development, or they had been sacrificed on ethical grounds when the tumor grew to a weight of 2 g.

In the present study, the population of jejunal enterocytes was chosen as a healthy tissue toxicity target in mice. Leukopenia is another known target of oxaliplatin toxicity in mice, but the main damage documented after time-scheduled injections of oxaliplatin was extensive jejunal mucosa necrosis [12]. For another cytotoxic drug, the bone marrow can be used as a target of drug toxicity, possibly using the same type of model, or more likely models of a different type, e.g., involving differential equations with delays in cell cycle models as reviewed e.g. in [13].

The total dose per course in the model simulations was limited to 20 mg/kg of oxaliplatin (300 μg of free platinum for a 30 g mouse). Actual doses in laboratory experiments consisted of four daily injections of 4 mg/kg of oxaliplatin [11].

1.4. Physiological hypotheses, literature data and model assumptions

1.4.1. Pharmacokinetics

Free platinum (Pt) is the active form of the drug; it binds *irreversibly* to all DNA bases, which is the assumed main mechanism of its efficacy and toxicity [14–17]. It also binds more avidly to sulphydryl radical-containing molecules, such as reduced glutathione, that protect cells from Pt toxicity [14] and also contribute to its elimination from blood by uptake and irreversible binding in erythrocytes. In oxaliplatin, Pt is linked to a diamminocyclohexane (DACH) nucleus (which is thought to be responsible for the poor DNA mismatch repair mechanisms and hence higher activity in colorectal cancer, in comparison to cisplatin [18]), and to an oxalate ion, a compound structure which endows it with relatively good blood solubility. Diffusion through membranes is ensured thanks to a transporter protein, a mechanism thought to be linear (i.e., no saturation is seen on outward/inward concentration transfer curves), based on in vitro assessments [19].

It has been assumed in this model that DACH–Pt oxalate (oxaliplatin) diffuses freely in the plasma and is eliminated as a free molecule from the (central) plasma compartment by binding irreversibly to plasma or hepatic proteins or to erythrocyte glutathione according to first-order kinetics [14,17,20]. In the periphery, DACH–Pt is transported through cell membranes according to a linear mechanism to the healthy cells and, in parallel, to the tumor cell compartment. Also according to first-order kinetics, either it is degraded there (mainly by intracellular glutathione) or it reaches its DNA target. This knowledge led to the definition of a single central compartment for soluble Pt and two peripheral compartments for nucleic acid-bound Pt, one for the tumor and one for the healthy tissue, here the jejunal mucosa. DACH–Pt binding to plasma proteins is fast and irreversible [14,20], and its intracellular binding either to DNA or to reduced glutathione and other detoxification molecules is also supposed to be rapid and irreversible. Its binding to plasma proteins and red blood cell reduced glutathione in the central compartment, on the one hand, and to peripheral cellular reduced glutathione and other detoxification molecules, on the other hand, may thus be represented by simple elimination terms. The parameters of natural Pt elimination in the tissues may be evaluated by the evolution of total Pt tissue concentrations, assuming proportionality between nucleic acid-bound and total Pt tissue concentrations.

1.4.2. Pharmacodynamics

Drug activity is represented by an efficacy/toxicity function (Hill function) inhibiting cell population growth in each peripheral compartment, healthy tissue or tumor. This function is here supposed to depend only on tissue drug concentration and the time of drug exposure, with a time-dependent amplitude modulation, here figured by a plain cosine function, representing circadian drug sensitivity.

1.4.3. Enterocyte population

The enterocyte population is known to respond to radiologic or cytologic insult by damped oscillations converging to its initial and stable equilibrium value [21,22]. The stability of this equilibrium is ensured physiologically by exact compensation (tissue homeostasis) of the villi cells eliminated into the intestinal lumen by the influx of young cells from the crypts.

It is also assumed that only crypt cells (the renewing ones, in which cell cycle activity exists) are subject to drug toxicity.

1.4.4. Tumor cell population

Without treatment, tumor growth is assumed to follow a Gompertz law [23]: firstly exponential growth, then convergence towards a plateau. This is representative of the early stages of tumor growth, before neoangiogenesis induces regrowth. The particular choice of the Gompertz model for such an S-shaped curve may be justified by considerations of the existence of proliferative and quiescent subpopulations in the tumor [24,25]. Though more elaborate models might be used, for instance using partial differential equations for tumor growth and inhibition by drug contact [26,27], or modifications of the Gompertz model, itself, obtained by making the upper limit, B_{max}, dependent on time so as to take angiogenesis into account [28,29], we chose to represent the first stages of tumor growth only, and to assess optimization procedures on such a

basic model endowed with but few parameters. Drug resistance may also optionally be introduced into the model as the probability for a given tumor cell to develop such resistance [30], though this is not considered here.

2. The model

2.1. Pharmacokinetics

The three dynamic variables considered here are Pt concentration (oxaliplatin being a compound DACH–Pt oxalate) in the central, or plasma, compartment, P, and nucleic acid-bound Pt concentrations in the healthy tissue (jejunal mucosa), C, and in the tumor, D. The first-order kinetic equations are:

$$\frac{dP}{dt} = -\lambda P + \frac{i(t)}{V_{di}} \tag{1}$$

$$\frac{dC}{dt} = -\mu C + \xi_C P \tag{2}$$

$$\frac{dD}{dt} = -\nu D + \xi_D P. \tag{3}$$

Here λ, μ and ν are decay parameters representing Pt elimination by *irreversible binding* to plasma proteins, hepatic or red blood cell glutathione, on the one hand (λ), and to intracellular glutathione or protective proteins, on the other hand (μ for healthy cells and ν for tumor cells). Parameter V_{di} is the drug distribution volume, which is assumed to be constant, in the central compartment, and i: $t \mapsto i(t)$ is the drug infusion flow control law. The flow i may be a constant function, in the case of constant continuous infusion, or a periodic one, in the case of a time-scheduled drug regimen, as is commonly used in clinical settings, and in the latter case may show different forms: square, sinusoid-like, or sawtooth-like waves, all of which are clinically implemented using programmable and portable infusion pumps like the ones that have been used for delivering the chronotherapy of cancer medications over the past several years; it may also be a brief, quasi-dirac-like impulsion function in the case of bolus administration, or any continuous function of time. Factors ξ_C and ξ_D before P in the second and third equations represent active drug transfer rates from the plasma to the peripheral compartments.

2.2. Pharmacodynamics: toxicity and therapeutic efficacy functions

These functions represent the mean drug activity in the healthy and tumor cell populations considered here, and are functions of the drug concentration, in the healthy tissue for toxicity, and in the tumor tissue for therapeutic efficacy. Both are Hill functions, modulated in amplitude by a circadian chronosensitivity factor:

$$f(C) = F \cdot \left\{1 + \cos\left(2\pi \frac{t-\varphi_S}{\mathcal{T}}\right)\right\} \cdot \frac{C^{\gamma_S}}{C_{S50}^{\gamma_S} + C^{\gamma_S}}$$

$$g(D) = H \cdot \left\{1 + \cos\left(2\pi \frac{t-\varphi_T}{\mathcal{T}}\right)\right\} \cdot \frac{D^{\gamma_T}}{D_{T50}^{\gamma_S} + D^{\gamma_T}}$$

where C and D are as defined earlier, γ_S and γ_T the Hill coefficients (>1 if drug activity is known to show cooperative reaction behavior as in certain enzymatic reactions, and by default equal to 1 if drug binding to its target, and subsequent cell death, is assumed, as will be the case here, to follow Michaelis–Menten kinetics), C_{S50} and D_{T50} half-maximum activity concentrations, F and H the half-maximum activities, $\mathcal{T}=24$ h (period of circadian drug sensitivity oscillations), and φ_S and φ_T are phases (in hours with reference to a fundamental 24-hour rhythm, i.e., taking into account 24-hour periodicity) of the maximum activities of functions f and g.

2.3. Enterocyte population

Growth of the enterocyte population evolution in an arbitrarily fixed volume of jejunal mucosa is represented by two dynamic variables: the mature villi cell population, A (in number of cells), and the flow, Z (in number of cells per time unit), of incoming young cells counted positively which migrate per each time unit from the crypts to replace ageing villi enterocytes that are eliminated into the intestinal lumen (Fig. 1):

$$\frac{dA}{dt} = Z - Z_{eq} \tag{4}$$

$$\frac{dZ}{dt} = \{-\alpha - f(C)\}Z - \beta A + \gamma. \tag{5}$$

Here $f(C)$ is the drug toxicity function in the healthy tissue introduced earlier, α a natural autoregulation factor in the crypt which the drug toxicity function thus modulates additively, β a mitosis inhibitory factor (a so-called "chalone") supposedly sent from the villi to the crypts, Z_{eq} the steady state (constant) flow from crypts to villi, and $A_{eq} = \frac{\gamma - \alpha Z_{eq}}{\beta}$ the steady the steady state villi population (without treatment). In healthy jejunal mucosa, tissue homeostasis (here represented, in the absence of drug damage, by constant cell population at steady state) is granted, so the equilibrium point (Z_{eq},A_{eq}) is a stable one. The parameters of the damped harmonic oscillator (Z,A) are entirely determined

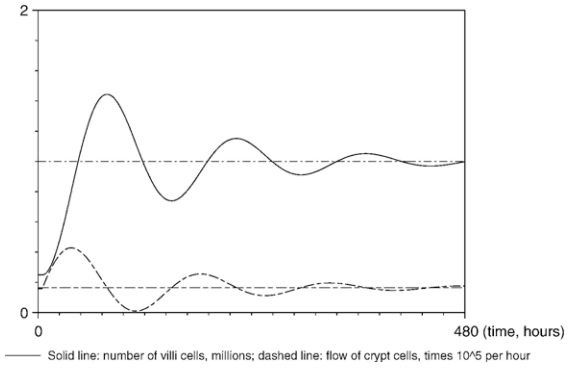

Fig. 1. Model oscillations of the population of enterocytes in response to a brief radiotoxic or cytotoxic insult shown over 20 days. Villi cells (top) and flow from crypts (bottom) are represented here recovering in a steady state behavior after an initial deviation from their equilibria at time zero. They may be seen as the linear approximation of a more complex phenomenon, e.g., as proposed in [31]. Units are in millions of cells for villi (solid line) and in units of 10^5 cells for the flow of cells from crypts (dashed line). Time (abscissa) is in hours.

if its period and dampening coefficient, together with the equilibrium point coordinates, are known (they can indeed be determined by elementary computation, as shown in the Appendix).

2.4. Tumor growth

Tumor growth is represented by the number of tumor cells, B, which is assumed to follow the Gompertz law without treatment, modified by a "therapeutic efficacy term" $-g(D)\cdot B$:

$$\frac{dB}{dt} = -a\cdot B\cdot \ln\left(B/B_{\max}\right) - g(D)\cdot B \qquad (6)$$

where $g(D)$ is the therapeutic efficacy function earlier introduced (here seen as a instantaneous death rate in the tumor cell population), $B_{\max}$ is the asymptotic (that is, maximal, since without $\frac{dB}{dt}>0$) treatment value of B, a is the Gompertz exponent, i.e., without treatment, one has $\frac{dB}{dt} = G.e^{-a(t-t_0)}\cdot B$, where $G = \frac{1}{B(t_0)}\frac{dB}{dt}|_{t=t_0}$ is the initial growth exponent if t_0 is the chosen initial observation time, conveniently estimated on the initial part of a tumor growth curve without treatment. Without treatment, this integrates immediately in $B(t) = B(t_0)e^{\frac{G}{a}\left(1-e^{-a(t-t_0)}\right)}$, whence $B_{\max} = B(t_0).e^{G/a}$. An example is shown in Fig. 2.

3. Model identification and computer simulation

3.1. Drug doses and pharmacokinetics

In the case of constant or periodic delivery regimens, the daily dose of active infused drug (Pt in oxaliplatin) was fixed as 60 μg of free Pt (corresponding to 4 mg/kg/d of oxaliplatin for a 30 g mouse, a common dosage for the laboratory, where the daily doses range between 4 and 17 mg/kg). Diffusion parameters (V_{di}=10 mL, λ=6, μ=0.015, ν=0.03) were estimated according to published laboratory data [20] on plasma concentration and half-life of free Pt in plasma and total Pt in peripheral tissues (jejunal mucosa for toxicity and red blood cells for therapeutic efficacy, in the absence of actual data on tumor tissue); the value $\nu=2\mu$ corresponds to the elimination of the total Pt from the tumor being twice as fast as in the healthy jejunum.

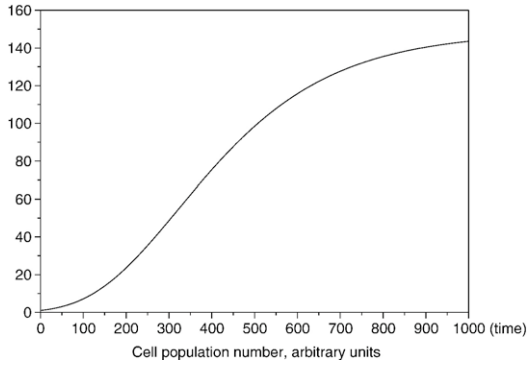

Fig. 2. Example of simple model Gompertzian growth: $B(t)=B_0e^{G/a(1-e^{-at})}$ where, $G/a = \ln\frac{B_{\max}}{B_0}$, a=0.005 and $B_{\max}/B_0$=150; time (x-axis) and number of cells are here in arbitrary units, from a minimum value B_0 arbitrarily set to 1 on the y-axis to a maximum value $B_{\max}$.

3.2. Pharmacodynamics

Hill exponents γ_S and γ_T were arbitrarily fixed as 1 in the absence of data on the actual concentration efficacy dependence, and C_{S50} and D_{T50} were set to a high value (10) compared to the average drug tissue concentrations in the model, so as to bring the efficacy/toxicity functions into a linear zone, in the absence of data on these Hill, or Michaelis–Menten functions at the tissue level.

The optimal injection phase (i.e., circadian time) of an oxaliplatin bolus was identified from laboratory experiments as 15 h after light onset (HALO), which corresponds to the middle of the activity time in the nocturnally active mice housed under a 12 h light–12 h dark regimen. This dosing time was observed to be optimal in both senses simultaneously: optimal in the sense that it yielded best anti-tumor efficacy and also optimal in the sense that it led to least drug-induced toxicity. This remarkable experimental result — a coincidence that has been always observed in experiments with mice in our laboratory, with no explanation so far, was obtained with a time resolution of 4 h by recording survival and tumor weight evolution in six different groups of mice, each group being defined by a specific HALO designation corresponding to the circadian time at which the animals received bolus injection of oxaliplatin for four consecutive days (see [11] for details). The maximal anti-tumor efficacy phase (φ_T=21 HALO) for a bolus was deduced by numerical variation along a one-hour step grid in simulations of the model. This delay $\Delta\varphi$ of approximately 6 h (from 15 HALO to 21 HALO) between the optimal injection phase φ_I – note that for a bolus the peak phase and the phase of the beginning of infusion, φ_I, coincide – and the maximal efficacy phase φ_T in the model may also be obtained by direct computation (see the Appendix). The maximal healthy tissue toxicity phase was estimated as φ_S =9 HALO based on two convergent considerations. First, we assumed by our cosine model of chronosensitivity a 12 h delay between highest and lowest drug-induced toxicity phases – and we already knew the circadian phase of lowest toxicity – and second, the circadian phase φ_S=9 is also known to be the phase of the minimum concentration of non-protein sulphydryl compounds (i.e., reduced glutathione and cysteine, the main actors in the tissue detoxification of oxaliplatin) in mouse jejunum cells [32].

In the absence of data on the evolution of jejunal cell population under treatment, the parameter F was adjusted (F=0.5) so as to yield a residual villi population always greater than 10% of the initial cell population for daily doses lower than 200 μg of free Pt (the approximate lethal dose effect for a 30 g mouse). The parameter H was estimated from tumor size evolution curves derived from animals under treatment (see Fig. 2) to obtain a likely value which was then fixed; the value then used in further simulations was H=2 (see the Appendix for details).

3.3. Healthy and tumor cell proliferation

The equilibrium point (Z_{eq},A_{eq}) for the enterocyte model was $(16{,}500,10^6)$, the latter value arbitrarily fixed and the former proportionally fixed according to data previously published in the literature [21]. The period of oscillations (6 days) and dampening coefficient (1/3) were also estimated using data found in the literature [21,31], whence α, β, γ (see Appendix for details). The initial growth exponent G and the Gompertz exponent a, whence $B_{max}/B(t_0)=e^{G/a}$, were first estimated based upon tumor size evolution curves (see Fig. 3) without treatment. Their values varied from one individual to the other (a between 0.005 and 0.1, B_{max} between 1.2 and 30 times the value of B at the beginning of its steep increase). Intermediate values chosen were $a=0.015$ and $G=0.025$, leading for the parameter B_{max} to a value of 5.3 times the initial observed value $B(t_0)$ at the onset of steep tumor growth. These values were retained so that further simulations might correspond to a human-like situation where the tumor grows rapidly, in a bounding environment, and being the object of an efficient chemotherapy (see Appendix for computational details).

The attainable parameters for model identification in clinical settings should thus be a and B_{max} for natural tumor growth, and H for therapeutic response.

3.4. Computer simulation

Numerical integration of the system of six ordinary differential equations was performed first in SCILAB or in MATLAB, then using programs written in fortran. The time unit was the hour, counted from 0 HALO on day 1. Integration (observation step: 0.1 h) began with treatment; the applied solvers were Adams and an implicit (BDF) scheme. The set of initial values was $(P_0=0,\ C_0=0,\ D_0=0,\ A_0=A_{eq}=10^6,\ Z_0=Z_{eq}=16{,}500,\ B_0=10^6)$. In clinical-like conditions that mimic hospital settings in where medications are delivered on a 24-hour basis, the chosen periodic control law was either a square, a sawtooth-like, or a sine wave.

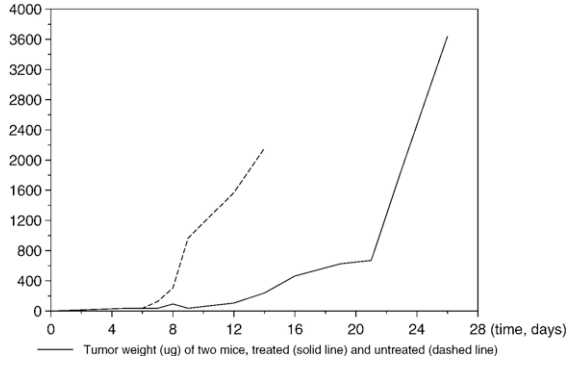

Fig. 3. Examples of tumor growth curves: without treatment (dashes) and after four evenly spaced injections (on days 5, 6, 7 and 8 following tumor inoculation into the test animals) of oxaliplatin, 4 mg/kg (solid line) in two $B6D2F_1$ mice bearing a Glasgow osteosarcoma. When tumor weight grew to two grams, animals were sacrificed on ethical grounds. Tumor weight is in units of mg (y-axis) and time is in units of days (x-axis).

4. Results: optimizing cancer chronotherapeutics

4.1. Frames for therapeutic optimization

In a first attempt, we adopted the types of drug-delivery regimens which are common in clinical therapeutics. Usually they entail infusion times of 1 to 12 h each day, periodically repeated on a 24-hour basis over four or five days, followed by a drug-free interval of time to allow patient recovery from drug-induced toxicity. This course of treatment is repeated every other week (when the duration of effective treatment is four days per course) or every third week (when the duration of effective treatment is five days per course). The optimal peak infusion time being known from previous experimental data, the search for optimality then consisted of obtaining the best infusion duration for the best daily regimen chosen among a limited dictionary of infusion profiles, of square, triangle, or sine wave shape. This best infusion was determined by varying this duration from 1 to 12 h by one-hour steps for each profile, and evaluating the resulting number of residual tumor cells.

Then we decided, using mathematical optimization techniques, to remove the periodical infusion scheme constraint, still taking into account the optimality of the peak infusion times, which is represented in the model by a sinusoidal modulation of the maximum effect. This yielded other optimal therapeutic drug-delivery schemes.

These two different attitudes toward therapeutic optimization and their results are described below.

4.2. Mimicking hospital routines: 24-hour periodic chemotherapy courses

A typical five day-infusion chemotherapy course, with the first five days of recovery, is represented in Fig. 4, where one can see the six variables of the dynamic system, from top to bottom: P, C, Z, A, D, and $\log_{10}(B)$. The objective function (to be minimized) is the minimal number of tumor cells (ideally zero) and tolerability consists of preserving a minimal number of villi cells, a percentage of the arbitrary initial value of 10^6 cells.

A graphic illustration of injection phase optimization in the model is presented in Fig. 5. The plateaus (centered on maximum anti-tumor efficacy phase φ_T) represent the logical variable $L=\left(a\ln\frac{B_{max}}{B}-g(D)<0\right)$ that is highly dependent on drug chronosensitivity in the tumor: 1 when the drug actually inhibits tumor growth, 0 when it does not. The optimization principle used here (numerically varying the circadian phase φ_I of the beginning time of infusion) may be seen as graphically superimposing the areas under peaks of tumor drug concentration (D, sawtooth line) on these plateaus ($L=1$). Tumor cell population evolution is shown in parallel on a logarithmic scale.

Therapeutic optimization may take place in two different contexts, depending on the patients' state of health, based on clinical criteria (to be evaluated by physicians), leading to two different schemes: either an aggressive curative scheme for patients who are able to tolerate a high degree of toxicity in the hope of obtaining complete tumor eradication, which is the

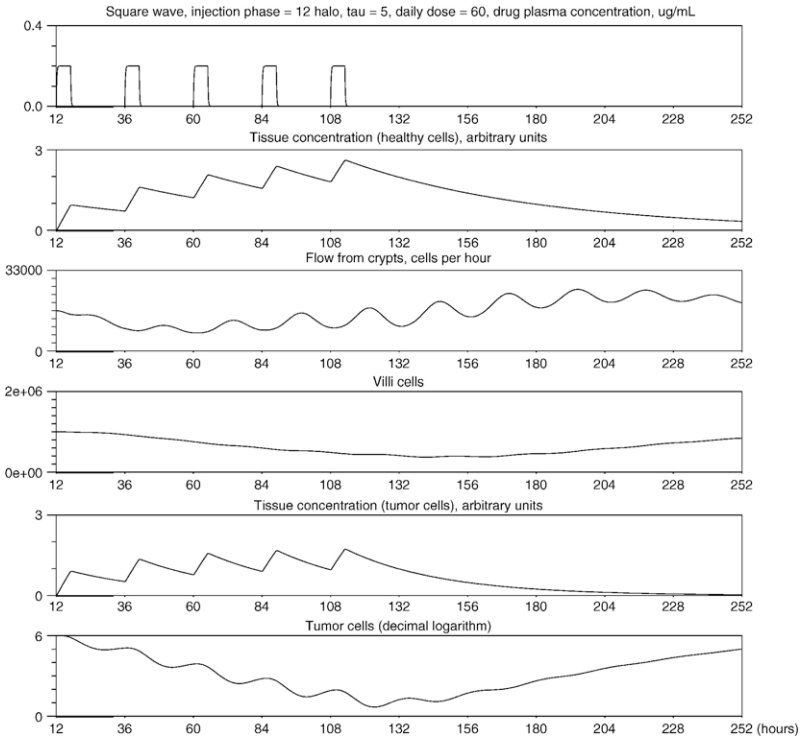

Fig. 4. A five-day optimal time-scheduled 24-hour periodic regimen followed by five days of recovery. Time (abscissa) is in hours and quantities in ordinates in units that depend on the track considered: μg/mL for drug plasma concentration, arbitrary units for tissue drug concentrations (depending on an unknown transfer constant from plasma to tissue) and cell populations in number of cells.

main goal of therapy; or a reduced toxicity scheme, leading only to tumor stabilization, i.e., forsaking eradication but maintaining an absolute limit of healthy cell toxicity, within which one is left with as few tumor cells as possible at the beginning of recovery time (usually followed by repeated subsequent courses of chemotherapy in order to contain the tumor). Transposed in the context of this model study, this choice between an aggressive and a reduced toxicity scheme led to the definition of two different types of simulations.

4.2.1. Simulations focusing on anti-tumor efficacy

The criterion for the "aggressive curative scheme" was to yield the smallest number of tumor cells during the course of chemotherapy (5 days of treatment and 16 days of recovery) for a standard daily dose of 60 μg/d of free platinum. A possible temporary decrease in the mature enterocyte population to as low as 35% of the initial population was allowed (compare this threshold with the previous one of 60% in the reduced toxicity scheme; these values are arbitrary in the absence of data known to us on the severity of diarrhea related to mucosal depletion, but they could easily be changed).

For the square wave control law, the best result (four residual tumor cells out of 10^6 initially) was obtained with an effective five-hour infusion duration that begins at 12 HALO. Even a better result (3 residual tumor cells) than with this five-hour square wave for the same daily dose was obtained with a sharp sinusoid-like model infusion law lasting five hours that begins at 12 HALO. Respect for the optimal injection phase is essential, since constant infusion yields worse results (16 cells) than square wave time-schedule beginning at optimal injection phase $\varphi_I = 12$ HALO (four cells), but achieves better results than the beginning time coinciding with the worst phase of 0 HALO (52 cells). In other words, this means that chronotherapy can be worse than constant infusion if the beginning infusion time φ_I is ill-chosen.

These simulations show in this theoretical framework the advantages of a time-scheduled regimen as compared to the conventional constant infusion scheme, *provided that the beginning infusion (circadian) time φ_I is accurately chosen*. Note that this last point is dependent on the chosen drug, not on the individual, inasmuch as the fundamental circadian rhythms

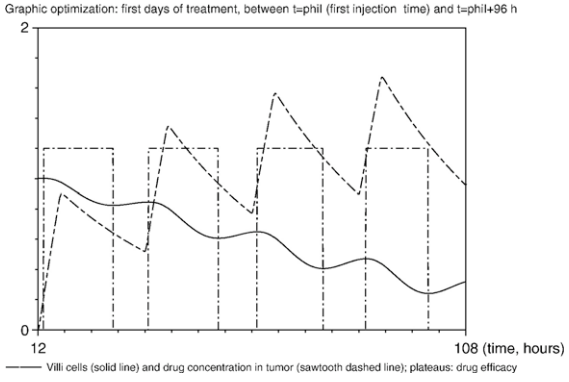

Fig. 5. Graphic chronotherapeutic optimization. Solid line = tumor population, logarithmic scale $\log_{10}(B)$; dashed line plateaus: up when the drug actually inhibits tumor growth, down when it does not; sawtooth dashed line = drug concentration in the tumor shown in arbitrary units; time shown in hours.

of the individuals in a population (as determined by their body circadian clocks [33]) are synchronized by environmental time signals of light, meals, social life, etc.; this was the case for the nocturnally active mice of this study that were all previously synchronized to a regimen of 12 h light alternating with 12 h darkness. These simulations also suggest that sinus-like waves actually used in clinical chronotherapies are a good approximation for optimality in this context.

4.2.2. Simulations focusing on treatment tolerability

The criterion for the reduced toxicity scheme was prohibition of the decrease of the mature enterocyte population below a given threshold (arbitrarily fixed between 40% and 60% of the initial population value) to obtain the therapeutic regimen yielding, by variation of the drug daily dose, the smallest number of tumor cells during the course of chemotherapy (in this case, 5 days of treatment and 16 days of recovery).

In the case of the threshold to preserve 60% of the initial population of enterocytes, the best result (2400 residual tumor cells out of 10^6 initially) was obtained with a right sawtooth-like infusion model law lasting 2 h (i.e., steep increase, then drop) beginning at $\varphi_I = 14$ HALO, allowing the infusion of a maximum dose of 33 µg/d of Pt. In the perspective of applications to clinical settings, the main drawback of this time schedule is the achievement of very high drug concentrations over a short period of time; in humans, at least a two-hour duration of oxaliplatin infusion is recommended to prevent acute muscular toxicity, in particular laryngeal spasm, an acute

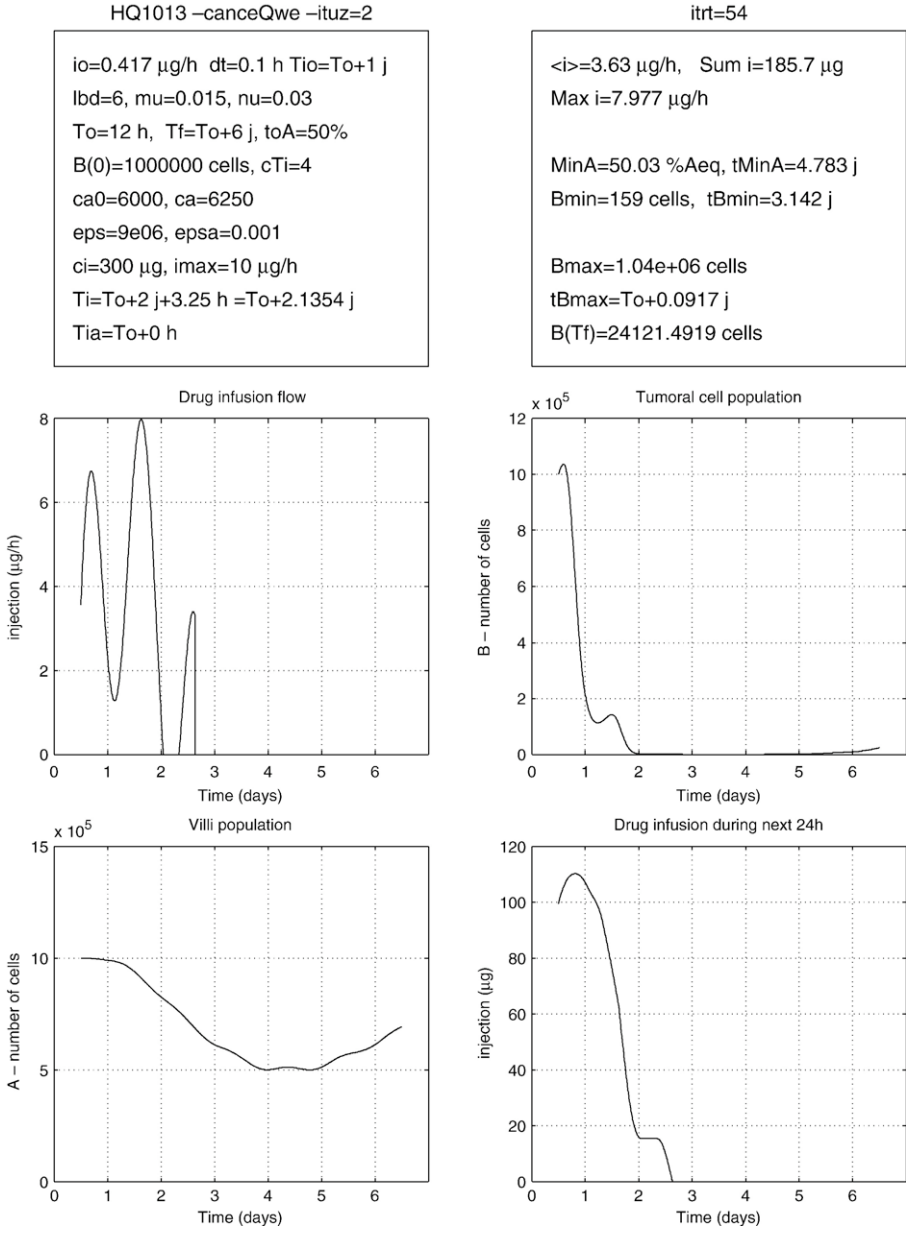

Fig. 6. Optimal eradication treatment preserving at least 50% of jejunal enterocytes: instantaneous drug infusion flow i (in µg/h), tumor cell population *B*, villi cell population *A*, and the resulting dose (in µg) – obtained by integration of *i* between times *t* and *t*+24 h – administered over a sliding window of 24-hour duration. Figure courtesy of C. Basdevant. See Ref. [38] for further details.

toxicity symptom which imposes termination of treatment. Such acute toxicity is excluded in the model, where chronic jejunal toxicity is the focus, by setting an upper limit to the drug infusion flow and its derivative with respect to time. The advantage of this reduced toxicity scheme is better anti-tumor outcome compared to the conventional constant infusion therapy that, for the same limit toxicity, imposes (in the model) a dose delivery no greater than 29 μg/d of Pt (7000 residual tumor cells).

These simulations illustrate in a modeling frame what is well known to oncologists involved in chronotherapeutics: first, a well chosen time-scheduled regimen can yield better results than a constant infusion scheme, and second, the shorter the infusion time, the less intolerance to treatment, as far as *chronic* toxicity is concerned.

4.3. Drug flow optimization in a general non-periodic frame

With the same model, but removing usual clinical chronotherapeutic requirements which impose 24-hour periodicity of the infusion scheme, we set the mathematical problem of therapeutic optimization as maximizing tumor cell death under

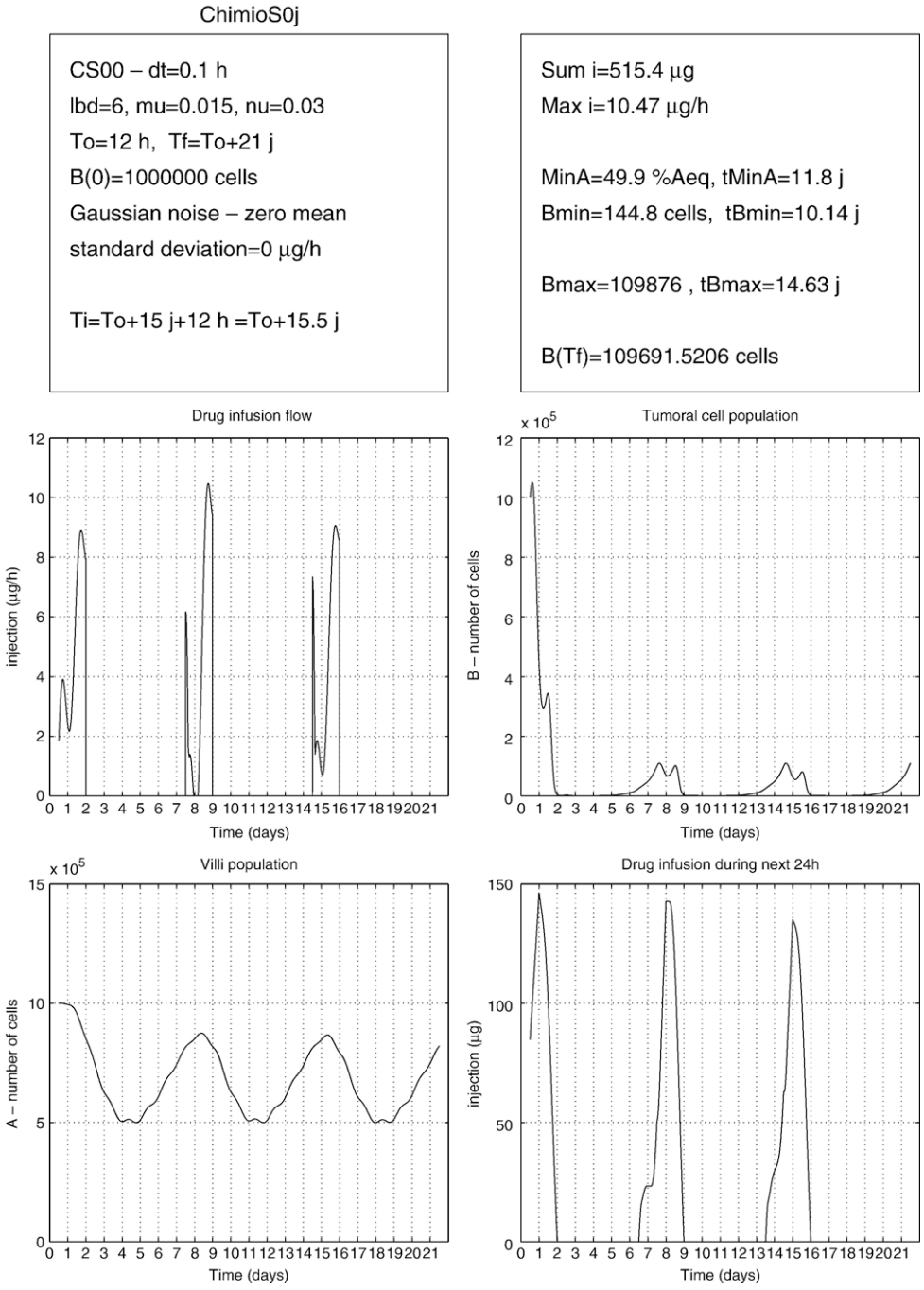

Fig. 7. Three weeks stabilization treatment with repeated chemotherapy courses of 1.5 of active medication 5.5 days medication-free interval: same variables as on Fig. 6. Figure courtesy of C. Basdevant. See Ref. [38] for further details.

the constraint of maintaining the healthy cell population always above a given threshold. This point of view has also been developed by other authors with different methods, in a similar context but with preservation of a different healthy cell population [36,37].

Whereas the clinical tolerability constraint is unequivocal (yet tunable by physicians according to the patient's state of health), the tumoral cell death maximizing goal may be understood in two different ways, since a tumor that has not been eradicated starts to regrow at the end of treatment. Either one assumes that complete eradication is possible and then the objective function to be minimized is the *minimum* number of tumor cells, as close as possible to zero, during a one course treatment; or one admits that there always will remain an ineradicable fraction of tumor cells, which may only be contained by repeated treatment courses under an acceptable threshold, compatible with patient survival. Then the objective function to be minimized is the *maximum* number of tumor cells during repeated treatment courses, in fact during the recovery period of the course.

This distinction leads to two different optimization strategies, respectively: the eradication strategy in a single course, and the stabilization strategy for repeated courses of the same treatment, which aims only at containing the tumor. This point of view has been extensively developed in a recent article, to which we refer for detailed results [38]. To briefly state the results obtained for each one of these two strategies, an optimal drug infusion flow (to be implemented using a programmable pump) is derived to minimize the tumor cell number (minimum or maximum) and to satisfy the conditions: a) the healthy cell population number remains above a given threshold; b) the total drug dose is lower than a prescribed level; and c) its instantaneous flow and its derivative with respect to time also remain below a prescribed level. Examples of these results are illustrated in Figs. 6 and 7. Since the resulting optimized infusion flows are not superimposable onto the 24-hour periodic sine wave like flows used in clinics, this suggests that classical repeated sine wave chronotherapeutic regimens are only approximations to optimality and may be further improved. Yet, in the absence of precise knowledge of all the parameters of the model, and their related confidence intervals, it would be hazardous to quantify in terms of tumor cell kill the gain expected from this optimized procedure as compared to the classical chronotherapeutic regimens.

5. Discussion and clinical perspectives

5.1. Advantages and limits of the model

The described model provides a semi-quantitative prediction tool. First, it shows that time-scheduled regimens are likely to yield a better treatment outcome than a constant infusion regimen, provided that the beginning time (with reference to circadian rhythms) φ_I of the infusion is well chosen. Second, it allows one to optimize time-scheduled regimens by acting on the beginning (or peak time) and duration of the infusion, and on the shape of the programmable infusion control law. To our knowledge, this is the first time that such clinical know-how has been set upon theoretical grounds.

The model was chosen to be a simple one to help parameter identification under the restraint of a relative scarcity of available data on the internal mechanisms of tumor growth and inhibition by medications. Its quasi-linear form without treatment (set $W=\ln B$ in the last equation and the model without treatment becomes completely linear) may be seen as a robust and natural approximation, in a neighborhood of its initial values, of a hypothetic, more complete and realistic model for cell proliferation. Some of its components, such as drug activity functions, remain unknown and were chosen according to the experience of pharmacologists working with different medications, such as antibiotics; in the same way, some parameters had to be estimated on questionable grounds, such as extrapolation from one tissue to another. Nonetheless, the other parameters were identified after experiments done in our laboratory on the effects of oxaliplatin treatment on GOS tumor-bearing $B6D2F_1$ mice.

5.2. Model assumptions

5.2.1. Healthy cell population

The linear system representing jejunal mucosa homeostasis may be seen as the linearization of an unknown non-linear system, which should describe the enterocyte population kinetics in a more accurate way (as in [31]), around its stable equilibrium point (Z_{eq},A_{eq}). Tissue homeostasis may be observed after brief radiologic or cytotoxic insult. In the case of a sudden perturbation, return to equilibrium with damped oscillations has been reported [22]. To guarantee the validity of this linear approximation, we make the additional assumption that this equilibrium point is hyperbolic, i.e., the linear tangent system has no zero or purely imaginary eigenvalues. Then linearization is valid, up to topological equivalence, in the vicinity of the equilibrium point, according to the Hartman–Grobman theorem (see for instance Perko [34]).

No basal (without treatment) circadian variation of the enterocyte population has been taken here into account; whereas, at least circadian variations in the enterocyte cell cycle have been known for some time [22,35]. The reason for this is the irrelevance of such variations for the follow up of the enterocyte population during a course of chemotherapy. The variables (Z,A) should rather be seen as sliding averages over the last 24 h of the population described beforehand. It is quite likely that instead of a basal equilibrium point, the non-linear system presents rather a stable limit cycle, with 24-hour period, but we are interested here only in controlling drug toxicity on an average villi population, since circadian variations of this population are negligible compared to the havoc produced by the drug-induced cytotoxicity.

Other toxicities such as neurotoxicity and hematotoxicity, known to be induced by oxaliplatin in human beings, were taken into account by imposing course scheduling designed as short treatment durations followed by sufficiently long recovery times, e.g., two days of treatment followed by five days of recovery in the case of repeated chemotherapy courses. Such a

recovery duration may seem short, but GOS is a fast growing tumor, with an apparent doubling time in exponential models being about 1.4 days; so, the long recovery times as used in clinical settings for curable human tumors (e.g., 10 days in 2 weeks or 16 days in 3 weeks) are not realistic here, since they would enable the tumor too much time for regrowth beyond its initial value after the end of the last infusion.

Neuropathy could not be experimentally examined in mice. Hematotoxicity (mainly leukopenia) was assumed in this study to be made up for by natural bone marrow proliferation during recovery. Post-mortem histology performed in animal experiments in our laboratory showed tolerable bone marrow depletion; in contrast, jejunal toxicity was most severe, with extensive necrosis of the mucosa [12,20].

5.2.2. Tumor cell population

The initial value for the tumor cell population number was arbitrarily fixed as 10^6 cells, and eradication was considered complete when it became lower than 1. These values could easily be replaced by 5×10^9 and 200 (oncologists agree on these figures, which represent a frequent lower limit for clinical or radiological discovery and a cell population number under which a tumor is usually considered as non-viable). The optimality, in the conditions of our model, of the infusion duration and initial phase (between 0 and 24, i.e., taking into account 24-hour periodicity) will not be changed by such modifications, given the homogeneity of Eq. (6) and the scale independence of the chosen criterion $\left(\min_{t\in[0,T]} B(t) \text{ or } \max_{t\in[0,T]} B(t)\right)$.

It is possible to introduce drug resistance in tumor cells, following Goldie and Coldman [30], by replacing in Eq. (6) the cell kill term $-\mathrm{g}(D).B$ by $-g(D).B.\frac{1+B^q}{2}$ where q is -2 times the probability for a cell to become resistant, a probability that in this formulation is independent of the time of or the amount of delivered dose, yielding a population of $B.\frac{1-B^q}{2}$ resistant cells; for instance, if one out of a thousand cells acquires drug resistance, then $q=-0.002$.

5.2.3. Pharmacodynamics

No cell cycle phase specificity of oxaliplatin has been reported, which is consistent with its supposed mechanism of action at the cell level, i.e., binding to DNA at any stage of the cell cycle. This makes inclusion of cell cycle kinetics in the present model unnecessary, at least as long as oxaliplatin is the only cytotoxic drug used for pharmacological control and circadian drug sensitivity is represented in the above-mentioned simplified way.

Drug toxicity and anti-tumor efficacy functions have been chosen to act as multiplicative factors on the population size of enterocytes and tumor cells. While this assumption is quite natural in the linear frame of the enterocyte model, where $f(C)$ is just an enhancement of the natural autoregulation coefficient α, it is more questionable for the Gompertz tumor growth model: it has the consequence "big tumor, big effect; small tumor, small effect". This may be true for oxaliplatin, but not for other drugs; other representations of the anti-tumor effect could be used instead of $-\mathrm{g}(D)B$, such as $-g(D)\frac{B}{K+B}$, as in [26].

The only place in the model where circadian variability occurs is by modulation of the maximal drug effect (parameters F and H). This simplifying assumption thus aggregates all possible circadian influences on one term in each peripheral compartment. The actual physiological circadian variation in drug sensitivity is more likely due to the variations in drug detoxification mechanisms in the central (hepatic enzymes, plasma proteins) and peripheral (cellular glutathione) compartments, but tissue measures which would be necessary to identify the parameters of these chronopharmacokinetic (i.e., biological rhythms in drug pharmacokinetics) mechanisms were not available to us, even though one may hope they will become available through future routine laboratory experiments or clinical data investigations.

The representation of drug chronosensitivity by a plain cosine intervening as a multiplying factor in the expression of the drug activity functions may be considered to be a coarse description of circadian rhythmicity. In the same way, this model does not include recent advances in the knowledge of the genetic determinants of mammalian circadian rhythms, such as the clock genes CLOCK, BMAL1, PER and CRY (and their proteins), nor of their influences on the cell cycle of the cellular populations involved [5–7]. In this respect, the cosine model might be replaced by a circadian oscillator model of the type developed by A. Goldbeter for *Drosophila* [2] or for mammals [3,4] or even by a simple Van der Pol oscillator, as suggested in [39]. But, as it is, this cosine function takes pragmatically into account the chronomodulation of the PD by circadian factors which has been observed in experimental and clinical settings.

5.3. Possible extensions of the model

5.3.1. Perspectives for clinical applicability

The design of this model originated from the desire to improve already existing time-scheduled regimens used in chronotherapeutics, mainly for metastatic colorectal cancer. But the present identification of its parameters in a population of mice, especially those related to untreated tumor progression, is not easily transposable to the clinic for evident ethical reasons. Yet if we want to apply chronotherapeutic optimization procedures outlined in this paper in clinical settings, we need to evaluate for a given cancer in a given patient the parameters of tumor growth dynamics and of drug response.

In particular, in order to give confidence intervals for the results of therapeutics optimized with the help of this model, a linear sensitivity analysis of the space of its parameters clearly remains to be done, and this will be accomplished in a future and extended version of this work. Nonetheless, individual patient tailoring of therapeutics involves developing for this model *population PK and PD* parameter evaluation methods which will require a better understanding of the various forms of tumor growth, relying on mathematical modeling and the analysis of in vitro, experimental and clinical data.

This presented model is thus intended to serve as an introductory example to the use of a general method for therapeutic optimization. Further modeling work is yet required to take

into account the accumulating knowledge of tumor growth dynamics and to apply this model in the everyday treatment of cancer patients, which uses combinations of different cytotoxic drugs.

5.3.2. Toxicities

Other toxicities need to be considered. In the perspective of future applications to medicine, it must be stated that oxaliplatin toxicity in human beings consists of peripheral sensory neuropathy, diarrhea and vomiting (taken here into account by jejunal toxicity), and hematological suppression [14].

Neurotoxicity is usually reversible in humans. As mentioned earlier, when it does not manifest itself as an acute symptom, such as laryngeal spasm which imposes immediate cessation of the treatment (this is normally avoided by averting high instantaneous drug concentration flows). it is a chronic toxicity, dependent on the total delivered dose, which imposes in clinical settings only a minimum recovery time between courses of chemotherapy. The prevention of acute neuropathy is taken into account in the model by imposing an upper limit to the drug infusion flow and its first derivative with respect to time.

In the perspective of clinical applications, hematotoxicity is not an issue in colorectal cancer *chronotherapeutics* by oxaliplatin and 5FU; whereas, intestinal toxicity is. For instance, it has been shown that in a pilot clinical trial [40] of oxaliplatin and 5-Fluorouracil (5FU) in patients with colorectal cancer, comparing chronotherapeutic time-scheduled regimen with the more widely used FOLFOX2 protocol, fewer episodes of neutropenia and more numerous episodes of diarrhea occurred in the chronotherapy arm.

It is clear that the future inclusion of other cytotoxic drugs in model therapeutics will imply considering the representation in the model of other such toxicities.

5.3.3. Molecular pharmacology modeling to explain drug synergies

Some future extensions of this model will be necessary to actually help oncologists, such as representation of several drugs acting in the same chemotherapy course (for instance oxaliplatin, 5FU and folinic acid, as currently used in combination for the treatment of human colorectal cancer). To account for synergies between drugs and their optimization, as much as possible such PD modeling should be led at the molecular level within a model of the cell cycle. For instance, oxaliplatin action should be represented by the damage it exerts directly on DNA as a function of its intracellular concentration; whereas, the PD of 5FU should be represented by its action on thymidylate synthase during the S phase of the cell cycle. The resulting cell kill in fast renewing tissues will then be due to phase transition blocking and apoptosis induction, in particular, by the protein p53. Models which partly take into account cell cycle dynamics of tumor growth and therapy already exist [41–43], but considerable work remains to be done to represent multidrug-induced modifications at the molecular level in a model that will be useable by oncologists in the clinic.

5.3.4. Drug resistance and other problems not considered here

Other options include representation of a tumor drug resistant cell population as an independent dynamic variable, as in [44,45] with possible dependence of the probability of transition to resistance on the drug dose level, genetic polymorphism in the response to cytotoxic drugs (this may be done more easily in molecular PK–PD models), and all other issues linked to metabolic and tissue environmental factors such as tumor angiogenesis, local and remote invasion, some of which are representable by reaction–diffusion equations for tumor growth and therapy, as in [26,27]. These manifestations of cancer growth may also be included as targets for anticancer therapy, i.e., included in an objective function to be optimized; whereas, emerging resistance linked to high drug doses provides a supplementary constraint comparable to clinical tolerability in healthy tissues. These complementary problems can thus be taken into account as objective functions and constraints for optimization methods in extended versions of the model without changing the principle of balancing therapeutic efficacy and unwanted adverse medication effects.

Acknowledgments

I am gratefully indebted to Michael Smolensky who did not spare his time in helping to revise the manuscript.

Appendix A. Parameter identification procedures

A.1. Enterocyte model

As mentioned in the text, tissue homeostasis (conservation of the cell population number, at least in the mean, i.e., averaged over 24 h and thus independent of circadian factors) of the jejunal mucosa may be represented by an equilibrium point of a dynamic system. Since convergence towards equilibrium is experimentally obtained with damped oscillations, the model should be of dimension 2 at least, but dimension 2 is also sufficient to design a linear oscillating model. Besides, assuming hyperbolicity of the equilibrium point, the Hartman–Grobman theorem allows us to replace, in a neighborhood of the equilibrium, the unknown system, one output of which is the villi cell number, by its linear tangent system (see for example Perko [34]).

To justify the particular form adopted for this linear system, first consider that the villi population is not submitted to a renewal process from itself, so $\frac{dA}{dt}$ is not dependent on A; besides, the factor 1 between $\frac{dA}{dt}$ and $Z - Z_{eq}$ is justified by the fact that eliminated villi cells may be reasonably assumed to be compensated one for one by the flow of young cells from the crypts. In this respect, Z_{eq} is clearly the mean rate of mature cells which are eliminated in the intestinal lumen: 1400/day for a villus of 3500 cells, according to [21], hence the number of approximately 16500 cells per time unit (=1 h) and for an equilibrium villi population of (arbitrarily) 10^6 cells.

Second, the estimation of the coefficients on the second line $\left(\frac{dZ}{dt}\right)$ comes from 3 equations:

a. The equation giving the dampening coefficient over one period (T):

$$s = \exp\left(-\frac{\alpha}{2}T\right)$$

since $-\frac{\alpha}{2}$ is the real part of the eigenvalues of the linear system, the characteristic polynomial of which is $\lambda^2 + \alpha\lambda + \beta$ (and $s=\frac{1}{3}$ after estimation based on literature data [22]).

b. The equation giving the period of oscillations: $T = \frac{2\pi}{\omega}$, where ω is the imaginary part of the complex eigenvalues of the linear system, i.e.

$$\omega = \sqrt{\beta - \frac{\alpha^2}{4}}$$

(T=6 days after estimation based on published data[22]).

c. The equilibrium equation

$$\alpha Z_{\mathrm{eq}} + \beta A_{\mathrm{eq}} = \gamma.$$

Hence the values of α, β, γ

$$\alpha = -2\frac{\ln s}{T},\ \beta = \frac{4\pi^2 + (\ln s)^2}{T^2},\ \gamma = \alpha Z_{\mathrm{eq}} + \beta A_{\mathrm{eq}}$$

A.2. Gompertz model for tumor growth without treatment

In principle, as the Gompertz model is without treatment linear in $W=\ln B$: $\frac{dW}{dt} = a(W_{\max} - W)$, it should be possible to obtain the slope $-a$ and intercept $aW_{\max}$ by linear interpolation on a data set $\left(\ln B(t_i),\ \frac{\ln B(t_{i+1}) - \ln B(t_i)}{B(t_i)(t_{i+1}-t_i)}\right)$. But such an identification procedure requires points rather close to one another on the S-shaped curve, which was not the case in our laboratory data set that showed only three points per week.

So we used another procedure, eliminating the unreachable value $B_{\max}$, based on the equation $\frac{dW}{dt} = a(W_{\max} - W)$: since

$$W_{\max} - W(t) = \mathrm{e}^{-a(t-t_0)}(W_{\max} - W(t_0))$$

i.e. for all i

$$\ln B_{\max} - \ln B(t_i) = \mathrm{e}^{-a(t_i-t_0)} \ln \frac{B_{\max}}{B(t_0)}$$

$$\ln B_{\max} - \ln B(t_{i+1}) = \mathrm{e}^{-a(t_{i+1}-t_0)} \ln \frac{B_{\max}}{B(t_0)}$$

whence

$$\frac{\ln B(t_{i+2}) - \ln B(t_i)}{\ln B(t_{i+1}) - \ln B(t_i)} = \frac{\mathrm{e}^{-a(t_{i+2}-t_0)} - \mathrm{e}^{-a(t_i-t_0)}}{\mathrm{e}^{-a(t_{i+1}-t_0)} - \mathrm{e}^{-a(t_i-t_0)}}.$$

Given three consecutive times t_i, t_{i+1}, t_{i+2}, the first member is known, and the second is a rational fraction in $X=\mathrm{e}^{-24a}$, since any t_i is of the form t_0+24k_i, $k_i \in \mathbb{N}$. This gives a polynomial equation in X, which has always one root strictly between 0 and 1, the natural logarithm of which is identified as $-24a$. For this procedure to be efficient, it is necessary to choose three points in the middle part of the evolution curve, not too close to its beginning, where $\ln B(t)$ is almost constant, and not too far, where other phenomena, e.g., linked to neoangiogenesis, may complicate the picture. This usually left hardly more than three points in our laboratory data set, e.g., measures at days 8, 9 and 12 on untreated animals, or days 16, 19 and 21 on treated animals.

We estimated $G = a\ln\frac{B_{\max}}{B(t_0)} = \frac{dB(t_1)}{B(t)dt}\big|_{t=t_0}$ by $\frac{B(t_1)-B(t_0)}{B(t_0)(t_1-t_0)}$ i.e., on the initial part of the curve, where $B(t_1)-B(t_0)$ is small, but non-zero, whence the determination of $B_{\max}=B(t_0).\mathrm{e}^{G/a}$. These primary estimations were then used as initial values for curve fitting algorithms, by using a least mean square procedure on each individual animal tumor growth evolution curve.

Only one pair of values (a=0.015, $B_{\max}=5.3\times B(t_0)$) was retained for further simulations and optimization procedures. These values correspond to a concave growth curve, since for parameter estimations we have focused on the fast growing part of each curve.

It means that we have in fact simulated an efficient treatment beginning at an advanced stage of tumor growth.

A.3. Pharmacodynamics

As mentioned above, the jejunal toxicity function ($f(C)$) could not be identified, and was arbitrarily set as yielding likely curves for the enterocyte population, with levels not under 10% of the equilibrium value for the drug doses in use at our laboratory. In the absence of data on the subject, for instance, 40% of villi population depletion was set to represent moderate toxicity, and 60% severe toxicity.

For the anti-tumor therapeutic efficacy function ($g(D)$), tumor size evolution curves under treatment were available. Animals which had previously been synchronized to an environmental regimen of 12 h of light alternating with 12 h of darkness and had received subcutaneous inoculation of Glasgow Osteosarcoma cells were treated with the same daily dose of oxaliplatin, according to a procedure described in [11] (where one can find that another daily dose of 5.25 mg/kg/d was also used, confirming the optimality of the 15 HALO injection phase). The treatment consisted of a bolus of 4 mg of oxaliplatin injected in the retroorbital venous sinus on four consecutive days with different groups of animals each one being treated consistently at one of six different HALO time points (each differing by 4 HALO from another). We could then compute the dynamics of the oxaliplatin concentration and therapeutic effect based on our model, as a function of its maximal value $2H$ (D_{T50} and γ_T being fixed respectively as 10 and 1, to obtain $g(D)\approx\frac{H}{D_{T50}}D$ for current levels of variable D, a quasi-linear behavior), and compare these calculations with the experimental curves. We started from the linear relation

$$\frac{dW}{dt} = -aW + aW_{\max} - g(D)$$

where $W=\ln B$; on integration, this becomes:

$$W(t) = W_{\max} + e^{at}(W_0 - W_{\max}) - e^{-at}\int_0^t \frac{HD(u)e^{au}}{D_{T50}+D(u)}\left\{1+\cos 2\pi\frac{(u-\varphi_T)}{24}\right\}du$$

whence

$$H = \frac{e^{at}\ln\frac{B_{\max}}{B(t)} - \ln\frac{B_{\max}}{B_0}}{\int_0^t \frac{e^{au}D(u)}{D_{T50}+D(u)}\left\{1+\cos 2\pi\frac{(u-\varphi_T)}{24}\right\}du}.$$

The integral was evaluated between time 0, representing the time of the last bolus of a series of four injections, on days 5, 6, 7 and 8 after tumor inoculation (the tumor being palpable on day 5), and other subsequent times, evenly spaced by multiples of 24 h. For instance, with $t=0$ corresponding to the last injection on day 8, time t for the upper bound of the integral was 13×24 h, corresponding to a measure on day 21, at the same given HALO.

Each bolus was injected at the same HALO for the same animal, and consisted of a unique dose (per day) of 4 mg/kg oxaliplatin (60 μg of free platinum for a 30 g mouse). Each bolus was taken as an initial condition $P_0=60$ μg, for the first equation, whence $D(t)$ (drug concentration in the tumor):

$$D(t) = \frac{P_0}{\lambda}\left(1+e^{-24v}+e^{-48v}+e^{-72v}\right)e^{-vt}.$$

In order to assess comparable data, we evaluated a and $B_{\max}$ on the same mouse chosen for the evaluation of H, but at the end of the tumor size curve, when drug concentration in the tumor was almost zero. As stated earlier, there were so large inter-individual differences in the evaluation of the Gompertz parameters G and $B_{\max}$ that we preferred this procedure, specifically for the evaluation of parameter H, rather than evaluating G and $B_{\max}$ on curves without treatment for other mice.

Based on these computations for the evaluation of H on different mice subject to oxaliplatin injections, we eventually used an H value of 2, which allowed us to qualitatively compare treatments in an effective way in model simulations.

The time difference $\Delta\varphi$ of approximately 6 h between the phase φ_T of maximal therapeutic effect and the optimal peak infusion phase φ_I (for a bolus, beginning and peak times are the same) may be obtained as follows.

Suppose a bolus of drug is injected at $t=0$, giving rise to an initial concentration P_0. Then by straightforward integration, plasma concentration will be $P(t)=P_0e^{-\lambda t}$ and tissue concentration, $D(t)=P_0=\frac{e^{-vt}-e^{-\lambda t}}{\lambda-v}\approx\frac{P_0}{\lambda}e^{-vt}$, since $v\ll\lambda$.

Replacing the pharmacodynamic function (with $\gamma_T=1$): $g(D)=H\frac{D}{D_{T50}+D}\left\{1+\cos\frac{2\pi}{24}(t-\varphi_T)\right\}$ by a linear approximation in D, $g(D)=H_0D\left\{1+\cos\frac{2\pi}{24}(t-\varphi_T)\right\}$, we have $g(D(t))=H_0\frac{P_0}{\lambda}e^{-vt}\left\{1+\cos\frac{2\pi}{24}(t-\varphi_T)\right\}$.

On integration between 0 and 24 h of the equation

$$\frac{d}{dt}\ln(B/B_{\max}) = \frac{dB}{Bdt} = -a.\ln(B/B_{\max}) - g(D)$$

we obtain

$$\ln(B(24)/B_{\max}) = \ln(B(0)/B_{\max})e^{-24a} - e^{-24a}\int_0^{24} H_0\frac{P_0}{\lambda}e^{(a-v)t} \times\left\{1+\cos\frac{2\pi}{24}(t-\varphi_T)\right\}dt$$

and we want to know for which value of φ_T this last integral takes its maximum: this value of φ_T will be the delay between the optimal injection time (known from experimental observations, here assumed to be zero) and the tissue optimal anti-tumor efficacy time φ_T. This maximum will be obtained when its derivative with respect to φ_T is zero, i.e., when

$$\int_0^{24} e^{(a-v)t}\left\{\sin\frac{2\pi}{24}(t-\varphi_T)\right\}dt = 0$$

which by simple computation is the case if and only if

$$(a-v)\sin\frac{2\pi}{12}\varphi_T + \frac{\pi}{12}\cos\frac{\pi}{12}\varphi_T = 0$$

leading to

$$\varphi_T = \frac{12}{\pi}\ \text{Arc tan}\ \frac{\pi}{12(v-a)}$$

with $v=0.03$ and $a=0.015$, this value is approximately 5.78 h, for which value of φ_T the second derivative

$$-\frac{2\pi}{24}\int_0^{24} e^{(a-v)t}\left\{\cos\frac{2\pi}{24}(t-\varphi_T)\right\}dt$$

of the integral with respect to φ_T is easily seen to be negative, showing that the integral actually reaches a maximum for this value of φ_T. Hence if the optimal injection time has been approximately determined as 15 HALO, then this means that $\varphi_T\approx 21$ HALO.

Acknowlegments

I am gratefully indebted to Michael Smolensky who did not spare his time in helping to revise the manuscript.

References

[1] A. Goldbeter, A model for circadian oscillations in the *Drosophila* period protein (PER), Proc. R. Soc. Lond. B 261 (1995) 319–324.
[2] A. Goldbeter, Computational approaches to cellular rhythms, Nature 420 (2002) 238–245.
[3] J.-C. Leloup, A. Goldbeter, Toward a detailed computational model of the mammalian circadian clock, Proc. Nat. Acad. Sci. 100 (12) (2003) 7051–7056.
[4] L. Fu, H. Pelicano, J. Liu, P. Huang, C.C. Lee, The circadian gene Period2 plays an important role in tumor suppression and DNA damage response in vivo, Cell 111 (2002) 41–50.
[5] M. Rosbash, J. Takahashi, The cancer connection, Nature 420 (2002) 373–374.
[6] L. Fu, C.C. Lee, The circadian clock: pacemaker and tumor suppressor, Nature Reviews 3 (2003) 351–361.
[7] F. Lévi, Cancer chronotherapeutics, Special Issue of Chronobiology International, 19 (1), 2002.

[8] B. Hecquet, Modélisation pour une chronopharmacologie, Pathologie-Biologie 35 (6) (1986) 937–941.
[9] J. Clairambault, D. Claude, E. Filipski, T. Granda, F. Lévi, Toxicité et efficacité antitumorale de l'oxaliplatine sur l'ostéosarcome de Glasgow induit chez la souris: un modèle mathématique, Pathologie-Biologie 51 (2003) 212–215.
[10] F. Lévi, B. Perpoint, et al., Oxaliplatin activity against metastatic colorectal cancer. A phase II study of 5-day continuous venous infusion at circadian rhythm modulated rate, Eur. J. Cancer 29A (9) (1993) 1280–1284.
[11] T.G. Granda, R.M. D'Attino, E. Filipski, et al., Circadian optimization of irinotecan and oxaliplatin efficacy in mice with Glasgow osteosarcoma, Brit. J. Cancer 86 (2002) 999–1005.
[12] N.A. Boughattas, F. Lévi, et al., Circadian rhythm in toxicities and tissue uptake of 1,2-diamminocyclohexane(*trans*-1)oxaloplatinum(II) in mice, Cancer Research 49 (1989) 3362–3368.
[13] C. Haurie, D.C. Dale, M.C. Mackey, Cyclical neutropenia and other hematological disorders: a review of mechanisms and mathematical models, Blood 92 (8) (1998) 2629–2640.
[14] F. Lévi, G. Metzger, C. Massari, G. Milano, Oxaliplatin: pharmacokinetics and chronopharmacological aspects, Clin. Pharmacokinet. 38 (2000) 1–21.
[15] S. Faivre, D. Chan, R. Salinas, B. Woynarowska, J.M. Woynarowski, DNA strand breaks and apoptosis induced by oxaliplatin in cancer cells, Biochemical pharmacology 66 (2003) 225–237.
[16] S.G. Chaney, S.L. Campbell, E. Bassett, Y.B. Wu, Recognition and processing of cisplatin-and oxaliplatin-DNA adducts, Clin. Rev. Oncol. Hematol. 53 (2005) 3–11.
[17] D.M. Kweekel, H. Gelderblom, H.-J. Guchelaar, Pharmacology of oxaliplatin and the use of pharmacogenomics to individualize therapy, Canc. Treatment Rev. 31 (2005) 90–105.
[18] D. Wang, S.L. Lippard, Cellular processing of platinum anticancer drugs, Nature Rev. Drug Discovery 4 (2005) 307–320.
[19] M. Mishima, G. Samimi, A. Kondo, X. Lin, S.B. Howell, The cellular pharmacology of oxaliplatin resistance, Eur. J. Cancer 38 (2002) 1405–1412.
[20] N.A. Boughattas, B. Hecquet, C. Fournier, B. Bruguerolle, A. Trabelsi, K. Bouzouita, B. Omrane, F. Lévi, Comparative pharmacokinetics of oxaliplatin (L-OHP) and carboplatin (CBDCA) in mice with reference to circadian dosing time, Biopharm Drug Dispos. 15 (1994) 761–773.
[21] C.S. Potten, M. Loeffler, Stem cells: attributes, cycles, spirals, pitfalls and uncertainties, Lessons Crypt. Dev. 110 (1990) 1001–1020.
[22] N. Wright, M. Alison, The Biology of Epithelial Cell Populations, vol.2, Clarendon Press, Oxford, 1984, pp. 842–869, chap.23.
[23] L. Edelstein-Keshet, Mathematical Models in Biology, McGraw-Hill, New York, 1988, pp. 210–270.
[24] M. Gyllenberg, G.F. Webb, Quiescence as an explanation of Gompertzian tumor growth, Growth, Development and Aging 53 (1989) 25–33.
[25] M. Gyllenberg, G.F. Webb, A nonlinear structured population model of tumor growth with quiescence, J. Math. Biol. 28 (1990) 671–694.
[26] T.L. Jackson, H.M. Byrne, A mathematical model to study the effects of drug resistance and vasculature on the response of solid tumors to chemotherapy, Math. Biosci. 164 (2000) 17–38.
[27] J.A. Sherratt, M.A.J. Chaplain, A new mathematical model for avascular tumour growth, J. Math. Biol. 43 (2001) 291–312.
[28] P. Hahnfeldt, D. Panigrahy, J. Folkman, L. Hlatky, Tumor development under angiogenic signaling: a dynamical theory of tumor growth, treatment response, and postvascular dormancy, Cancer Research 59 (1999) 4770–4775.
[29] A. Ergun, K. Camphausen, L.M. Wein, Optimal scheduling of radiotherapy and angiogenic inhibitors, Bull. Math. Biol. 65 (2003) 407–424.
[30] J.H. Goldie, A.J. Coldman, A mathematic model for relating the drug sensitivity of tumors to their spontaneous mutation rate, Cancer Treat. Rep. 63 (1979) 1727–1733.
[31] N.F. Britton, N.A. Wright, J.D. Murray, A mathematical model for cell population kinetics in the intestine, J. Theor. Biol. 98 (1982) 531–541.
[32] X.M. Li, G. Metzger, E. Filipski, G. Lemaigre, F. Lévi, Modulation of nonprotein sulphydryl compounds rhythm with buthionine sulphoximine: relationship with oxaliplatin toxicity in mice, Arch. Toxicol. 72 (1998) 574–579.
[33] M.H. Hastings, A.B. Reddy, E.S. Maywood, A clockwork web: circadian timing in brain and periphery, in health and disease, Nat. Rev./Neurosci. 4 (2003) 649–661.
[34] L. Perko, Differential Equations and Dynamical Systems, 2nd edition, Springer, 1996, pp. 119–129.
[35] L.E. Scheving, E.R. Burns, J.E. Pauly, T.H. Tsai, Circadian variations in cell division of the mouse alimentary tract, bone marrow and corneal epithelium, Anat. Rec. 191 (1978) 479–486.
[36] A. Iliadis, D. Barbolosi, Optimising drug regimens in cancer chemotherapy by an efficacy-toxicity mathematical model, Computers Biomed. Res. 33 (2000) 211–226.
[37] A. Iliadis, D. Barbolosi, Optimising drug regimens in cancer chemotherapy: a simulation study using a PK–PD model, Computers Biol. Med. 31 (2001) 157–172.
[38] C. Basdevant, J. Clairambault, F. Lévi, Optimisation of time-scheduled regimen for anti-cancer drug infusion, Math. Model. Numer. Anal. 39 (6) (2005) 1069–1086.
[39] D.B. Forger, R.E. Kronauer, Reconciling mathematical models of biological clocks by averaging on approximate manifolds, SIAM J. Appl. Math. 62 (4) (2002) 1281–1296.
[40] F.A. Levi, N. Tubiana-Mathieu, C. Focan, C. Brézault-Bonnet, B. Coudert, C. Carvalho, D. Genet, S. Giacchetti, M.-A. Lentz, B. Baron, First line infusion of 5-fluorouracil, leucovorin and oxaliplatin for metastatic colorectal cancer: 4-day chronomodulated (FFL410) versus 2-day FOLFOX2, A Multicenter Randomized Phase III Trial of the Chronotherapy Group of the European Organization for Research and Treatment of Cancer (EORTC 05963). ASCO Meeting Abstracts, 22, 2004, p. 3526.
[41] J.C. Panetta, A mathematical model of drug resistance: heterogeneous tumors, Math. Biosci. 147 (1998) 41–61.
[42] F. Kozusko, P.H. Chen, S.G. Grant, B.W. Day, J.C. Panetta, A mathematical model of in vitro cancer cell growth and treatment with the antimitotic agent curacin A, Math. Biosci. 170 (2001) 1–16.
[43] J. Clairambault, P. Michel, B. Perthame, Circadian rhythm and tumour growth, C. R. Acad. Sci. (Paris) 342 (1) (2006) 17–22.
[44] J.C. Panetta, A mathematical model of breast and ovarian cancer treated with Paclitaxel, Math. Biosci. (1997) 89–113.
[45] J.L. Boldrini, M.I.S. Costa, Therapy burden, drug resistance, and optimal treatment regimen for cancer therapy, IMA J. Math. Appl. Med. Biol. 17 (2000) 33–51.

J. Math. Biol.
DOI 10.1007/s00285-007-0147-x

Mathematical Biology

An age-and-cyclin-structured cell population model for healthy and tumoral tissues

Fadia Bekkal Brikci · Jean Clairambault · Benjamin Ribba · Benoît Perthame

Received: 22 August 2006 / Revised: 13 November 2007

Abstract We present a nonlinear model of the dynamics of a cell population divided into proliferative and quiescent compartments. The proliferative phase represents the complete cell cycle (G_1–S–G_2–M) of a population committed to divide at its end. The model is structured by the time spent by a cell in the proliferative phase, and by the amount of *Cyclin D/*(*CDK4 or 6*) complexes. Cells can transit from one compartment to the other, following transition rules which differ according to the tissue state: healthy or tumoral. The asymptotic behaviour of solutions of the nonlinear model is analysed in two cases, exhibiting tissue homeostasis or tumour exponential growth. The model is simulated and its analytic predictions are confirmed numerically.

Mathematics Subject Classification (2000) 35P05 · 92B05 · 35F20 · 92D25

1 Introduction

Living tissues, subject to renewal, are constituted of two different categories of cells: proliferating cells (p) and quiescent cells (q). Proliferating cells grow and divide, giving "birth" at the end of the cell cycle to new cells, or else transit to the quiescent compartment (often referred to as the G_0 phase), whereas quiescent cells do not grow nor divide but either transit to the proliferative compartment or else stay in G_0 and eventually differentiate according to the tissue type.

F. Bekkal Brikci · J. Clairambault (✉) · B. Perthame
Projet BANG, UR Rocquencourt, Institut de Recherche en Informatique et en Automatique,
BP 105, Le Chesnay Cedex 78150, France
e-mail: jean.clairambault@inria.fr

B. Ribba
Institute for Theoretical Medicine, Clinical Pharmacology Department EA3736,
Faculty of Medecine RTH Laennec, University Lyon 1, Paradin st, 69376 Lyon Cedex 08, France

In a tumour cell population the number of proliferating cells increases continuously as long as it is malignant and active, whereas in a normal (healthy) cell population, the size of the proliferative compartment remains bounded since the total number of cells, proliferating and quiescent, remains constant (at least in the mean, e.g. by averaging over 24 h) so as to maintain tissue homeostasis.

During the first phase (often referred to as G_1) of the proliferation cell cycle, until the restriction point (R) in late G_1 has been reached, proliferating cells may enter the quiescent G_0 phase and stop proliferation. Indeed, experiments by Zetterberg and Larsson [12,44] showed that the restriction point (R) divides the G_1 phase into two parts: before R, cells may enter the quiescent phase, but once it has been passed, they are committed to proceed through the other phases (S, G_2, M, which will not be considered here as such) until cell division.

The switching of cells between quiescence and proliferation depends on extracellular environmental conditions such as growth and antigrowth factors, and is regulated differently in normal and tumour cells, due to differences in the expression of the involved genes.

The model we present in this paper belongs to the category of *physiologically structured population dynamics* (see [3,23,25,35,43] for a general approach). It relies on Partial Differential Equations structured both in age and cyclin content for cell populations. Cell population models with proliferative and quiescent compartments have been investigated by several authors (e.g., Arino, Gyllenberg, Rossa, Sanchez, Webb) who studied their asynchronous exponential growth property [4,17,18,34]. Our goal here is to design a generic cell population model applicable to both cancer and normal tissue growth.

Unlimited tumour growth, by opposition to healthy tissue homeostasis, can be seen in particular as a deregulation of transitions between proliferative and quiescent compartments. Furthermore, recent measurements [19] indicate that cyclins are the most determinant control molecules for phase transitions.

For these reasons, and since we are interested in studying in parallel the behaviour of healthy and tumour cell populations, we structure our cell population model in age and cyclin content, a process which we describe step by step in Sects. 2 and 3. In Sect. 4, we analyse the theoretical properties of the model, which we illustrate by numerical simulations in Sect. 5. Finally, some comments and future prospects are briefly developed in Sect. 6.

2 Molecular mechanisms involved in the G_1 phase

A variety of proteins are produced during the proliferative cell cycle. The progression of a cell through the cycle is controlled by complexes composed of two proteins: a cyclin (structural protein) and a cyclin dependent kinase (or CDK), an enzyme which is needed for the cyclin to activate. Each phase of the cell cycle has specific *Cyclin/CDK* complexes. In particular, *Cyclin D/*(*CDK4 or 6*) and *Cyclin E/CDK2* activate during the G_1 phase. Cyclin D is the first cyclin which is synthesized at the beginning of the cell cycle. The level of Cyclin D is controlled by the extracellular environment.

Thus, Cyclin D synthesis is induced by specific growth factors (GFs) [6], and its level decays when cells are deprived of GFs. GFs bind to specific receptors on the external

cytoplasmic membrane, stimulating an intracellular signalling pathway (*Ras/Raf/Map kinase*) by means of which Cyclin D is eventually synthesized (see [2,5,37], for more details). Experiments reported in [20,39,45] show the important role of Cyclin D as a regulator of the transition between G_1 and G_0. They show that a reduced exit from G_1 to G_0 occurs when Cyclin D is overexpressed, whereas non-overexpressing cells remain in G_0. Progression through the restriction point (R) is essentially related to Cyclin D level in as much as when there is a sufficient amount of Cyclin D, cells pass the restriction point and are committed to proceed through the rest of the cell cycle.

The passage through the restriction point is also dependent on the cyclin dependent kinase inhibitor *p27(Kip1)* concentrations, since it has been shown [21] that the intracellular levels of *p27(Kip1)* are strongly and negatively correlated to the probability for a cell to pass through the restriction point.

Moreover, Cyclin D makes complexes with either CDK4 or CDK6 kinases and these complexes are able to phosphorylate other proteins which are important for cell progression in the G_1 phase through the restriction point and further for the rest of the cell division cycle: DNA replication, mitosis and cell division [38,39]. It is also known (see e.g. [31] and articles cited therein) that an important role of the *Cyclin D/(CDK4 or 6)* complexes is to bind to p27 and thus fight its inhibitory activity in the passage of cells through the restriction point. This mechanism naturally relates, in a competing manner, *Cyclin D/(CDK4 or 6)* to *p27(Kip1)* concentrations, so that the balance between *Cyclin D/(CDK4 or 6)* and *p27(Kip1)* concentrations may be seen as a reliable marker of the cells that have passed this restriction point.

In this paper, we are interested in the molecular interactions that are related to the activity of the *Cyclin D/(CDK4 or 6)* complexes *in fast renewing cell populations* (not in individual cells as such). In the same way, the molecular concentrations we use must be understood only as averaged concentrations in the subpopulations considered (quiescent or proliferating), without regard of between cell variability or molecular density distribution within these subpopulations.

Several authors [29,30,32,41] have described and simulated, under specific assumptions, part of the complex molecular reactions involved. Here, we give a simple model to describe the activity of a lumped variable representing the activity of *Cyclin D/(CDK4 or 6)* induced by growth factors, which is known to balance the *p27(Kip1)* CDK inhibitor. This switch-like dynamics models the irreversible passage through the restriction point, and it has been also represented in a comparable way by other authors who used models with more variables ([29,41] and other references therein). In fact, it may be shown (material not presented here) that the complex molecular dynamics of *Cyclin D/(CDK 4 OR6)* linking to p27, as modelled e.g. in [29], may be seen to yield a variable such as $[Total\ Cyclin\ D]/[Unbounded\ Kip1]$, representing a balance between active Cyclin D and p27, that shows a time dynamics very close to that of the lumped variable x we will describe now. It must be stressed that we use it only as a variable leading the passage of a cell population through the restriction point, which is essential in modelling the exchanges between proliferative and quiescent phases. It is also clear that we would have to be more specific in the design of another Cyclin D model if we wanted to include these G_0 to G_1 exchanges in a detailed model of the cell cycle with phases G_1, S, G_2 and M, as presented elsewhere [11].

For its present use in this simplified cell population model of the exchanges between a proliferative and a quiescent compartments, described by a reduced set of equations, we consider it as physiologically plausible enough and sufficient for our needs.

Let x be the amount of complexes *Cyclin D/(CDK4 or 6)* (or the ratio of concentrations [*Cyclin D/(CDK4 or 6)*]/[*Free p27*], if one is to take the inhibitory role of p27 into account) in the cell populations considered, and w another aggregated variable representing the amount of the various molecules (*Ras/Raf/. . .MAPK*) involved in the production of active Cyclin D. We assume that the stimulation of active Cyclin D production by the aforementioned complex signalling pathways (Ras/Raf/MAPK), that are triggered upstream by growth factors, involves a limited positive feedback from Cyclin D itself, in as much as these growth factors (w) are supposed to impinge directly, but in a saturable manner as stated earlier, our lumped variable x, which may be seen to represent more Cyclin D itself.

We consider x and w as regulating variables in a simple nonlinear system of ordinary differential equations (ODEs) with respect to age a in the G_1 phase. We assume in this system an infinite reservoir, with constant production rate, of w, only dependent on upstream growth factors, and no (or negligible) consumption by x (Cyclin D), i.e., no feedback from x, and participation, in a limited way, of Cyclin D itself in its synthesis, which is triggered by variable w. Clearly, a simple bilinear equation (e.g. $\dot{x} = awx - bx$, $\dot{w} = c - dw$) to represent this positive feedback of Cyclin D by a law of mass action in its production is not relevant and must be excluded, since solution x would burst exponentially, as shown by straightforward computation. We thus hypothesize Michaelis–Menten-like dynamics of the lumped variable x for the contribution of Cyclin D in its synthesis triggered by the aggregated variable w, replacing awx by $\frac{awx}{1+x}$ in the first equation. A simple ODE model with these features can thus be written as follows:

$$\begin{cases} \frac{dx}{da} = c_1 \frac{x}{1+x} w - c_2 x, \quad x(0) = x_0 > 0, \\ \frac{dw}{da} = c_3 - c_4 w, \quad w(0) = w_0 > 0. \end{cases} \tag{1}$$

The saturable influence of x in its production is the only nonlinear part in this system and it is this term which yields its switch-like dynamics: S-shaped monotone convergence from low initial values to a plateau. The coefficient c_2 is the linear degradation rate of Cyclin D, c_3 is the constant production rate of the lumped variable w, and c_4 is a coefficient describing its linear degradation rate. All coefficients $c_i (1 \leq i \leq 4)$ are strictly positive. Substituting the solution of the second equation of (1), we can reduce (1) to one equation in x:

$$\frac{dx}{da} = c_1 \frac{x}{1+x} \left(\frac{c_3}{c_4} + e^{-c_4 a} \left(w_0 - \frac{c_3}{c_4} \right) \right) - c_2 x, \quad x(0) = x_0. \tag{2}$$

This holds only for the G_1 phase since we assume that cyclin amount x and age a remain constant in G_0 phase. A natural quantity arises in the qualitative analysis of (2), the x -nullcline:

$$X(a) = \frac{c_1}{c_2}\left(\frac{c_3}{c_4} + e^{-c_4 a}\left(w_0 - \frac{c_3}{c_4}\right)\right) - 1.$$

We assume that $w_0 \leq \frac{c_3}{c_4}$ and $c_1 c_3 > c_2 c_4$ which is a way to express that the lumped variable w is increasing from its initial to its asymptotic value, and that in the early G_1 phase the overall synthesis of the chemicals involved in the progression of the G_1 phase overcomes their degradation. Therefore, a fundamental property of Eq. (2) is that the cyclin concentration x is limited by:

$$x_{\max} = \frac{c_1 c_3}{c_2 c_4} - 1 > 0. \tag{3}$$

We keep this simple model for our next purpose which is to describe a population of cells, in proliferative or quiescent state.

3 Physiologically structured model

In the cell population model we will now present, we consider only two phases: a quiescent one (physiologically G_0) and a proliferative one (physiologically G_1–S–G_2–M). The cell populations we study are firstly structured by the time spent inside the proliferative phase. This phase represents the complete cell division cycle since cell birth, and time in the phase will hereafter be referred to as a, for physiological age in the cycle. As proposed in [7,42], we also structure the model by the amount of (active, not bound to *p27*) *cyclin D/*(*CDK4 or 6*) complexes, denoted by variable x. Indeed, as mentioned earlier, this biological quantity is the most important determinant of progression up to the restriction point R in the late G_1 phase.

Let $p\,(t, a, x)$and $q\,(t, a, x)$ be respectively the densities of proliferating and quiescent cells with age a and content x in *Cyclin D/*(*CDK4 or 6*) complexes at time t. We also consider a "total weighted population", i.e., an effective population density, N defined by

$$N\,(t) = \int_0^{+\infty}\int_0^{+\infty}\left(\varphi^*(a, x)p\,(t, a, x) + \psi^*(a, x)q\,(t, a, x)\right)da\,dx. \tag{4}$$

Here the weights φ^* and ψ^* represent environmental factors such as growth and anti-growth factors acting on the populations of proliferating and quiescent cells, respectively. N is the density of the fraction of the total population consisting in the cells that are sensitive to these factors and are thus qualified to influence, for example by a mechanism related to density inhibition, the G_0/G_1 transition. This excludes for instance apoptotic or pre-apoptotic cells.

Exits from the quiescent compartment are due either to apoptosis (physiological cell death) at a nonnegative rate d or to transition to the proliferative phase according to a "recruitment" or "getting in the cycle" function G, which is assumed to depend on the total weighted population N. We also assume that cells may leave the proliferative compartment for the quiescent one according to a "demobilisation" or "leak" function

$L(a,x)$. These functions L and G, which represent the core mechanism of exchange from proliferation to quiescence and vice-versa, respectively, in our model, will be described in Sect. 3.2. Quiescent cells are assumed to be halted in their individual physiological evolution, in the sense that once a cell becomes quiescent, its age and cyclin content are fixed at their last values as belonging to a proliferative cell. In this way, quiescent cells do not age and do not change their cyclin content.

The model, the coefficients of which, unless otherwise specified, will always be strictly postive, may be written as

$$\begin{cases} \frac{\partial}{\partial t} p(t,a,x) + \frac{\partial}{\partial a}\left(\Gamma_0 p(t,a,x)\right) + \frac{\partial}{\partial x}\left(\Gamma_1(a,x)\, p(t,a,x)\right) \\ \quad = -\left(L(a,x) + F(a,x) + d_1\right) p(t,a,x) + G(N(t))\, q(t,a,x), \\ \frac{\partial}{\partial t} q(t,a,x) = L(a,x)\, p(t,a,x) - \left(G(N(t)) + d_2\right) q(t,a,x). \end{cases} \tag{5}$$

The parameter Γ_0 denotes the evolution speed of physiological age a with respect to time t, which is assumed to be constant in this model; if for example $\Gamma_0 = 0.5$, it means that physiological age a evolves twice as slowly as real time t. Similarly, the function Γ_1 represents the evolution speed of *Cyclin D/*(*CDK4 or 6*) with respect to time, i.e., Γ_0 times the speed $\frac{dx}{da}$ of x with respect to physiological age a, which is given by Eq. (2), with $w_1 = w_0 - \frac{c_3}{c_4} < 0$:

$$\frac{dx}{da} = \frac{\Gamma_1(a,x)}{\Gamma_0} = c_1 \frac{x}{1+x}\left(\frac{c_3}{c_4} + e^{-c_4 a} w_1\right) - c_2 x.$$

The parameters d_1, d_2 are apoptosis rates for proliferating and quiescent cells respectively, and $F(a,x)$ is the fraction of cells which leave the proliferative population to divide according to a process which will be described later.

To complete the description of the model (5), we specify initial conditions:

$$p(0,a,x) = p_i(a,x), \quad a \geq 0, \ x \geq 0, \tag{6}$$

and

$$q(0,a,x) = q_i(a,x), \quad a \geq 0, \ x \geq 0, \tag{7}$$

where p_i and q_i are nonnegative functions.

In the following section, we describe a condition for entering the proliferative phase (physiologically in G_1) at age $a = 0$, but note that no such condition is needed at $x = 0$, since cyclin level $x = 0$ is never reached in the process described by (2) because Γ_1 vanishes at $x = 0$.

3.1 Unequal division

The distribution of the cellular material between daughter cells is assumed to be unequal. Due to variability in cyclin content between the two daughter cells when division occurs (see [22,40] for a relation with aging), some cells may inherit a larger amount of certain proteins such as cyclins, whereas others start the cycle with a smaller

amount of the same proteins. We consider that the distribution of the amount of *cyclin D/(CDK4 or 6)* between the two daughter cells is given by a conditional density $f\,(a, x, y)$ such that the probability for a daughter cell, born from a mother cell with content y in *Cyclin D/(CDK4 or 6)* with $x_1 \leq y \leq x_2$, to have itself content x in *Cyclin D* is

$$\frac{\int_{x_1}^{x_2} f\,(a, y, x)\,dy}{\int_0^{+\infty} f\,(a, y, x)\,dy}.$$

We also consider that all newborn cells are at birth in the proliferative compartment. Then we have the following condition at the boundary $a = 0$,

$$p\,(t, 0, x) = \frac{2}{\Gamma_0} \int_0^{+\infty} \int_0^{+\infty} f\,(a, x, y)\; p\,(t, a, y)\,da\,dy. \tag{8}$$

The following conditions follow from the earlier interpretation:

(1) The amount of cyclin in a daughter cell is smaller than that of its mother cell at the time of division:

$$f(a, x, y) = 0 \quad \text{if } x > y.$$

(2) The amount y of cyclin of the mother cell is exactly conserved and shared by the two daughters

$$f(a, x, y) = f(a, y - x, y)$$

and

$$\int_0^{+\infty} f(a, x, y)dx = F\,(a, y)\,,$$

where $F(a, y)$ is the fraction of cells which at age a and cyclin content y leave the proliferative phase to undergo cell division. These cells disappear and are replaced by two daughter cells which immediately restart in the proliferative phase for their own part.

We choose for F a standard Hill function:

$$F\,(a, y) = \frac{k_1 y^{\gamma_1}}{k_2^{\gamma_1} + y^{\gamma_1}} \mathbb{1}_{[A^*, +\infty[}(a),$$

where $\mathbb{1}_J$ is the indicator function of interval J (i.e., $\mathbb{1}_J(x) = 1$ if $x \in J$, else 0), k_1 is the maximum effect of Cyclin D on cell division, k_2 is the cyclin content yielding its half-maximum effect, γ_1 is the Hill coefficient tuning the steepness of the switch

at $y = k_2$ between 0 and k_1 for the effect, and A^* is the minimal cell cycle duration; we also consider that cyclin repartition is uniform after division:

$$f(a, x, y) = \frac{F(a, y)}{y} \mathbb{1}_{[0,y]}(x).$$

3.2 Transition control between proliferation and quiescence

Lynch et al. [24] have studied the effect of a transcription factor that inhibits the proliferation of human colon cancer cells by reducing Cyclin D gene expression and hence inducing an accumulation of cells in G_0. Deprivation of growth factors (GFs) in the early G_1 phase also leads to a low Cyclin D level in cells, when *Cyclin D/CDK4* is the only Cyclin/CDK complex present, and the low level of Cyclin D is such that cells exit G_1 to enter the G_0 phase.

We firstly assume that transition from proliferation to quiescence depends on age and cyclin content of the cell. At the beginning of the cell cycle, the cell remains in the proliferative phase but from a certain age on, if its content in *Cyclin D/*(*CDK4 or 6*) is not high enough, the cell passes to the quiescent phase.

We set the "demobilisation" function from proliferation to quiescence as:

$$L(a, x) = A_1 \frac{A_2^{\gamma_2}}{A_2^{\gamma_2} + x^{\gamma_2}} \mathbb{1}_{[\bar{A}, +\infty[}(a).$$

In this setting, if the Hill exponent γ_2 is high enough (e.g. between 5 and 10), A_2 is the "switching" cyclin content value x beyond which the "leak" function L becomes close to zero, preventing escape to quiescence. At this point, the cell population is irreversibly committed to proceed into the proliferative phase until division. The value A_2 may thus be interpreted as the *Cyclin D/*(*CDK4 or 6*) level determining the restriction point, in the sense of Zetterberg and Larsson [44]. The steep switch in function L represents the fact that transition from G_1 to G_0 is preceded by a rapid increase in physiological cyclin-dependent kinase inhibitors (CDKIs), such as *p15*, *p21*, and especially *p27*, significantly reducing the activities of the G_1 CDKs [36].

Secondly, as regards the reverse transition from quiescence to proliferation (the "recruitment" function), it may be assumed to depend on the total population of cells (see e.g. [15]). In the present model we assume, as stated above, that the recruitment depends on those cells (subpopulation N of the total population) that are "qualified" to be sensitive to growth or anti-growth factors. Two cases are studied here, since we assume healthy tissues and tumours to behave differently with respect to the transition from G_0 to G_1:

(1) For a healthy tissue, the fraction of the quiescent cells that re-enter the proliferative phase decreases when the total population grows; in this case we define the recruitment function G as a monotone Hill function of N decreasing to zero, representing density inhibition:

$$G(N) = \frac{\alpha_1 \theta^n}{\theta^n + N^n}, \tag{9}$$

where the parameters α_1, θ and n have the same meaning as k_1, k_2 and γ_1 for function $F(a, x)$, see, except that the switch is from α_1 to zero instead of zero to k_1.

(2) For a tumour, the fraction of the quiescent cells that enter the proliferative phase is also decreasing with the total population, but asymptotically tends towards a non-zero value when the population is very large, representing a population density inhibition less complete than in healthy tissues. So, in the tumoral case, we take G as follows:

$$G(N) = \frac{\alpha_1 \theta^n + \alpha_2 N^n}{\theta^n + N^n} \quad \text{with } 0 < \alpha_2 < \alpha_1 \text{ to ensure decay.} \tag{10}$$

We then analyse the qualitative behaviour of the model, which enables us to distinguish a healthy tissue from a tumour by the asymptotic behaviour of their cell densities.

4 Analysis and qualitative behaviour

We now perform the analysis of the model developed above. We use the method of Generalised Relative Entropy (GRE), which was recently introduced by Michel et al. [26–28]. It allows us to deal with the model in its full generality. The GRE method is based on the study of eigenproblems for linearised systems and relies on the Krein–Rutman theorem for compact positive operators (see [13]). The use of other methods is possible, for instance methods based on the theory of abstract semigroups with structural conditions as described below or, in special cases, reduction to differential equations with delay (see [1] for instance).

4.1 Linear problem

The linear problem associated with (5) assumes that the transition rate from the quiescent to the proliferative state is a constant $\tilde{G}$, such that:

$$\begin{cases} \frac{\partial p}{\partial t} + \frac{\partial(\Gamma_0 p)}{\partial a} + \frac{\partial(\Gamma_1(a,x)p)}{\partial x} \\ \quad = -\left(L(a,x) + F(a,x) + d_1\right) p(t,a,x) + \tilde{G} q(t,a,x), \\ \frac{\partial q}{\partial t} = L(a,x)\, p(t,a,x) - (\tilde{G} + d_2) q(t,a,x), \\ p(t,0,x) = \frac{2}{\Gamma_0} \int_0^{+\infty} \int_0^{+\infty} f(a,x,y)\, p(t,a,y) da\, dy. \end{cases} \tag{11}$$

Gyllenberg and Webb, studying a similar linear problem by methods relying on the theory of continuous semigroups, proved the existence and uniqueness of a positive solution for the system, and also proved that it has the property of asynchronous exponential growth [17] (note that this results in fact from variants of the Krein–Rutman theorem [13]). It means the following: the growth rate associated with (11)-the so-called Malthus parameter- i.e., the first eigenvalue of the problem, also referred to as the Perron eigenvalue in the finite-dimensional case, is defined as the only λ yielding a nonnegative steady state (P, Q) solution of:

$$\begin{cases} \lambda P + \frac{\partial(\Gamma_0 P)}{\partial a} + \frac{\partial(\Gamma_1(a,x)P)}{\partial x} = -\left(L\left(a,x\right) + F(a,x) + d_1\right) P + \tilde{G} Q, \\ (\lambda + \tilde{G} + d_2) Q = L\left(a,x\right) P, \\ P(0,x) = \frac{2}{\Gamma_0} \int_0^{+\infty} \int_0^{+\infty} f\left(a,x,y\right) P\left(a,y\right) da\, dy. \end{cases} \tag{12}$$

Of course this system can be reduced to a single equation on P, and λ depends continuously upon $\tilde{G}$. For an age-structured model it can be solved by the method of characteristics.

At this stage, it is also useful to introduce the adjoint system, following the theory developed in [26]. The adjoint problem reads:

$$\begin{cases} \lambda\varphi - \Gamma_0 \frac{\partial\varphi}{\partial a} - \Gamma_1\left(a,x\right) \frac{\partial\varphi}{\partial x} - 2\int_0^{+\infty} \varphi\left(0,y\right) f\left(a,y,x\right) dy \\ \quad = -\left(L\left(a,x\right) + F(a,x) + d_1\right)\varphi + L\left(a,x\right)\psi, \\ (\lambda + \tilde{G} + d_2)\psi = \tilde{G}\varphi, \end{cases} \tag{13}$$

with $\varphi \geq 0$, $\psi \geq 0$, and normalisation by the condition:

$$\int_0^{+\infty}\int_0^{+\infty} \Big(\varphi(a,x) P\left(a,x\right) + \psi(a,x) Q\left(a,x\right)\Big)\, da\, dx = 1.$$

These equations imply that solutions of (11) satisfy:

$$\begin{aligned} &\int_0^{+\infty}\int_0^{+\infty} \Big(\varphi(a,x) p\left(t,a,x\right) + \psi(a,x) q\left(t,a,x\right)\Big)\, da\, dx \\ &= e^{\lambda t} \int_0^{+\infty}\int_0^{+\infty} \Big(\varphi(a,x) p_i\left(a,x\right) + \psi(a,x) q_i\left(a,x\right)\Big)\, da\, dx\,, \end{aligned} \tag{14}$$

a condition that clearly expresses exponential growth with rate λ.

In the following, we explain why these growth rates can allow us to qualitatively distinguish between healthy and tumoral tissues. This will be done according to the behaviour of the first eigenvalue λ for the system linearised at the extreme values of the recruitment function G, $G(0) = \alpha_1$ and $G_\infty = \alpha_2$. We then present the main features of the nonlinear problem using a method introduced in [10] enforcing conditions on the linearised problem.

4.2 Healthy tissue: non-extinction (a priori bound from below)

Coming back to the nonlinear problem, we first state conditions enforcing non-extinction. For this purpose, we need to investigate the linearised problem around $N(t) = 0$ and its first eigenvalue.

We assume that the coefficients are such that the following qualitative properties hold true:

(H1) For $\tilde{G} = G(0) = \alpha_1$, the first eigenvalue, denoted here as λ_0, of system (12) and its adjoint (13), is positive ($\lambda_0 > 0$).

(H2) For the corresponding solutions to (12) and (13) obtained for $\tilde{G} = G(0)$, (p_0, q_0) and (φ_0, ψ_0), there exists a constant C_0, such as $\varphi^* \leq C_0\varphi_0$ and $\psi^* \leq C_0\psi_0$ (φ^*, ψ^* as defined in (4)).

These assumptions express that even if there are very few cells in the healthy tissue, the population can be regenerated spontaneously. Note that if we a priori assume the existence of a maximum possible age, then the positivity of φ_0 and ψ_0 implies that (H2) is automatically satisfied for any pair of bounded functions (φ^*, ψ^*).

Lemma 1 *Under hypotheses* $(H1)$ *and* $(H2)$ *there exists a number* m_0 *such that*:

$$\int_0^{+\infty}\int_0^{+\infty} \Big(\varphi_0(a,x)p(t,a,x) + \psi_0(a,x)q(t,a,x)\Big)\,da\,dx \geq m_0 > 0 \quad \forall t \geq 0.$$

Proof of Lemma 1 Indeed, setting:

$$S_0(t) = \int_0^{+\infty}\int_0^{+\infty} \Big(\varphi_0(a,x)p(t,a,x) + \psi_0(a,x)q(t,a,x)\Big)\,da\,dx,$$

and using (5) and (13), we have, by the same duality principle used for deriving (14):

$$\frac{dS_0}{dt}(t) = \lambda_0 S_0(t) - \frac{\lambda_0 + d_2}{G(0)}(G(0) - G(N(t))) \int_0^{+\infty}\int_0^{+\infty} \psi_0(a,x)q(t,a,x)da\,dx\,,$$

whence, because $p \geq 0$:

$$\frac{dS_0}{dt}(t) \geq \left(\frac{\lambda_0 + d_2}{G(0)}G(N(t)) - d_2\right) S_0(t).$$

Therefore, firstly:

$$S_0(t) \geq S_0(0)\exp\left\{\int_0^t \left(\frac{\lambda_0 + d_2}{G(0)}G(N(u)) - d_2\right) du\right\} > 0.$$

Now, if the minimum of $S_0(t)$ is attained at $t = 0$, then $S_0(t) \geq S_0(0) > 0$; otherwise it is attained at some point t_0 (possibly at infinity), where $\frac{dS_0}{dt}(t_0) = 0$, which yields:

$$G(N(t_0))\frac{\lambda_0 + d_2}{G(0)} - d_2 \leq 0,$$

or equivalently:

$$G(N(t_0)) \leq \frac{d_2}{\lambda_0 + d_2} G(0).$$

Since G is continuous and decreasing to 0, there exists a number $N_0 > 0$ such that:

$$G(N_0) = \frac{d_2}{\lambda_0 + d_2} G(0).$$

Thus $G(N(t_0)) \leq G(N_0)$, which implies that $N(t_0) \geq N_0 > 0$ and by (H2), for all $t \geq 0$, $S_0(t) \geq S_0(t_0) \geq \frac{N_0}{C_0}$. Therefore we have proved the result with

$$m_0 = \min\left(\frac{N_0}{C_0}, S_0(0)\right).$$

4.3 Healthy tissue: limited growth (a priori bound from above)

We also need conditions enforcing tissue homeostasis, meaning that the total cell population density is limited in its growth: for this purpose we assume that for some $\lambda_{\lim}$ with $-d_2 < \lambda_{\lim} < 0$ (recall that d_2 is the apoptosis rate in the quiescent phase), there exist a real number $N_{\lim} > 0$ and nonnegative functions $(\varphi_{\lim}, \psi_{\lim})$ satisfying:

(H3) For $\tilde{G} = G(N_{\lim}) = \frac{\alpha_1 \theta^n}{\theta^n + N_{\lim}^n}$, the first eigenvalue, denoted here as $\lambda_{\lim}$, of system (12) and its adjoint(13), is negative ($\lambda_{\lim} < 0$).

(H4) For the corresponding solutions to (12) and (13) obtained for $\tilde{G} = G(N_{\lim})$, $(p_{\lim}, q_{\lim})$ and $(\varphi_{\lim}, \psi_{\lim})$, there exists a constant $C_{\lim}$, such that $\varphi^* \geq C_{\lim}\varphi_{\lim}$ and $\psi^* \geq C_{\lim}\psi_{\lim}$.

These assumptions express that a large excess of cells is regulated negatively and thus the population remains bounded.

Lemma 2 *Under hypotheses* $(H3)$ *and* $(H4)$ *there is a number* $m_{\lim}$ *such that*:

$$\int_0^{+\infty}\int_0^{+\infty} (\varphi_{\lim}(a,x)p(t,a,x) + \psi_{\lim}(a,x)q(t,a,x))da\,dx \leq m_{\lim}, \quad \forall t \geq 0.$$

Proof of Lemma 2 Indeed as in the proof of Lemma 1, we define

$$S_{\lim}(t) = \int_0^{+\infty}\int_0^{+\infty} (\varphi_{\lim}(a,x)p(t,a,x) + \psi_{\lim}(a,x)q(t,a,x))da\,dx.$$

Then,

$$\begin{aligned}\frac{dS_{\lim}}{dt}(t) &= \lambda_{\lim} S_{\lim}(t) - (G(N_{\lim}) - G(N(t)))\,\frac{\lambda_{\lim}+d_2}{G(N_{\lim})} \\ &\quad \times \int_0^{+\infty}\int_0^{+\infty} \psi_{\lim}(a,x) q(t,a,x)\,da\,dx \\ &\leq \lambda_{\lim} S_{\lim}(t) - (G(N_{\lim}) - G(C_{\lim} S_{\lim}(t)))\,\frac{\lambda_{\lim}+d_2}{G(N_{\lim})} \\ &\quad \times \int_0^{+\infty}\int_0^{+\infty} \psi_{\lim}(a,x) q(t,a,x)\,da\,dx,\end{aligned}$$

because, due to assumption (H4):

$$N(t) \geq C_{\lim} S_{\lim}(t).$$

Therefore, following the arguments,

$$S_{\lim}(t) \leq \max\left(S_{\lim}(0), \frac{N_{\lim}}{C_{\lim}}\right) := m_{\lim}.$$

4.4 Tumoral tissue: unlimited growth

Following Sect. 3.2, in the tumoral case, the recruitment function from quiescence to proliferation is given by the function (10):

$$G\ (N) = \frac{\alpha_1 \theta^n + \alpha_2 N^n}{\theta^n + N^n}.$$

Here, we expect that the population will show unlimited growth, and a condition leading to this property is:

(H5) For $\tilde{G} = G(\infty) = \alpha_2$, the first eigenvalue, denoted here as λ_1, of system (12) and its adjoint (13), is strictly positive ($\lambda_1 > 0$).

(H6) For the corresponding solutions to (12) and (13) obtained for $\tilde{G} = G(\infty)$, (p_1, q_1), (φ_1, ψ_1), there exists a constant C_1, such that $\varphi^* \geq C_1 \varphi_1$ and $\psi^* \geq C_1 \psi_1$.

Lemma 3 *Under hypotheses (H5) and (H6), we have*

$$N(t) \underset{t\to+\infty}{\longrightarrow} +\infty,$$

and

$$\int_0^{+\infty}\int_0^{+\infty} \Big(\varphi_1(a,x)p(t,a,x) + \psi_1(a,x)q(t,a,x)\Big)\,da\,dx \underset{t\to+\infty}{\longrightarrow} +\infty.$$

Proof of Lemma 3 Indeed, we define:

$$S_1(t) = \int_0^{+\infty}\int_0^{+\infty} (\varphi_1(a,x)p(t,a,x) + \psi_1(a,x)q(t,a,x))da\,dx.$$

We have, since G is decreasing,

$$\begin{aligned}\frac{dS_1}{dt}(t) &= \lambda_1 S_1(t) - (G(\infty) - G(N(t)))\,\frac{\lambda_1 + d_2}{G(\infty)}\int_0^{+\infty}\int_0^{+\infty} \psi_1(a,x)q(t,a,x)da\,dx \\ &\geq \lambda_1 S_1(t).\end{aligned}$$

This implies that $S_1(t)$ has exponential growth. Finally, due to (H6) we have $N(t) \geq C_1 S_1(t)$. We conclude that $N(t)$ tends to infinity and Lemma 3 is proved.

Note that we can also consider the case $\lambda_1 = 0$ in (H5). In this case, $S_1(t)$ would have unlimited, but not exponential growth, and we would be closer to experimental observations of tumour growth [9,14]. Such polynomial-like growth behaviour may actually be obtained in the model by incorporating specific exchange functions L and G between G_0 and G_1 actually yielding $\lambda_1 = 0$, as shown elsewhere [8].

4.5 Steady state for healthy tissue

Numerical experiments show that in the case of healthy tissues, the cell population goes to a steady state that represents tissue homeostasis. This can be analysed in the present model, since a steady state (p^*, q^*) for (5) satisfies the following system of equations:

$$\begin{cases} \frac{\partial(\Gamma_0 p^*)}{\partial a} + \frac{\partial(\Gamma_1(a,x)p^*)}{\partial x} \\ \quad = -\left(L(a,x) + F(a,x) + d_1\right)p^*(a,x) + G(N^*)\,q^*(a,x), \\ L(a,x)\,p^*(a,x) - (G(N^*) + d_2)\,q^*(a,x) = 0, \\ p^*(0,x) = \frac{2}{\Gamma_0}\int_0^{+\infty}\int_0^{+\infty} f(a,x,y)p^*(a,y)\,da\,dy, \end{cases}$$

with

$$N^* = \int_0^{+\infty}\int_0^{+\infty}\left(\varphi^*(a,x)p^*(a,x) + \psi^*(a,x)q^*(a,x)\right)da\,dx. \tag{15}$$

Substituting q^*, we obtain the equation:

$$\begin{cases} \frac{\partial(\Gamma_0 p^*)}{\partial a} + \frac{\partial(\Gamma_1(a,x)p^*)}{\partial x} = -r(a,x,N^*)p^*(a,x), \\ p^*(0,x) = \frac{2}{\Gamma_0}\int_0^{+\infty}\int_0^{+\infty} f(a,x,y)p^*(a,y)\,da\,dy, \end{cases} \tag{16}$$

with

$$r(a,x,N^*) = \frac{d_2}{G(N^*)+d_2}L(a,x) + F(a,x) + d_1.$$

Proposition 4.1 *With the assumptions* $(H1)$, $(H2)$, $(H3)$ *and* $(H4)$, *the system* (15), (16) *has a unique positive solution* (p^*, q^*).

Proof of Proposition 4.1 Equation (16) is an eigenproblem as is Eq. (12); therefore, given a steady state population number N^*, we can find $\lambda(N^*)$ solution of (12). We know by (H1), (H2) that $\lambda(0) > 0$ and by (H3) and (H4) that $\lambda(N_{\lim}) < 0$. Because $\lambda(N^*)$ is continuous, and decreasing since r is increasing with N^*, there is a unique value of N^* such that $\lambda(N^*) = 0$. It remains to normalise the eigenvectors properly to obtain (15).

Remark 1 From (H5) and (H6) we deduce that, for tumour growth, (5) has no steady state.

5 Numerical simulations

Some of the model parameters are known for specific cells in other settings for functions used in a similar context. For stem cells, the parameters are well documented in the literature on the subject (see e.g. [15]), and we chose parameter values according to these sources, knowing that actually identifying these values on other cell lines would be necessary for experimental validation of the model. Parameter values come from [41] for c_1, c_2, c_4, and from [15] for d_1, d_2, α_1, n, θ. The factors determining transition from proliferation to quiescence have been proved to be directly related to Cyclin D [6,20,24,45], but the exact rates are not known. In the same way, parameters A_1, A_2, k_1, k_2, γ_1, γ_2, w_0, Γ_0, α_2, A^*, $\overline{A}$ are not known, but the choices made have been determined either by fixing arbitrary values -as likely as possible, e.g. $A^* = 24$ h, $\overline{A} = 15$ h or by giving a range of values within which our numerical simulations exhibit a behaviour illustrating the theoretical properties of the model demonstrated under assumptions $(H1)$–$(H6)$ (Table 1).

In our numerical simulations, we have used $\varphi^* = \psi^* \equiv 1$, which means that all cells are eligible for recruitment control (by cell density inhibition, growth or antigrowth factors) in phase G_1.

For healthy tissues, Fig. 1 shows the trend towards a steady state as stated in Proposition 4.1 and Fig. 2 shows the distribution of cells according to their age and *Cyclin D/(CDK4 or 6)* concentrations in the quiescent and proliferative phases.

Table 1 Parameters and values used in simulations

Parameters	Values	Parameters	Values
c_1	0.04	γ_1	5 – 10
c_2	0.03	A^*	24 h
c_3	0.3	A_1	0.8 – 1
c_4	0.01	A_2	25
w_0	1	γ_2	5 – 10
Γ_0	0.5	$\overline{A}$	15 h
d_1	0.07 day^{-1}	α_1	0.8 day^{-1}
d_2	0.07 day^{-1}	θ	0.095×10^6
k_1	1	n	1
k_2	20	α_2	0.7 day^{-1}

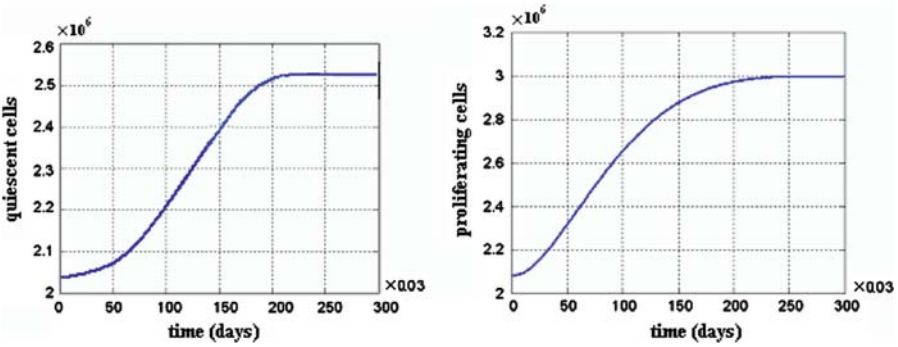

Fig. 1 Time evolution of total population for a healthy tissue. *Left* total quiescent cells $\int_0^{+\infty}\int_0^{+\infty} q(t,a,x)dadx$; *right* total proliferating cells $\int_0^{+\infty}\int_0^{+\infty} p(t,a,x)da\,dx$

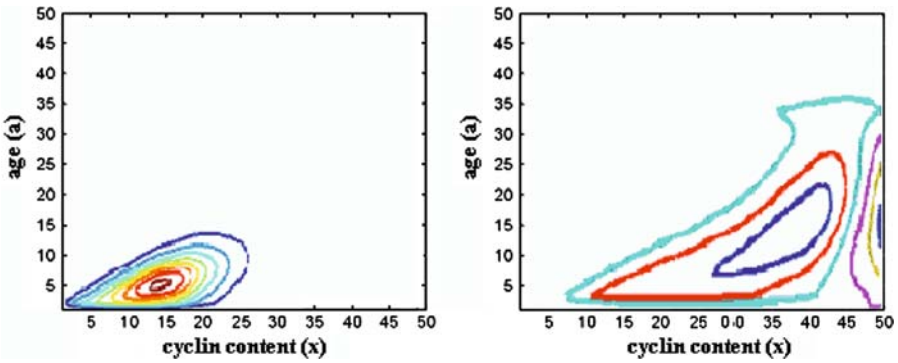

Fig. 2 Isovalues of the total cell population for a healthy tissue at steady state (p^*, q^*): variable x (cyclin content) is in abscissae, variable a (age in the proliferative phase) in ordinates, and level lines indicate constant p^* or q^* values. *Left* quiescent cells $q^*(a,x)$; *right* proliferating cells $p^*(a,x)$

We have verified that assumptions (H1) and (H3) hold true. The so-called power algorithm [16] allowed us to obtain numerically the first eigenvalue for system (12).

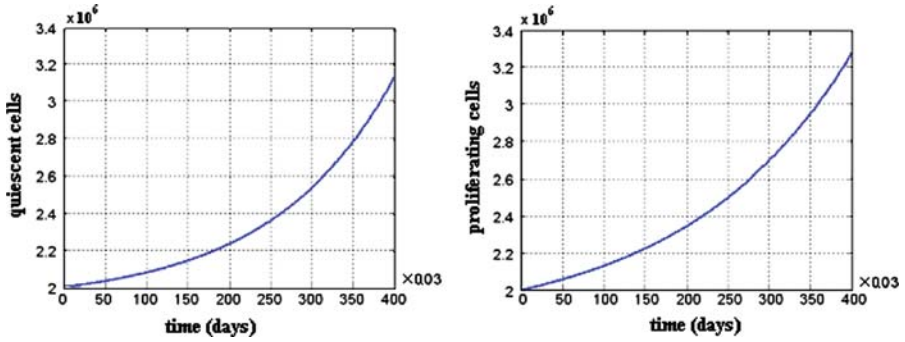

Fig. 3 Time evolution of total population for a tumoral tissue. *Left* total quiescent cells $\int_0^{+\infty}\int_0^{+\infty} q(t,a,x)dadx$; *right* total proliferating cells $\int_0^{+\infty}\int_0^{+\infty} p(t,a,x)dadx$

For $\tilde{G} = \alpha_1 = 0.8$, we have obtained $\lambda_0 = 0.026$, which is compatible with (H1); we have also numerically determined $N_{\text{lim}} = 5.6 \times 10^6$, and obtained $\lambda_{\text{lim}} = -0.12$ for $\tilde{G} = G(N_{\text{lim}}) = \frac{\alpha_1 \theta^n}{\theta^n + N_{\text{lim}}^n}$, which is compatible with (H3) since the cell population has limited growth.

For a tumoral tissue, Fig. 3 shows that the population has unlimited exponential growth in both the quiescent and proliferative phases.

6 Discussion and conclusion

We have considered a nonlinear model to describe a cell population structured by its age and its amount of cyclin with two compartments: proliferating and quiescent cells. We have structured our cell population model by the amount of *Cyclin D/(CDK4 or 6)* since it is the cyclin/CDK complex, or rather the balance between *Cyclin D/(CDK4 or 6)* and *p27(Kip1)* concentrations, which is the most determinant factor for the progression in the cell cycle through the restriction point, and it is also important for the transition from proliferation to quiescence, since there is only one proliferating phase in the model, i.e., other cyclins (E, A, B) have not been considered. We have also assumed that the transition from quiescence to proliferation depends on the total ("qualified") cell population: this nonlinear feedback has been introduced on purpose to allow for a possible cell population steady state which is the norm in fast renewing healthy tissues. Our cell population model can thus be applied to both cancer and normal tissue growth.

The analysis we have carried out, assuming reasonable hypotheses on the parameters, exhibits a steady state for a healthy tissue and, on the contrary, unlimited growth for tumoral tissue. In addition, the numerical simulations confirm these results, as illustrated by Figs. 1, 2 and 3.

Throughout our analysis, we have particularly studied the role of transitions between quiescence and proliferation, focusing on the intracellular amount of Cyclin D, to connect the physiological behaviour of individual cells with the asymptotic behaviour

of the corresponding cell populations with respect to their growth dynamics, for both healthy and tumoral tissues.

In this paper, we did not take space into account, a choice which was unlikely to yield, for the solutions of the equations, the Fisher-KPP-like long-term behaviour which has been observed by various authors for the growth of solid spheroid tumours [9,14], i.e., $R(t) \simeq kt$ for the tumour radius as a function of time. But note that these observations deal with tumours that have in common to be described at a late stage, when space limitations are essential to tumour growth kinetic mechanisms. In this respect, the present model, in the tumoral case, may be suitable only for the phenomenological representation of the initial exponential step of solid tumour growth, or of tumours of the hematopoietic system. Other models [33] take both space and cell cycle control into account, and adding space as a structuring variable (i.e., designing in the future a model structured in age, cyclin content and space) is an open option.

We can hope that a better understanding of the cell cycle and its control can be used practically in cancer therapy. Drugs used in cancer chemotherapies affect only proliferating cells, often in a specific phase of the cell cycle and are often specific to particular proteins of the cell cycle. In the future, we will add to this model the representation of the effects on the cell cycle of drugs such as antagonists of *EGFRs* (epidermal growth factor receptors). These receptors, on stimulation by growth factors, act on the G_1 phase, inducing quiescent cells to enter the proliferating phase and these drugs, which are more and more widely used in clinics, inhibit this recruitment. We will also separate the proliferating phase (i.e., the complete cell division cycle) into specific phases (G_1/S–G_2/M) onto which specific drugs act, e.g. 5 Fluorouracil on S phase.

Such modelling principles will allow us to represent separately the cytotoxic effects of alkylating agents, such as e.g. platinum compounds, non-phase-specific, of antimetabolites, S phase-specific, as well as the cytostatic effects of *EGFR* antagonistic drugs on transitions between quiescent and proliferative states. Taking into account the effects of such different drugs is indeed a necessity in order to actually help clinicians, since modern treatments in oncology use combinations of drugs in standard therapeutic protocols.

References

1. Adimy, M., Crauste, F., Pujo-Menjouet, L.: On the stability of a nonlinear maturity structured model of cellular proliferation. Discrete Contin. Dyn. Syst. **12**(3), 501–502 (2005)
2. Alberts, B., Bray, D., Lewis, J., Raff, M., Roberts, K., Watson, J.D.: Molecular Biology of the Cell. Garland, New York (1994)
3. Arino, O.: A survey of structured cell population dynamics. Acta Biotheor. **43**(1–2), 3–25 (1995)
4. Arino, O., Sanchez, E., Webb, G.F.: Necessary and sufficient conditions for asynchronous exponential growth in age structured cell populations with quiescence. J. Math. Anal. Appl. **215**(2), 499–513 (1997)
5. Bagowski, C.P., Besser, J., Frey, C.R., Ferrell, J.E.: The JNK cascade as a biochemical switch in mammalian cells: ultrasensitive and all-or-none responses. Curr. Biol. **13**(4), 315–320 (2003)
6. Blagosklonny, M.V., Pardee, A.B.: The restriction point of the cell cycle. Cell Cycle **1**(2), 103–10 (2002)
7. Bekkal Brikci, F., Bekkal Brikci, F.: Modélisation du cycle cellulaire et couplage avec la dynamique de population cellulaire. PhD Thesis (in French), Université Pierre-et-Marie-Curie (Paris 6), 2005
8. Bekkal Brikci, F., Clairambault, J., Perthame, B.: Analysis of a molecular structured population model with possible polynomial growth for the cell division cycle. Math. Comput. Model. (2007) (in press)

9. Brú, A., Albertos, S., Subiza, J.L., Gareia-Asenjo, J.L., Brú, I.: The universal dynamics of tumor growth. Biophys. J. **85**(5), 2948–2961 (2003)
10. Carrillo, J.A., Cuadrado, S., Perthame, B.: Adaptive dynamics via Hamilton-Jacobi approach and entropy methods for a juvenile-adult model. Math. Biosci. **205**(1), 137–161 (2007)
11. Clairambault, J., Michel, P., Perthame, B.: Circadian rhythm and tumour growth. C. R. Acad. Sci. (Paris), Mathématique, **342**(1), 17–22 (2006)
12. Cooper, S.: On the Proposal of a G0 phase and the restriction point. FASEB J. **12**(3), 367–373 (1998)
13. Dautray, R., Lions, J.-L.: Mathematical analysis and numerical methods for sciences and technology, Springer, Chap. VIII, pp. 187–199 (1990)
14. Drasdo, D., Höhme, S.: A single-cell-based model of tumor growth in vitro: monolayers and spheroids. Phys Biol. **2**(3), 133–147 (2005)
15. Foley, C., Bernard, S., Mackey, M.C.: Cost-effective G-CSF therapy strategies for cyclical neutropenia: Mathematical modelling based hypotheses. J. Theor. Biol. **238**(4), 754–763 (2006)
16. Golub, G.H., Van Loan, C.F.: Matrix Computations 3rd edn. Johns Hopkins University Press, Baltimore (1996)
17. Gyllenberg, M., Webb, G.F.: A nonlinear structured population model of tumor growth with quiescence. J. Math. Biol. **28**(6), 671–694 (1990)
18. Gyllenberg, M., Webb, G.F.: Age–size structure in populations with quiescence. Math. Biosci. **86**(1), 67–95 (1987)
19. Hartwell, L.H., Kastan, M.B.: Cell cycle control and cancer. Science **266**(5192), 1821–1828 (1994)
20. Hitomi, M., Stacey, D.W.: Cellular ras and cyclin D1 are required during different cell cycle phases in cycling NIH 3T3 cells. Mol. Cell. Biol. **19**(7), 4623–4632 (1999)
21. Hitomi, M., Yang, K., Guo, Y., Frethold, J., Harwalkar, J., Stacey, D.W.: p27 Kip1 and cyclin dependent kinase 2 regulate passage through the restriction point. Cell Cycle **5**(19), 2281–2289 (2006)
22. Kimmel, M., Darzynkiewicz, Z., Arino, O., Traganos, F.: Analysis of a cell cycle model based on unequal division of metabolic constituents to daughter cells during cytokinesis. J. Theor. Biol. **110**(4), 637–664 (1984)
23. Lebowitz, J.L., Rubinow, S.I.: A theory for the age and generation time distribution of a microbial population. J. Math. Biol. **1**(1), 17–36 (1974)
24. Lynch, J., Keller, M., Guo, R.J., Yang, D., Traber, P.: Cdx1 inhibits the proliferation of human colon cancer cells by reducing cyclin D1 gene expression. Oncogene **22**(41), 6395–6407 (2003)
25. Metz, J.A.J., Diekmann, O.: The dynamics of physiologically structured populations. Lecture Notes in Biomathematics vol. 68, Springer, Heidelberg (1986)
26. Michel, P., Mischler, S., Perthame, B.: General relative entropy inequality: an illustration on growth models. J. Math. Pures Appl. **84**(9), 1235–1260 (2005)
27. Michel, P.: Existence of a solution to the cell division eigenproblem. Math. Mod. Meth. App. Sci. **16**(7, suppl.), 1125–1153 (2006)
28. Mischler, S., Perthame, B., Ryzhik, L.: Stability in a nonlinear population maturation model. Math. Mod. Meth. Appl. Sci. **12**(12), 1751–1772 (2002)
29. Novak, B., Tyson, J.J.: A model for restriction point control of the mammalian cell cycle. J. Theor. Biol. **230**(4), 563–579 (2004)
30. Obeyesekere, M., Zimmerman, S.O.: A model of cell cycle behavior dominated by kinetics of A pathway stimulated By growth factors. Bull. Math. Biol. **61**(5), 917–934 (1999)
31. Philipp-Staheli, J., Payne, S.R., Kemp, C.J.: $p27^{Kip1}$: regulation and function of a haploinsufficient tumor suppressor and its misregulation in cancer. Exp. Cancer. Res. **264**(1), 148–168 (2001)
32. Qu, Z., Weiss, J.N., MacLellan, W.R.: Regulation of the mammalian cell cycle: a model of the G1-to-S transition. Am. J. Physiol. Cell. Physiol. **284**(2), C349–C364 (2003)
33. Ribba, B., Colin, T., Schnell, S.: A multiscale mathematical model of cancer, and its use in analyzing irradiation therapies. Theor. Biol. Med. Model. **3**, 7 (2006) Published online Feb 10
34. Rossa, B.: Asynchronous exponential growth in a size structured cell population with quiescent compartment. In: Arino et al., O. (ed) Carcinogenesis and Cell and Tumor Growth. vol. 2, Chap. 14, pp. 183–200 (1995)
35. Rotenberg, M.: Transport theory for growing cell populations. J. Theor. Biol. **103**(2), 181–199 (1983)
36. Sangfelt, O., Erickson, S., Castro, J., Heiden, T., Gustafsson, A., Einhorn, S., Grander, D.: Molecular mechanisms underlying interferon-alpha-induced G0/G1 arrest: CKI-mediated regulation of G1 Cdk-complexes and activation of pocket proteins. Oncogene **18**(18), 2798–2810 (1999)
37. Sherr, C.J.: D-type cyclins. Trends Biochem. Sci. **20**(5), 187–190 (1995)

38. Sherr, C.J.: CDK inhibitors: Positive and negative regulators of G_1-phase progression. Genes Dev. **13**(12), 1501–1512 (2007)
39. Stacey, D.W.: Cyclin D1 serves as a cell cycle regulatory switch in actively proliferating cells. Curr. Option. Cell Biol. **15**(2), 158–163 (2003)
40. Stewart, E.J., Madden, R., Paul, G., Taddei, F.: Aging and death in an organism that reproduces by morphologically symmetric division. PLoS Biol. **3**(2), e45 (2005)
41. Swat, M., Kel, A., Herzel, H.: Bifurcation analysis of the regulatory modules of the mammalian G1/S transition. Bioinformatics **20**(10), 1506–1511 (2004)
42. Val, J., Tyson, J.: A purely deterministic model for the population dynamics of budding yeast. In: Arino, O., Axelrod, D., Kimmel, M. (eds.) Advances in Mathematical Population Dynamics—Molecules, Cells and Man. World Scientific, Singapore (1997)
43. Webb, G.F.: Theory of nonlinear Age-dependent Population Dynamics Monographs and Textbooks in Pure and Applied Mathematics. Marcel Dekker, New York (1985)
44. Zetterberg, A., Larsson, O.: Cell cycle progression and cell growth in mammalian cells: kinetic aspects of transition events. In: Hutchinson, C., Glover, D.M. (eds.) Cell Cycle Control, pp. 206–227. Oxford University Press, Oxford (1995)
45. Zwijsen, R.M., Klompmaker, R., Wientjens, E.B., Kristel, P.M., van der Burg, B., Michalides, R.J.: Cyclin D1 triggers autonomous growth of breast cancer cells by governing cell cycle exit. Mol. Cell. Biol. **16**(6), 2554–2560 (1996)

Proceedings of the 28th IEEE
EMBS Annual International Conference
New York City, USA, Aug 30-Sept 3, 2006

Physiologically based modelling of circadian control on cell proliferation

Jean Clairambault
INRIA, Domaine de Voluceau, BP 105, F78153 Rocquencourt, France
Email: jean.clairambault@inria.fr

Abstract— **The molecular circadian clock which is present in almost all cells of animal organisms exerts a control on the cell division cycle in proliferating tissues by modulating the activity of cyclins and cyclin dependent kinases (CDKs), the proteins which determine transitions from one phase of the cell cycle to the following one, until effective division. Each peripheral cell circadian clock is under the synchronising control of a central hypothalamic pacemaker which itself receives inputs, synchronising or disruptive, from external light and from circulating molecules such as cytokines.**

Principles for modelling these interacting systems are exposed. They rely on age-structured partial differential equations for cell proliferation in a population of cells and ordinary differential equations for the control of cell cycle phase transtions and for the circadian system presented as a network of oscillators with synchronisation and desynchronisation. These physiological cellular systems are coupled together and subject to pharmacological inputs, e.g. from anticancer therapies, which may be synchronised with cell cycle timing by the knowledge of the body circadian clock status, investigated by noninvasive measurements.

The output of the controlled cell proliferation is a population growth exponent identifiable by in vivo tissue measurements; it allows to assess the proliferative status of the tissues under investigation, as a function of the circadian clock status, well fit or disrupted, and of pharmacological inputs such as used in anticancer treatments.

I. Introduction

Cancer growth and response to therapy by anticancer drugs have been shown to be dependent on circadian clock inputs ([9], [15]). Indeed, tumour growth is enhanced by perturbations of the central hypothalamic clock ([6], [7]) and this is most likely related to cell cycle control disruption ([8], [9]). What are the relationships between molecular circadian clock and cell cycle timings? How should anticancer therapeutics be designed so as to induce efficient recovering of such control mechanisms? To answer these questions, an integrative physiology model has been designed, taking into account cell proliferation at the level of a population of cells by age-structured partial differential equations (PDEs), its control by cell cycle proteins (variables in ordinary differential equations, ODEs), and the control of these molecular mechanisms by the circadian system, designed as a network of coupled oscillators also described by ODEs.

II. Cell proliferation: populations of cells

In tissues subject to renewal, in particular in tumours, but also in fast renewing healthy tissues such as gut, skin and bone marrow, the individual cell is the fundamental level of description for the interacting molecular mechanisms at stake in cell cycle progression and circadian clock timing systems. But it is tissue proliferation which is at stake in cancer growth, and also in healthy tissue homeostasis, and that is a matter of cell population dynamics. This leads to consider age-structured cell populations, which are described, for each phase of the cell division cycle, classically divided in phases G_1, $S-G_2$ and M, by evolution equations for cell densities dependent on time and age spent in each phase. Cells in renewing tissues are either in the quiescent, or G_0, phase (where nothing happens), or in the proliferating phases G_1, S (for DNA synthesis, i.e., genome duplication), G_2 and M (for mitosis, or actual cell division). Exchanges of cells between phases G_0 and G_1 may occur at any time in phase G_1 as long as the so-called *restriction point* has not been reached; afterwards, a proliferating cell is irreversibly committed to proceed until actual division -unless it is stopped, e.g. by anticancer drugs, in its progression at cell cycle phase transition *checkpoints*, the most important of which occur at the G_1/S and G_2/M transitions. The transition rates from one phase to the following one (hereafter noted $K_{i\to i+1}$ in the model) are the main targets of the circadian (and pharmacological) control on cell cycle progression.

A. An age-structured partial differential equations (PDE) model of the cell cycle

The model chosen ([4]) is linear and of the Von Foerster-McKendrick type. For each phase i ($1 \leq i \leq I$) of the cell division cycle, $n_i = n_i(t,a)$ denotes the density of cells of age a in phase i at time t. Inside each phase, the variation of the density of cells is due either to a spontaneous death rate $d_i = d_i(t,a)$ or to a transition rate $K_{i\to i+1} = K_{i\to i+1}(t,a)$ from phase i to phase $i+1$ (with the convention $I+1=1$):

$$\begin{cases} \frac{\partial}{\partial t} n_i + \frac{\partial}{\partial a}\left[v_i(a) n_i\right]) + \left[d_i + K_{i\to i+1}\right] n_i = 0, \\ \\ v_i(0) n_i(t, a=0) = \displaystyle\int_{\alpha\geq 0} K_{i-1\to i}(t,\alpha)\; n_{i-1}(t,\alpha)\; d\alpha, \\ \quad 2 \leq i \leq I \\ \\ n_1(t, a=0) = 2 \displaystyle\int_{\alpha\geq 0} K_{I\to 1}(t,\alpha)\; n_I(t,\alpha)\; d\alpha, \end{cases}$$

where $\displaystyle\sum_{i=1}^{I} \int_{\alpha\geq 0} n_i(t,\alpha) d\alpha = 1$, $v_i(a)$ denotes a "speed" function of age a in phase i with respect to time t, and $K_{i\to i+1}(t,a) = \psi_i(t) \mathbf{1}_{\{a\geq a_i\}}(a)$.

The transition rates are chosen as $\psi_i(t)\mathbf{1}_{\{a\geq a_i\}}(a)$, which means that a minimum age, from 0 to a_i, must be spent in phase i, and that a dynamic control $t \mapsto \psi_i(t)$ is exerted on the transition. The control function ψ_i integrates physiological control, such as hormonal or circadian, as well as external environmental and pharmacological influences. Another possibility to take circadian control into account would be by action on the death rates d_i, but it can be shown that at least by itself such control is not compatible with observations from laboratory experiments on tumour growth with modifications of the circadian clock ([4]).

B. Tumoral cells: unlimited growth

As it is, with positive functions as parameters, this linear model is bound to show exponential growth. It can be shown indeed that it yields a so-called *Malthus exponent* λ which governs the asymptotic behaviour of the solutions n_i, in the sense that for all i, the normalised solutions $t \mapsto e^{-\lambda t} n_i(t)$ are bounded, asymptotically constant if ψ_i is constant, and asymptotically periodic if ψ_i is periodic, with the same period. This Malthus exponent λ may be assessed in the case of solid tumours by in vivo tissue growth measurements (only approximately, if one neglects the presence of necrotic material) by $\lambda = \dfrac{\ln 2}{T_d}$, if T_d is the apparent doubling time of tumour size.

C. Healthy cells: tissue homeostasis

In the case of healthy cells, of course there can be no exponential growth, and tissue homeostasis must be ensured, in the sense that for healthy renewing tissues, cell loss must be made up for, and with no excess, by influx from newly formed cells. This can be modelled by the introduction of a G_0 (or quiescent) phase exchanging cells with the G_1 phase, taking into account in the control of these exchange mechanisms a limitation by cell density dependent inhibition, see [2]. In this case, the Malthus exponent λ is zero since the asymptotic growth behaviour of the total population of cells is evolution to stationarity or periodicity, and there is no exponential growth.

An interest in simultaneously representing a tumoral and a healthy cell population is, in the perspective of therapeutic optimisation, to control unwanted toxicity on healthy tissues, a constant side effect in anticancer therapies. These unwanted effects on the healthy cell division cycle are also dependent on the control of cell cycle phase transition by the circadian clock, but possibly with phase differences, as compared with tumours, which may explain observed differences between worst toxicity and best efficacy times for drug infusion ([15]). In this respect, the therapeutic control objective may be seen as to obtain a negative Malthus exponent for tumour cells, and zero growth for healthy cells.

III. Cell proliferation control: cyclins and CDKs

A. Control of cell cycle phase transitions by cyclins and CDKs

Cyclins and their activating kinases (Cyclin dependent kinases, or CDKs) are the proteins which are the most important determinants for the processing through cell cyle phases and transitions between phases. In particular, Cyclin E associated with CDK2 is essential for the G_1/S transition, and Cyclin B associated with CDK1 must be at a level high enough to allow G_2/M transition.

B. Circadian control on cyclins and CDKs

Of these two mechanisms, the most known is the inhibition of G_2/M transition by the circadian clock-controlled kinase Wee1, which deactivates CDK1, thus blocking cells in G_2. It has been described by A. Goldbeter in [10] by an ODE system in which Wee1 is a mere parameter. This system oscillates with an intrinsic frequency which depends on its parameters, but which may be entrained at a 24 h period by Wee1 if Wee1 becomes an output of the molecular circadian clock. A simulation of the entrainment of the normalised M-cell population $t \mapsto e^{-\lambda t} \displaystyle\int_0^{+\infty} n_2(t,a)\, da$, in a simplified 2-phase model ($n_1 =$ cells in $G_1 - S - G_2$, $n_2 =$ cells in M) of the population, by a 24 h-entrained CDK1 is shown on Figure 1.

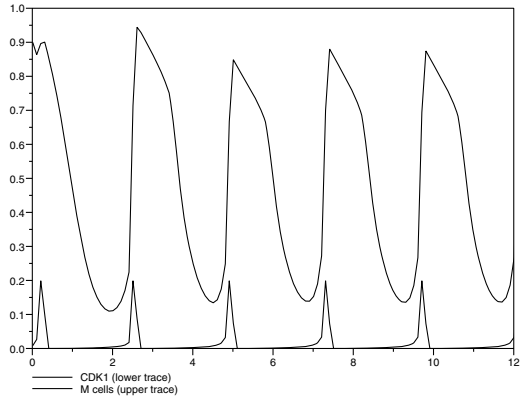

Fig. 1. (abscissae: tens of hours; ordinates: arbitrary units) Entrainment of G2/M transition in a simplified 2-phase cell cycle population model (n_1: G1-S-G2 cells; n_2: M cells) by the circadian clock: CDK1 kinase (lower trace), taken as function ψ in the cell cycle model and entrained by Wee1 (square wave, not shown, of 4 h duration with 24 h period) in A. Goldbeter's mitotic oscillator model, and normalised population of cells in M phase (upper trace).

C. Pharmacological control on cyclins and CDKs

Cell cycle control proteins such as $p53$ act both at the G_1/S and G_2/M checkpoints as sensors of DNA damage and effectors of cell cycle arrest by inhibiting the formation of Cyc E/CDK2 and Cyc B/CDK1 complexes. Anticancer drugs such as alkylating agents act by damaging DNA, and thus provoke cell cycle arrest by triggering p53 and its effects on phase transitions at G_1/S and G_2/M ([18]). And it has been shown that $p53$ on the one hand, and many cellular enzymatic drug detoxification mechanisms (such as reduced glutathione) on the other hand, are dependent on the cell circadian clock, showing 24 h periodicity in their gene expression ([3]). Hence the molecular circadian clock exerts its control on cell cycle transitions both physiologically and when an external pharmacological control is applied. In this modelling frame, the

target of both controls will be on the time-dependent transition functions $t \mapsto \psi_i(t)$ introduced above.

IV. The circadian system: a network of oscillators

This circadian clock control on the cell division cycle is not a constant independent of individual or environmental factors. Though it is endowed with an intrinsic *circa 24 h (circa diem)* period given by a hypothalamic pacemaker - the suprachiasmatic nuclei-, it is dependent on photic inputs (entrainment by the light/dark cycle through the retinohypothalamic tract), and also on the disruptive input of circulating molecules such as cytokines, often elevated in cancers, which may perturb its amplitude so deeply that any physiological body circadian rhythm (temperature, cortisol, rest/activity, etc.) becomes undetectable. Indeed, it has been shown that patients with cancer showing disrupted circadian rhythms are less responsive to chemotherapy and have poorer prognosis than patients with preserved circadian rhythmicity ([15], [17]).

A. The network and its constituents

The body circadian clock ([12], [16]), as far as its control on peripheral cell proliferation is concerned, may be seen as an orchestra consisting in the same basic individual oscillators: cell molecular circadian clocks, since the molecular mechanisms are the same whatever the cells, its peripheral constituents ("the musicians") being slaves, hardly or not communicating together, to the central pacemaker located in the suprachiasmatic nucleus ("the conductor").

Various physiological ODE models of individual circadian clocks have been published in the last ten years. They rely on transcriptional regulation, a mechanism possibly yielding limit cycles, which is a natural mathematical way to represent robust periodic behaviour ([10], [11], [13]). The simplest such physiological model of circadian clock is the 3-dimensional ODE model of FRQ (or PER) protein regulation in *Neurospora Crassa* ([13]), and it was chosen for the individual cell clock model. In this model (see next paragraph for detailed equations), PER and $mRNA$ stand for the PER cytoplasmic protein and its messenger RNA concentrations, and Z for a transcriptional retroinhibition factor linked to PER synthesis.

B. The conductor: the suprachiasmatic nuclei (SCN)

1) Diffusive neuronal coupling in the SCN: From this individual clock model, a network of circadian oscillators results by diffusive coupling of PER. Such coupling may be physiologically achieved either through gap junction connections between suprachiasmatic neurons, or through local release in the intercellular space of neurotransmitters such as vasointestinal peptide (VIP), abundant in the ventrolateral part of these nuclei, where the main pacemaker is supposed to be located, and binding to $VPAC_2$ membrane receptors on these same neurons, or even through electrical signalling with glial participation ([14]). This coupling is thus not necessarily instantaneous, possibly relying mainly on slow tissue diffusion through gap junctions or ligand-receptor connections, but nevertheless may be considered as fast at a time scale of 24 hours, relevant for cell division cycle timing. The coupling is formulated as:

$$\begin{cases} \dfrac{dmRNA(i)}{dt} = V_s \dfrac{K^n}{K^n + Z(i)^n} - V_m(i) \dfrac{mRNA(i)}{K_m + mRNA(i)} \\ \dfrac{dPER(i)}{dt} = k_s mRNA(i) - V_d \dfrac{PER(i)}{K_d + PER(i)} - k_1 PER(i) \\ \qquad\qquad + k_2 Z(i) + K_e \displaystyle\sum_{j \neq i} [PER(j) - PER(i)] \\ \dfrac{dZ(i)}{dt} = k_1 PER(i) - k_2 Z(i) \end{cases}$$

where $1 \leq i, j \leq N$, N being the number of neurons connected in the pacemaker network. The degradation rate V_m of the messenger RNA is supposed to differ from one neuron to the other (with random distribution around a central value) and thus holds variability in individual PER level period. The output of this pacemaker network,to be transmitted to the periphery, is an average $\dfrac{1}{N} \displaystyle\sum_{i=1}^{N} PER(i)$ between neurons, which shows as higher amplitude in its periodic variations (i.e., good synchronisation) as the coupling strength K_e is stronger.

2) Synchronising photic inputs: But it is also known that light, through the retinohypothalamic tract, modulates, equally for all neurons, the transcription rate V_s, which is thus supposed to be $V_s = V_{s_0} \left[1 + L \cos \dfrac{2\pi t}{24}\right]$, and this modulation actually entrains the suprachiasmatic pacemaker, initially endowed with a period dependent on the parameters, e.g. 21 h 30 with our parameter set, to a forced 24 h period, provided that the entrainment by light L is strong enough to overcome the spontaneous period yielded by diffusive coupling between neurons inside the pacemaker.

3) Disruptive inputs from cytokines and drugs: Circulating molecules such as cytokines (interferon, interleukins), either secreted by the immune system in the presence of cancer cells, or delivered by therapy, are known to have a disruptive effect on the circadian clock, most likely at the central pacemaker level, and elevated levels of cytokines have been shown to be correlated with *fatigue* ([17]), a symptom constantly found in cancer, and which presents close relationships with the "jet-lag" of transmeridian flights. This has also been found with anticancer drugs, and is supposed to be a result of drug toxicity on the suprachiasmatic nuclei. It may be taken into account in the model by a positive effect on variable Z, which represents transcriptional inhibition, in the central neuronal clocks.

C. Transmission pathways from the centre to peripheral cells

These pathways are not completely known, but the autonomic nervous system, and neurohormonal ways using the hypothalamo-corticosurrenal axis, are likely candidates to this role. The messengers may be represented by supplementary evolution equations (not shown) describing a chain between messengers: intercentral, hormonal (such as ACTH) and tissular (such as cortisol), the terminal control being exerted on peripheral cells by acting on the transcription of cell clock

variables, acting themselves on cell cycle control proteins in the case of proliferating cells, in the model through the target functions ψ_i introduced above.

D. The musicians: peripheral cell circadian clocks

This terminal control is supposed, as in the case of cytokines in the pacemaker, to be exerted at the transcriptional level through a modification of variable Z in individual cell clocks. Clocks in peripheral cells will be entrained by the central pacemaker at a 24 h rhythm if the transmitted rhythm is strong enough. To illustrate this, Figure 2 shows variables $mRNA$, PER and Z of the model circadian clock averaged in a population of peripheral cells subject to entrainment by the central pacemaker when it is itself entrained or not by light.

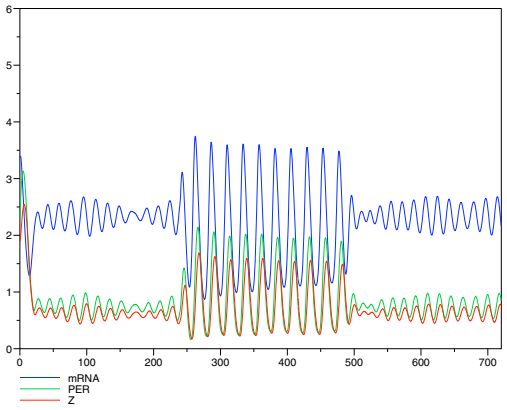

Fig. 2. (abscissae: hours; ordinates: arbitrary units) 3 epochs of 240 h for variables $mRNA$, PER and Z of a peripheral circadian clock: a) without entrainment by light (L=0); b) with entrainment (L=1); c) without (L=0).

V. Conclusion

This paper presents a modelling frame for the circadian control of cell and tissue proliferation. It aims at providing a rationale for therapeutic optimisation of cancer chemotherapies, that is, maximisation of tumour cell kill with shielding of healthy renewing tissues from unwanted toxic side effects, by using synchronisation of the drug delivery schedule and its cell processing with intrinsic cell cycle timing. Such synchronisation naturally relies on the circadian system and it has been in use in clinical ([15]) and in theoretical ([1], [5]) settings in oncology with macroscopic modelling for drug delivery regimen and therapeutic efficacy and unwanted toxicity representation. Anticancer drugs are delivered at the whole organism level, but act at the cell and tissue level on cell cycle control mechanisms. This multiscale modelling framework provides oncologists with a theoretical tool -still under construction- to bridge the gap between the pharmaceutical clinical control level and the molecular pharmacological hidden level of drug action; optimal design of pharmacological control on the cell cycle thus may rely on the knowledge of the natural synchronising control of both cell proliferation and cell drug processing mechanisms by the circadian system, which may be routinely assessed by noninvasive measurements in clinics. Future modelling developments will aim at designing practical clinical rules for dynamic drug delivery schedule optimisation based on molecular pharmacokinetic-pharmacodynamic data for the drugs in use and drug enzymatic metabolism and circadian profiles for patients under anticancer treatment.

Acknowledgments

The author would like to thank Benoît Perthame and Fadia Bekkal Brikci for their essential contributions to cell cycle modelling, Béatrice Laroche for helping deriving the circadian system oscillator network model, and Sonia Montanes for helpful information on present biological knowledge on synchronisation in the suprachiasmatic nuclei.

References

[1] C. Basdevant, J. Clairambault and F. Lévi, *Optimisation of time-scheduled regimen for anti-cancer drug infusion*, Mathematical Modelling and Numerical Analysis, 39(6):1069-1086, 2005.

[2] F. Bekkal Brikci, J. Clairambault, B. Ribba and B. Perthame, *A cell population model with proliferation and quiescence for healthy and tumoral tissues*, submitted, 2006.

[3] G.A. Bjarnason, R.C.K. Jordan and R.B. Sothern, *Circadian variation in the expression of cell-cycle proteins in the human oral epithelium*, Am.J. Pathol., 154:613-622, 1999.

[4] J. Clairambault, Ph. Michel and B. Perthame, *Circadian rhythm and tumour growth*, C. R. Acad. Sci. Paris 342(1):17-22, 2006.

[5] J. Clairambault, *Modelling oxaliplatin drug delivery to circadian rhythms in drug metabolism and host tolerance*, Advanced Drug Delivery Reviews, invited paper (submitted), 2006.

[6] E. Filipski, F. Delaunay, V.M. King, M.W. Wu, B. Claustrat, A. Gréchez-Chassiau, C. Guettier, M.H. Hastings and F. Lévi, *Effects of Chronic Jet Lag on Tumor Progression in Mice*, Cancer Res., 64(21):7879-7885, 2004.

[7] E. Filipski, P. Innominato, M.X. Wu, X.M. Li, S. Iacobelli, L.J. Xian and F. Lévi, *Effects of Light and Food Schedules on Liver and Tumor Molecular Clocks in Mice.*, J. Natl. Cancer Inst., 97(7):507-517, 2005.

[8] L.N. Fu, H. Pelicano, J. Liu, P. Huang and C.C. Lee, *The circadian gene Per2 plays an important role in tumor suppression and DNA damage response in vivo* Cell, 111:41-50, 2002.

[9] L.N. Fu and C.C. Lee, *The circadian clock: pacemaker and tumor suppressor*, Nature reviews / Cancer, 3:350-361, 2003.

[10] A. Goldbeter, *Biochemical oscillations and cellular rhythms*, Cambridge University Press, 1996.

[11] D. Gonze, S. Bernard, C. Wassermann, A. Kramer and H. Herzel, *Spontaneous synchronization of coupled circadian oscillators*, Biophys. J. 89(1):120-129, 2005.

[12] M.H. Hastings, A.B. Reddy and E.S. Maywood, *A clockwork web: circadian timing in in brain and periphery, in health and disease*, Nature Reviews / Neuroscience, 4:649-661, 2003.

[13] J.-C. Leloup, D. Gonze and A. Goldbeter, *Limit cycle models for circadian rhythms based on transcriptional regulation in* Drosophila *and* Neurospora, J. Biol. Rhythms, 14(6):433-448, 1999.

[14] S. Montanes, *Study of the biological clock within the Suprachiasmatic Nucleus (SCN) in mammals' brain*, Internal report, Benjamin Franklin Klinikum für medizinische Informatik, Charité-Universitätsmedizin, Berlin, 2006.

[15] M.-C. Mormont and F. Lévi, *Cancer chronotherapy: principles, applications and perspectives*, Cancer, 97(1):155-169, 2003.

[16] S.M. Reppert and D.R. Weaver, *Coordination of circadian timing in mammals*, Nature, 418:935-941, 2002.

[17] T. Rich, P.F. Innominato, J. Boerner, M.-C. Mormont, S. Iacobelli, B. Baron, C. Jasmin and F. Lévi, *Elevated serum cytokines correlated with altered behavior, serum cortisol rhythm, and dampened 24-hour rest-activity patterns in patients with metastatic colorectal cancer*, Clin. Cancer Res. 11(5):1757-64, 2005.

[18] S. You, P.A. Wood, Y. Xiong, M. Kobayashi, J. Du-Quiton and W.J.M. Hrushesky, *Daily coordination of cancer growth and circadian clock gene expression*, Breast Canc. Res. Treatment, 91:47-60, 2005.

Bibliographie

[1] Bourgey, L. Observation et expérience chez les médecins de la Collection Hippocratique, Vrin, coll. Bibliothèque d'Histoire de la Philosophie, Paris (2005, 1re édition 1953).

[2] Boissin, J., Canguilhem, B. Les rythmes du vivant. Nathan Université, Paris (1998).

[3] Labrecque, L., Sirois-Labrecque, M. Chronopharmacologie. Presses de l'Université de Montréal (2003).

[4] Goldbeter, A. Biochemical oscillations and cellular rhythms. Cambridge University Press (1996).

[5] Rosenblueth, A., Simeone, F.A. The interrelations of vagal and accelerator effects on the cardiac rate. Am. J. Physiol. 110:42-55 (1934).

[6] Sayers, B.Mc A. nalysis of heart rate variability, Ergonomics, 16;1:85-97 (1973).

[7] Katona, P.G., Jih, F. Respiratory sinus arrhythmia: Noninvasive measure of parasympathetic control, J. Appl. Physiol., 30, pp. 801-805 (1975).

[8] Akselrod, S. et al. Power spectrum analysis of heart rate fluctuation : a quantitative probe of beat to beat cardiovascular control. Science, 213:220-222 (1981).

[9] B. Pomeranz et al. Assesment of autonomic function in humans by heart rate spectral analysis. Am. J. Physiol. 248 (Heart Circ. Physiol. 17):H151-H153 (1985).

[10] Nawab, S.H., Quatieri, T.F. Short-Time Fourier Transform. In: Advanced topics in signal processing, pp. 289-337. Editors: J.S. Lim, A.V. Oppenheim. Prentice-Hall, Englewood Cliffs, NJ (1988).

[11] Shin, S.J. Assessment of autonomic regulation of heart rate variability by the method of complex demodulation. IEEE Transact. Biomed. Eng. 36, 2:274-283 (1989).

[12] Lachenbruch, P.A. Discriminant analysis, Chapter 7. Hafner Press, Mac Millan Publishing Co (1975).

[13] Celeux, G. et al. L'analyse discriminante. In : Classification automatique des données, environnement statistique et informatique, pp. 237-275. Dunod, Paris (1989).

[14] Dempster, A., Laird, N., Rubin, D. Maximum likelihood from incomplete data via the EM algorithm (with discussion). J.R.S.S. B, 39:1-38 (1977).

[15] Celeux, G., Diebolt, J. The SEM Algorithm: a probabilistic teacher algorithm derived from the EM algorithm for the mixture problem. Computational Statistics Quaterly, 2:73-82 (1985).

[16] Juang, B.H., Rabuiner, L.R. Hidden Markov Models for Speech Recognition. Technometrics, 251-272 (199)1.

[17] Guckenheimer, J., Holmes, P. Nonlinear oscillations, dynamical systems, and bifurcations of vector fields. Springer (1983).

[18] Eckmann, J.-L., Ruelle, D. Ergodic theory of chaos and strange attractors. Rev. Modern Phys., 57:617-656 (1985).

[19] Grassberger, P., Procaccia, I. Measuring the strangeness of strange attractors. Physica D, 9:189-208 (1983).

[20] Pincus, S.M., Cummins, T.R., Haddad, G.G. Heart rate control in normal and aborted-SIDS infants. Am. J. Physiol., 264:R638-R646 (1993).

[21] Pincus, S.M., Goldberger, A.L. Physiological time series: what does regularity quantify? Am. J. Physiol., 266:H1643-H1656 (1994).

[22] Wolf, A., Swift, J.B., Swinney, HL, Vasta, J.A. Determining Lyapunov exponents from a time series. Physica D, 16:285-317 (198).

[23] Eckmann, J.-P., Oliffson Kamphorst, S., Ruelle, D., Ciliberto, S. Lyapunov exponents from time series. Phys. Rev. A, 34:4971-4979 (1986).

[24] Briggs, K. An improved method for estimating Liapunov exponents of chaotic time series. Phys. Lett. A, 151:27-32 (1990).

[25] Abarbanel, H.D.I., Brown, R., Sidorowich, J.J., Tsimring, L. Sh. The analysis of observed chaotic data in physical systems. Rev. Modern Phys., 65:1331-1392 (1993).

[26] Theiler, J., Eubank, S., Longtin, A., Galdrikian, B., Farmer, J.D. Testing for nonlinearity in time series: the method of surrogate data. Physica D, 58:77-94 (1992).

[27] Sugihara, G., May, R.M. Nonlinear forecasting as a way of distinguishing chaos from measurement error in time series. Nature, 344:734-741 (1990).

[28] Yanagihara, K., Noma, A., Irisawa, H. Reconstruction of sino-atrial node pacemaker potential based on the voltage clamp experiments. Jap. J. Physiol., 30:841-857 (1980).

[29] Mokrane, A., LeBlanc, A.R., Nadeau, R. Modeling of the basic mechanisms of short-term control of heart rate. Proc. of the IFAC symposium on modeling and control in biomedical systems, Galveston, TX, USA, pp. 142-143 (1994).

[30] Lévi, F., Perpoint, B. et al., Oxaliplatin Activity against Metastatic Colorectal Cancer. A Phase II Study of 5-Day Continuous Venous Infusion at Circadian Rhythm Modulated Rate. Eur. J. Cancer 29A (9):1280-1284 (1993).

[31] Lévi, F. (Ed.) Cancer chronotherapeutics. Special issue of Chronobiology International Vol. 19(1) (2002).

[32] Mormont, M.-C., Lévi, F. Cancer chronotherapy: principles, applications and perspectives. Cancer, 97(1): 155-169 (2003).

[33] N.A. Boughattas, F. Lévi, et al., Circadian Rhythm in Toxicities and Tissue Uptake of 1,2-diamminocyclohexane(trans-1)oxaloplatinum(II) in Mice. Cancer Research 49 (1989) 3362-3368.

[34] T.G. Granda, R.M. D'Attino, E. Filipski, et al., Circadian optimization of irinotecan and oxaliplatin efficacy in mice with Glasgow osteosarcoma. Brit. J. Cancer 86 (2002) 999-1005.

[35] Dautray, R., Lions, J.-L. Mathematical analysis and numerical methods for sciences and technology, Springer, Ch VIII:187-199 (1990).

[36] Filipski, E., Innominato, P. F., Wu, M. W., Li, X. M., Iacobelli, S, Xian, L. J., Lévi, F. Effect of light and food schedules on liver and tumor molecular clocks in mice. J. Natl Cancer Inst., 97 (7): 507-517 (2005).

[37] Matsuo, T., Yamaguchi, S., Mitsui, S., Emi, A., Shimoda, F., Okamura, H. Control mechanism of the circadian clock for timing of cell division in vivo. Science 302: 255-259 (2003).

[38] Blagosklonny, M.V., Pardee, A.B. The restriction point of the cell cycle. Cell Cycle, Mar-Apr 1(2):103-10 (2002).

[39] Brú, A., Albertos, S., Subiza, J.L., Gareia-Asenjo, J.L., Brú,I. The universal dynamics of tumor growth. Biophys. J. 85:2948-2961 (2003).

[40] Lévi, F, Metzger, G, Massari, C, Milano, G. Oxaliplatin: Pharmacokinetics and Chronopharmacological Aspects. Clin. Pharmacokinet. 38:1-21, 2000.

[41] Faivre, S., Chan, D., Salinas, R., Woynarowska, B., Woynarowski, J.M. DNA strand breaks and apoptosis induced by oxaliplatin in cancer cells. Biochemical pharmacology, 66:225-237, 2003.

[42] Su FX et al. Glutathion S Transferase π indicates chemotherapy resistance in breast cancer. J. Surg. Res. 113:102-108 (2003).

[43] Viguier, J. et al. ERCC1 codon 118 polymorphism is a predictive factor for the tumor response to oxaliplatin/5-fluorouracil combination chemotherapy in patients with advanced colorectal cancer. Clin Cancer Res. 11(17):6212-7 (2005).

[44] Li, XM, Metzger, G. Filipski, E., Boughattas, N., Lemaigre, G., Hecquet, B., Filipski, J., Lévi, F. Pharmacologic modulation of reduced glutathione circadian rhythms with buthionine sulfoximine: relationship with cisplatin toxicity in mice. Tox. Appl. Pharmacol. 143:281-290 (1997).

[45] Li, XM, Metzger, G., Filipski, E., Lemaigre, G., Lévi, F. Modulation of nonprotein sulphydryl compounds rhythm with buthionine sulphoximine: relationship with oxaliplatin toxicity in mice. Arch.Toxicol. 72:574-579 (1998).

[46] Goldbeter, A. A model for circadian oscillations in the Drosophila period protein (PER). Proc. R. Soc. Lond. B, 261:319-324, 1995.

[47] Leloup, J.-C., Gonze, D., Goldbeter, A. Limit cycle models for circadian rhythms based on transcriptional regulation in Drosophila and Neurospora, J. Biol. Rhythms, 14(6):433-448, 1999.

[48] Goldbeter, A. A minimal cascade model for the mitotic oscillator involving cyclin and cdc2 kinase. Proc. Natl. Acad. Sci. U S A. 88(20):9107-11 (1991).